Synthesis and reactivity of metal complexes containing functionalized N-heterocyclic carbene ligands for catalytic applications

Pengfei Ai

UNIVERSITÉ DE STRASBOURG

ÉCOLE DOCTORALE DES SCIENCES CHIMIQUES

Institute de Chimie, UMR7177

THÈSE présentée par :

Pengfei AI

soutenue le : **24 sept 2015**

pour obtenir le grade de : **Docteur de l'université de Strasbourg**

Discipline/ Spécialité : Chimie

Synthèse et réactivité de complexes métalliques contenant des ligands carbéniques N-hétérocycliques et des ligands fonctionnels pour des applications catalytiques

THÈSE dirigée par :

M. BRAUNSTEIN Pierre	Directeur de recherche émérite CNRS, Université de Strasbourg Membre de l'Académie des sciences
M. DANOPOULOS Andreas	Fellow USIAS, Université de Strasbourg

RAPPORTEURS :

M. SEVERIN Kay	Professeur à l'École polytechnique fédérale de Lausanne
M. DRIESS Matthias	Professeur à la Technische Universität Berlin

Acknowledgement

This work was carried out in the Laboratoire de Chimie de Coordination (UMR 7177 CNRS) of the Université de Strasbourg, directed by Prof. Pierre Braunstein. I am very grateful to all the kind people around me because it would not have been possible for me to finish my doctoral thesis without their help and support.

Firstly I wish to thank my supervisor Prof. Pierre Braunstein. He is a nice, respected supervisor and his vast experience and profound knowledge in the area has helped me during my PhD research. He always gave me constant encouragement and suggestions in spite of his busy agenda. In addition to research, he also taught me about the French culture and life, especially wines, which has become one of my favorite hobbies. It has been my honor to be his PhD student.

I then would like to express my special thanks to my co-supervisor Dr. Andreas Danopoulos. He is a kind and diligent researcher with constructive thoughts. He taught me a lot of experimental skills and helped me pursue my work in a very interesting research topic. His constructive suggestions helped me overcome all the difficulties during my PhD. He also helped me broaden my chemical experience.

I would like to express my sincere gratitude to the members of my jury, Prof. Kay Severin and Prof. Matthias Driess, for agreeing to be the external evaluators and participate in the defense of this thesis.

I thank Dr Kirill Yu. Monakhov (now in Aachen) for his contribution to the DFT calculations in this thesis. I also thank Dr. Matteo Mauro and Prof. Luisa de Cola (ISIS, Strasbourg) for investigating the photophysical properties of some of the complexes I prepared and Dr. Christophe Gourlaouen (Institut de Chimie, Strasbourg) for performing theoretical calculations on them.

I would like to thank all the members of the NMR, X-ray Crystallography, Elemental Analysis and Mass Spectrometry services of the Université de Strasbourg for their contribution and assistance.

I am grateful to the present and former secretaries for all their help: Nadia

Bouaouina, Sandrine Garcin and Soumia Hnini. I also thank the present and former members in our lab (in random order): Dr. Jacky Rosé, Dr. Marcel Wesolek, Dr. Lucie Routaboul, Dr. Béatrice Jacques, Dr. Pierre de Frémont, Mélanie Boucher, Marc Mermillon-Fournier, Alessio Ghisolfi, Sophie Hameury, Martin Jagenbrein, Alexandre Massard, Paulin Buchwalter, Valentine Charra, Fan He, Minghui Yuan, Xiaoyu Ren, Serena Orbisaglia, Mary Garner, Venkatesh Subbiah. In particular, I want to thank Thomas Simler. We entered the lab in the same year and he gave me a lot of help in research and in life.

I want to express my thanks to all my Chinese friends in Strasbourg. Without them, my life abroad would not be so interesting.

Lastly, I would like to thank my parents, my girlfriend and my sister for all their encouragement and support.

Pengfei Ai

Strasbourg

July 2015

CONTENTS

Introduction Générale

1 Carbènes N-Hétérocycliques

1.1 Une brève histoire des Carbènes N-Hétérocycliques.

Les carbènes sont des composés neutres contenant un atome de carbone divalent à six électrons de valence et les carbènes N-Hétérocycliques (abrégés dans la suite NHCs pour « N-Heterocyclic Carbenes ») sont définis comme des espèces hétérocycliques contenant un atome de carbone carbénique et au moins un atome d'azote dans le cycle.[1] En raison de leur grande réactivité et courte durée de vie, ils n'ont généralement été considérés que comme des intermédiaires de réaction fugaces. Les premiers complexes métalliques possédant des ligands NHC furent décrits indépendamment par Öfele et Wanzlick et collaborateurs en 1968 (Figure 1).[2] Cependant, ce n'est qu'en 1991 que le premier NHC stable fut isolé par Arduengo, 1,3-di(adamantyl)imidazol-2-ylidene (**IAd**, Figure 1).[3] Depuis, une très grande diversité de ligands NHCs ont été synthétisés et on assiste à une véritable explosion du nombre d'études expérimentales et théoriques les concernant.[1a,4] Etant d'excellents ligands pour les métaux de transition, les NHCs ont trouvé des applications très nombreuses en catalyse homogène, en chimie médicinale et en science des matériaux.[5]

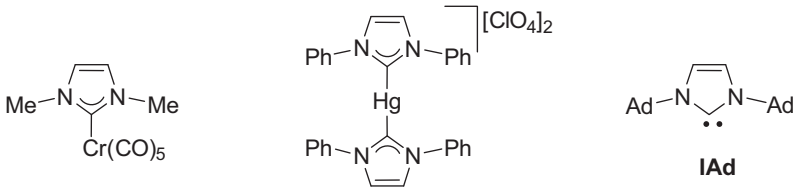

Schéma 1

1.2 Propriétés électroniques et stériques des NHCs

La configuration électronique des NHCs est un singulet à l'état fondamental avec deux électrons de spins opposés occupant une orbitale σ alors qu'une orbitale *p* est vacante. Ces ligands possèdent en général des substituants encombrés sur les atomes d'azote, tels que l'adamantyle (Ad), qui contribuent à leur stabilisation

Pour les références bibliographiques, voir page 15

cinétique en défavorisant leur dimérisation en oléfine correspondante.[1a,4a,4c] L'importante stabilisation électronique apportée par les atomes d'azote adjacents au carbone carbénique opère de deux manières: l'effet inductif (les azotes sont σ-attracteurs) provoque un abaissement de l'énergie de l'orbitale occupée σ et l'effet mésomère (les azotes sont π-donneurs) apporte de la densité électronique dans l'orbitale vide p_π (Figure 2).[5k,6]

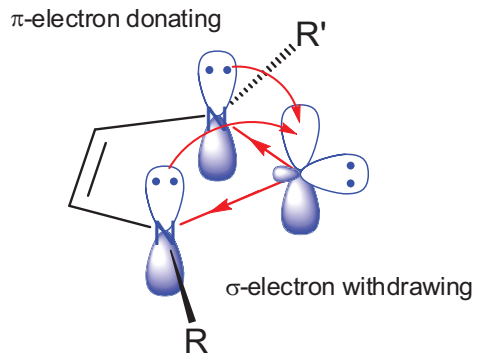

Schéma 2

Les propriétés électroniques des NHCs dépendent du type d'hétérocycle et des substituants du cycle alors que les substituants de l'azote ont une importance considérable sur les propriétés stériques. La quantification de ces deux propriétés se fait en utilisant deux paramètres maintenant couramment utilisés, respectivement le paramètre électronique de Tolman (TEP) et le pourcentage de volume occupé par les atomes (buried volume (% V_{bur})).[5k,6]

Initialement développé pour évaluer les propriétés donneur d'électron des phosphines par Tolman en 1970, le TEP est basé sur la valeur de la fréquence infra-rouge de vibration d'élongation A_1 dans un complexe carbonyle de métal de transition modèle, tel que $[Ni(CO)_3L]$.[7] Plus le ligand apporte de la densité électronique au métal, plus la retro-coordination π sera importante vers les ligands carbonyles, affaiblissant ainsi la liaison triple CO et abaissant la fréquence de vibration ν(CO). Du fait de la grande toxicité de $[Ni(CO)_3L]$, les complexes *cis*-$[IrCl(CO)_2L]$ and *cis*-$[RhCl(CO)_2L]$ sont de plus en plus utilisés à cet effet.[4h]

Pour les références bibliographiques, voir page 15

Le concept de volume occupé (% V_{bur}) fut développé et affiné par Nolan, Cavallo *et al*. en 2003.[8] Ce paramètre est défini comme le pourcentage d'une sphère autour du métal (avec un rayon r) occupée par le ligand sur la base de données cristallographiques (Figure 3). Les paramètres à utiliser pour ce calcul sont: une distance de 2.0 Å ou 2.28 Å pour la liaison métal-ligand (d) et un rayon de 3.0 Å ou 3.5 Å pour la sphère (r). Plus le ligand est encombré stériquement, plus la valeur % V_{bur} sera élevée. Ce concept peut d'ailleurs être étendu à d'autres familles de ligands en chimie de coordination.[9]

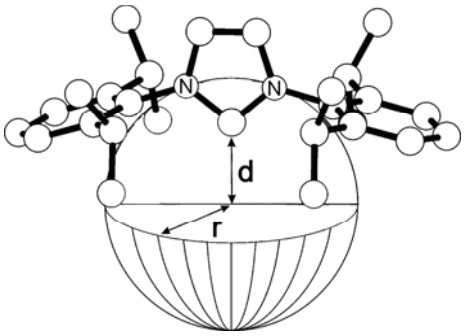

Schéma 3

2 Ligands Hybrides

Les ligands hybrides possèdent au moins deux atomes donneurs chimiquement différents, séparés par un espaceur, et sont censés combiner les propriétés favorables de chaque type de donneur et/ou montrer des propriétés uniques que ne possèdent pas les ligands à mêmes atomes donneurs.[10]

On peut identifier trois modes de coordination pour les ligands hybrides (Figure 4): (*i*) monodente, seul un donneur est coordiné au métal; (*ii*) chélatant, où les deux groupes donneurs fixés sur le même métal présentent des interactions métal-ligand différentes; (*iii*) pontant, où chaque donneur est fixé sur un centre métallique différent, des interactions métal-métal pouvant ou non exister entre eux.[10a]

Pour les références bibliographiques, voir page 15

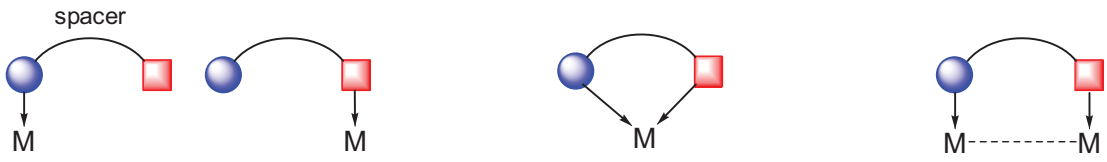

Schéma 4

En grande partie motivés par la capacité des ligands hybrides à présenter un comportement hémilabile, les chercheurs ont produit dans les dernières années un très grand nombre de tels ligands et ont utilisé leurs complexes métalliques en catalyse homogène.[10c,11] En particulier, des ligands NHC avec un groupe fonctionnel tel que phosphine, amine, amide, éther, aryloxy, alkoxy et cyclopentadienyle (Cp), attirent une attention croissante.[12] Mon travail portera plus particulièrement sur des ligands hybrides contenant un groupe NHC associé à une phosphine.

3 Proligands et ligands fonctionnels *N*-phosphanyl-NHC

Bien que les ligands NHC soient considérés comme mimant bien le comportement des phosphines, ils possèdent des propriétés électroniques σ-donneur/π-accepteur et stériques différentes.[5k,13] Les complexes contenant à la fois des donneurs NHC et phosphine sur le même métal ont montré des propriétés catalytiques supérieures à celles des complexes analogues contenant que des ligands NHC ou phosphines.[14] Cet effet coopératif ainsi que l'intérêt général porté aux ligands hybrides ont conduit à l'idée prometteuse de vouloir combiner ces fonctions au sein d'un même ligand pour former des ligands NHC phosphorés. Ils peuvent être de deux types, soit avec un espaceur entre N_{imid} et l'atome de P, soit avec une liaison directe P-N. Puisque la première catégorie a été l'objet d'une revue récente par Gaillard *et al.*,[12c] nous nous concentrerons dans cette Introduction sur le deuxième type, les ligands et proligands fonctionnels *N*-phosphanyl-NHC. Ce sont principalement les groupes de Kostyuk et de Hofmann qui ont abordé ce domaine avant nous. Puisque notre propre contribution sera présentée au cours des chapitres qui suivent, nous porterons ici

Pour les références bibliographiques, voir page 15

notre attention sur le travail des autres. Dans la suite de ce chapitre, les complexes métalliques NHC seront représentés par le dessin de gauche du Schéma 5,[4g] indiquant la délocalisation électronique entre les atomes d'azote et aucune charge et un simple trait entre le carbone et le métal, alors qu'une liaison dative est typiquement utilisée pour décrire la liaison entre le phosphore et le métal dans les complexes phosphine des métaux de transition (Figure 5 droite).

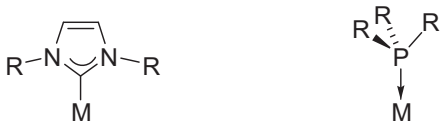

Schéma 5

Les premières études traitant de sels d'imidazolium *N*-phosphorylés datent de 1999 où ils furent observés comme intermédiaires par ^{31}P NMR au cours de la préparation de 1-alkyl-2-diphénylphosphanyl imidazole (Schéma 6).[15] Plus de 10 ans plus tard, Kostyuk *et al*. furent les premiers à isoler le bromure de 1-méthyl-3-diphenylphosphanyl-imidazolium et montrèrent que dans les travaux précédents, le signal à ca. 30 ppm en ^{31}P NMR avait été attribué par erreur au sel d'imidazolium *N*-phosphorylé (68 ppm).[16]

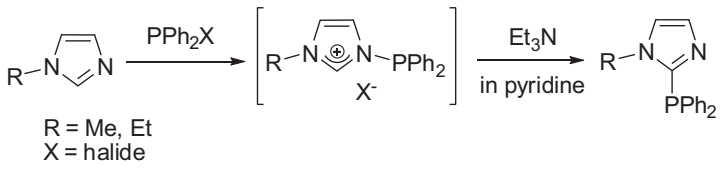

Schéma 6

Au même moment, ils ont préparé une série de (pro-)ligands fonctionnels NHC *N*-phosphanyle. Depuis, cette nouvelle famille de ligands hybrides rigides attire une attention croissante.[12c,17] Le schéma 7 regroupe tous les proligands fonctionnels NHC *N*-phosphanyle (**1**-**10**) et les ligands (**11**-**18**) caractérisés jusqu'à juin 2015 inclus.

Pour les références bibliographiques, voir page 15

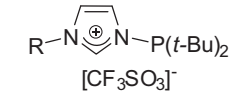

R = Me (**a**), Mes (**b**), Dipp (**c**), 2,6-diethylphenyl (**d**).
R = Et; anion = BF_4.

1

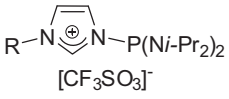

R = Me, *t*-Bu.

2

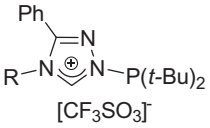

R = Me (**a**), Et (**b**), *i*-Pr (**c**).

3

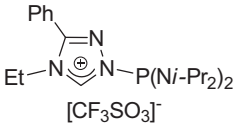

4

R = Me, *i*-Pr.

5

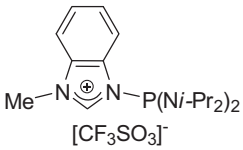

6

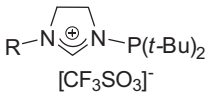

R = Ph (**a**), Mes (**b**).

7

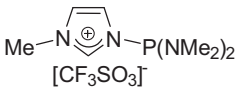

8

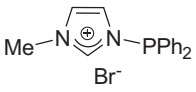

9

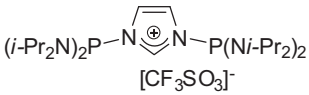

10

***N*-Phosphanyl functionalized NHC pro-ligands**

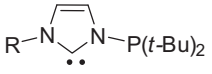

R = Me (**a**), Et (**b**), *t*-Bu (**c**), Mes (**d**), Dipp (**e**), Adam (**f**), 2,6-diethylphenyl (**g**).

11

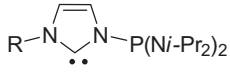

R = Me, *t*-Bu.

12

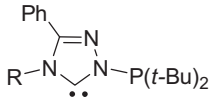

R = Me (**a**), Et (**b**), *i*-Pr (**c**).

13

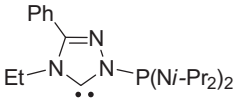

14

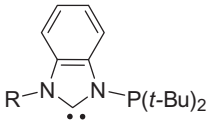

R = Me (**a**), *i*-Pr (**b**), *t*-Bu (**c**), Adam (**d**),

15

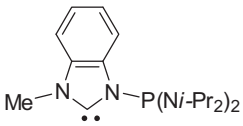

16

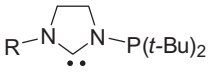

R = Ph (**a**), Mes (**b**)

17

18

***N*-Phosphanyl functionalized NHC ligands**

Schéma 7

Le contre-anion associé à ce type de pro-ligands NHC a une très grande importance sur leur stabilité et le triflate s'est révélé le meilleur. Les principales approches synthétiques consistent en: (*i*) la réaction d'imidazole (ou benzimidazole, imidazoline ou triazole) *N*-substitutée avec des bromo- (ou chloro-)phosphines en présence de triflate de sodium; (*ii*) la réaction d'imidazole (ou benzimidazole) *N*-substitutée avec le triflate d'un composé phosphoré; (*iii*) l'alkylation d'imidazole (ou benzimidazole ou triazole) *N*-phosphanyle avec un triflate d'alkyle (Schéma 8). La

Pour les références bibliographiques, voir page 15

liaison P-N des proligands est très labile and susceptible d'être cassée par des nucléophiles (tels que H_2O, CH_3OH ou Me_2NH).[17c]

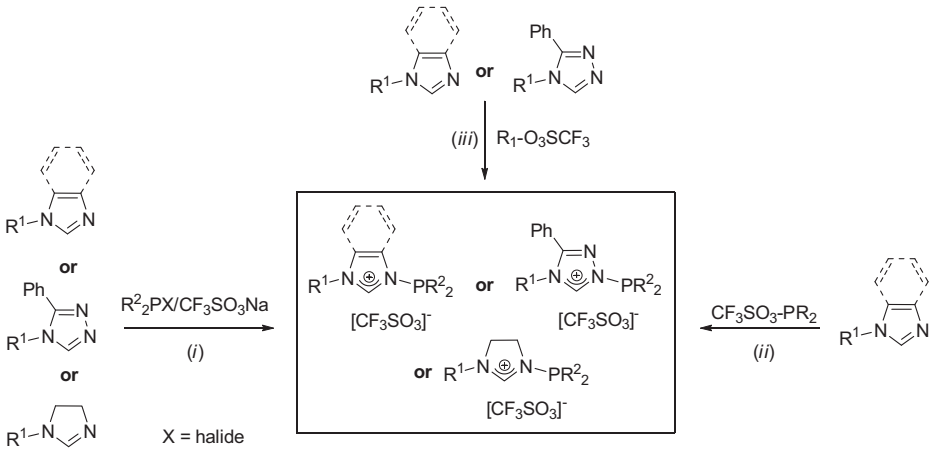

Schéma 8

Bien que divers proligands fonctionnels *N*-phosphanyl-NHC puissent être facilement préparés, leur déprotonation pour obtenir le carbène libre dépend du choix du dérivé phosphoré. Les ligands NHC libres n'ont pu être obtenus que lorsque les substituants du phosphore sont *t*-Bu ou *i*-Pr_2N. Dans le cas contraire, une migration du groupe phosphine se produit de N vers C2.[16] Un exemple avec un groupe imidazole est montré dans le Schéma 9. Engendrer avec succès des carbènes libres par déprotonation des proligands dependra aussi de la nature de la base et seules des bases fortes, telles que les alkyl lithiens, NaHMDS ou KHMDS, le permettent. Il a été observé que NaOH et NaOMe conduisent à l'ouverture du N-hétérocycle.[17c] Un autre accès à ce type de ligands NHC met en oeuvre la déprotonation de l'imidazole *N*-substitutée par *n*-BuLi, suivie de la réaction avec la di-*tert*-butylchlorophosphine (Scheme 9).[17d]

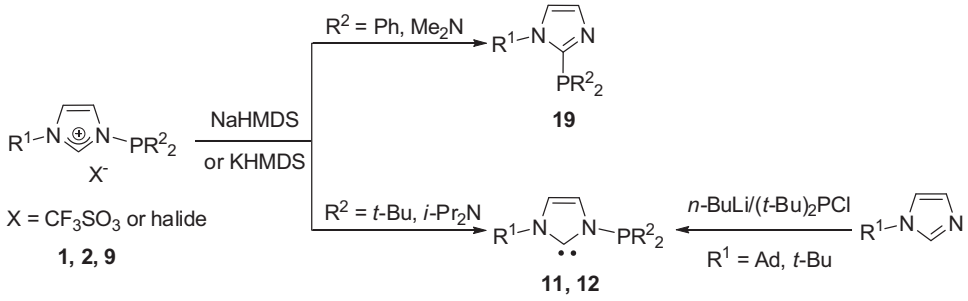

Schéma 9

Pour les références bibliographiques, voir page 15

Les caractéristiques propres de ces ligands NHC incluent: (*i*) un petit angle de pince (bite angle) et une grande rigidité; (*ii*) une liaison covalente P-N(hétérocycle) qui facilite la communication électronique directe entre les atomes donneurs; (*iii*) une aptitude du fragment phosphanyle à opérer une migration-1,2 du N(hétérocycle) au C2(hétérocycle).

4 Réactivité des ligands fonctionnels *N*-phosphanyl-NHC

4.1 Ligands pontants

Les complexes organométalliques contenant des *N*-phosphanyl-NHCs contiennent principalement les métaux du groupe 11 (Cu, Ag, Au), avec ces ligands en mode pontant. Hofmann *et al*.[17a] ont décrit les complexes dinucléaires du Cu(I) **20a** et **20d**, obtenus par réaction des carbènes libres **11a** et **11d** avec $[Cu(MeCN)_4]PF_6$, respectivement (Schéma 10). Les centres Cu(I) sont doublement pontés par deux ligands via les donneurs C_{NHC} et P selon un mode μ_2-κ*C*,κ*P*. Les courtes distances Cu-Cu, respectivement de 2.613 et 2.575 Å, indiquent la présence d'interactions d^{10}-d^{10}.[18] Le remplacement des groupes méthyle ou mésityle par le substituant plus volumineux *t*-Bu conduisit au complexe mononucléaire du Cu(I) **21** où le métal est linéairement coordiné à deux ligands par les donneurs C_{NHC} (Schéma 10).

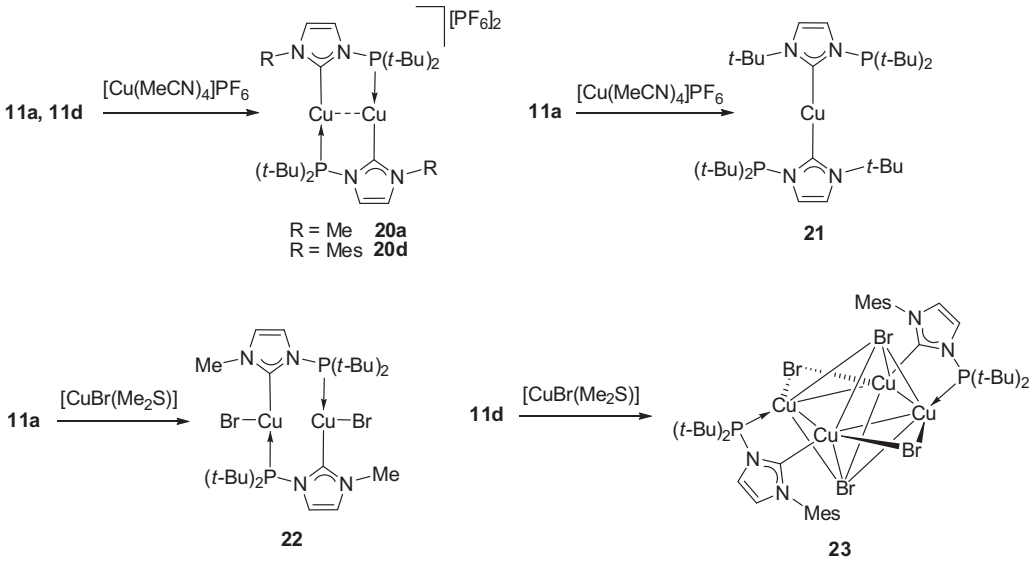

Schéma 10

Pour les références bibliographiques, voir page 15

Le remplacement du précurseur métallique par [CuBr(Me_2S)] a conduit avec le ligand **11a** au complexe dinucléaire **22** ayant le même mode de coordination que **20** mais avec un ligand bromure lié à chaque Cu (Schéma 10), ce qui amène une élongation de la distance Cu-Cu (2.9977 Å). Utiliser **11d** dans les mêmes conditions a conduit au complexe tétranucléaire centrosymétrique **23** avec un coeur Cu_4 rectangulaire. Deux ligands bromures sont liés de manière μ_4 au coeur Cu_4 plane et deux autres sont liés en mode μ_2.[18] Les distances Cu-Br sont comprises entre 2.4437 et 2.8553 Å.

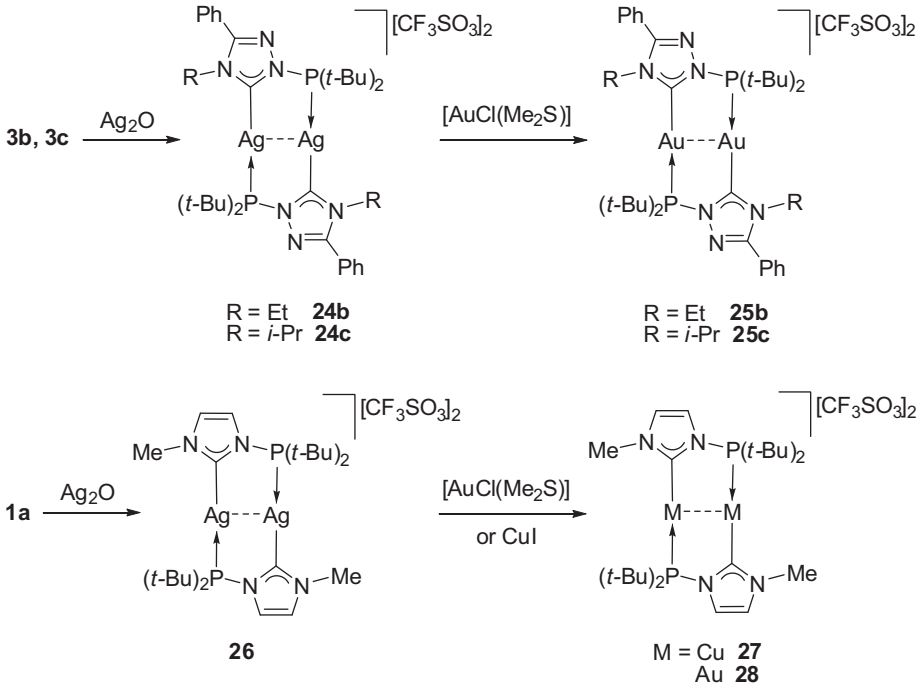

Schéma 11

Au cours de la même année, Kostyuk *et al*.[17e,17f] ont préparé les complexes dinucléaires d'Ag(I) **24b**, **24c** et **26** par réaction des proligands **3b**, **3c** et **1a** avec Ag_2O, respectivement (Schéma 11). Des transmétallations ultérieures avec [AuCl(Me_2S)] ou CuI ont donné les complexes correspondants d'Au(I) ou de Cu(I). La structure des complexes d'Ag(I) et d'Au(I) a révélé des distances métal-métal courtes (2.881 Å pour **24b**, 2.8221 Å pour **26**, 2.8554 Å pour **25b** et 2.8099 Å pour **28**) en accord avec des interactions d^{10}-d^{10}.[18e,19] Les propriétés de **27** et **28** ont aussi été étudiées: le complexe de cuivre **27** a donné d'excellents résultats dans des réactions de transfert

Pour les références bibliographiques, voir page 15

de nitrène, alors que le complexe d'or **28** n'a donné qu'une émission négligeable sous irradiation UV, malgré la présence d'interactions aurophiles.

Les sels d'imidazolium **7a** et **7b** furent synthétisés récemment et leur réaction avec Ag_2O a conduit respectivement aux complexes dinucléaires **29a** et **29b** (Schéma 12), qui peuvent également être obtenus directement par coordination à $[AgO_3SCF_3]$ du carbène libre correspondant **17a** et **17b**.[17i] Les transmétallations de **29b** ont conduit à la formation des complexes dinucléaires de Cu(I) **30** et d'Au(I) **31** qui possèdent des interactions d^{10}-d^{10} (Schéma 12). La préparation de complexes d'Au et de Cu fut aussi réalisée par addition de $[AuCl(Me_2S)]$ ou CuI au carbene libre **17b**, mais un mélange de deux complexes dinucléaires fut obtenu **32** et **33** ou **34** et **35**, respectivement, d'où un produit pur ne put être isolé (Schéma 13).

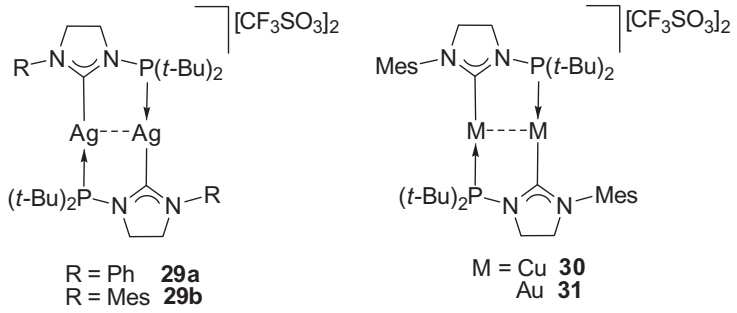

Schéma 12

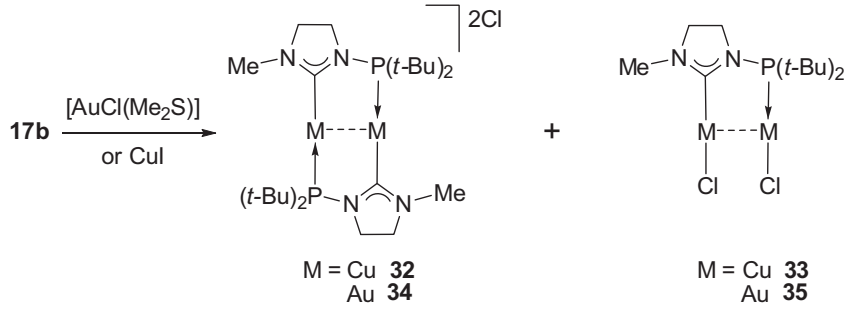

Schéma 13

4.2 Ligands chélatants

Outre leur mode de liaison pontant, les ligands *N*-phosphanyl-NHC peuvent se comporter en chélates par les donneurs C_{NHC} et P, ce qui ne fut décrit que par Hofmann *et al.* Ils ont observé la formation de complexes possédant un chélate à quatre chaînons par coordination directe des carbènes libres **11b**, **11d** et **11e**

Pour les références bibliographiques, voir page 15

(Schéma 14). La valeur de l'angle de pince est situé entre 65.25° dans **42** et 70.15° dans **41**.[17b]

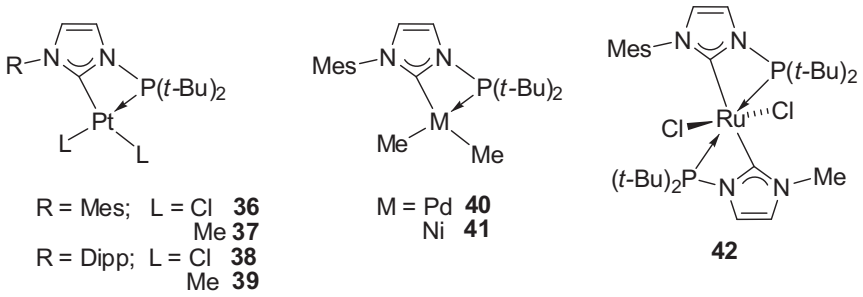

Schéma 14

La réactivité du complexe diméthyle de palladium **40** a été étudiée en vu de transformations ultérieures.[17b] Sa réaction avec des alcynes pauvres en électrons, comme le diméthyl acétylène dicarboxylate (DMAD), a donné le complexe de type palladacyclopentadiène **43** alors qu'avec le fumaronitrile (FN) ou l'anhydride maléique (MA), une élimination réductrice a conduit aux complexes de Pd(0) **44** et **45**, respectivement (Schéma 15).

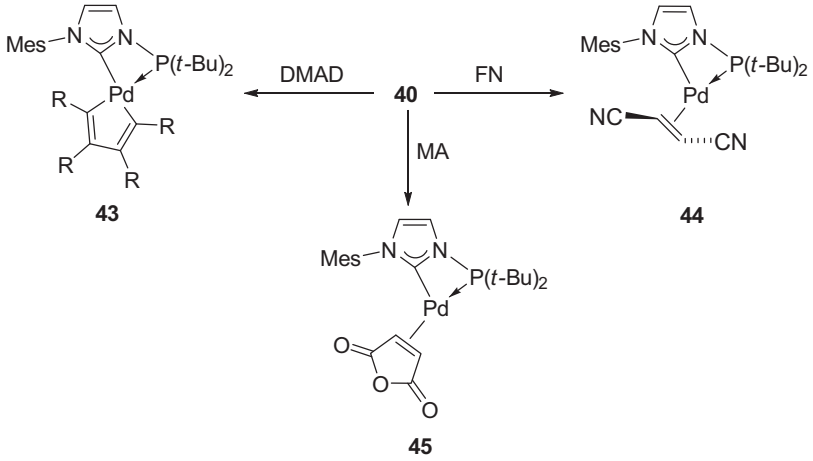

Schéma 15

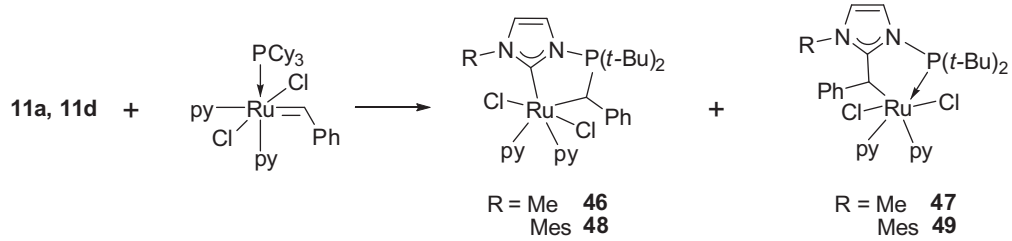

Schéma 16

Pour les références bibliographiques, voir page 15

Ces auteurs ont également observé la formation de cycles à cinq chaînons suite à la formation de nouvelles liaisons C-P ou C-C par réaction du carbène libre **11a** ou **11d** avec $[RuCl_2(Pcy_3)py_2(CHPh)]$ (Schéma 16).[17g] Des calculs DFT ont montré que ces réactions étaient sous contrôle cinétique et pouvaient avoir un lien avec les réactions de désactivation du catalyseur en métathèse des oléfines.

5 Objectifs et plan de ma thèse

Comme déjà mentionné, les ligands fonctionnels *N*-phosphanyl-NHC ont essentiellement été du type bidentate avec une liaison P-N alors que des tridentes avec deux liaisons P-N ne sont connus que pour **18**, porteur de groupes $(i\text{-}Pr_2N)_2P$. Il possède trois sites donneurs (C_{NHC} et deux P) intéressants pour une chimie multimétallique et ses applications. Cependant, la faible capacité de coordination de **18** limite son application en chimie de coordination et des réactions de décomposition furent observées lors de tentatives infructueuses avec les métaux du groupe 11. L'objectif de cette thèse a été de synthétiser de nouveaux ligands tridentes stables, de type NHC *N*,*N*'-diphosphanyle et d'explorer leur chimie de coordination.

Faisant suite à l'Introduction, huit chapitres seront présentés concernant un nouveau ligand tridente *N*,*N*'-bis(di-tert-butylphosphanyl)-imidazole-2-ylidene (**$PC_{NHC}P$**) et ses complexes métalliques. Ces chapitres seront présentés sous forme de publications (parues ou à soumettre) et ont donc leur propre bibliographie.

Les chapitres 1, 2, 4 et 5 portent sur la synthèse du ligand **$PC_{NHC}P$** et ses complexes avec les métaux du groupe 11 (Cu, Ag, Au), à configuration électronique d^{10} et donnant lieu à des interactions métallophiles d^{10}-d^{10}. Le chapitre 3 porte sur deux diphosphines imidazole régioisomères et leurs complexes avec les métaux du groupe 10 (Ni, Pd, Pt). Les chapitres 6 et 7 présenteront des complexes hétéronucléaires Cu/Pd et Ag/Pd et homonucléaires du palladium. Le chapitre 8 porte sur des complexes du Cr(II) et Cr (III) et leurs propriétés catalytiques en

Pour les références bibliographiques, voir page 15

oligomérisation de l'éthylène. Enfin, le chapitre 10 visera à déterminer l'acidité π de ligands sur la base des adduits NHC-Se et complexes du bore, du Rh(I) et du Fe(II).

Pour les références bibliographiques, voir page 15

1.6 Références

(1) (a) Bourissou, D.; Guerret, O.; Gabbaï, F. P.; Bertrand, G. *Chem. Rev.* **2000**, *100*, 39-92. (b) de Frémont, P.; Marion, N.; Nolan, S. P. *Coord. Chem. Rev.* **2009**, *253*, 862-892.

(2) (a) Öfele, K. *J. Organomet. Chem.* **1968**, *12*, P42-P43. (b) Wanzlick, H. W.; Schönherr, H. J. *Angewandte Chemie* **1968**, *80*, 154-154.

(3) Arduengo, A. J.; Harlow, R. L.; Kline, M. *J. Am. Chem. Soc.* **1991**, *113*, 361-363.

(4) (a) Herrmann, W. A.; Köcher, C. *Angew. Chem. Int. Ed. Engl.* **1997**, *36*, 2162-2187. (b) Arduengo, A. J. *Acc. Chem. Res.* **1999**, *32*, 913-921. (c) Böhm, V. P. W.; Herrmann, W. A. *Angew. Chem. Int. Ed.* **2000**, *39*, 4036-4038. (d) Nolan, S. P. *N-Heterocyclic Carbenes in Synthesis*; Wiley-VCH Verlag GmbH & Co. KGaA: Weinheim, 2006. (e) Díez-González, S.; Nolan, S. P. *Coord. Chem. Rev.* **2007**, *251*, 874-883. (f) Hahn, F. E.; Jahnke, M. C. *Angew. Chem. Int. Ed.* **2008**, *47*, 3122-3172. (g) Schmidt, A.; Wiechmann, S.; Freese, T. *Arkivoc* **2013**, 424-469. (h) Nelson, D. J.; Nolan, S. P. *Chem. Soc. Rev.* **2013**, *42*, 6723-6753. (i) Crabtree, R. H. *Coord. Chem. Rev.* **2013**, *257*, 755-766. (j) Jahnke, M. C.; Hahn, F. E. *Coord. Chem. Rev.* **2015**, *293–294*, 95-115. (k) Waters, J. B.; Goicoechea, J. M. *Coord. Chem. Rev.* **2015**, *293–294*, 80-94.

(5) (a) Herrmann, W. A. *Angew. Chem. Int. Ed.* **2002**, *41*, 1290-1309. (b) Crudden, C. M.; Allen, D. P. *Coord. Chem. Rev.* **2004**, *248*, 2247-2273. (c) Peris, E.; Crabtree, R. H. *Coord. Chem. Rev.* **2004**, *248*, 2239-2246. (d) Glorius, F. *N-Heterocyclic Carbenes in Transition Metal Catalysis*; Springer Berlin Heidelberg, 2007. (e) Pugh, D.; Danopoulos, A. A. *Coord. Chem. Rev.* **2007**, *251*, 610-641. (f) Kantchev, E. A. B.; O'Brien, C. J.; Organ, M. G. *Angew. Chem. Int. Ed.* **2007**, *46*, 2768-2813. (g) Díez-González, S.; Marion, N.; Nolan, S. P. *Chem. Rev.* **2009**, *109*, 3612-3676. (h) McGuinness, D. *Dalton Trans.* **2009**, 6915-6923. (i) Riener, K.; Haslinger, S.; Raba, A.; Högerl, M. P.; Cokoja, M.; Herrmann, W. A.; Kühn, F. E. *Chem. Rev.* **2014**. (j) Visbal, R.;

Pour les références bibliographiques, voir page 15

Gimeno, M. C. *Chem. Soc. Rev.* **2014**, *43*, 3551-3574. (k) Hopkinson, M. N.; Richter, C.; Schedler, M.; Glorius, F. *Nature* **2014**, *510*, 485-496.

(6) Dröge, T.; Glorius, F. *Angew. Chem. Int. Ed.* **2010**, *49*, 6940-6952.

(7) Tolman, C. A. *Chem. Rev.* **1977**, *77*, 313-348.

(8) Hillier, A. C.; Sommer, W. J.; Yong, B. S.; Petersen, J. L.; Cavallo, L.; Nolan, S. P. *Organometallics* **2003**, *22*, 4322-4326.

(9) Clavier, H.; Nolan, S. P. *Chem. Commun.* **2010**, *46*, 841-861.

(10) (a) Braunstein, P.; Naud, F. *Angew. Chem. Int. Ed.* **2001**, *40*, 680-699. (b) Braunstein, P. *J. Organomet. Chem.* **2004**, *689*, 3953-3967. (c) Zhang, W.-H.; Chien, S. W.; Hor, T. S. A. *Coord. Chem. Rev.* **2011**, *255*, 1991-2024.

(11) Liu, X.; Braunstein, P. *Inorg. Chem.* **2013**, *52*, 7367-7379.

(12) (a) Kühl, O. *Functionalised N-Heterocyclic Carbene Complexes*; Wiley, Weinheim, 2010. (b) Tornatzky, J.; Kannenberg, A.; Blechert, S. *Dalton Trans.* **2012**, *41*, 8215-8225. (c) Gaillard, S.; Renaud, J.-L. *Dalton Trans.* **2013**, *42*, 7255-7270.

(13) (a) Öfele, K.; Herrmann, W. A.; Mihalios, D.; Elison, M.; Herdtweck, E.; Scherer, W.; Mink, J. *J. Organomet. Chem.* **1993**, *459*, 177-184. (b) Herrmann, W. A.; Öfele, K.; Elison, M.; Kühn, F. E.; Roesky, P. W. *J. Organomet. Chem.* **1994**, *480*, c7-c9. (c) Lee, M.-T.; Hu, C.-H. *Organometallics* **2004**, *23*, 976-983. (d) Crabtree, R. H. *J. Organomet. Chem.* **2005**, *690*, 5451-5457.

(14) (a) Scholl, M.; Ding, S.; Lee, C. W.; Grubbs, R. H. *Org. Lett.* **1999**, *1*, 953-956. (b) Frey, G. D.; Schütz, J.; Herdtweck, E.; Herrmann, W. A. *Organometallics* **2005**, *24*, 4416-4426. (c) Schmid, T. E.; Jones, D. C.; Songis, O.; Diebolt, O.; Furst, M. R. L.; Slawin, A. M. Z.; Cazin, C. S. J. *Dalton Trans.* **2013**, *42*, 7345-7353.

(15) Tolmachev, A. A.; Yurchenko, A. A.; Merculov, A. S.; Semenova, M. G.; Zarudnitskii, E. V.; Ivanov, V. V.; Pinchuk, A. M. *Heteroatom Chemistry* **1999**, *10*, 585-597.

(16) Marchenko, A. P.; Koidan, H. N.; Huryeva, A. N.; Zarudnitskii, E. V.; Yurchenko, A. A.; Kostyuk, A. N. *J. Org. Chem.* **2010**, *75*, 7141-7145.

Pour les références bibliographiques, voir page 15

(17) (a) Kühnel, E.; Shishkov, I. V.; Rominger, F.; Oeser, T.; Hofmann, P. *Organometallics* **2012**, *31*, 8000-8011. (b) Nägele, P.; Herrlich, U.; Rominger, F.; Hofmann, P. *Organometallics* **2012**, *32*, 181-191. (c) Marchenko, A. P.; Koidan, H. N.; Hurieva, A. N.; Pervak, I. I.; Shishkina, S. V.; Shishkin, O. V.; Kostyuk, A. N. *Eur. J. Org. Chem.* **2012**, *2012*, 4018-4033. (d) Marchenko, A. P.; Koidan, H. N.; Pervak, I. I.; Huryeva, A. N.; Zarudnitskii, E. V.; Tolmachev, A. A.; Kostyuk, A. N. *Tetrahedron Lett.* **2012**, *53*, 494-496. (e) Marchenko, A. P.; Koidan, H. N.; Zarudnitskii, E. V.; Hurieva, A. N.; Kirilchuk, A. A.; Yurchenko, A. A.; Biffis, A.; Kostyuk, A. N. *Organometallics* **2012**, *31*, 8257-8264. (f) Marchenko, A. P.; Koidan, H. N.; Hurieva, A. N.; Gutov, O. V.; Kostyuk, A. N.; Tubaro, C.; Lollo, S.; Lanza, A.; Nestola, F.; Biffis, A. *Organometallics* **2013**, *32*, 718-721. (g) Brown, C. C.; Plessow, P. N.; Rominger, F.; Limbach, M.; Hofmann, P. *Organometallics* **2014**, *33*, 6754-6759. (h) Kirilchuk, A. A.; Yurchenko, A. A.; Kostyuk, A. N.; Rozhenko, A. B. *J. Comput. Chem.* **2014**, n/a-n/a. (i) Marchenko, A.; Koidan, H.; Hurieva, A.; Kurpiieva, O.; Vlasenko, Y.; Kostyuk, A.; Tubaro, C.; Lenarda, A.; Biffis, A.; Graiff, C. *J. Organomet. Chem.* **2014**, *771*, 14-23. (j) Wang, T.; Stephan, D. W. *Chem. Eur. J.* **2014**, *20*, 3036-3039.

(18) (a) Mehrotra, P. K.; Hoffmann, R. *Inorg. Chem.* **1978**, *17*, 2187-2189. (b) Pyykkö, P. *Chem. Rev.* **1997**, *97*, 597-636. (c) Zuo, J. M.; Kim, M.; O'Keeffe, M.; Spence, J. C. H. *Nature* **1999**, *401*, 49-52. (d) Fu, W.-F.; Gan, X.; Che, C.-M.; Cao, Q.-Y.; Zhou, Z.-Y.; Zhu, N. N.-Y. *Chem.–Eur. J.* **2004**, *10*, 2228-2236. (e) Gray, T. G.; Sadighi, J. P. In *Molecular Metal-Metal Bonds*; Wiley-VCH Verlag GmbH & Co. KGaA: 2015, p 397-428.

(19) (a) Bardajía, M.; Laguna, A. *Eur. J. Inorg. Chem.* **2003**, *2003*, 3069-3079. (b) Katz, M. J.; Sakai, K.; Leznoff, D. B. *Chem. Soc. Rev.* **2008**, *37*, 1884-1895. (c) Schmidbaur, H.; Schier, A. *Chem. Soc. Rev.* **2008**, *37*, 1931-1951. (d) Sculfort, S.; Braunstein, P. *Chem. Soc. Rev.* **2011**, *40*, 2741-2760. (e) Schmidbaur, H.; Schier, A. *Chem. Soc. Rev.* **2012**, *41*, 370-412. (f) Tiekink, E. R. T. *Coord. Chem. Rev.* **2014**, *275*, 130-153. (g) Schmidbaur, H.; Schier, A. *Angew. Chem. Int. Ed.* **2015**, *54*, 746-784.

Pour les références bibliographiques, voir page 15

Chapter 1

A novel, rigid diphosphine with an active NHC spacer; di- and trinuclear complexes of d^{10} coinage metals

This chapter is written in the form of a publication. This article was published in *Chemical Communications* **2014**, 50, 103-105.

My contribution in this work included the synthesis of the ligands and complexes, their characterization and the preparation of the draft of the publication. The calculations were performed by Dr. Kirill Yu. Monakhov.

Unpublished results are presented in the annex to this chapter.

A novel, rigid diphosphine with an active NHC spacer; di- and trinuclear complexes of d^{10} coinage metals

Pengfei Ai,[a] Andreas A. Danopoulos,*[a,b] Pierre Braunstein*[a] and Kirill Yu. Monakhov[c]

[a] Laboratoire de Chimie de Coordination, Institut de Chimie (UMR 7177 CNRS), Université de Strasbourg, 4 rue Blaise Pascal, 67081 Strasbourg Cedex (France). E-mail: danopoulos@unistra.fr, braunstein@unistra.fr

[b] Institute for Advanced Study, USIAS, Université de Strasbourg.

[c] Institut für Anorganische Chemie, RWTH Aachen University, Landoltweg 1, 52074 Aachen, Germany.

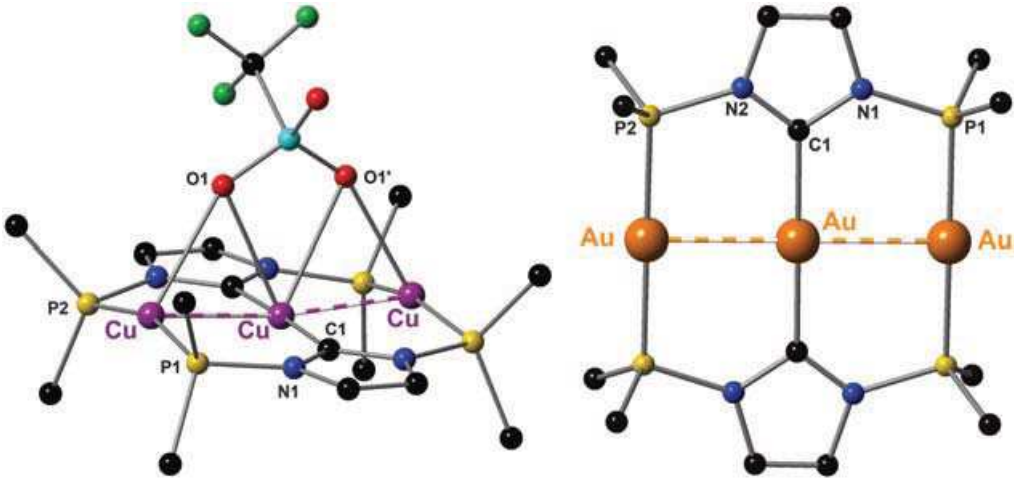

Supporting information for this chapter is available on the internet under http://pubs.rsc.org/en/Content/ArticleLanding/2014/CC/C3CC47370H

For references, see P24

Résumé du Chapitre 1

Deux sels d'imidazolium *N,N'*-diphosphanyl **1a** et **1b** ont été synthétisés et leur déprotonation a conduit respectivement à la formation d'un carbène N-hétérocyclique (NHC) *N,N'*-diphosphanyl fonctionalisé **2a** et à une diphosphine **3b** dont les groupes phosphorés sont différents (Schéma 1). Le chauffage de **2a** à 120 °C pendant la nuit conduit à la diphosphine **3a** analogue à **3b** après migration d'un groupe $P(t\text{-}Bu)_2$ de N vers C2.

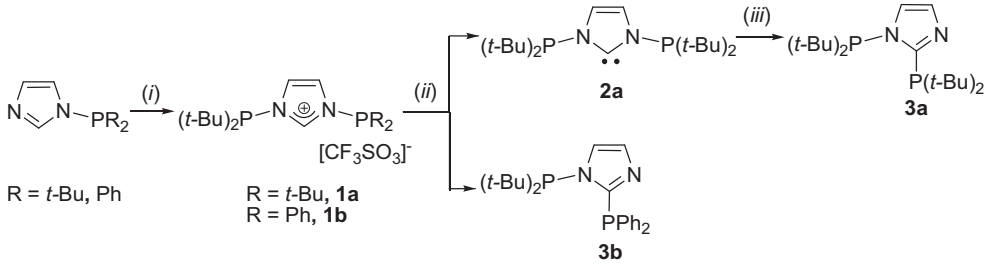

Schéma 1 Réactifs et conditions: (*i*) NaO_3SCF_3, $PBr(t\text{-}Bu)_2$, THF, 0 °C à temp. amb.; (*ii*) $NaN(SiMe_3)_2$, éther, 0 °C à temp. amb.; (*iii*) chauffage à 120 °C, pendant la nuit.

Nous montrons également que le ligand NHC tridente rigide **2a** constitue une plateforme unique pour la synthèse de nouveaux complexes di- et trinucléaires avec les métaux du groupe 11 (Cu, Ag et Au) (Schéma 2).

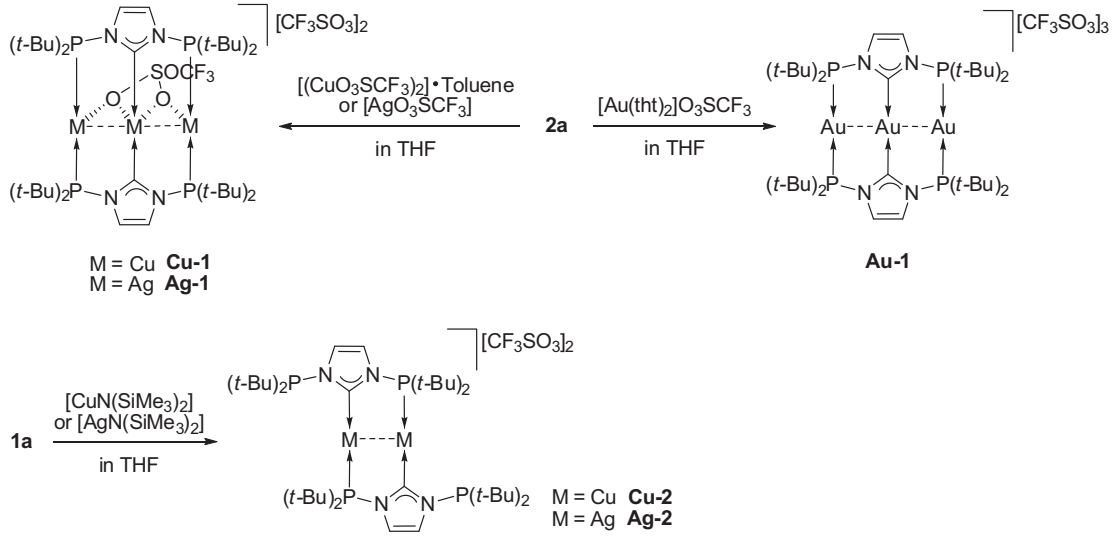

Schéma 2

For references, see P24

La distance métal-métal dans les complexes trinucléaires est très courte (2.5761(9) Å pour **Cu-1**, 2.7599(3) Å pour **Ag-1** et 2.7584(2) Å pour **Au-1**), ainsi que dans le complexe dinucléaire (2.6827(12) Å pour **Cu-2**), ce qui indique l'existence d'interactions métallophiles d^{10}-d^{10} entre les métaux.

For references, see P24

ChemComm

COMMUNICATION

View Article Online
View Journal | View Issue

A novel, rigid diphosphine with an active NHC spacer; di- and trinuclear complexes of d^{10} coinage metals†‡

Cite this: *Chem. Commun.*, 2014, **50**, 103

Received 26th September 2013,
Accepted 22nd October 2013

DOI: 10.1039/c3cc47370h

www.rsc.org/chemcomm

Pengfei Ai,[a] Andreas A. Danopoulos,*[ab] Pierre Braunstein*[a] and Kirill Yu. Monakhov[c]

A novel *N,N′*-diphosphanyl-imidazol-2-ylidene acts as a stable, hybrid $PC_{NHC}P$ ligand for M_2 or linear M_3 (M = Cu, Ag, Au) arrays with metallophilic interactions.

The coordination of both NHC and P donors to the same metal has led to complexes with superior catalytic properties to their all-NHC or all-P analogues.[1] Although the origins of this synergism are mechanistically diverse and not yet fully understood,[2] advancements can be anticipated by precisely tuning the metal coordination sphere through the use of multidentate P-functionalized NHC ligands, featuring donor atoms in fixed positions relative to each other. P-functionalized NHC pro-ligands and ligands[3] are thus of high current interest.[4] Very recently, a few *N*-phosphanyl imidazoliums and their corresponding NHCs have been described (Scheme 1).[5] Distinctive characteristics of these ligands include: (i) a narrow bite angle and high rigidity; (ii) covalent P–N(heterocycle) bonds facilitating direct electronic communication between the donors; (iii) aptitude of the phosphanyl fragment for 1,2-migration from N(heterocycle) to C2(heterocycle) which, in order to be suppressed, places constraints on the nature of the P-substituents. Recent focus[5] has mainly been on bidentate (pro)-ligands of type **A** and their complexes with group 10 and 11 metals. In contrast, molecules of type **B** are only known for Y = Z = P(Ni-Pr_2)$_2$,[5a] which limits their scope in coordination chemistry; although combining P- and NHC-strong σ-donors

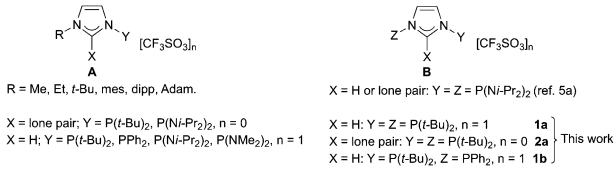

Scheme 1

should have obvious potential in multimetallic chemistry and relevant applications, especially with coinage metals.[6]

Here we describe novel rigid diphosphines of type **B** (Scheme 1) with an imidazolium or an NHC spacer, investigate their stability by experimental and DFT methods with respect to phosphanyl migration aptitude from the N to the $NC_{NHC}N$ carbon atom, and characterise rare NHC, phosphine complexes,[3c,5c,7] with either κ^2-*PC*$_{NHC}$P or unprecedented, rigid κ^3-$PC_{NHC}P$ bonding to two or three coinage metals, respectively.

Critical for the successful isolation of **1a,b** is the use of the non-nucleophilic triflate anion (Scheme 2)‡.[5a,b]

Deprotonation of **1a** with NaN(SiMe_3)$_2$ in ether gave **2a** while similar attempts with **1b** under various conditions led to the non-symmetric diphosphine **3b**, after PPh_2 migration (see the DFT study below). The air sensitive **2a** is thermally stable at room temperature ($t_{1/2} \simeq 6$ h at 120 °C) and has been fully characterised, including by X-ray diffraction (Fig. 1) (for comparison the structure of **1a** was also determined; Fig. S1 and Table S1, ESI‡).

In the highly symmetrical **1a** and **2a**,‡ the orientation of the lone pairs at P differs: in **1a** it is *syn* to the proton at (crystallographic)C1 but in **2a** *anti* to the lone pair at the C_{NHC}. These *syn*,

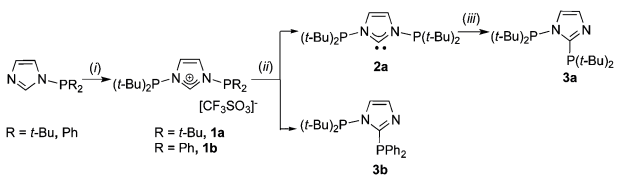

Scheme 2 *Reagents and conditions*: (i) NaO_3SCF_3, PBr(*t*-Bu)$_2$, THF, 0 °C to RT; (ii) NaN(SiMe_3)$_2$, ether, 0 °C to RT; (iii) heating to 120 °C, overnight.

[a] *Laboratoire de Chimie de Coordination, Institut de Chimie (UMR 7177 CNRS), Université de Strasbourg, 4 rue Blaise Pascal, 67081 Strasbourg Cedex, France. E-mail: danopoulos@unistra.fr, braunstein@unistra.fr*
[b] *Institute for Advanced Study, USIAS, Université de Strasbourg, France*
[c] *Institut für Anorganische Chemie, RWTH Aachen University, Landoltweg 1, 52074 Aachen, Germany*

† Dedicated to Michael I. Bruce on this occasion of his 75th birthday, with our warmest congratulations.

‡ Electronic supplementary information (ESI) available: Experimental details and full characterisation of all compounds; crystal structure data for **1a**, **2a**, **Cu-1**·2CH_2Cl_2, **Ag-1**·2CH_2Cl_2, **Au-1**·2MeCN and **Cu-2** (CCDC 963084–963089); and computational details. For ESI and crystallographic data in CIF or other electronic format see DOI: 10.1039/c3cc47370h

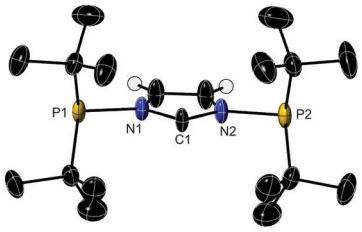

Fig. 1 Structure of **2a**. H atoms except those attached to the heterocycle are omitted. Selected bond lengths (Å) and angles [°]: C1–N1 1.3763(15); C1–N2 1.3779(14); N1–P1 1.7475(10); N2–P2 1.7531(11); N1–C1–N2 102.54(10).

anti-orientations were also found by DFT calculations at the BP86/TZ2P level to be energetically favoured (Tables S2 and S3, ESI‡). Similar conformations have been observed in other 'pincer' type NHCs[8] and mono-*N*-phosphanyl-substituted NHC ligands.[5e]

The stability of **2a** in conjunction with unsuccessful efforts to isolate or detect spectroscopically analogous NHCs with PR_2 groups where R ≠ *t*-Bu (Scheme 2 for R = Ph) prompted us to attempt to rationalize our observations by DFT methods.‡ Molecule **3a**§ with the N(C–PR_2) bond is thermodynamically more stable than **2a** with the N_{imid}–PR_2 bonds by *ca.* 90 kJ mol^{-1} (R = *t*-Bu); the same applies to R = Ph, the energy difference being 100 kJ mol^{-1}; Scheme S1, ESI.‡ In contrast, the HOMO–LUMO gaps (ΔE_{H-L}) of the N(C–PR_2) and N_{imid}–PR_2 isomers (R = *t*-Bu, Ph) are very different and follow the order for R = *t*-Bu: $\Delta E_{H-L}[N_{imid}–PR_2] = 4.05$ eV > $\Delta E_{H-L}[N(C–PR_2)] = 3.75$ eV and for R = Ph: $\Delta E_{H-L}[N_{imid}–PR_2] = 2.87$ eV < $\Delta E_{H-L}[N(C–PR_2)] = 3.53$ eV (Scheme S1, ESI‡). These results may suggest that the formation of **2a** is kinetically controlled. This is also supported by a Hirshfeld charge analysis for the R_2P^+ and (*t*-Bu)$_2$P-NHC$^-$ fragments. The charge on P in Ph_2P^+ (+0.32) is less positive than that in *t*-Bu_2P^+ (+0.36).[9] In turn, the charges on the N_{imid} and C_{NHC} sites in the anionic fragment are −0.30 and −0.19, respectively. Combining these fragments leads preferentially to **2a** and **3b**. The rearrangement from the N_{imid}–PR_2 to N(C–PR_2) bond isomer requires a higher energy barrier for R = *t*-Bu than for R = Ph. Further theoretical analyses of these and related molecules are in progress.

Complexation studies of **2a** (Scheme 3) showed that the nature of the reaction product dramatically depends on the combination of a metal precursor and the nature of the ligand source (*i.e.* imidazolium *vs.* free NHC).

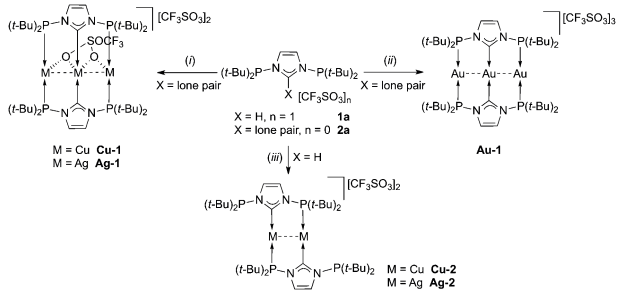

Scheme 3 Synthesis of (κ^3-$PC_{NHC}P$) trinuclear **Cu-1**, **Ag-1**, **Au-1** and (κ^2-*P*C_{NHC}P) dinuclear **Cu-2**, **Ag-2** complexes. (i) $(CuO_3SCF_3)_2$·toluene or AgO_3SCF_3, THF; (ii) $[Au(tht)_2]O_3SCF_3$, THF; (iii) $CuN(SiMe_3)_2$ or $AgN(SiMe_3)_2$, THF.

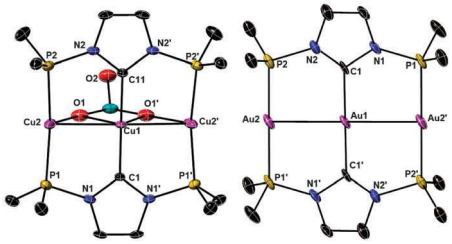

Fig. 2 Structures of the cation in **Cu-1**·2CH_2Cl_2 (left) and one, centrosymmetric cation in **Au-1**·2MeCN (right). H atoms, CF_3 group of coordinated triflate, uncoordinated triflate anions, the *t*-Bu Me groups and solvent molecules are omitted.‡ Selected bond lengths (Å) and angles [°] for **Cu-1**·2CH_2Cl_2: Cu1–C1 1.947(8), Cu1–C11 1.943(8), Cu2–P1 2.222(2), Cu2–P2 2.226(2), Cu1–Cu2 2.5761(9), Cu2–O1 2.611, Cu1–O1 2.700, C1–Cu1–C11 177.1(3), Cu2–Cu1–Cu2′ 171.81(7), P1–Cu2–P2 161.86(9). For **Au-1**·2MeCN: Au1–C1 2.068(5), Au2–P2 2.3168(14), Au2′–P1 2.3141(15), Au1–Au2 2.7584(2), P1–Au2′–P2′ 178.69(5).

All complexes were air stable as solids for short periods of time (*ca.* 1–2 h). Particularly diagnostic are: (i) the ^{31}P NMR singlet at δ 102.1 for **Cu-1**, two doublets centered at δ 119.4 for **Ag-1** ($J_{P-^{109}Ag}$ = 541.0 Hz, $J_{P-^{107}Ag}$ = 467.3 Hz) and one singlet at δ 141.0 for **Au-1**; (ii) the shift of the ^{13}C NMR signals due to C_{NHC} from δ 232.7 in **2a** to δ 194.2 (t, $^2J_{P-C}$ = 22.4 Hz) in **Cu-1**, to δ 200.3 (overlapping m, $^1J_{C-^{109}Ag}$ = 213.1 Hz, $^1J_{C-^{107}Ag}$ = 184.2 Hz) for **Ag-1**, and to δ 194.3 (t, $^2J_{P-C}$ = 14.6 Hz) for **Au-1**.

The structures of **Cu-1** and **Ag-1** (Fig. 2 left and Fig. S3, ESI‡) are very similar: the complex cation features an almost linear (171.81° and 171.41°, respectively) trinuclear metal arrangement with two bridging ligands **2a** coordinated in such a way that the internal metal is bound to two NHC donors, and the two terminal metals to two P donors from different ligands.

The terminal and internal metal centres are μ_2-bridged pairwise by two different oxygen atoms of a triply-bridging triflate. We are not aware of any other example of triflate bridging three different metals in a linear arrangement *via* two oxygen atoms. The geometry around the internal metal (not considering the M–M interactions) can be described as 'sawhorse' and that of the terminal metals as distorted 'T-shaped'. The short metal–metal distances (2.5761(9) Å for **Cu-1** and 2.7599(3) Å for **Ag-1**) imply fully-supported metallophilic d^{10}–d^{10} interactions.[6d] Discrete molecular, open (*i.e.* non-triangular), nearly linear M_3 species (M = Cu^I, Ag^I) are rare.[10] **Cu-1** and **Ag-1** constitute unique examples of linear M_3 species with NHC donors.

The structure of **Au-1** contains two different trinuclear Au_3 cations in the unit cell (Fig. 2 right),‡ one featuring strictly linear (symmetry imposed) metal arrangement and the other slightly deviating from it. There are also two bridging **2a** ligands coordinated as in the Cu and Ag analogues; however, no triflate coordination is observed. Here too, metallophilic d^{10}–d^{10} interactions are present (2.7584(2) and 2.7628(2) Å). Discrete molecular, linear Au_3 species are uncommon, fully-supported by linear triphosphines with ethylene or methylene linkers, semi-supported or unsupported.[10d,11] Amongst these examples, **Au-1** shows the shortest Au–Au distances.

Further insight into the coordination chemistry of **2a** was obtained by attempts to form dinuclear complexes (Scheme 3).

For references, see P24

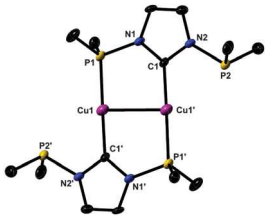

Fig. 3 Structure of the cation in **Cu-2**. Hydrogen atoms, the *t*-Bu Me groups and triflate anions are omitted. Selected bond lengths (Å) and angles [°]: P1–Cu1 2.1936(13); Cu1–C1′ 1.923(4); Cu1–Cu1′ 2.6827(12); C1–Cu1′–P1′ 177.81(13); C1–Cu1′–Cu1 86.81(12); P1–Cu1–Cu1′ 92.93(4).

Particularly revealing is the reaction of **1a** with $CuN(SiMe_3)_2$ (in a 1 : 1 ratio in THF), which led cleanly to the new dinuclear complex **Cu-2**. This molecule (Fig. 3) features a dinuclear complex with the $[Cu_2(\mathbf{2a})_2]$ core,‡ with each metal exhibiting an identical coordination sphere comprising one NHC and one P donor in an almost linear *trans*-arrangement; the second P donor remains dangling. This behaviour is analogous to that of bidentate ligands recently reported,[5c,g] where NHC coordination and dangling P donors have also been observed. Interestingly, the orientation of the lone pairs of the dangling P donors in **Cu-2**, as judged from the observed conformation in the crystal, is towards the metal. The NHC rings and the coordinated Cu centres are coplanar. The internuclear distance [2.6827(12) Å] is longer than that in the trinuclear **Cu-1**. The Cu–C_{NHC} or Cu–P bond lengths in **Cu-2** are shorter compared to those in **Cu-1**. The solution structure of **Cu-2** at room temperature cannot be deduced with certainty due to the broad NMR resonances. Thus, the ^{31}P-NMR spectrum shows one broad peak at δ 94.5; broad features are also observed for the *t*-Bu groups in ^{1}H NMR and ^{13}C NMR spectra implying nonrigidity in solution which could originate from intermolecular ligand exchange or partial dissociation of the P donors followed by rotation around the Cu–C_{NHC} bond; this will be addressed in future studies.

Similarly, **Ag-2**, tentatively formulated as a related dinuclear species, was obtained from **1a** and a solution of $AgN(SiMe_3)_2$ generated *in situ*. The ^{31}P-NMR spectrum showed two broad multiplets, also observed in the reaction of **1a** with Ag_2O in CH_2Cl_2. However, after attempting crystallisation in CH_2Cl_2 the product was converted to **Ag-1**. Understanding the details of this process is under study.

In conclusion, we have prepared a novel stable and rigid tridentate diphosphanylated-imidazol-2-ylidene and gained experimental and computational information on its stability. It serves as a unique platform for the synthesis of novel complexes with the coinage metals, exhibiting rare structural features. Dinuclear complexes with this tridentate ligand have also been isolated and exhibit one dangling P-donor. We are currently investigating their potential as precursors towards trinuclear species. Preliminary data show that **Au-1** is luminescent under sunlight or UV-light in acetonitrile solution. The study of further aspects of the donor properties, stability and the versatile coordination chemistry of phosphorylated-imidazol-2-ylidenes is in progress in our laboratory.

A.A.D. thanks the CNRS, the Région Alsace, the Département du Bas-Rhin and the Communauté Urbaine de Strasbourg for a Gutenberg Excellence Chair (2010–2011). K.Y.M. is grateful to the DFG for a postdoctoral reintegration fellowship. We thank the CNRS, the MESR (Paris), the UdS, China Scholarship Council, and the ucFRC (www.icfrc.fr) for financial support and the Service de Radiocristallographie (Institut de Chimie, Strasbourg) for the determination of the crystal structures.

Notes and references

§ This molecule has been obtained in a direct way: see M. Brill, L. Weigel, K. Rübenacker, F. Rominger and P. Hofmann, *Heidelberg Forum of Molecular Catalysis*, 28 June 2013, poster P60.

1 (*a*) M. Scholl, S. Ding, C. W. Lee and R. H. Grubbs, *Org. Lett.*, 1999, **1**, 953; (*b*) G. D. Frey, J. Schütz, E. Herdtweck and W. A. Herrmann, *Organometallics*, 2005, **24**, 4416; (*c*) T. E. Schmid, D. C. Jones, O. Songis, O. Diebolt, M. R. L. Furst, A. M. Z. Slawin and C. S. J. Cazin, *Dalton Trans.*, 2013, **42**, 7345.
2 K. Albert, P. Gisdakis and N. Rösch, *Organometallics*, 1998, **17**, 1608.
3 (*a*) W. A. Herrmann, C. Köcher, L. J. Goußen and G. R. J. Artus, *Chem.–Eur. J.*, 1996, **2**, 1627; (*b*) A. A. Danopoulos, S. Winston, T. Gelbrich, M. B. Hursthouse and R. P. Tooze, *Chem. Commun.*, 2002, 482; (*c*) X. Liu and P. Braunstein, *Inorg. Chem.*, 2013, **52**, 7367 and references therein.
4 (*a*) O. Kühl, *Functionalised N-Heterocyclic Carbene Complexes*, Wiley, Weinheim, 2010; (*b*) P. G. Edwards and F. E. Hahn, *Dalton Trans.*, 2011, **40**, 10278; (*c*) S. Gaillard and J.-L. Renaud, *Dalton Trans.*, 2013, **42**, 7255 and references therein.
5 (*a*) A. P. Marchenko, H. N. Koidan, A. N. Huryeva, E. V. Zarudnitskii, A. A. Yurchenko and A. N. Kostyuk, *J. Org. Chem.*, 2010, **75**, 7141; (*b*) A. P. Marchenko, H. N. Koidan, I. I. Pervak, A. N. Huryeva, E. V. Zarudnitskii, A. A. Tolmachev and A. N. Kostyuk, *Tetrahedron Lett.*, 2012, **53**, 494; (*c*) E. Kühnel, I. V. Shishkov, F. Rominger, T. Oeser and P. Hofmann, *Organometallics*, 2012, **31**, 8000; (*d*) A. P. Marchenko, H. N. Koidan, E. V. Zarudnitskii, A. N. Hurieva, A. A. Kirilchuk, A. A. Yurchenko, A. Biffis and A. N. Kostyuk, *Organometallics*, 2012, **31**, 8257; (*e*) P. Nägele, U. Herrlich, F. Rominger and P. Hofmann, *Organometallics*, 2012, **32**, 181; (*f*) H. Salem, M. Schmitt, U. Herrlich, E. Kühnel, M. Brill, P. Nägele, A. L. Bogado, F. Rominger and P. Hofmann, *Organometallics*, 2013, **32**, 29; (*g*) A. P. Marchenko, H. N. Koidan, A. N. Hurieva, O. V. Gutov, A. N. Kostyuk, C. Tubaro, S. Lollo, A. Lanza, F. Nestola and A. Biffis, *Organometallics*, 2013, **32**, 718.
6 (*a*) J. C. Garrison and W. J. Youngs, *Chem. Rev.*, 2005, **105**, 3978; (*b*) J. C. Y. Lin, R. T. W. Huang, C. S. Lee, A. Bhattacharyya, W. S. Hwang and I. J. B. Lin, *Chem. Rev.*, 2009, **109**, 3561; (*c*) S. Sculfort and P. Braunstein, *Chem. Soc. Rev.*, 2011, **40**, 2741; (*d*) H. Schmidbaur and A. Schier, *Chem. Soc. Rev.*, 2012, **41**, 370; (*e*) R. Visbal, I. Ospino, J. M. López-de-Luzuriaga, A. Laguna and M. C. Gimeno, *J. Am. Chem. Soc.*, 2013, **135**, 4712 and references therein.
7 P. L. Chiu and H. M. Lee, *Organometallics*, 2005, **24**, 1692.
8 A. A. Danopoulos, S. Winston and W. B. Motherwell, *Chem. Commun.*, 2002, 1376.
9 J. M. Slattery and S. Hussein, *Dalton Trans.*, 2012, **41**, 1808.
10 (*a*) J. Beck and J. Strähle, *Angew. Chem., Int. Ed. Engl.*, 1985, **24**, 409; (*b*) X. He, K. Ruhlandt-Senge, P. P. Power and S. H. Bertz, *J. Am. Chem. Soc.*, 1994, **116**, 6963; (*c*) Y. Takemura, T. Nakajima, T. Tanase, M. Usuki, H. Takenaka, E. Goto and M. Mikuriya, *Chem. Commun.*, 2009, 1664; (*d*) G. S. M. Tong, S. C. F. Kui, H.-Y. Chao, N. Zhu and C.-M. Che, *Chem.–Eur. J.*, 2009, **15**, 10777; (*e*) V. T. Yilmaz, E. Soyer and O. Büyükgüngör, *Polyhedron*, 2010, **29**, 920.
11 (*a*) W. Schuh, H. Kopacka, K. Wurst and P. Peringer, *Chem. Commun.*, 2001, 2186; (*b*) S. D. Hanna, S. I. Khan and J. I. Zink, *Inorg. Chem.*, 1996, **35**, 5813; (*c*) S. J. Hsu, K. M. Hsu, M. K. Leong and I. J. B. Lin, *Dalton Trans.*, 2008, 1924.

Annex

Unpublished results

The trinuclear complex **Cu-1'** with three PF_6^- anions, analoguous to **Cu-1**, was also prepared by the reaction of the NHC ligand **2a** with $[Cu(CH_3CN)_4]PF_6$. It is not stable in MeCN and decomposes after one day by losing one of the phospine groups and protonation of its carbene function by MeCN gave a polymer **Poly-Cu** (eq 1), as established by crystallography (Figure S1). The cation in **Poly-Cu** shows a zigzag conformation (Figure S2) and the Cu atom is coordinated by one phosphine group, two acetonitrile ligands and one neutral N atom from the other imidazole ring, leading to a tetrahedral coordination geometry (Figure S1).

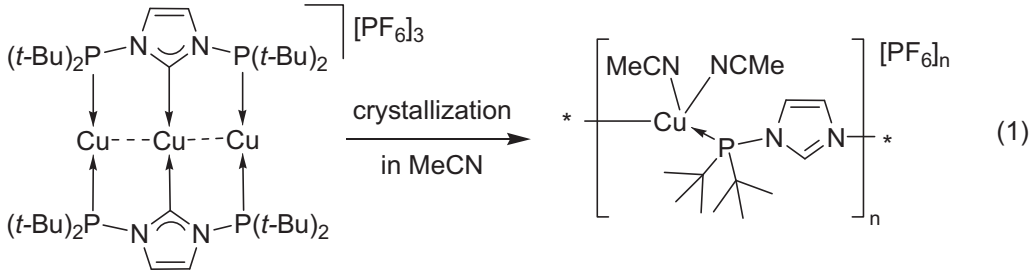

(1)

Cu-1' **Poly-Cu**

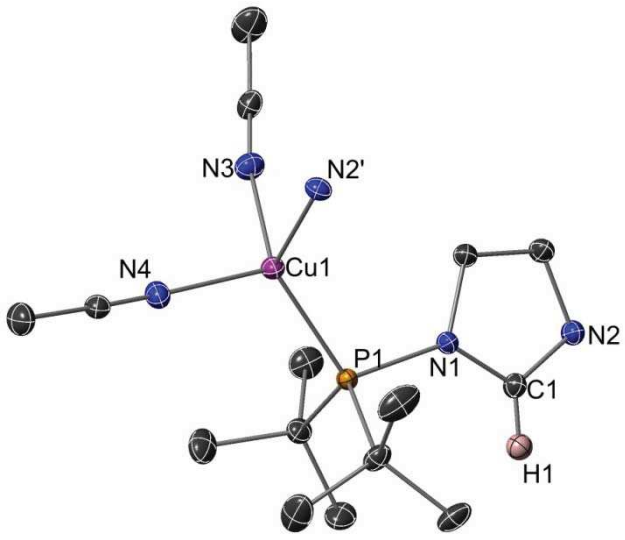

Figure S1. Thermal ellipsoid representation (30% probability level) of one repeat

For references, see P24

cation unit in **Poly-Cu**. H atoms (except H1 on C1 atom) and one PF_6 anion are omitted for clarity. Selected bond lengths (Å) and angles [°]: Cu1-N2' 2.078(2), Cu1-N3 2.063(2), Cu1-N4 2.021(2), Cu1-P1 2.2157(5), C1-N2 1.310(3), C1-N1 1.364(2), N1-P1 1.762(2); N2'-Cu1-P1 122.91(5), N3-Cu1-N2' 93.98(7), N3-Cu1-P1 117.19(5), N4-Cu1-N3 105.55(8), N4-Cu1-N2' 96.27(7), N4-Cu1-P1 116.78(5), Cu1-P1-N1 109.50(5).

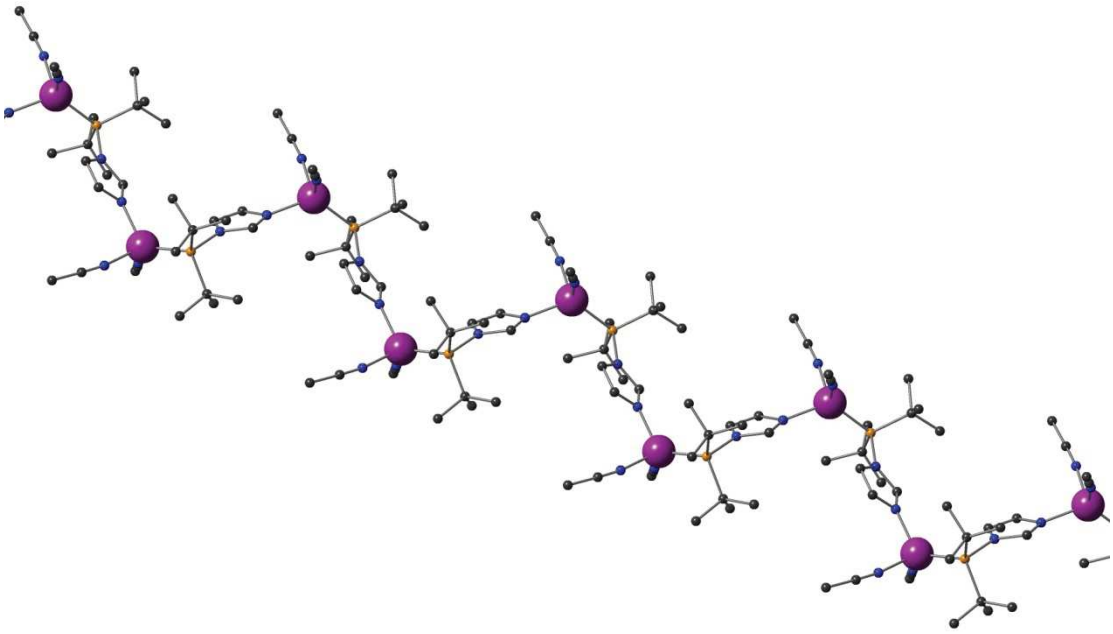

Figure S2. The zigzag conformation of the cations of **Poly-Cu**. All the hydrogen atoms have been omitted for clarity. The Cu atoms are in purple, P in orange and N in blue.

Experimental section:

1.1 Synthesis of **Cu-1'**.

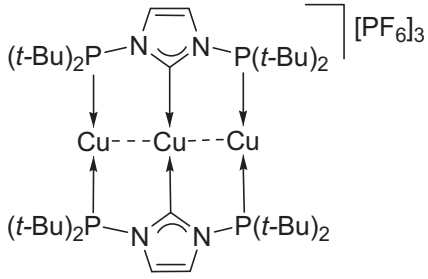

The preparation of **Cu-1'** is similar to that of **Cu-1**: $[Cu(CH_3CN)_4]PF_6$ was reacted with the corresponding free carbene **2a** in THF (5 ml) at -10 °C. It is not soluble in CH_2Cl_2. For **Cu-2**: ^{1}H NMR (400 MHz, CD_3CN): δ 7.73 (s, 4H, im-*H*), 1.33 (d, 72H, *J* = 14.4 Hz, C(CH_3)$_3$). $^{13}C\{^1H\}$ NMR (125 MHz, CD_3CN): δ 126.7 (im-*C*), 36.3 (d,

For references, see P24

$^{1}J_{CP}$ = 9.6 Hz, *C*$(CH_3)_3$), 28.7 (d, $^{2}J_{CP}$ = 11.7 Hz, C(*C*$H_3)_3$), the carbene carbon is not detected. $^{31}P\{^{1}H\}$ NMR (161 MHz, CD_3CN): δ 103.1 (s, P(*t*-Bu)$_2$), 144.6 (sept, $^{1}J_{PF}$ = 706.1 Hz, PF_6).

1.2 Synthesis of **Poly-Cu**.

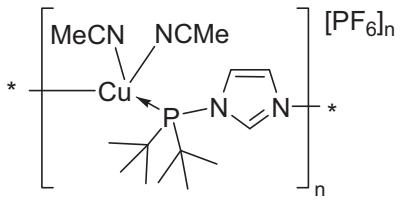

Cu-1' is not stable in MeCN and decomposes after one day. Diffusion of ether into a MeCN solution of **Cu-1'** led to the formation of X-ray quality crystals (colorless) for **Poly-Cu**. For **Poly-Cu**: ^{1}H NMR (400 MHz, CD_3CN): δ 7.96 (br, 1H, im-*H2*), 7.50 (s, 1H, im-*H4/5*), 7.20 (s, 1H, im-*H4/5*), 1.23 (d, 72H, *J* = 14.8 Hz, C(C*H*$_3)_3$). $^{31}P\{^{1}H\}$ NMR (161 MHz, CD_3CN): δ 90.4 (br, P(*t*-Bu)$_2$), 144.6 (sept, $^{1}J_{PF}$ = 706.1 Hz, PF_6).

Table S1. Crystal data for **Poly-Cu.**

	Poly-Cu		**Poly-Cu**
Chemical formula	$C_{15}H_{27}CuF_6N_4P_2$	Space group	*P 21/c*
Formula Mass	502.88	Formula units / cell, *Z*	4
Crystal system	Monoclinic	Absorption coefficient, μ/mm^{-1}	1.200
a/Å	13.6567(6)	No. of reflections measured	17110
b/Å	11.4684(5)	No. of independent reflections	5834
c/Å	15.8637(6)	R_{int}	0.0428
α/°	90	Final R_1 values ($I > 2\sigma(I)$)	0.0359
β/°	118.105(3)	Final $wR(F^2)$ values ($I > 2\sigma(I)$)	0.0760
γ/°	90	Final R_1 values (all data)	0.0620
Unit cell volume/Å^3	2191.61(17)	Final $wR(F^2)$ values (all data)	0.0814
Temperature/K	173(2)	Goodness of fit on F^2	0.956

For references, see P24

Chapter 2

Aurophilicity-Triggered Assembly of Novel Cyclic Penta- and Hexa-nuclear Au(I) Complexes with Rigid Anionic NHC-Type Ligands

This chapter is written in the form of a publication. This article was published in *Inorganic Chemistry* **2015**, 54, 3722-3724 (cover article).

My contribution in this work included the synthesis of the complexes, their characterization and the preparation of the draft of the publication.

Aurophilicity-Triggered Assembly of Novel Cyclic Penta- and Hexa-nuclear Au(I) Complexes with Rigid Anionic NHC-Type Ligands

Pengfei Ai,[a] Andreas A. Danopoulos,*[a,b] Pierre Braunstein*[a]

[a] Laboratoire de Chimie de Coordination, Institut de Chimie (UMR 7177 CNRS), Université de Strasbourg, 4 rue Blaise Pascal, 67081 Strasbourg Cedex (France). E-mail: danopoulos@unistra.fr, braunstein@unistra.fr

[b] Institute for Advanced Study (USIAS), Université de Strasbourg, 4 rue Blaise Pascal, 67081 Strasbourg Cedex (France)

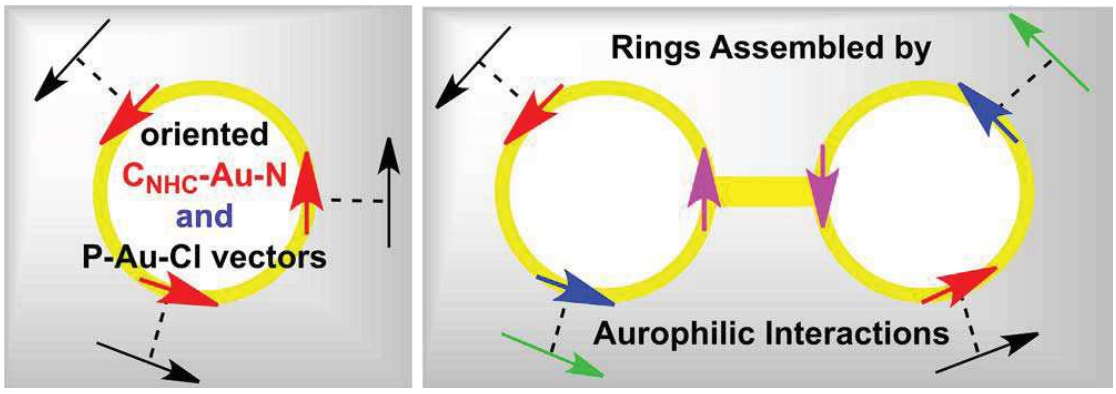

Supporting information for this chapter is available on the internet under http://pubs.acs.org/doi/suppl/10.1021/acs.inorgchem.5b00276

For references, see P34

Résumé du Chapitre 2

La nature des produits de réaction entre *N,N'*-diphosphanyl-imidazol-2-ylidene (**P-C-P**) et les complexes précurseurs d'Au(I) dépend de la nature des anions associés. Contrairement à la réaction observée avec [Au(tht)$_2$(*OTf)*] (voir Chapitre 1), l'utilisation de [Au*Cl*(tht)] a conduit à la rupture d'une liaison P-N pour donner le nouveau complexe hexanucléaire **1** (Schéma 1), qui possède un squelette $Au_6(\mu_3$-**P-C**,κ*C*,κ*N*,κ*P*$)_3$.

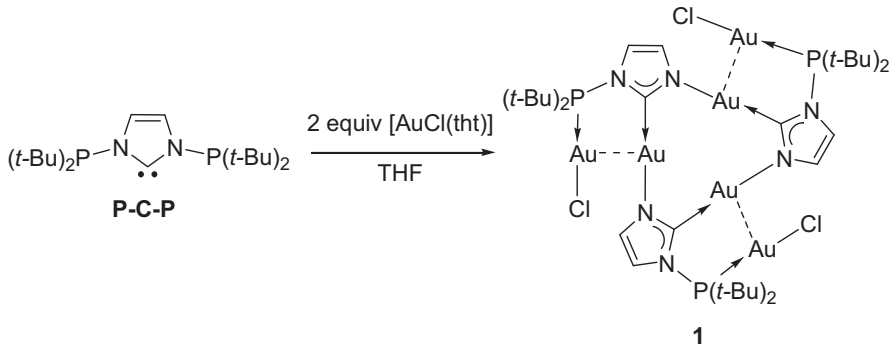

Schéma 1

Un accès plus directe à ce complexe fut tenté au départ de l'imidazolidure de lithium **P-C-Li**, obtenu par déprotonation 1-(di-*t*-butylphosphanyl)imidazole. La réaction effectuée en partant du sel isolé **P-C-Li** et de [AuCl(tht)] a produit **1** (Schéma 2), ainsi qu'un sel inattendu et très original de formule $[Au_5Cl(\mu_3$-**P-C**-κ*P*,κ*C*,κ*N*$)_3]_2[AuCl_2]_2$ (**2**) qui renferme des sous-unités $[Au_5(\mu_3$-**P-C**-κ*P*,κ*C*,κ*N*$)]^+$.

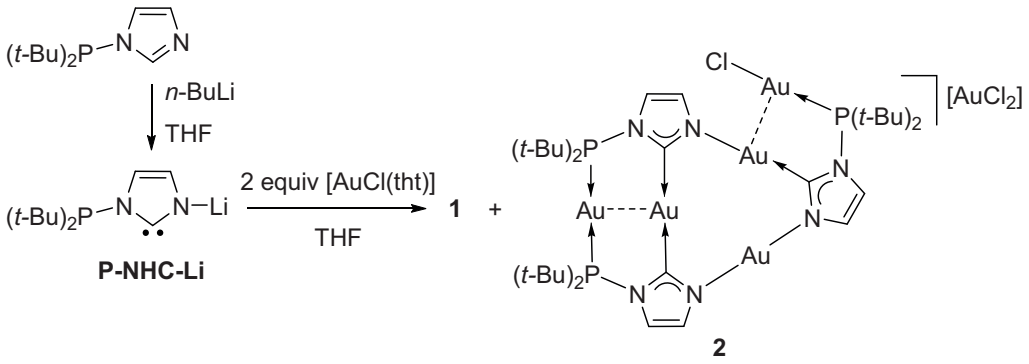

Schéma 2

For references, see P34

Inorganic Chemistry
including bioinorganic chemistry
April 20, 2015
Volume 54, Number 8
pubs.acs.org/IC

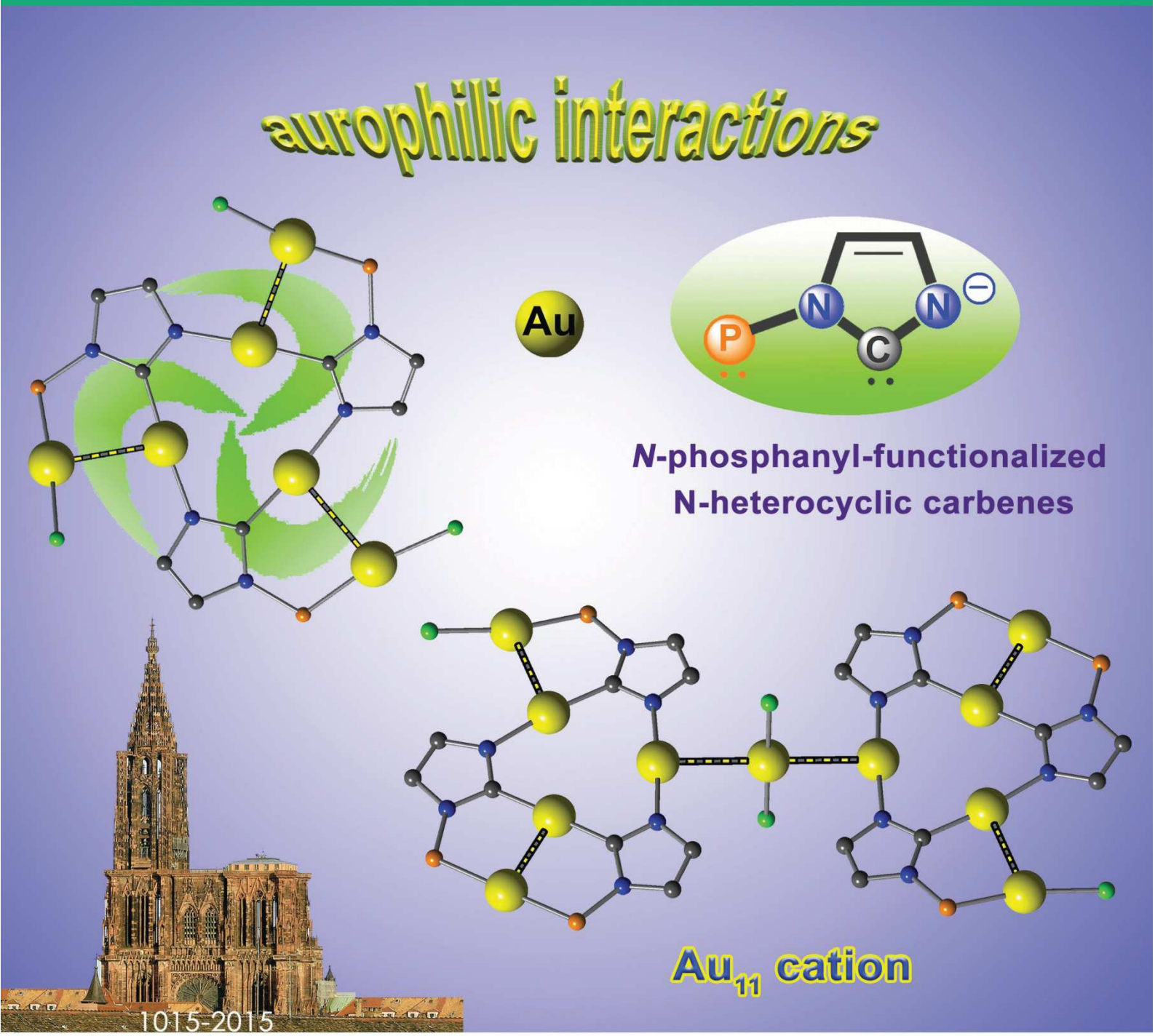

ACS Publications
Most Trusted. Most Cited. Most Read.
www.acs.org

For references, see P34

Inorganic Chemistry

Communication

pubs.acs.org/IC

Aurophilicity-Triggered Assembly of Novel Cyclic Penta- and Hexanuclear Gold(I) Complexes with Rigid Anionic NHC-Type Ligands

Pengfei Ai,[†] Andreas A. Danopoulos,*[,†,‡] and Pierre Braunstein*[,†]

[†]Laboratoire de Chimie de Coordination, Institut de Chimie (UMR 7177 CNRS), and [‡]Institute for Advanced Study (USIAS), Université de Strasbourg, 4 rue Blaise Pascal, 67081 Strasbourg Cedex, France

Supporting Information

ABSTRACT: The products of the reaction between *N*,*N*′-diphosphanylimidazol-2-ylidene (**P−C−P**) and gold(I) precursors depend on the nature of the anions associated with the latter. In contrast to the reported reaction with $[Au(tht)_2(OTf)]$, the use of [AuCl(tht)] led to the new hexanuclear complex **1**, which features a $Au_6(\mu_3\text{-}\mathbf{P{-}C},\kappa C,\kappa N,\kappa P)_3$ skeleton. The reaction of lithium imidazolide (**P−C−Li**) and [AuCl(tht)] also afforded **1**, together with an unusual salt of the general formula $[Au_5Cl(\mu_3\text{-}\mathbf{P{-}C}\text{-}\kappa P,\kappa C,\kappa N)_3]_2[AuCl_2]_2$ (**2**), which contains $[Au_5(\mu_3\text{-}\mathbf{P{-}C}\text{-}\kappa P,\kappa C,\kappa N)]^+$ subunits. In the solid state, one of these Au_5 cations is associated with an $[AuCl_2]^-$ anion, while two other cations interact through their unique dicoordinated N−Au−N center with a $[AuCl_2]^-$ anion, with the charge of the resulting monocation being compensated for by another $[AuCl_2]^-$ anion to give a Au_{12} salt. Remarkably, the latter displays seven different bonding types at Au^I: C−Au−C, N−Au−N, P−Au−P, Cl−Au−Cl, C−Au−N, P−Au−Cl, and Au···Au.

Since the first report in 1970 of the cyclic trigold(I) $[Au(\mu\text{-}N^1,C^2\text{-pyridyl})]_3$,[1] similar complexes have attracted considerable attention owing to their fascinating structures and relevance to supramolecular chemistry, metallophilic interactions, and optoelectronic properties.[2] This family of complexes possesses a planar, nine-membered ring with alternating Au^I centers and bidentate C,N- or N,N-bound monoanionic ligands. In the solid state, they can assemble into 1D stacks, with or without the incorporation of electrophiles.[2c,g,i,3] The only example of a cyclic trigold(I) complex bearing N-heterocyclic carbene (NHC) ligands, $[Au(\mu\text{-}C^2,N^3\text{-benzylimidazolide})]_3$,[4] has a high π basicity,[2f] and it can sandwich Tl^+ and Ag^+ ions[3a,b] or interact with $[Hg_3(\mu\text{-}C_6F_4)_3]$, TCNQ, C_6F_6, and F_8-naphthalene to produce supramolecular structures with interesting luminescence properties.[2c,e,g,3c,d]

Recently, bulky *N*-phosphanyl-functionalized NHC ligands have been reported by us and others.[5] They feature two or more different coordination sites (C_{NHC} and one or two P-donor functionalities) and support polynuclear complexes with promising applications.[2j,5b,c] In particular, *N*,*N*′-diphosphanylimidazol-2-ylidene (**P−C−P**) led to the remarkable linear trinuclear complex $[Au_3\{\mu_3\text{-}\kappa^3(\mathbf{P{-}C{-}P})\}_2][OTf]_3$ (**A**), which contains a very short Au···Au interaction [2.7584(2) Å]. Related P,C,P-donor ligands with a flexible ethylene spacer between the P and C donors have very recently been used to support gold complexes but with longer intermetallic distances.[6]

We have now found that the outcome of the reaction of **P−C−P** with gold(I) precursors dramatically depends on the nature of their associated anion. Thus, the reaction of **P−C−P** with [AuCl(tht)] (tht = tetrahydothiophene) in tetrahydrofuran (THF) at −78 °C led to a novel cyclic hexanuclear gold(I) complex, $[Au_2Cl(\mu_3\text{-}\mathbf{P{-}C}\text{-}\kappa P,\kappa C,\kappa N)]_3$ (**1**; eq 1 and Figure 1)

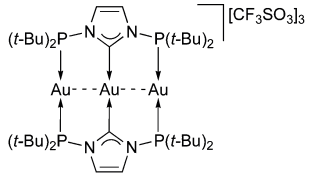

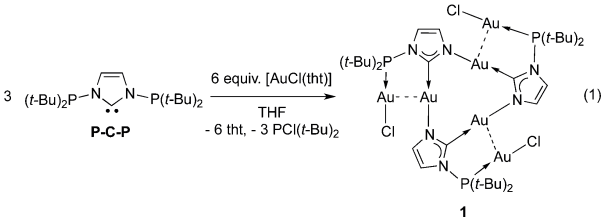

after cleavage of one $t\text{-}Bu_2P{-}N_{imid}$ bond of **P−C−P**. The formation of $PCl(t\text{-}Bu)_2$ was evidenced in the reaction mixture as the only other P-containing product (δ 145 in $^{31}P\{^1H\}$ NMR).

Complex **1** exhibits a cyclic structure of approximate C_3 symmetry characterized by an internal nine-membered planar ring (maximum deviation 0.109 Å for the N2 atom) formed by the assembly through N−Au bonds of three identical "modules" comprising one anionic **P−C** ligand bridging two Au atoms. The Au atoms within the internal ring form an almost equilateral triangle, in which the metal−metal separations (ave 3.491 Å) are too long to represent bonding interactions, although there is a slight inward bending of the N−Au−C angles [173.9(5)−176.7(5)°]. The Au−N and Au−C distances are in the ranges 2.048(11)−2.056(11) and 1.974(13)−2.009(13) Å, respectively. Each $P(t\text{-}Bu)_2$ donor is coordinated to one Au−Cl moiety, which flanks the internal nine-membered ring (aver. P−Au−Cl 170.6°). All six Au^I centers are almost coplanar (max. deviation 0.397 Å for

Received: February 4, 2015
Published: March 9, 2015

For references, see P34

DOI: 10.1021/acs.inorgchem.5b00276
Inorg. Chem. 2015, 54, 3722−3724

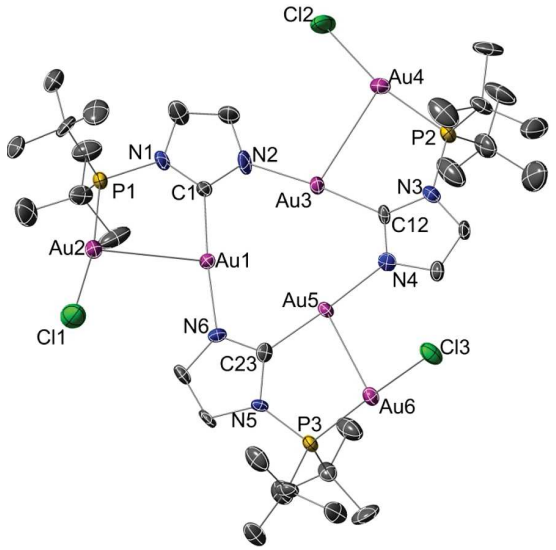

Figure 1. Structure of **1** in **1**·THF. One molecule of THF and H atoms are omitted for clarity. Selected bond distances (Å) and angles [deg]: Au1−C1 2.009(13), Au1−N6 2.048(11), Au3−C12 2.002(12), Au3−N2 2.056(12), Au5−C23 1.974(13), Au5−N4 2.056(11), Au2−P1 2.238(4), Au2−Cl1 2.284(4), Au4−P2 2.239(4), Au4−Cl2 2.294(5), Au6−P3 2.240(3), Au6−Cl3 2.300(4), Au1···Au2 3.0659(7), Au3···Au4 3.1300(8), Au5···Au6 3.0430(7); C1−Au1−N6 174.7(5), C12−Au3−N2 173.9(5), C23−Au5−N4 176.7(5), P1−Au2−Cl1 170.7(1), P2−Au4−Cl2 168.4(2), P3−Au6−Cl3 172.7(1).

Au1), as a result of aurophilic interactions between the "internal" and "external" Au^{I} centers (aver. Au···Au = 3.080 Å).[7] No intermolecular Au···Au contacts were observed (the closest intermolecular Au···Au distance is 6.258 Å).

Although details of the formation of **1** are not yet clear, it is plausible that the chloride ligand displaced from [AuCl(tht)] acted as a nucleophile toward the uncoordinated P−N bond of a partially (i.e. via one P and/or C) coordinated **P−C−P** ligand (neither the free **P−C−P** ligand nor **A** is degraded by chloride ions) and led to the formation of PCl(*t*-Bu)$_2$ and Au{**P−C**}$^-$ moieties, with the latter assembling to give **1**. We thus envisaged a more direct access to **1** from lithium imidazolide (**P−C−Li**), preformed by the deprotonation of 1-(di-*tert*-butylphosphanyl)-imidazole with *n*-BuLi (see the Supporting Information, SI).

Interestingly, the reaction of preisolated **P−C−Li** with [AuCl(tht)] in THF indeed afforded **1**, but a new gold complex, **2**, was also obtained (Scheme 1) in a ca. 1:1 ratio (from ^{31}P NMR spectra). Pure **2** was obtained by repeated washing of the precipitate obtained from the reaction mixture with THF, in which **2** is much less soluble than **1**. As solids, **1** and **2** are air-stable for several hours but are better stored under an inert atmosphere. Reactions of [AuCl(tht)] with a mixture of 1-(di-*tert*-butylphosphanyl)imidazole and *n*-BuLi in THF failed because of the competing reduction of [AuCl(tht)] by *n*-BuLi.

Scheme 1. Synthesis of 1 and 2

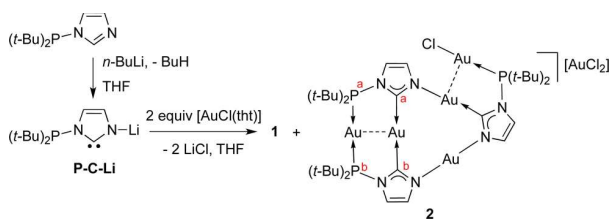

In the solid state, the structure of **2**·CH_2Cl_2 can be described as containing, first, one pentanuclear cation of the formula [Au_5(μ_3-**P−C**-$\kappa P,\kappa C,\kappa N$)]$^+$ (Figure 2), the positive charge of which

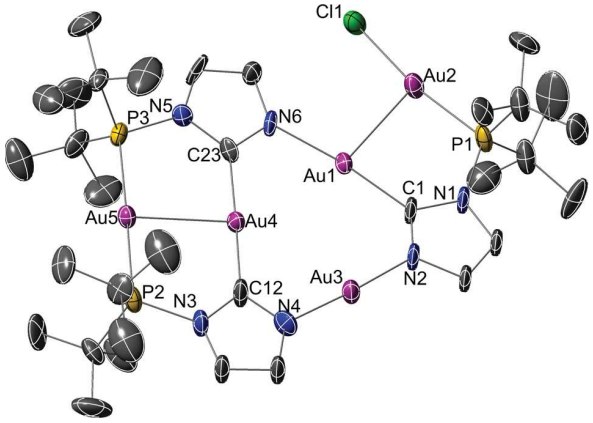

Figure 2. Structure of one of the pentanuclear cations present in the asymmetric unit of **2**·CH_2Cl_2. Selected bond distances (Å) and angles [deg]: Au1−C1 2.01(1), Au1−N6 2.044(11), Au3−N2 2.001(11), Au2−P1 2.232(4), Au3−N4 2.01(1), Au4−C12 2.00(1), Au4−C23 2.03(1), Au5−P2 2.305(4), Au5−P3 2.314(4), Au1···Au2 3.0846(8), Au4···Au5 2.7523(7). In the other pentanuclear cation present in the asymmetric unit of **2**·CH_2Cl_2, a contact is established between the unique N−Au−N atom and one of the [$AuCl_2$]$^-$ anions (Scheme 2).

(formally associated with the P → Au ← P unit) is compensated for by a [$AuCl_2$]$^-$ anion, and second, a centrosymmetric Au_{11} monocation, balanced by another [$AuCl_2$]$^-$ anion. The Au_{11} monocation comprises two pentanuclear cations connected through their unique dicoordinated N−Au−N center to the Au atom of one linear [$AuCl_2$]$^-$ anion. The latter Au atom occupies a center of symmetry (Scheme 2 and Figure S1 in the SI). Overall,

Scheme 2. Representation of 2 in 2·CH_2Cl_2 Containing Two [Au_5(μ_3-P−C-$\kappa P,\kappa C,\kappa N$)]$^+$ Cations That Establish d^{10}−d^{10} Interactions with a Central [$AuCl_2$]$^-$ Anion [Au8···Au11 = 3.0863(5) Å; Au11 Occupies a Center of Symmetry]

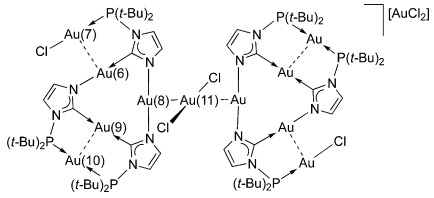

this gives for **2** a formulation corresponding to [Au_5Cl(μ_3-**P−C**-$\kappa P,\kappa C,\kappa N$)$_3$]$_2$[$AuCl_2$]$_2$. The metrical data within the Au_5 units are almost identical. The Au8···Au11 distance of 3.0863(5) Å is consistent with aurophilic interactions.[7] Like in **1**, in each pentanuclear unit, there are three $N_{imidazolide}$−Au bonds. Whereas the internal Au^{I} centers in **1** were all in the same coordination environment (with three C−Au−N vectors forming a topologically oriented nine-membered ring), the different assembling orientations of the bridging ligand in **2** result in three different environments for the Au^{I} centers: C−Au−C, N−Au−N, and C−Au−N. The Au−Cl distances in the two types of [$AuCl_2$]$^-$ anions present (ave. 2.248 Å) are very similar to that in [*n*-

DOI: 10.1021/acs.inorgchem.5b00276
Inorg. Chem. 2015, 54, 3722−3724

$Bu_4N][AuCl_2]$ [2.257(4) Å].[8] The Au8−Au11−Cl plane makes an angle of 75.63° with the Au6−Au8−Au9 plane.

Although the alternating assembly of mononuclear cationic and anionic gold(I) complexes resulting from electrostatic interactions is well-known,[7a,d] we are not aware of literature precedents for the arrangements displayed by **2**.

It is worth noting that **1** and **2** are actually formula isomers, but whereas in **1** there are only two types of gold(I) coordination environments (neglecting the aurophilic interactions), i.e., P−Au−Cl and C−Au−N, six different types are present in **2**: C−Au−C, N−Au−N, P−Au−P, Cl−Au−Cl, C−Au−N, and P−Au−Cl. This remarkable diversity within the same complex appears unprecedented. The shorter Au···Au distances in **2** are associated with the $\kappa C,\kappa N,\kappa P$ bonding mode of the μ_3-**P−C** ligand [2.7523(7) and 2.7608(7) Å for Au4···Au5 and Au9···Au10, respectively] and are similar to those observed in the linear trinuclear gold complex **A** [2.7584(2) Å].[5c] However, these short distances cannot be solely ascribed to the short-bite effect of the ligand because the longer Au1···Au2 and Au6···Au7 separations [3.0846(8) and 3.0863(5) Å, respectively] are also spanned by this ligand in the same bridging mode. The latter values are similar to those for the "peripheral" Au···Au interactions in **1**.

Preliminary experiments have not led to the observation of any remarkable photophysical properties for **1** and **2**, despite the presence of numerous Au···Au interactions. This is probably related to the presence of bulky *t*-Bu groups on the P atoms that prevent the establishment of closer intermolecular contacts.

The Au_6 and Au_5 cores found in **1** and **2**, respectively, are retained in solution, as evidenced by NMR spectroscopy. Particularly diagnostic in this respect are (i) the $^{31}P\{^1H\}$ NMR singlet at δ 111 for **1**, in contrast to the AB pattern (δ 126.5, 124.8; $^2J_{AB}$ = 289.5 Hz) for the two trans atoms P_a and P_b (the AB pattern originating from the lack of any symmetry element relating these two nuclei) and a singlet at δ 115.1 in **2** and (ii) the equivalence of all three C_{NHC} atoms in **1**, which gives rise to a doublet at δ 178.6 (d, $^2J_{CP}$ = 30.5 Hz), whereas in **2**, the C_{NHC} atoms C_a and C_b appear as dd at δ 193.8 (dd, $^2J_{CP}$ = 25.9 Hz, $^4J_{CP}$ = 2.7 Hz) and 192.1 (dd, $^2J_{CP}$ = 25.4 Hz, $^4J_{CP}$ = 2.3 Hz), and the C_{NHC} atom trans to N appears at δ 179.0 (d, $^2J_{CP}$ = 30.9 Hz), a value very similar to the corresponding one in **1**.

In conclusion, the nucleophilic Cl^- liberated from the precursor [AuCl(tht)] is thought to be responsible for the change of the reaction course of the **P−C−P** ligand with [AuCl(tht)] compared to $[Au(tht)_2(OTf)]$. While the rational synthesis of **1** based on the use of the isolated **P−C−Li** as a ligand source was successful, it also afforded the unusual Au_{12} complex **2**, which exhibits seven different types of coordination environments for Au^I. Significant energetic contributions responsible for the assembly of these remarkable complexes are thought to involve aurophilic interactions.

■ ASSOCIATED CONTENT

Supporting Information

Experimental details, NMR data, and crystal data for **1** and **2**. This material is available free of charge via the Internet at http://pubs.acs.org. CIF files have been deposited with the CCDC, 12 Union Road, Cambridge CB2 1EZ, U.K., and can be obtained upon request free of charge by quoting the publication citation and deposition numbers 1046767 and 1046768.

■ AUTHOR INFORMATION

Corresponding Authors

*E-mail: danopoulos@unistra.fr.

*E-mail: braunstein@unistra.fr.

Notes

The authors declare no competing financial interest.

■ ACKNOWLEDGMENTS

The USIAS, CNRS, Région Alsace, and Communauté Urbaine de Strasbourg are acknowledged for the award of fellowships and a Gutenberg Excellence Chair (2010−2011) to A.A.D. We thank the CNRS and MESR (Paris) for funding and the Service de Radiocrystallographie (UdS) for determination of the crystal structures. We thank Dr. M. Mauro (ISIS) for preliminary photophysical measurements. We are grateful to the China Scholarship Council for a Ph.D. grant to P.A. and to Johnson Matthey PLC for a generous loan of gold precursors.

■ DEDICATION

Dedicated to Prof. H. Schmidbaur on the occasion of his 80th birthday (December 31, 2014), with our warmest congratulations.

■ REFERENCES

(1) Vaughan, L. G. *J. Am. Chem. Soc.* **1970**, *92*, 730−731.

(2) (a) Minghetti, G.; Bonati, F. *Angew. Chem., Int. Ed. Engl.* **1972**, *11*, 429−429. (b) Olmstead, M. M.; Jiang, F.; Attar, S.; Balch, A. L. *J. Am. Chem. Soc.* **2001**, *123*, 3260−3267. (c) Fackler, J. P., Jr. *Inorg. Chem.* **2002**, *41*, 6959−6972. (d) Burini, A.; Mohamed, A. A.; Fackler, J. P., Jr. *Comments Inorg. Chem.* **2003**, *24*, 253−280. (e) Omary, M. A.; Mohamed, A. A.; Rawashdeh-Omary, M. A.; Fackler, J. P., Jr. *Coord. Chem. Rev.* **2005**, *249*, 1372−1381. (f) Tekarli, S. M.; Cundari, T. R.; Omary, M. A. *J. Am. Chem. Soc.* **2008**, *130*, 1669−1675. (g) Elbjeirami, O.; Rashdan, M. D.; Nesterov, V.; Rawashdeh-Omary, M. A. *Dalton Trans.* **2010**, *39*, 9465−9468. (h) Hettiarachchi, C. V.; Rawashdeh-Omary, M. A.; Korir, D.; Kohistani, J.; Yousufuddin, M.; Dias, H. V. R. *Inorg. Chem.* **2013**, *52*, 13576−13583. (i) Ni, W.-X.; Li, M.; Zheng, J.; Zhan, S.-Z.; Qiu, Y.-M.; Ng, S. W.; Li, D. *Angew. Chem., Int. Ed.* **2013**, *52*, 13472−13476. (j) Visbal, R.; Gimeno, M. C. *Chem. Soc. Rev.* **2014**, *43*, 3551−3574.

(3) (a) Burini, A.; Fackler, J. P., Jr.; Galassi, R.; Pietroni, B. R.; Staples, R. J. *Chem. Commun.* **1998**, 95−96. (b) Burini, A.; Bravi, R.; Fackler, J. P., Jr.; Galassi, R.; Grant, T. A.; Omary, M. A.; Pietroni, B. R.; Staples, R. J. *Inorg. Chem.* **2000**, *39*, 3158−3165. (c) Burini, A.; Fackler, J. P., Jr.; Galassi, R.; Grant, T. A.; Omary, M. A.; Rawashdeh-Omary, M. A.; Pietroni, B. R.; Staples, R. J. *J. Am. Chem. Soc.* **2000**, *122*, 11264−11265. (d) Rawashdeh-Omary, M. A.; Omary, M. A.; Fackler, J. P., Jr.; Galassi, R.; Pietroni, B. R.; Burini, A. *J. Am. Chem. Soc.* **2001**, *123*, 9689−9691.

(4) Bonati, F.; Burini, A.; Pietroni, B. R.; Bovio, B. *J. Organomet. Chem.* **1989**, *375*, 147−160.

(5) (a) Gaillard, S.; Renaud, J.-L. *Dalton Trans.* **2013**, *42*, 7255−7270. (b) Marchenko, A. P.; Koidan, H. N.; Hurieva, A. N.; Gutov, O. V.; Kostyuk, A. N.; Tubaro, C.; Lollo, S.; Lanza, A.; Nestola, F.; Biffis, A. *Organometallics* **2013**, *32*, 718−721. (c) Ai, P.; Danopoulos, A. A.; Braunstein, P.; Monakhov, K. Yu. *Chem. Commun.* **2014**, *50*, 103−105. (d) Marchenko, A.; Koidan, H.; Hurieva, A.; Kurpiieva, O.; Vlasenko, Y.; Kostyuk, A.; Tubaro, C.; Lenarda, A.; Biffis, A.; Graiff, C. *J. Organomet. Chem.* **2014**, *771*, 14−23. (e) Wang, T.; Stephan, D. W. *Chem.—Eur. J.* **2014**, *20*, 3036−3039. (f) Brill, M.; Marrwitz, D.; Rominger, F.; Hofmann, P. *J. Organomet. Chem.* **2015**, *775*, 137−151.

(6) Bestgen, S.; Gamer, M. T.; Lebedkin, S.; Kappes, M. M.; Roesky, P. W. *Chem.—Eur. J.* **2015**, *21*, 601−614.

(7) (a) Katz, M. J.; Sakai, K.; Leznoff, D. B. *Chem. Soc. Rev.* **2008**, *37*, 1884−1895. (b) Schmidbaur, H.; Schier, A. *Chem. Soc. Rev.* **2008**, *37*, 1931−1951. (c) Sculfort, S.; Braunstein, P. *Chem. Soc. Rev.* **2011**, *40*, 2741−2760. (d) Schmidbaur, H.; Schier, A. *Chem. Soc. Rev.* **2012**, *41*, 370−412. (e) Tiekink, E. R. T. *Coord. Chem. Rev.* **2014**, *275*, 130−153.

(8) Braunstein, P.; Müller, A.; Bögge, H. *Inorg. Chem.* **1986**, *25*, 2104−2106.

For references, see P34

DOI: 10.1021/acs.inorgchem.5b00276
Inorg. Chem. 2015, 54, 3722−3724

Chapter 3

Non-symmetric diphosphines based on the imidazole scaffold: Unusual group interchange involving Pd-CH_3 and (imidazole)P-Ph cleavage

This chapter is written in the form of a publication. This article was published in *Dalton Transactions* **2014**, 43, 1957-1960.

My contribution in this work included the synthesis of the ligands and complexes, their characterization and the preparation of the draft of the publication.

Non-symmetric diphosphines based on the imidazole scaffold: Unusual group interchange involving Pd-CH_3 and (imidazole)P-Ph cleavage

Pengfei Ai,[a] Andreas A. Danopoulos,*[a,b] Pierre Braunstein*[a]

[a] Laboratoire de Chimie de Coordination, Institut de Chimie (UMR 7177 CNRS), Université de Strasbourg, 4 rue Blaise Pascal, 67081 Strasbourg Cedex, France. E-mail: danopoulos@unistra.fr, braunstein@unistra.fr

[b] Institute for Advanced Study, USIAS, Université de Strasbourg, France.

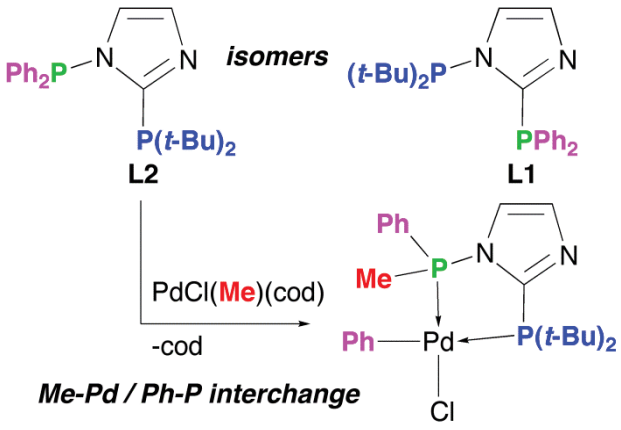

Supporting information for this chapter is available on the internet under http://pubs.rsc.org/en/content/articlelanding/2014/dt/c3dt53025f

For references, see P41

Résumé du Chapitre 3

Deux $P^{C2}P^{N}$-imidazoles régio-isomères, non symétriques $t\text{-Bu}_2\text{P}\overline{\text{NCH=CHNC}}(\text{PPh}_2)$ (**L1**, P^{C2} = PPh_2, P^{N} = P(*t*-Bu)$_2$); $\text{Ph}_2\text{P}\overline{\text{NCH=CHNC}}[\text{P}(t\text{-Bu})_2]$ (**L2**, P^{C2} = P(*t*-Bu)$_2$, P^{N} = PPh_2) ont été obtenus par différents chemins (Schéma 1).

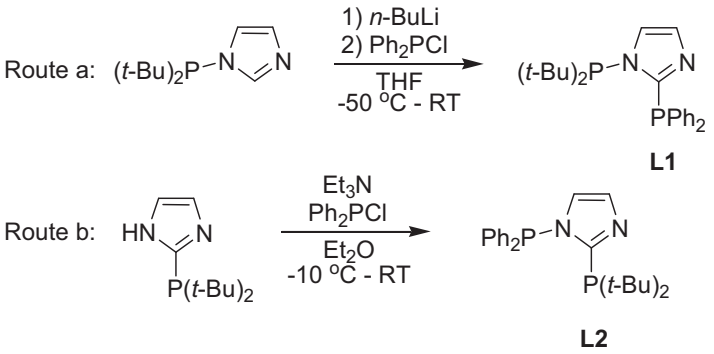

Schéma 1

La chimie de coordination de **L1** et **L2** fut étudiée vis-à-vis de différents précurseurs de Pd (Schéma 2). Ces ligands montrent des différences de réactivité considérables de la phosphine liée à N. L'isomère **L2** est extrêmement sensible à la rupture de liaison P-N par les nucléophiles et lorsqu'il est coordiné au fragment Pd(Me)Cl, il donne lieu à un échange facile d'un phényle de P^{N} avec le méthyle provenant du Pd.

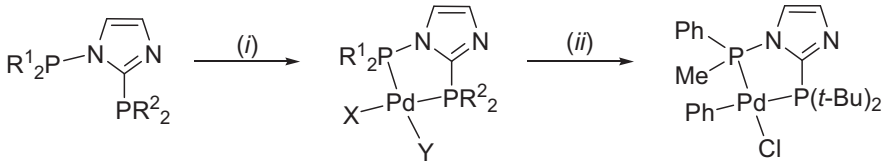

Schéma 2. Conditions de réaction: (*i*) [$PdCl_2$(cod)] ou [PdClMe(cod)], THF; (*ii*) THF ou CH_2Cl_2, temp. amb., 5 jours.

For references, see P41

Dalton Transactions

COMMUNICATION

View Article Online
View Journal | View Issue

Non-symmetric diphosphines based on the imidazole scaffold: an unusual group interchange involving Pd–CH_3 and (imidazole)P–Ph cleavage†

Cite this: *Dalton Trans.*, 2014, **43**, 1957

Received 26th October 2013,
Accepted 25th November 2013

DOI: 10.1039/c3dt53025f

www.rsc.org/dalton

Pengfei Ai,[a] Andreas A. Danopoulos*[a,b] and Pierre Braunstein*[a]

Two regioisomeric, non-symmetric $P^{C2}P^{N}$-imidazoles, *t*-Bu_2PNCH=CHNC(PPh_2) (L1, P^{C2} = PPh_2, P^{N} = P(*t*-Bu)$_2$) and Ph_2PNCH=CHNC[P(*t*-Bu)$_2$] (L2, P^{C2} = P(*t*-Bu)$_2$, P^{N} = PPh_2), respectively, show dramatic differences in the reactivity of the N-bound phosphine group; the L2 isomer is extremely sensitive to P–N bond cleavage by nucleophiles, and when coordinated to the PdCl(Me) fragment it undergoes facile interchange of one P^{N} phenyl with the methyl originating from Pd.

Functional phosphine ligands of the type $PR_n(Het)_{3-n}$, R = alkyl or aryl, Het = aza-heteroaryl, n = 0, 1, 2, are well studied for Het = *m*-pyridyl[1] (m = 2, 3, 4), but less so with other N-heteroaryls. $PR_n(m\text{-pyridyl})_{3-n}$ were used as ligands for the Pd-catalysed alkoxycarbonylation of propyne.[2] More recently 2-(di-alkyl- or -aryl-phosphino)-1*R*-imidazole ligands (R = H, alkyl or aryl) were employed for the hydration of alkynes,[3] the isomerisation of alkenes,[4] and for carbonylative cross-coupling reactions;[5] in the cases reported, catalytic performances were superior compared to non-heteroaryl analogues. Attempts to gain insight into the role of the N-heteroaryl group have pointed to its ability to be involved in the formation of small bite angle (P, N)-chelates with potential hemilability,[6] in intramolecular or intermolecular hydrogen bonding and to provide a basic site facilitating proton transfer during catalysis.[3c,7] Information on the donor characteristics of 2-(di-alkyl- or -aryl-phosphino)-1*R*-imidazoles is scarce but supports similarities (based on the electronic Tolman parameter) to analogous PR_2Ph ligands.[8] Recently, complexes with the chelating flexible 1,2-bis-(2-diphenylphosphino-imidazolyl)-benzene and 1,2-bis-(2-diphenylphosphino-imidazolium)-benzene have been reported.[9]

Ligands of the type 1-(di-*t*-butyl- or -aryl-phosphino)-imidazole, -imidazolium, and 1-(di-*t*-butylphosphino)-N-heterocyclic carbene (NHC), with a P–N covalent bond, belong to the broad class of aminophosphines[10] and have only recently become available,[11] attracting interest as ligands and as intermediates for the synthesis of imidazolium salts and NHCs.[11b,d,12]

Due to our long-standing efforts in the chemistry of ligands with P–N bonds[13] we set out to study the chemistry of the chelating regioisomeric diphosphines *t*-Bu_2PNCH=CHNC(PPh_2) (**L1**) and Ph_2PNCH=CHNC-[P(*t*-Bu)$_2$] (**L2**) shown in Scheme 1, which result from a swap of the PPh_2 and P(*t*-Bu)$_2$ donors between the 1- and 2-positions of the heterocycle. Such ligands offer a platform to explore rigid, chelating imidazole-based diphosphines, with one P–N and one P–C bond and thus one less donating, more π-acidic P donor and a more donating, less π-acidic P donor, respectively. There are two previous reports on bidentate $P^{C2}P^{N}$-imidazoles[11b,14] formed as undesired products from the coordination of 2-dimethylphosphanyl-imidazole on a W(0) carbonyl centre and the synthesis of *N*-phosphanyl-NHCs. More recently, the synthesis of the bis-(di-*t*-butyl) analogue of **L1** and **L2** has been reported.[15]

The high yielding and rational routes a and b (Scheme 1) can provide **L1** and **L2** in gram quantities and are based on the

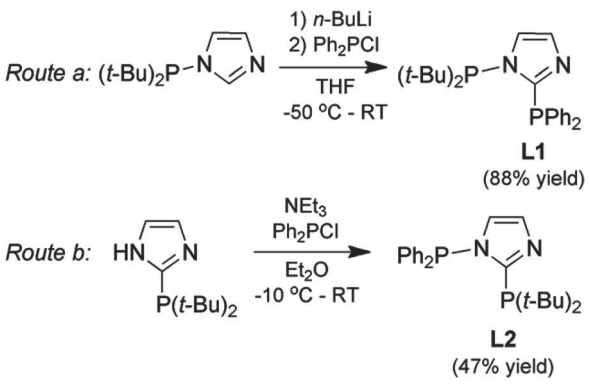

Scheme 1 The ligands **L1** and **L2** and their synthesis.

[a]*Laboratoire de Chimie de Coordination, Institut de Chimie (UMR 7177 CNRS), Université de Strasbourg, 4 rue Blaise Pascal, 67081 Strasbourg Cedex, France. E-mail: danopoulos@unistra.fr, braunstein@unistra.fr*
[b]*Institute for Advanced Study, USIAS, Université de Strasbourg, France*

†Electronic supplementary information (ESI) available: Experimental details and full characterisation of all compounds; crystal structure data for **L1**, **L2**, **1b**, **2a**, **2b** and **2c**. CCDC 968367–968372. For ESI and crystallographic data in CIF or other electronic format see DOI: 10.1039/c3dt53025f

For references, see P41

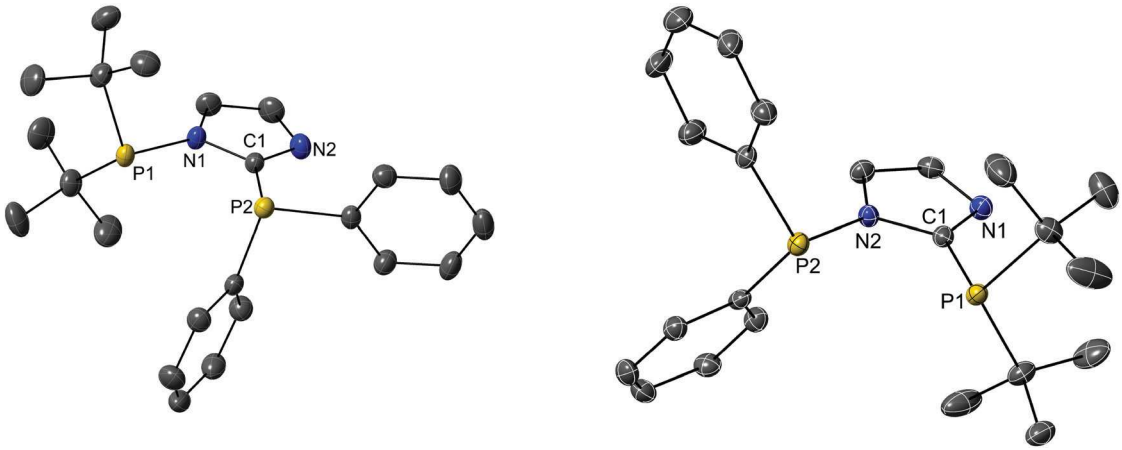

Fig. 1 Thermal ellipsoid representation (30% probability level) of the structure of **L1** (left) and **L2** (right). Selected bond lengths (Å) and angles [°]: for **L1**: P1–N1 1.763(1), N1–C1 1.389(2), C1–P2 1.828(1), C1–N2 1.321(2); N2–C1–N1 111.6(1), N2–C1–P2 126.1(1), N1–C1–P2 122.16(9), C1–N1–P1 122.17(9). For **L2**: P1–C1 1.828(3), C1–N1 1.321(3); C1–N2 1.396(4); N2–P2 1.751(2); N1–C1–N2 110.5(2), N1–C1–P1 128.4(2), N2–C1–P1 121.2(2), C1–N2–P2 125.6(2).

reaction of PPh_2Cl with C2 lithiated 1-(di-*tert*-butylphosphino)-imidazole and 2-(di-*tert*-butylphosphino)-imidazole. An indirect, less convenient formation of **L1** has recently been described.[11a] Interestingly, attempted preparation of **L2** by deprotonation of 1-(diphenylphosphino)imidazole with *n*-BuLi (in a sequence analogous to route a) led to the cleavage of the Ph_2P–N_{imid} bond and the formation of $Ph_2P(n\text{-Bu})$ (identified by ^{31}P NMR spectroscopy: δ −16 ppm). This demonstrated the weakness of the Ph_2P–N_{imid} bond (compared to $(t\text{-Bu})_2P$–N_{imid}) and its susceptibility to the presence of strong nucleophiles. Ligand **L1** is stable in air, while **L2** is very sensitive to both water and oxygen. Their different behaviour is not mirrored by major structural differences (*e.g.* P–N bond in **L1** (1.763(1) Å) and **L2** (1.751(2) Å) (see Fig. 1).

Preliminary comparative studies of the coordination chemistry of **L1** and **L2** gave some unexpected results (see Scheme 2).

All characterisation data point to the retaining of the integrity of the basic ligand framework after complexation both in solution and in the solid state (Fig. 2–4). The Pd centre in **2a** shows a typical distorted square planar coordination geometry; the ligand bite angle is 89.04(1)°. Slight shortening of the Ph_2P–N bond and reduction of the P2–N1–C1 angle are noticeable on coordination. There are significant differences between the two Pd–P bond distances, [Pd–PPh_2 (2.2070(4) *vs.* Pd–P(*t*-Bu)$_2$) (2.2850(4) Å], but not between the two Pd–Cl bonds.

Reaction of **L1** and **L2** with [PdCl(Me)(cod)] gave complexes **1b** and **2b** (see ESI†). The two doublets in ^{31}P NMR at δ 114.9 (d, $^{2+3}J_{PP}$ = 37.2 Hz, $P(t\text{-Bu})_2$) and 27.4 (d, $^{2+3}J_{PP}$ = 37.2 Hz, PPh_2), 85.9 (d, $^{2+3}J_{PP}$ = 35.4 Hz, PPh_2) and 41.4 (d, $^{2+3}J_{PP}$ = 35.4 Hz, $P(t\text{-Bu})_2$), respectively, in combination with the two doublets assignable to the Pd–CH_3, in the ^1H NMR spectrum due to ^3J-coupling of the methyl group protons with the P atoms are diagnostic for complex formation. Attempts to obtain X-ray quality crystals were straightforward for **1b** but were

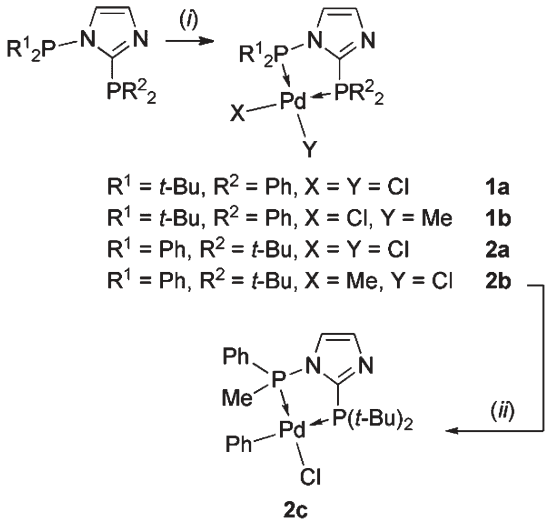

R^1 = *t*-Bu, R^2 = Ph, X = Y = Cl **1a**
R^1 = *t*-Bu, R^2 = Ph, X = Cl, Y = Me **1b**
R^1 = Ph, R^2 = *t*-Bu, X = Y = Cl **2a**
R^1 = Ph, R^2 = *t*-Bu, X = Me, Y = Cl **2b**

2c

Scheme 2 Synthesis of palladium complexes **1a/b** and **2a/b/c**. Reaction conditions: (*i*) [$PdCl_2$(cod)] or [PdCl(Me)(cod)], THF; (*ii*) THF or CH_2Cl_2, room temperature, quantitative after 5 days.

complicated for **2b** due to a rearrangement reaction described below. Therefore, crystallisation of **2b** had to be carried out at −38 °C in the glove box. However, after successful isolation, the solids **1b** and **2b** are air-stable. The structures of **1b** and **2b** are shown in Fig. 3 and 4.

The coordination geometry around the Pd centre in both complexes is distorted square planar; the ligand bite angles are 88.62(2)° and 89.41(3)°, respectively. In both cases, the chloride is located *trans* to the PPh_2 group with Pd–Cl bond distances of 2.3792(7) and 2.369(1) Å and the *Pd–C*H_3 bond distances of 2.091(2) and 2.121(3) Å, respectively. There are significant differences between the two Pd–P bond lengths in each structure, [Pd–P(*t*-Bu)$_2$ 2.361(1) Å and Pd–PPh_2 2.1808(9) Å for **2b**; Pd–P(*t*-Bu)$_2$ 2.2072(6) Å and Pd–PPh_2 2.3632(6) Å for **1b**].

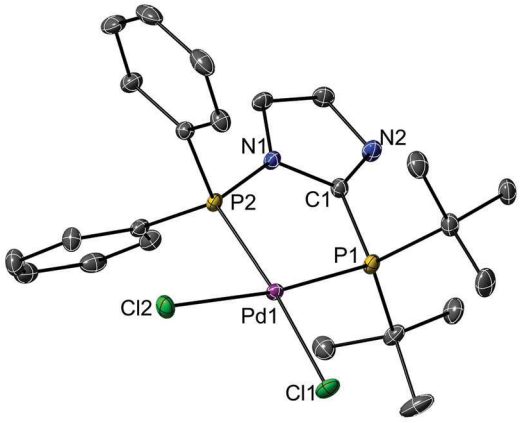

Fig. 2 Thermal ellipsoid representation (30% probability level) of the structure of **2a**. Selected bond lengths (Å) and angles [°]: Pd1–P1 2.2850(4), Pd1–P2 2.2070(4), Pd1–Cl1 2.3507(3), Pd1–Cl2 2.3634(4); P1–C1 1.831(2), C1–N1 1.378(2), C1–N2 1.316(2), N1–P2 1.721(1); Cl1–Pd1–Cl2 91.12(2), P1–Pd1–P2 89.04(1), P1–Pd1–Cl1 97.56(2), P2–Pd1–Cl1 173.34(2), P1–Pd1–Cl2 171.29(2), P2–Pd1–Cl2 82.28(1), N1–C1–N2 111.7(1), N1–C1–P1 117.7(1), N2–C1–P1 130.5(1), C1–N1–P2 121.9(1), C1–P1–Pd1 103.66(5), N1–P2–Pd1 107.26(4).

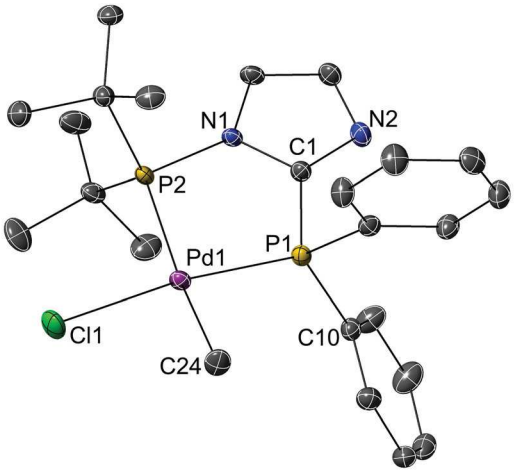

Fig. 3 Structure of **1b**. Selected bond lengths (Å) and angles [°]: Pd1–C24 2.091(2), Pd1–Cl1 2.3792(7), Pd1–P1 2.2072(6), Pd1–P2 2.3632(6), C1–N2 1.317(3), C1–N1 1.378(3), C1–P1 1.817(2), N1–P2 1.749(2); N2–C1–N1 112.7(2), N2–C1–P1 127.4(2), N1–C1–P1 119.8(2), C1–N1–P2 121.4(2), C1–P1–Pd1 106.36(8), N1–P2–Pd1 103.72(7), C24–Pd1–P1 88.73(8), C24–Pd1–P2 172.21(8), P1–Pd1–P2 88.62(2), C24–Pd1–Cl1 86.61(8), P1–Pd1–Cl1 172.57(3), P2–Pd1–Cl1 96.73(2).

Solutions of **2b** in THF or CH_2Cl_2 undergo a facile rearrangement ($t_{1/2} \sim 2$ days at room temperature), in which the methyl group bound to Pd exchanges with one of the Ph groups in PPh_2 to give the new complex **2c** cleanly and quantitatively after 5 days (Scheme 2). This could be confirmed by the appearance in the ^{31}P NMR of two new doublets at δ 72.1 (d, $^{2+3}J_{PP}$ = 35.3 Hz) and 42.0 (d, $^{2+3}J_{PP}$ = 35.3 Hz) and in the ^{1}H NMR the disappearance of the original two doublets

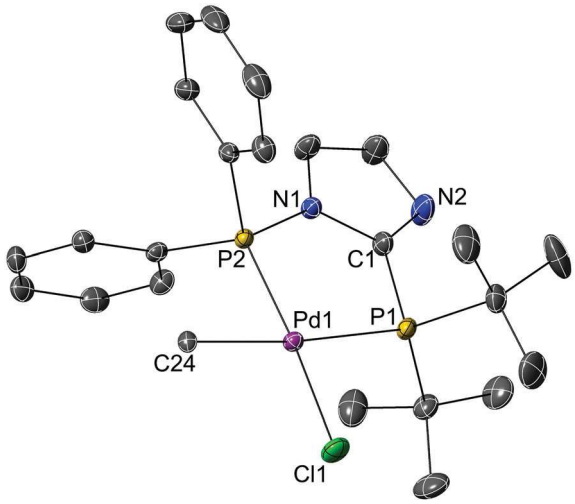

Fig. 4 Structure of **2b**. Selected bond lengths (Å) and angles [°]: Pd1–C24 2.121(3), Pd1–Cl1 2.369(1), Pd1–P1 2.361(1), Pd1–P2 2.1808(9), C1–N2 1.324(5), C1–N1 1.377(5), C1–P1 1.824(4), N1–P2 1.736(3); N2–C1–N1 111.4(3), N2–C1–P1 130.1(3), N1–C1–P1 118.5(3), C1–N1–P2 123.0(3), C1–P1–Pd1 101.8(1), N1–P2–Pd1 107.2(1), C24–Pd1–P2 84.5(1), C24–Pd1–P1 173.9(1), P2–Pd1–P1 89.41(3), C24–Pd1–Cl1 88.7(1), P2–Pd1–Cl1 172.78(4), P1–Pd1–Cl1 97.33(4).

assignable to the CH_3 and the appearance of one doublet at δ 2.04 (d, $^{2}J_{PH}$ = 9.7 Hz). The structure of the molecule is given in Fig. 5.

In **2c** the Pd is adopting a square planar geometry (ligand bite angle, 88.81(4)°). The chloride is still *trans* to P-phenyl and the Pd–Cl bond is longer compared to **2b**. The Pd–P bonds in **2c** are longer than those in **2b**. There is no significant difference between the N_{imid}–*P*PhMe and N_{imid}–*P*Ph_2 bond lengths.

Although the electronic characteristics of the P^N and P^C are not precisely known, it is reasonable to assume that the P^C-(t-Bu)$_2$ is the strongest donor in the systems studied, and therefore should weaken in **2b** the Pd–Me bond that is *trans* to it; the rearrangement results in positioning the Ph (with stronger Pd–C_{aryl}) *trans* to the P^C(tBu$_2$). It also places the electron releasing Me on the electron deficient (and therefore electrophilic) P^N centre. A relevant rearrangement occurring in a Rh-methyl phosphine complex has been recently described,[16] and the implications of P–C/Pd–C bond cleavage/formation for homogeneous catalysis have been emphasised.[17] Recently the mechanistic diversity of the transition metal-mediated P–C/X exchange has been reviewed.[18] From the mechanistic scenario proposed, the intramolecular nucleophilic attack on the electrophilic P^N is plausible with the current ligand system. Our experimental observations on Pd–Me/P–Ph interchange may have relevance to reaction pathways or catalysts deactivation in *e.g.* cross-coupling reactions.

A. A. D. thanks the CNRS for support, the Région Alsace, the Département du Bas-Rhin and the Communauté Urbaine de Strasbourg for a Gutenberg Excellence Chair (2010–2011) and USIAS for a fellowship. We thank the CNRS, the MESR (Paris), the UdS, the China Scholarship Council (PhD grant to

For references, see P41

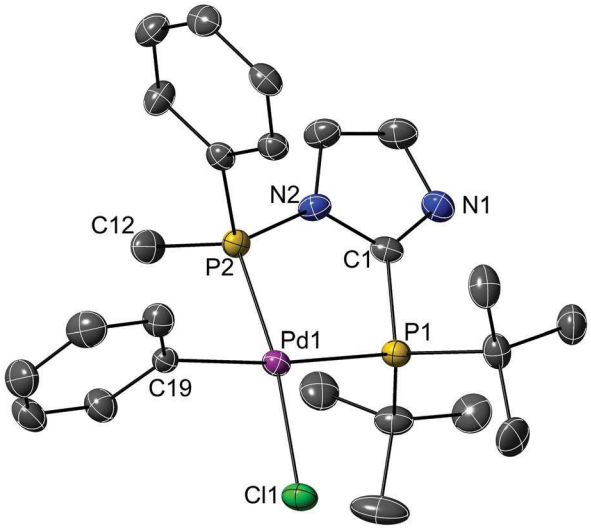

Fig. 5 Thermal ellipsoid representation (30% probability level) of the structure of **2c**. Selected bond lengths (Å) and angles [°]: Pd1–C19 2.089(4), Pd1–Cl1 2.380(1), Pd1–P1 2.378(1), Pd1–P2 2.198(1), C1–N1 1.323(5), C1–N2 1.375(5), C1–P1 1.820(4), C12–P2 1.802(4), N2–P2 1.729(4); N1–C1 N2 111.7(4), N1–C1–P1 130.6(4), N2–C1–P1 117.7(3), C1–N2–P2 124.0(3), C1–P1–Pd1 102.1(2), N2–P2–C12 103.7(2), N2–P2–Pd1 106.9(1), C12–P2–Pd1 115.2(2), C19–Pd1–P2 84.5(1), C19–Pd1–P1 173.2(1), P2–Pd1–P1 88.81(4), C19–Pd1–Cl1 88.0(1), P2–Pd1–Cl1 171.90(4), P1–Pd1–Cl1 98.53(4).

A.P.), and the ucFRC (http://www.icfrc.fr) for financial support and the Service de Radiocristallographie (Institut de Chimie, Strasbourg) for the determination of the crystal structures.

References

1 G. R. Newkome, *Chem. Rev.*, 1993, **93**, 2067.
2 E. Drent, W. W. Jager, J. J. Keijsper and F. G. M. Niele, *Applied Homogeneous Catalysis with Organometallic Compounds*, VCH, Weinheim, 2002.
3 (*a*) D. B. Grotjahn, C. D. Incarvito and A. L. Rheingold, *Angew. Chem., Int. Ed.*, 2001, **40**, 3884; (*b*) D. B. Grotjahn, Y. Gong, A. G. DiPasquale, L. N. Zakharov and A. L. Rheingold, *Organometallics*, 2006, **25**, 5693; (*c*) L. Hintermann, T. T. Dang, A. Labonne, T. Kribber, L. Xiao and P. Naumov, *Chem.–Eur. J.*, 2009, **15**, 7167.
4 D. B. Grotjahn, C. R. Larsen, J. L. Gustafson, R. Nair and A. Sharma, *J. Am. Chem. Soc.*, 2007, **129**, 9592.
5 X.-F. Wu, H. Neumann, A. Spannenberg, T. Schulz, H. Jiao and M. Beller, *J. Am. Chem. Soc.*, 2010, **132**, 14596.
6 P. Braunstein and F. Naud, *Angew. Chem., Int. Ed.*, 2001, **40**, 680.
7 (*a*) D. B. Grotjahn, *Dalton Trans.*, 2008, 6497; (*b*) E. Drent, P. Arnoldy and P. H. M. Budzelaar, *J. Organomet. Chem.*, 1994, **475**, 57; (*c*) E. Drent, P. Arnoldy and P. H. M. Budzelaar, *J. Organomet. Chem.*, 1993, **455**, 247; (*d*) G. Kiss, *Chem. Rev.*, 2001, **101**, 3435; (*e*) G. Franciò, R. Scopelliti, C. G. Arena, G. Bruno, D. Drommi and F. Faraone, *Organometallics*, 1998, **17**, 338.
8 D. B. Grotjahn, X. Zeng, A. L. Cooksy, W. S. Kassel, A. G. DiPasquale, L. N. Zakharov and A. L. Rheingold, *Organometallics*, 2007, **26**, 3385.
9 Y. Canac, N. Debono, C. Lepetit, C. Duhayon and R. Chauvin, *Inorg. Chem.*, 2011, **50**, 10810.
10 (*a*) D. Benito-Garagorri and K. Kirchner, *Acc. Chem. Res.*, 2008, **41**, 201; (*b*) J. Cheng, Y. Sun, F. Wang, M. Guo, J.-H. Xu, Y. Pan and Z. Zhang, *J. Org. Chem.*, 2004, **69**, 5428.
11 (*a*) P. Ai, A. Danopoulos, P. Braunstein and K. Monakhov, *Chem. Commun.*, 2014, **50**, 103; (*b*) A. P. Marchenko, H. N. Koidan, A. N. Huryeva, E. V. Zarudnitskii, A. A. Yurchenko and A. N. Kostyuk, *J. Org. Chem.*, 2010, **75**, 7141; (*c*) A. P. Marchenko, H. N. Koidan, I. I. Pervak, A. N. Huryeva, E. V. Zarudnitskii, A. A. Tolmachev and A. N. Kostyuk, *Tetrahedron Lett.*, 2012, **53**, 494; (*d*) P. Nägele, U. Herrlich, F. Rominger and P. Hofmann, *Organometallics*, 2012, **32**, 181.
12 (*a*) E. Kühnel, I. V. Shishkov, F. Rominger, T. Oeser and P. Hofmann, *Organometallics*, 2012, **31**, 8000; (*b*) A. P. Marchenko, H. N. Koidan, A. N. Hurieva, O. V. Gutov, A. N. Kostyuk, C. Tubaro, S. Lollo, A. Lanza, F. Nestola and A. Biffis, *Organometallics*, 2013, **32**, 718.
13 (*a*) S. Zhang, R. Pattacini and P. Braunstein, *Organometallics*, 2010, **29**, 6660; (*b*) R. Pattacini, G. Margraf, A. Messaoudi, N. Oberbeckmann-Winter and P. Braunstein, *Inorg. Chem.*, 2008, **47**, 9886; (*c*) P. Braunstein, *Chem. Rev.*, 2005, **106**, 134.
14 Z. Chen, H. W. Schmalle, T. Fox, O. Blacque and H. Berke, *J. Organomet. Chem.*, 2007, **692**, 4875.
15 M. Brill, L. Weigel, K. Rübenacker, F. Rominger and P. Hofmann, *Heidelberg Forum of Molecular Catalysis*, 28 June 2013, poster P60.
16 B. K. Shaw, B. O. Patrick and M. D. Fryzuk, *Organometallics*, 2012, **31**, 783.
17 (*a*) D. K. Morita, J. K. Stille and J. R. Norton, *J. Am. Chem. Soc.*, 1995, **117**, 8576; (*b*) F. E. Goodson, T. I. Wallow and B. M. Novak, *J. Am. Chem. Soc.*, 1997, **119**, 12441.
18 S. A. Macgregor, *Chem. Soc. Rev.*, 2007, **36**, 67.

For references, see P41

Chapter 4

Luminescent Properties of Au(I) Complexes Bearing *N*,*N*'-Diphosphanyl NHC Ligands

This chapter is written as a publication to be submitted

My contribution in this work included the synthesis of the complexes, their characterization and the preparation of the draft of the publication (synthetic part). The photophysical properties are being characterized by Dr Matteo Mauro and Prof. Luisa de Cola and the theoretical calculations is being performed by Dr Christophe Gourlaouen in Strasbourg.

Luminescent Properties of Au(I) Complexes Bearing *N*,*N*'-Diphosphanyl NHC Ligands

Pengfei Ai,[a] Matteo Mauro,[b] Christophe Gourlaouen,[c] Andreas A. Danopoulos,*[a,d] Pierre Braunstein,*[a] Luisa De Cola*[b]

[a] Laboratoire de Chimie de Coordination, Institut de Chimie (UMR 7177 CNRS), Université de Strasbourg, 4 rue Blaise Pascal, 67081 Strasbourg Cedex, France. E-mail: danopoulos@unistra.fr, braunstein@unistra.fr

[b] ISIS & icFRC, Université de Strasbourg & CNRS, 8 rue Gaspard Monge, 67000 Strasbourg, France

[c] Laboratoire de Chimie Quantique, Institut de Chimie (UMR 7177 CNRS), Université de Strasbourg, 1 rue Blaise Pascal, 67008 Strasbourg, France

[d] Institute for Advanced Study, USIAS, Université de Strasbourg, France.

For references, see P81

Résumé du Chapitre 4

La réaction de transmétallation du complexe trinucléaire d'argent (I) **PCP-Ag3** avec 3 équiv. de [AuCl(tht)] dans l'acétonitrile a conduit au complexe **PCP-Au3** ainsi qu'à un nouveau complexe minoritaire, **PCP-Au3Cl2THT** (Scheme 1).

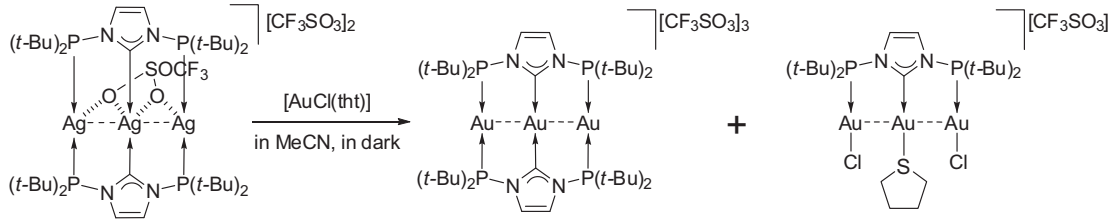

Schéma 1

Le complexe dinucléaire d'or(I), **PCP-Au2**, fut préparé par réaction du sel d'imidazolium **PCHP** avec [(Ph_3P)Au{$N(SiMe_3)_2$}], en présence d'une petite quantité de **PCP** (ca. 0.17 equiv.) dans le THF (Schéma 2). Avec deux groupes phosphines pendants, **PCP-Au2** peut servir de plateforme pour la préparation de complexes polynucléaires très originaux, dont le complexe homotrinucléaire **PCP-Au3** et le complexe hétérotrinucléaire **PCP-Au2Ag** (Schéma 2).

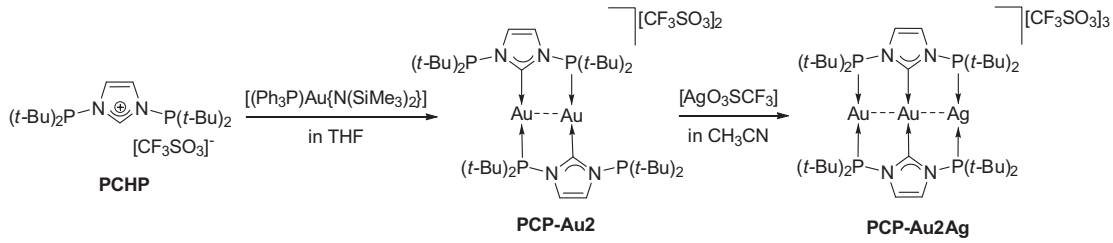

Schéma 2

For references, see P81

Luminescent Properties of Au(I) Complexes Bearing *N*,*N*'-Diphosphanyl NHC Ligands

Pengfei Ai,[a] Matteo Mauro,[b] Christophe Gourlaouen,[c] Andreas A. Danopoulos,*[a,d] Pierre Braunstein,*[a] Luisa De Cola*[b]

[a] Laboratoire de Chimie de Coordination, Institut de Chimie (UMR 7177 CNRS), Université de Strasbourg, 4 rue Blaise Pascal, 67081 Strasbourg Cedex, France. E-mail: danopoulos@unistra.fr, braunstein@unistra.fr

[b] ISIS & icFRC, Université de Strasbourg & CNRS, 8 rue Gaspard Monge, 67000 Strasbourg, France

[c] Laboratoire de Chimie Quantique, Institut de Chimie (UMR 7177 CNRS), Université de Strasbourg, 1 rue Blaise Pascal, 67008 Strasbourg, France

[d] Institute for Advanced Study, USIAS, Université de Strasbourg, France.

ABSTRACT

Transmetallation of the silver (I) complex **PCP-Ag3** with 3 equiv. of [AuCl(tht)] in acetonitrile afforded the trinuclear complex **PCP-Au3** in high yield, accompanied by the **PCP-Au3Cl2THT** bearing only one supporting **PCP** ligand. A comparison with the dinuclear gold (I) complex **PCP-Au2** is presented. With two dangling phosphines, it serves as a platform for the preparation of homotrinuclear **PCP-Au3** or heterotrinuclear complex **PCP-Au2Ag** complexes.

For references, see P81

INTRODUCTION

Luminescent d^{10} coinage metal complexes with structural diversity have been widely investigated due to their intriguing photophysical properties.[1] Amongst them, Au(I) complexes occupy a special position,[2] since the heavy gold metal center is responsible for efficiency enhancements originating from spin-orbit coupling, and promotes access to triplet excited states via intersystem crossing processes.[1a,3] The precise ligand environment and aurophilic interactions caused by dispersion/correlation effects and strengthened by relativistic effects,[4] add additional elements of versatility and tuning options for the emissive properties of Au(I) complexes[1a,1c,3] as well as for their photocatalytic activities.[5] The interest for such class of Au(I) complexes is driven by the fact that their photophysical and photocatalytic properties are generally sensitive to small environmental changes, such as (counter-)ion, solvent and pressure.[6] Classical donor-, functional-groups encountered in luminescent Au(I) complexes include amongst others phosphines, alkynyls, thiolates, chalcogenido, *etc.*.[1b]. Moreover, apart from mononuclear derivatives, polynuclear Au(I) counterparts with attractive aurophilic interactions are also of particular interest in view of their luminescent and catalytic properties.[7] In particular, such class of compounds bearing polydentate P-based ligands has been object of intense study since long time.[1g,8] Furthermore, the nature of the excitation processes along with that of the emitting lowest-lying exited state is often debated and a clear structure–properties relationship elusive.[2d,9] This is in spite of the fact that some of the derivative display very interesting photophysical properties with photoluminescence quantum yield (PLQY) in some cases approaching unity,[2d,10] as well as tunable emission color by proper choice of the coordinating ligands. Overall such features make mono- and poly-nuclear luminescent Au(I) great candidate as photoactive materials and low-molecular weight gelating agents suitable for sensing,[6a] light-emitting devices[11] and biomedical application.[12]

Since the first report of luminescent Au(I) benzimidazole-2-ylidene complexes by Lin and coworkers,[13] a great number of *N*-heterocyclic carbene (NHC) Au(I)

For references, see P81

complexes have been prepared which show interesting optical properties.[1b,1c,6d,10] In this respect, photoactive NHC-containing complexes are able to engage strong M−C_{NHC} coordination bonds and they currently play a pivotal role due to their attractive electronic properties. Indeed, upon coordination to a metal center, the strong σ-donation ability exerted by the NHC moiety push-up the energy of quenching *d-d* metal-centered (MC) states, thus reducing the nonradiative deactivation pathways. Also, as consequence of the weak π-accepting ability of NHC ligands, π* orbitals located on such moieties lies to higher energy with respect to other, widely employed, chromophoric ligands. These feature allows highly emissive excited state to lie in higher energy regions, in particular falling into the blue to ultraviolet (UV) portion of the electromagnetic spectrum: an important feature in view of their possible application in light-emitting devices.[10]

Recently, bulky *N*-phosphanyl- or *N,N'*-diphosphanyl-functionalized NHC ligands have attracted attention as tunable scaffolds, providing rigid arrangement, thanks to the two adjacent donor types (NHC and PR_3).[14] The trifunctional rigid, small natural bite angle *N,N'*-diphosphanyl-imidazol-2-ylidene (**$PC_{NHC}P$**) ligand (P = P(*t*-Bu)$_2$) was found to be stable enough towards N_{imid} to C_{NHC} phosphorus migration to provide an entry into the coordination chemistry of linear trinuclear chain complexes amenable to 'σ-donation fine grading' and with potentially promising physical properties.[1b,14b,14c] Compared to related P,C_{NHC},P donor ligands with a flexible ethylene spacer between the P and C donors that also support di- and tri-nuclear gold complexes, *N,N'*-diphosphanyl-functionalized NHC impose shorter intermetallic distances, in the range 2.70 – 2.80 Å.[2c] The remarkable linear trinuclear complex $[Au_3\{\mu_3\text{-}\kappa^3(\mathbf{PC_{NHC}P})\}_2][CF_3SO_3]_3$ (**Au_3-($PC_{NHC}P)_2$**) indeed displays a very short Au···Au interaction (2.7584(2) Å).[14c] Compared to the all phosphine analogues (**$P^{Ph}P^{Ph}P^{Ph}$**) and (**$P^RP^RP^R$**), R = Me, Cy, with methylene linkers (as the extreme means to impose rigidity in this case) an intermetallic distance of 2.9323(8) Å (R = Cy) has been observed in the linear Au_3 arrangement in the related (**Au3-($PPP)_2$**),[2d] but the ligand flexibility may lead to deviations from Au_3 linearity (R = Me, Ph) and occasionally to higher nuclearity complexes.[15] Therefore, the complex **Au_3-($PC_{NHC}P)_2$** provides a

For references, see P81

unique opportunity to establish relationships between the structure and the physical and chemical properties of closely spaced, 'σ-loaded' Au centers. The short Au···Au separation, shorter than in bulk Au (2.88 Å) makes this complex an excellent candidate for identifying the metal-metal vibrations by Raman spectroscopy and performing photophysical studies, with the possible involvement of metal cooperativity.

We report here a good yield transmetallation route to **Au_3-($PC_{NHC}P)_2$** and another trinuclear gold complex **Au_3-$PC_{NHC}P$** with only one supporting **$PC_{NHC}P$** ligand and longer Au···Au separations. The novel dinuclear gold complex **Au_2-($PC_{NHC}P)_2$** and its derivative heterotrimetallic complex **Au_2Ag-($PC_{NHC}P)_2$** were also prepared. The photophysical properties were investigated, compared and rationalized on the basis of computational studies.

RESULTS AND DISCUSSION

Synthesis and characterization of complexes.

Initial attempts were focused at optimizing the selectivity and yield of the **Au_3-($PC_{NHC}P)_2$** synthesis. Transmetallation of the trinuclear silver (I) complex **Ag_3-($PC_{NHC}P)_2$**,[14c] with 3 equiv. of [AuCl(tht)] (tht = tetrahydrothiophene) in acetonitrile afforded the complex **Au_3-($PC_{NHC}P)_2$** in high yield (80%) together with a new air stable gold(I) complex, **Au_3-$PC_{NHC}P$**, as by-product (Scheme 1). The two complexes can easily be separated and purified by washing the mixture by small amount of CH_2Cl_2 (See experiment). The multinuclear NMR characterization of **Au_3-$PC_{NHC}P$** included peaks at δ 3.33 (m, 4H) and 1.87 (m, 4H) assignable to one tht molecule and at 1.53 (d, $^3J_{HP}$ = 17.8 Hz) for *t*-Bu; in the $^{31}P\{^1H\}$ NMR spectrum a singlet at δ 133.7 shows equivalence of the two coordinated phosphine groups. The molecular structure of **Au_3-$PC_{NHC}P$** crystallized from acetonitrile is shown in Figure 1.

For references, see P81

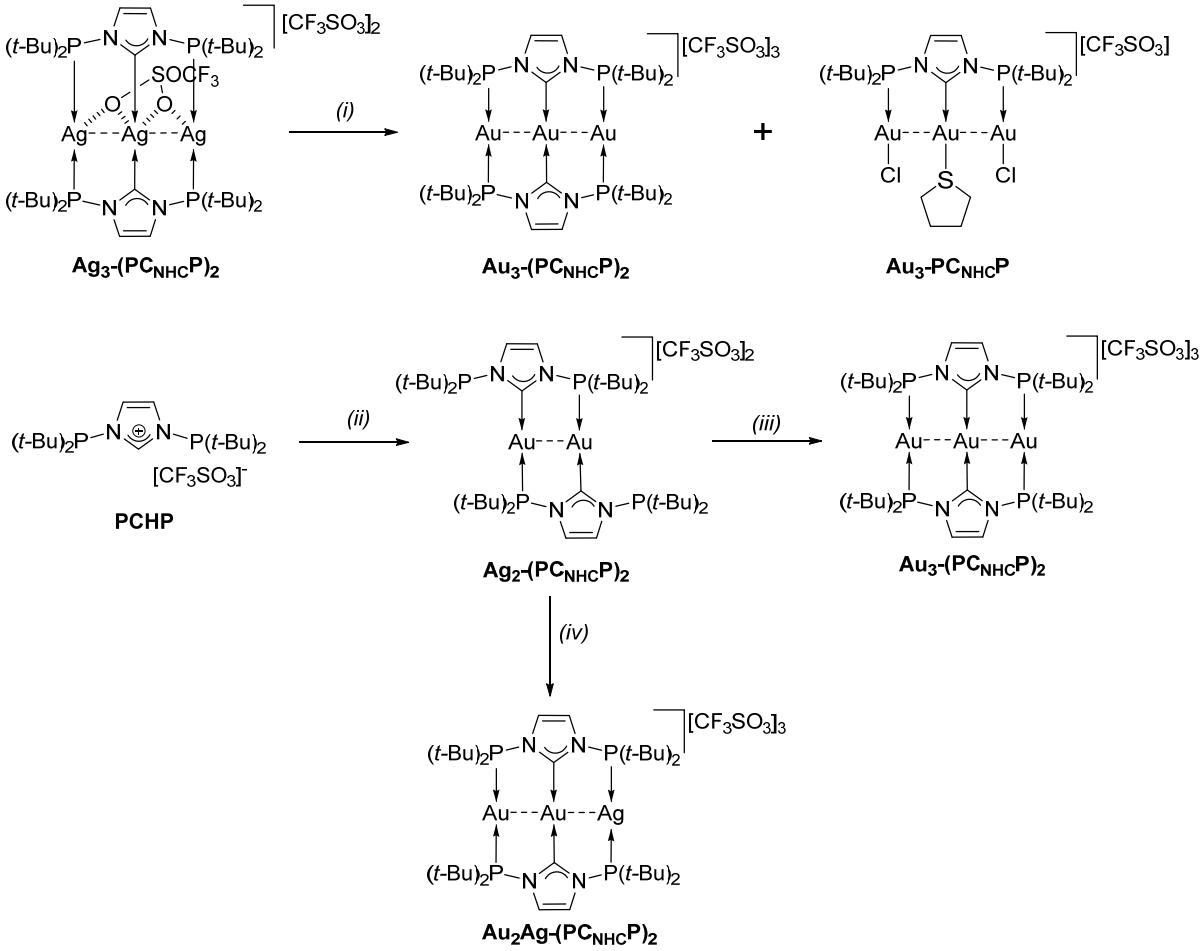

Scheme 1. Synthesis of the Au(I) complexes. Reagents and conditions: (*i*) [AuCl(tht)], in MeCN, RT, in dark; (*ii*) [(Ph_3P)Au{$N(SiMe_3)_2$}], in THF, 3 days, RT; (*iii*) [$Au(tht)_2$](CF_3SO_3), in CH_3CN, RT; (*iii*) [AgO_3SCF_3], in CH_3CN, RT.

The complex of **Au_3-$PC_{NHC}P$** contains an Au_3 array bridged by one **$PC_{NHC}P$** (*i.e.* μ_3-**$PC_{NHC}P$**, κ*P*,κ*C*,κ*P* mode). A chloride ligand is bound to each of the two outer and one THT ligand to the central Au atoms. The coordination geometries at all three Au centers are virtually linear (P1-Au1-Cl1 172.76(9)° and C1-Au2-S1 178.5(3)°). In the molecule there is a plane of symmetry (through C1, Au2, S1) but, interestingly, the Au1-Au2-Au1' vector deviates significantly from linearity (148.94(2)) highlighting the important role of the second PCP ligand in constraining geometrically the Au_3 substructure. This is further demonstrated by the significant elongation of the intermetallic distances compared to the **Au_3-$(PC_{NHC}P)_2$** (Au(1)-Au(2) distance of 2.9710(4) Å vs. 2.7584(2) Å in **Au_3-$(PC_{NHC}P)_2$**). The NHC ring and the central Au atom are coplanar. The Au-C_{NHC} (2.004(13) Å), Au-P (2.235(2) Å) and Au-Cl (2.285(3) Å)

For references, see P81

distances are in the expected range.[2b,2c,16] The implication of the differences metrical data on the photophysical properties is discussed below.

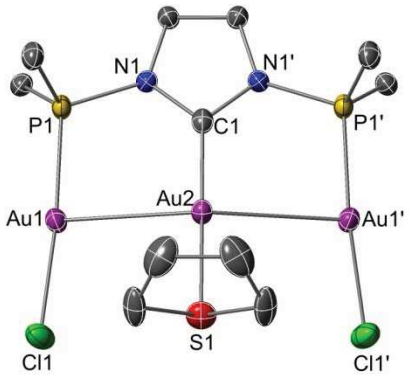

Figure 1. Structure of cationic part of **Au_3-$PC_{NHC}P$**•MeCN. H atoms, the *t*-Bu methyl groups and one molecule of MeCN are omitted for clarity. Anisotropic displacement parameters are depicted at the 30% probability level. Selected bond lengths (Å) and angles [°]: Au2-C1 2.004(13), Au1-P1 2.235(2), Au1-Cl1 2.285(3), Au1-Au2 2.9710(4), Au2-S1 2.318(4); P1-Au1-Cl1 172.76(9), C1-Au2-S1 178.5(3), Au1-Au2-Au1' 148.94(2).

Attempts to expand the scope and diversify the PCP Au coordination chemistry were focused on the synthesis of suitable building blocks that could be used to assemble polynuclear structures. In this respect the air stable gold (I) complex, **Au_2-($PC_{NHC}P$)$_2$**, was prepared by the reaction of the imidazolium salt **PCHP** in the presence of a small amount of **$PC_{NHC}P$** (ca. 0.17 equiv) in THF, with the precursor [(Ph_3P)Au{$N(SiMe_3)_2$}] featuring the strong internal base $N(SiMe_3)_2$, the conjugate acid of which is not detrimental to the P-N bonds that are sensitive to protic reagents (Scheme 1). The structure of **Au_2-($PC_{NHC}P$)$_2$** was established crystallographically (Figure 3, see below) confirming its dinuclear nature and a μ_2-**$PC_{NHC}P$** κ*C*,κ*P* bonding mode of the ligand. However, the appearance of the $^{31}P\{^1H\}$ NMR spectrum in CD_2Cl_2 or CD_3CN solutions (two sets of singlets at δ 134.8, 110.6 and δ 132.7, 119.7, in a 1:5 ratio) implies the presence of two, presumably isomeric, species; in the solid-state (CP-MAS ^{31}P NMR spectroscopy) only two singlets (δ 130.8, 115.8) were observed (see Experimental section and Figure 2).

In order to further understand the difference between the solution and the

For references, see P81

solid-state spectra, a variable-temperature $^{31}P\{^{1}H\}$-NMR study was carried out. The complex **Au_2-($PC_{NHC}P)_2$** was dissolved in precooled (-78 ^{o}C) CD_2Cl_2 and the spectra were recorded on a precooled probe, from -60 ^{o}C to room temperature (Figure 2). At -60 ^{o}C, only two singlets are present at δ 131.0 (s) and 117.8 (s), which correspond to the values observed in the solid state (**A** in scheme 2). When the temperature was raised to -20 ^{o}C, the second species (**B** in Scheme 2) appeared initially in a ratio of **B**/**A** of 1/25, which increased to 1/9 at -10 ^{o}C, finally reaching a constant value of 1/5 at 10 ^{o}C. Recooling the sample to -60 ^{o}C did not change this ratio. The chemical shifts of B evidence that it comprises dangling and coordinated P donors and likely an isomer of A. Furthermore, it appears to be thermodynamically more stable than **A** (Scheme 2) and provides a favourably pre-organized disposition of the danging non-coordinated phosphorus atoms to capture another metal cation. This hypothesis may explain the smooth reaction of **Au_2-($PC_{NHC}P)_2$** with $[Au(tht)_2](CF_3SO_3)$ to give the trinuclear **Au_3-($PC_{NHC}P)_2$**. Thus, in the presence of $[Au(tht)_2](CF_3SO_3)$, the equilibrium between **A** and **B** would be shifted in favor of **B** to yield **Au_3-($PC_{NHC}P)_2$,** whereas simple addition products of **A** with $[Au(tht)_2](CF_3SO_3)$ to give tetranuclear complexes, even in the presence of two equivalents of $[Au(tht)_2](CF_3SO_3)$, have never been observed.

For references, see P81

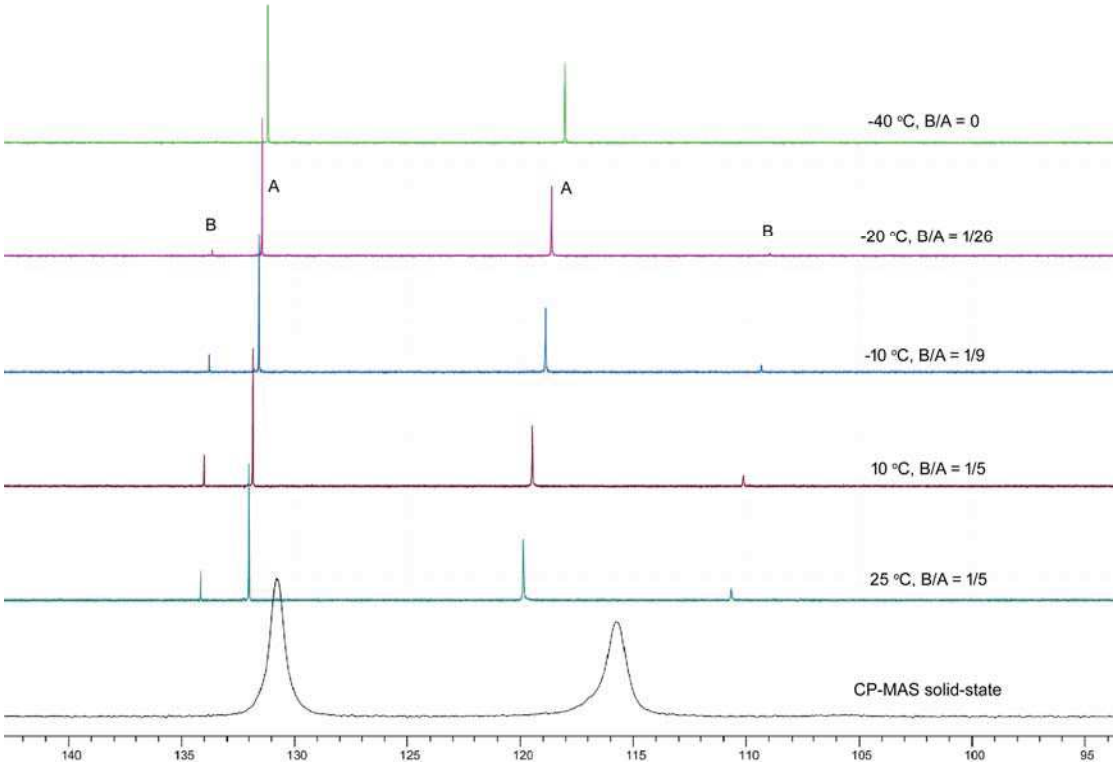

Figure 2. $^{31}P\{^{1}H\}$ NMR spectrum of **Au_2-($PC_{NHC}P)_2$**. (1) In CH_2Cl_2 at different temperatures: -40 °C (green), -20 °C (purple), -10 °C (blue), 10 °C (red), 25 °C (cyan). (2) CP-MAS solid-state (below, black).

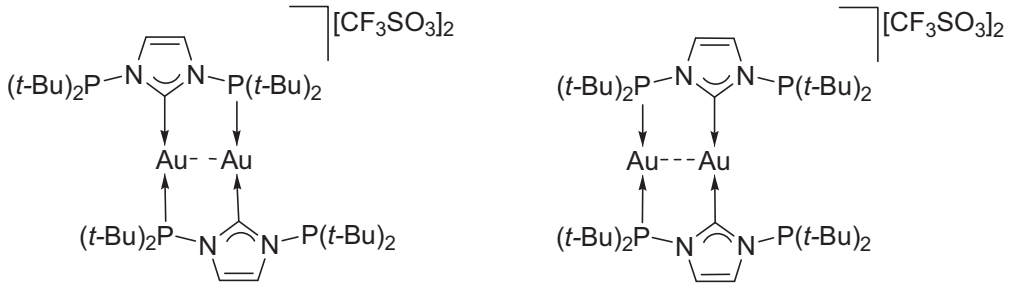

A **B**

Scheme 2. The regioisomers **A** (heteroleptic, C_2) and **B** (homoleptic, C_{2v}) of **Au_2-($PC_{NHC}P)_2$**.

In the solid state the complex **Au_2-($PC_{NHC}P)_2$** is centrosymmetric (C_2) with each of the two **$PC_{NHC}P$** ligands acting as P,C_{NHC} bridge between two Au centers and the remaining P donor dangling; each Au centre is heteroleptic (P and NHC donor sets) in

For references, see P81

a linear geometry (Figure 3).This donor situation is similar to that observed in related digold complexes containing a bidentate P,C_{NHC} ligand.[14b,14c,17] The orientation of the lone pair of the uncoordinated P atoms is the same as that of the coordinated P. The metal-metal separation of 2.8320(6) Å reflects the occurrence of aurophilic interactions but is longer than that in the trinuclear gold complex **Au_3-($PC_{NHC}P)_2$** (2.7584(2) Å). This is consistent with the slight outward bending of the C1-Au1-P1' angle (176.2(2)°) and shows that the shorter metal-metal distances observed in **Au_3-($PC_{NHC}P)_2$** result from the presence of two **$PC_{NHC}P$** ligands spanning the metal-metal chain. We assign this structure to isomer **A**. It is plausible that the species **B** formed in solution is isomeric **A** exhibiting homoleptic (P, P and NHC, NHC donor sets) Au centers with C_{2v} symmetry (Scheme 2).

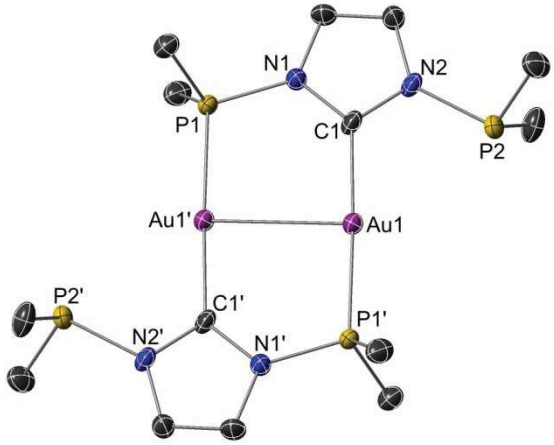

Figure 3. Structure of cationic part of **Au_2-($PC_{NHC}P)_2$**. H atoms and the *t*-Bu Me groups are omitted for clarity. Anisotropic displacement parameters are depicted at the 30% probability level. Selected bond lengths (Å) and angles [°]: Au1-C1 2.038(8), Au1-P1' 2.287(2), Au1-Au1' 2.8320(6), C1-Au1-P1' 176.2(2), C1-N1-P1 124.1(5), C1-N2-P2 118.1(5).

Since it became clear that **Au_2-($PC_{NHC}P)_2$** with the dangling phosphines can be used as precursor to homonuclear complexes of higher nuclearity e.g. **Au_3-($PC_{NHC}P)_2$,** it was also conceivable that hetero-tri nuclear complexes could be become accessible by proper choice of metal precursors. Thus the reaction of **Au_2-($PC_{NHC}P)_2$** with [AgO_3SCF_3] in MeCN afforded the mixed-metal chain complex **Au_2Ag-($PC_{NHC}P)_2$**. The

For references, see P81

$^{31}P\{^{1}H\}$ NMR of the new complex is very informative: one singlet at δ 137.2 corresponds to the phosphine coordinated with Au and two doublets centered at δ 121.7 ($J_{P\text{-}109Ag}$ = 542.9 Hz, $J_{P\text{-}107Ag}$ = 469.5 Hz) correspond to the phosphine coordinated to Ag. Structural elucidation of **$Au_2Ag\text{-}(PC_{NHC}P)_2$** crystallographically clearly established the presence in **$Au_2Ag\text{-}(PC_{NHC}P)_2$** with two adjacent homoleptic gold atoms (P-Au-P and C-Au-C) in a metal chain; however an Ag centre with full occupancy was not unambiguously established. Despite numerous recrystallization attempts, the problem persisted. It appears that the problem is rather a crystallographic artefact (MORE???) since the presence of the P-Ag-P subunit is unambiguously demonstrated by the $^{31}P\{^{1}H\}$ NMR solution data. **$Au_2Ag\text{-}(PC_{NHC}P)_2$** is air-stable and photoluminescent.

Photophysical properties.

The photophysical properties of the novel complex **$Au_3\text{-}(PC_{NHC}P)_2$**, **$Au_3\text{-}PC_{NHC}P$**, **$Au_2\text{-}(PC_{NHC}P)_2$** and **$Au_2Ag\text{-}(PC_{NHC}P)_2$** were investigated by means of steady state and time-resolved techniques. The electronic absorption spectrum of the complexes in dilute condition in either MeCN or CH_2Cl_2 solution is depicted in Figure 4 and the photophysical data are listed in Table 1.

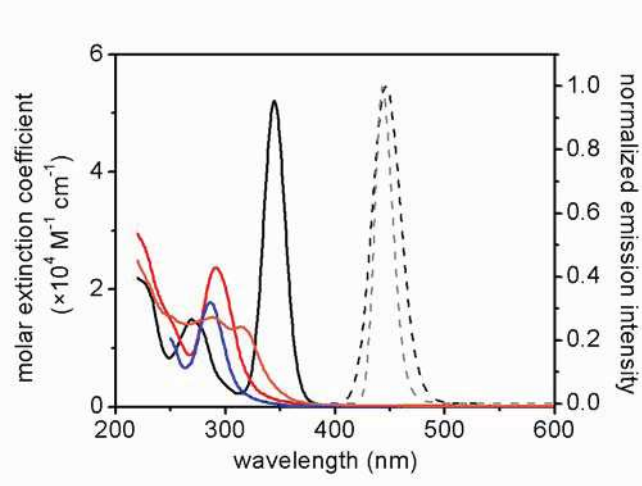

Figure 4. Electronic absorption spectrum for **$Au_3\text{-}(PC_{NHC}P)_2$** (black), **$Au_2\text{-}(PC_{NHC}P)_2$** (red) and **$Au_2Ag\text{-}(PC_{NHC}P)_2$** (orange) in MeCN and **$Au_3\text{-}PC_{NHC}P$** (blue) in CH_2Cl_2 are displayed as solid traces. Normalized emission intensity (dashed traces) for complex

For references, see P81

Au_3-($PC_{NHC}P)_2$ in MeCN at room temperature (black) and 77 K frozen matrix (grey) upon excitation at λ_{exc} = 340 nm.

As far as the experimental spectra are concerned, the electronic absorption of complex **Au_3-($PC_{NHC}P)_2$** in CH_3CN is characterized by narrow intense featureless bands in the ultraviolet region with λ_{max} = 345 and 270 nm ($\varepsilon = 5.21\times10^4$ and 1.49×10^4 M^{-1} cm^{-1}, respectively). The former can be attributed to the spin- and optically-allowed singlet-manifold $^1[5d\sigma^*\rightarrow6p\sigma]$ transition with strong metal centered (MC) character. Ideally, such optical excitation process can be seen such as promotion of the electronic density from the anti-bonding d_z^2 to the bonding $6s/6p_z$ orbital, where *z* represent the Au···Au···Au interaction axis, and increasing metal···metal interaction (see also computational section). The higher-energy band observed in the absorption to the singlet-manifold transition involving the NHC units with admixed intraligand (^{1}IL) and ligand (phosphine) to metal-ligand (Au–NHC) charge transfer ($L_PML'_{NHC}CT$) nature. Such assignments were made also as comparison with similar previously reported Au(I) complexes,[5d,10a] also bearing optically transparent phosphine ligands.[2d] Noteworthy, such intense lower energy band is absent for complex **Au_2-($PC_{NHC}P)_2$** and **Au_3-$PC_{NHC}P$**, while their absorption spectra are characterized by a slightly more intense ^{1}IL bands at λ_{max} = 292 ($\varepsilon = 2.37\times10^4$ M^{-1} cm^{-1}) and 286 nm ($\varepsilon = 1.78\times10^4$ M^{-1} cm^{-1}), respectively. Moreover, dilute sample of complex **Au_2Ag-($PC_{NHC}P)_2$** in CH_3CN display relatively intense band in the region 315–247 nm ($\varepsilon \approx 1.3 - 1.6 \times10^4$ M^{-1} cm^{-1}) attributable to a combination of spin-allowed ^{1}ILCT and ^{1}MLCT excitation processes.

To further investigate the nature of the absorption transition for complex **Au_3-($PC_{NHC}P)_2$**, a solvent effect study was carried out and the photophysical properties recorded in CH_3CN compared with those in CH_2Cl_2 and DMF solution and the results are displayed in Figure 5 and listed in Table 2. As shown in Figure 5, the lowest-energy absorption band did not show any modulation of the absorption max upon variation of the solvent polarity ruling out any charge transfer (CT) nature in the excitation process and supporting the assignment of a mainly metal-centered (MC)

For references, see P81

nature of the transition. Although, a neat decrease of the extinction coefficient was observed when DMF – a more polar solvent with better solvation ability for ionic compounds – was used. This finding may indicate a partial involvement of the triflate counterion into coordination sphere around the trinuclear complex influencing the electronic ground-state properties of the latter and/or an involvement of the solvent molecules with high donor number into the coordination sphere of the complex.[2d] On the other hand, a slight modulation of the absorption maximum at higher energy was found going form the more polar CH_3CN to the less polar CH_2Cl_2 (λ_{abs} = 270 *vs.* 278 nm, respectively), confirming the partial CT nature of the transition involved.

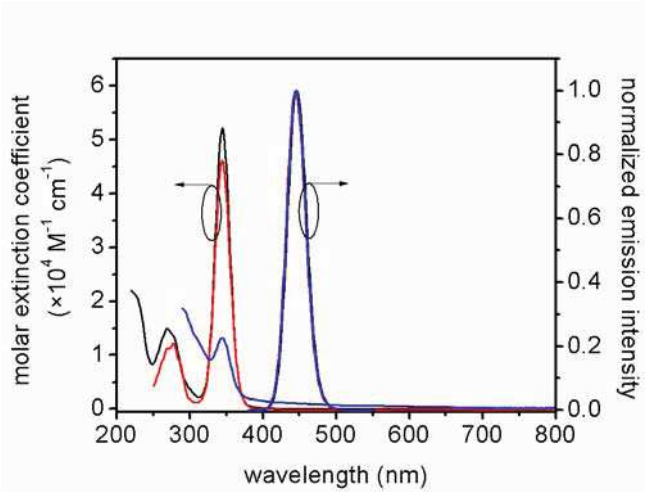

Figure 5. Electronic absorption and normalized emission spectra for **Au_3-($PC_{NHC}P)_2$** in MeCN (black), CH_2Cl_2 (red) and DMF (blue) recorded at room temperature upon excitation at λ_{exc} = 350 nm.

For references, see P81

Table 1. Photophysical data obtained for complex **Au_3-($PC_{NHC}P)_2$**, **Au_2-($PC_{NHC}P)_2$** and **Au_2Ag-($PC_{NHC}P)_2$** in MeCN and **Au_3-$PC_{NHC}P$** in CH_2Cl_2 in dilute condition at room temperature and in frozen matrix at 77 K.

	room temperature						*77 K matrix*	
cmpd	λ_{abs} (ε) [nm, ($\times 10^4$ M^{-1} cm^{-1})]	λ_{em} [nm]	τ	PLQY[a] (%)	τ μ	PLQY[b] (%)	λ_{em} [nm]	τ μ
Au_3-($PC_{NHC}P)_2$	345 (5.21), 270 (1.49), 225 (2.14)	446	510	11	3.9	82	443[e]	4.2[e]
Au_2-($PC_{NHC}P)_2$	292 (2.37), 246sh (1.63), 225 (2.79)	446, 560	–	–	4.0[c] 6.9 (64%)[d] 1.6 (36%)	–	527[e]	16.6[e]
Au_2Ag-($PC_{NHC}P)_2$	315 (1.36), 288 (1.53), 247sh (1.56), 229sh (2.14)	442	–	–	–	–	415, 515	1.8 (65%) 4.3 (35%)[g] 8.7 (71%)[h] 2.1 (29%)
Au_3-$PC_{NHC}P$	286 (1.78)	719	–	–	5.9 (66%) 0.85 (34%)	0.8	440[f]	1.4 (36%)[f] 3.8 (64%)

[a] air-equilibrated ; [b] degassed; [c] λ_{em} = 447 nm; [d] λ_{em} = 520 nm; [e] in CH_3CN; [f] in CH_2Cl_2:EtOH 1:4; [g] recorded at λ_{em} = 410 nm; [h] recorded at λ_{em} = 550 nm; [sh] denotes a shoulder

For references, see P81

Table 2. Photophysical data obtained for the solvent effect carried out on dilute samples of complex **Au_3-($PC_{NHC}P)_2$** in CH_2Cl_2 and DMF at room temperature. Data in MeCN are also reported for sake of comparison. The samples were excited at λ_{exc} = 350 nm.

		a			*d*	
	λ_{abs} (ε) [nm, ($\times 10^4$ M^{-1} cm^{-1})]	λ_{em} [nm]	τ μ	PLQY (%)	τ μ	PLQY (%)
MeCN	345 (5.21), 270 (1.49), 225 (2.14)	446	510	11	3.9	82
CH_2Cl_2	344, (4.61), 278 (1.22), 270 (1.13)	445	1.1	27	3.0	74
DMF	345 (1.32)	445	0.193 (17%) 0.061 (11%) 0.009 (72%)	5	2.0	35

Upon photoexcitation in the region 290–300 nm at room temperature, dilute samples of complex **Au_2-($PC_{NHC}P)_2$** clearly show an irradiation-time dependent emission spectrum as displayed in Figure S1 (see ESI). As for comparison of the excitation spectra with the electronic absorption profile, it appears that upon irradiation of **Au_2-($PC_{NHC}P)_2$** at λ_{exc} = 290 nm, the photochemical product is most likely the trinuclear **Au_3-($PC_{NHC}P)_2$** derivative, due to the close resemblance of the excitation spectra recorded at λ_{em} = 450–470 nm with respect to the corresponding absorption spectrum of **Au_3-($PC_{NHC}P)_2$** (Figure 4 and Figure S1 in ESI). Also, sequential emission spectra upon photoirradiation of a solution of complex **Au_2-($PC_{NHC}P)_2$** shows

For references, see P81

a clear presence of an isosbestic point at about λ_{em} = 480 nm, supporting the idea that the rise of the chemical species associated to the emission band at higher energy is a direct consequence of the photochemical degradation of the parental dinuclear complex. Nonetheless, such photodegradation process appears slower upon degassing the sample by freeze-pump-thaw (see Figure S1 in ESI).

Emission spectra for complex **Au_2Ag-$(PC_{NHC}P)_2$** in dilute MeCN are displayed in Figure S2 (ESI). The sample showed at emission maximum centered at 442 nm during the first emission measurement, but a steady decrease of the emission intensity and the concomitant appearance of a second band at longer wavelength is visible, attributable to a photodecomposition product during the experiment.

On the other hand, upon irradiation at λ_{exc} = 290 nm, complex **Au_3-$PC_{NHC}P$** in dilute degassed CH_2Cl_2 displays a rather weak (PLQY = 0.8%) luminescence with a broad and featureless profile centered at λ_{em} = 719 nm, with an excitation spectrum that overlaps the electronic absorption profile and a bi-exponential decay kinetics of τ_1 = 850 ns (34%) and τ_2 = 5.9 μs (66%) (Table 2 and Figure S1 in ESI).

Noteworthy, upon irradiation at the lower energy absorption band at λ_{exc} = 300–350 nm, dilute samples of complex **Au_3-$(PC_{NHC}P)_2$** display a wavelength-independent highly intense emission spectrum with narrow profile and λ_{em} = 446 nm (see Figure 4) with a Stokes shift as small as 6560 cm^{-1}. The excitation spectrum recorded at such emission band nicely corresponds to the absorption profile as displayed in Figure S3 (ESI). Going from air-equilibrated to degassed condition **Au_3-$(PC_{NHC}P)_2$** samples did not show any change in the emission profile, yet, a strong increase of the photoluminescence quantum yield, namely PLQY, was observed with values going from 0.11 to as high as 0.82. The increase of PLQY was mirrored by a concomitant prolongation of the excited state lifetime from 510 ns to 3.9 μs, respectively, which strongly supports the triplet-manifold nature of the emitting excited-state. Noteworthy, the recorded chromaticity based on the 1931 Commission Internationale de l'Eclairage coordinates, CIE(*x*,*y*), is *x* = 0.157, *y* = 0.024, corresponding to a saturated blue-violet emission (*i.e.*, $x \approx 0.15$, $y < 0.08$). To further investigate the nature of the radiative process involved in such strong emission, the

For references, see P81

photoluminescence properties upon solvent polarity variation were investigated (Table 2 and Figure 5). The independence of the solvent polarity onto the emission energy as well as the dependence of the excited state lifetime and PLQY on the presence of quenching dioxygen support triplet-manifold MC character of the emitting state that can be described as to be ^{3}[5dσ*6pσ] in nature, similarly to what reported for closely-related Au(I) complexes.[2d,5d]

Moving from fluid solution at room temperature to glassy matrix at 77 K, samples of **Au_3-($PC_{NHC}P$)$_2$** in frozen CH_3CN matrix show a bright emission that is only slightly hypsochromically shifted (152 cm^{-1}) with respect to the profile recorded at room temperature (see Figure 4, grey trace and Figure S3 in ESI) pointing towards a low charge transfer character of the emitting excited state. The excitation spectrum recorded upon monitoring such emission band nicely corresponds to the electronic absorption spectrum at room temperature, indicating that the origin of such photoluminescence process is the same in both cases. Similarly to the room temperature, compound **Au_2-($PC_{NHC}P$)$_2$, Au_2Ag-($PC_{NHC}P$)$_2$** and **Au_3-$PC_{NHC}P$** clearly shows a photochemical degradation process that was even faster for the **Au_2-($PC_{NHC}P$)$_2$** and **Au_3-$PC_{NHC}P$** species (see Figure S4 in ESI).

Finally, the photoluminescence properties in solid state as neat samples were investigated and the corresponding data are shown in Figure 6 and listed in Table 3. While Au2 is not photostable even in the solid state as neat powder (data not shown), complex **Au_3-($PC_{NHC}P$)$_2$** and **Au_2Ag-($PC_{NHC}P$)$_2$** display a very strong emission band centered at λ_{em} = 442 and 404 nm, respectively. As far as complex **Au_3-($PC_{NHC}P$)$_2$** is concerned, the emission maximum and photoluminescence profile is very similar to the spectra recorded in CH3CN solution and PLQY retains the high value of 80%. On the basis of such similarities we can attribute such radiative process to an emission with mainly ^{3}[5dσ*6pσ] character.

Table 3. Photophysical data obtained for complex **Au_3-($PC_{NHC}P$)$_2$, Au_3-$PC_{NHC}P$** and **Au_2Ag-($PC_{NHC}P$)$_2$** in solid state as neat powder.

For references, see P81

	λ_{em} [nm]	τ μ	PLQY (%)
Au_3-($PC_{NHC}P$)$_2$	442	2.7	80
Au_3-$PC_{NHC}P$	665	– [a]	– [a]
Au_2Ag-($PC_{NHC}P$)$_2$	404	0.83 (42%) 1.8 (58%)	38

[a] emission too weak to be recorded.

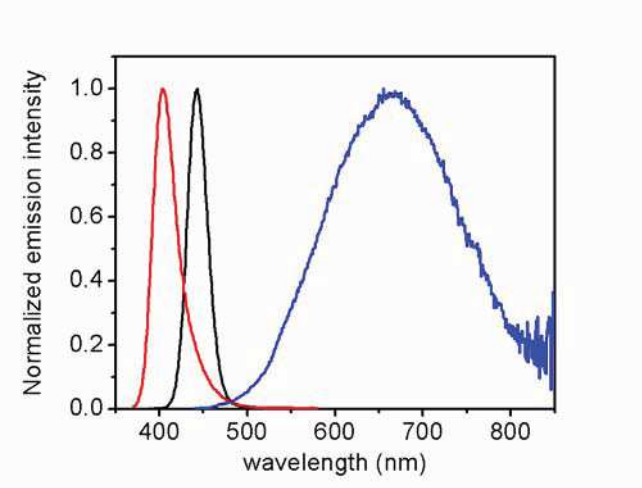

Figure 6. Emission spectra of complex **Au_3-($PC_{NHC}P$)$_2$** (black trace), **Au_3-$PC_{NHC}P$** (blue trace) and **Au_2Ag-($PC_{NHC}P$)$_2$** (red trace) in solid state as neat powder upon excitation at λ = 300 nm.

Electrochemical Characterization.

The electrochemical properties have been investigated in acetonitrile using two different types of supporting electrolytes, namely $TBAPF_6$ and NaOTf. The reduction potentials, $E°_{red}$, associated with the Au centers reduction process over scan rate in the range 0.05–1 V s^{-1} are listed in Table 4, while the corresponding cyclic voltammogramms are displayed in Figure 7.

Table 4. Electrochemical data of complex **Au_3-($PC_{NHC}P$)$_2$** in MeCN with two different types of electrolytes, using GC as working electrode. [a] Potential referred to the

For references, see P81

couple Fc/Fc^+. All the processes were found to be irreversible.

scan rate [mV s^{-1}]	$E°_{,red}$ [a] $TBAPF_6$ [V]	$E°_{,red}$ [a] NaOTf [V]
50	–1.53, –1.95, –2.50	–1.55, –2.00
100	–1.54, –1.95, –2.43	–1.55, –2.00
200	–1.55, –1.96, –2.41	–1.55, –2.01, –2.17
500	–1.57, –1.99, –2.41	–1.60, –2.04, –2.19
1000	–1.58, –2.02, –2.43	–1.62, –2.06, –2.24

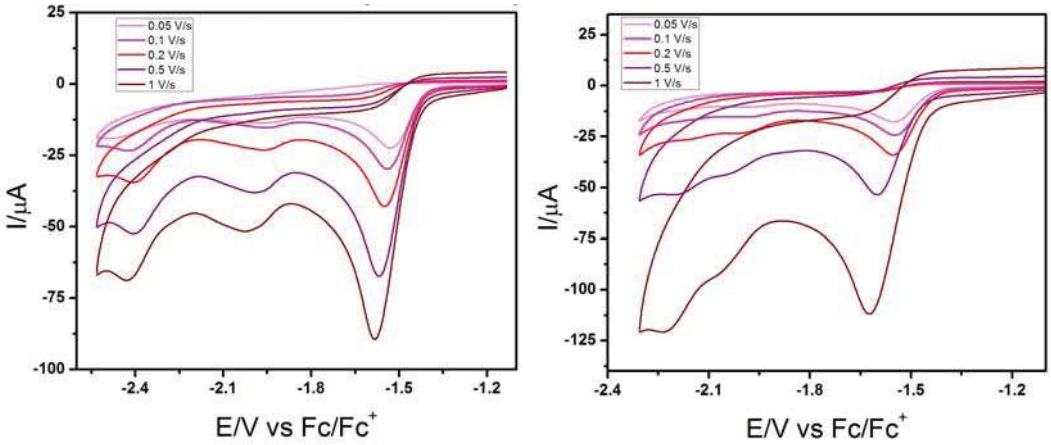

Figure 7. Cyclic voltammogramms recorded for the complex **Au_3-($PC_{NHC}P)_2$** in CH_3CN at concentration of 1 mM, using 0.1 M $TBAPF_6$ (left) and NaOTf (right) as supporting electrolyte and GC as working electrode. Scan rate 0.05–1 V s^{-1}.

In MeCN containing 0.1 M $TBAPF_6$, the trinuclear complex does not show any anodic peak attributable to the oxidation of the metal center, while it displays well-defined cathodic processes attributable to the reduction of the metallic centers. The cathodic peaks are irreversible because of the instability of reduced species formed electrochemically upon potential scan. In fact, cyclic voltammetry performed at scan rates slower than 0.05 V s^{-1} has shown that after the first scan no more peaks in reduction can be observed. When the supporting electrolyte is changed from $TBAPF_6$ to NaOTf, the clear presence of the higher potential peak (*i.e.*, more negative

For references, see P81

value) is scan-rate dependent and it is only visible at higher scan rate (*i.e.*, 0.2–1 V s^{-1}). Such finding can be explained on the basis of the different supporting electrolyte employed and indeed it is already reported in literature that this can have an effect on the relative electrochemical spacing of the different potentials (Figure 8). [18]

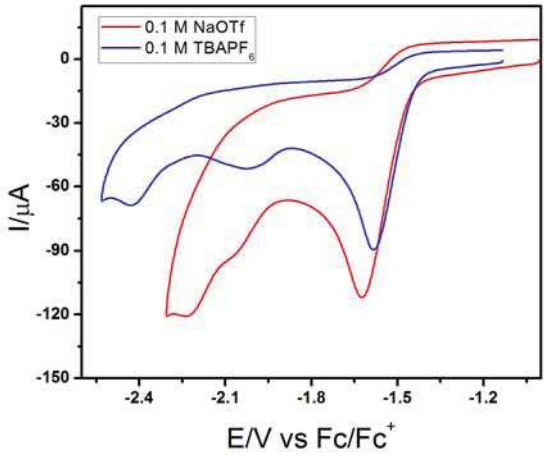

Figure 8. Cyclic voltammogramms recorded for complex **Au_3-($PC_{NHC}P)_2$** in 1 mM CH_3CN, using 0.1 M $TBAPF_6$ (blue trace) and NaOTf (red trace) as supporting electrolyte and GC as working electrode. Scan rate is 1 V s^{-1}.

To better visualize the different electrochemical processes present, differential pulsed voltammetry (DPV) has been performed also by employing the two different supporting electrolytes and the corresponding data are displayed in Figure 9.

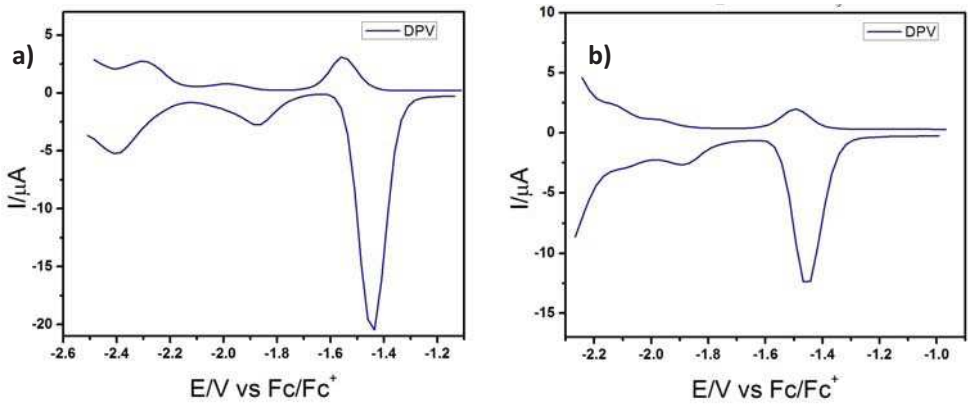

Figure 9. Differential pulsed voltammogramms recorded for complex **Au_3-($PC_{NHC}P)_2$** in CH_3CN at concentration of 1 mM using a) 0.1 M $TBAPF_6$ and b) NaOTf as supporting electrolyte and GC as working electrode. Pulse height is 0.025 V.

For references, see P81

Firstly, it is important to notice that there is an interaction between the anions produced at the end of the electrochemical process and the electrolyte cations, which in this case changes from tetrabutylammonium (TBA^+) to sodium. This interaction can lead to a variation in the $\Delta E_{1/2}$ that increases going from Na^+ to TBA^+ (Figure 9–10). Indeed, the TBA^+ stabilizes better the anion produced during the reduction process, leading to a more difficult reduction of the second metal center. When Na+ is employed, this stabilization effect appears to be lower yielding much closer cathodic waves to such an extent that they collapse in only one peak at slower scan rate.

Secondly, the NaOTf decreases the electrochemical window of MeCN and in particular in the cathodic side because it is not resistant to the reduction.

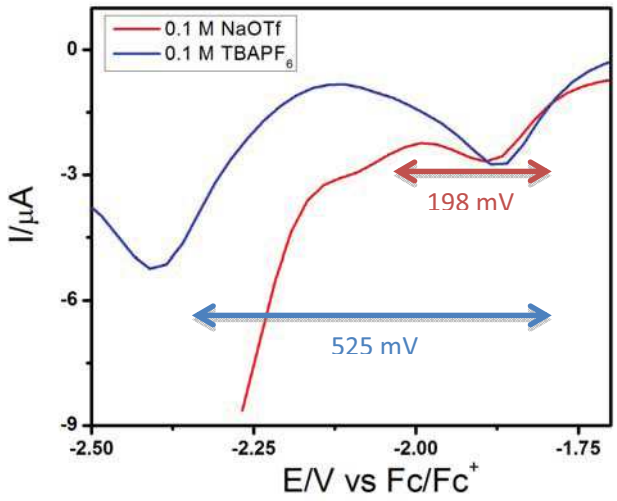

Figure 10. Differential pulsed voltammogramms recorded for complex **Au_3-($PC_{NHC}P)_2$** in MeCN at concentration of 1 mM, using a) 0.1 M $TBAPF_6$ (blue trace) and b) NaOTf (red trace) as supporting electrolyte and GC as working electrode. Pulse height is 0.025 V.

The redox behavior of molecules containing multiple (formally) chemically equivalent redox centers is well documented in the literature. [19] In the present case,

For references, see P81

the electron density is not the same for each of the three gold centers, but all of them are formally Au(I). Then, the possible redox reactions occurring on the system Au(I)-Au(I)-Au(I) are the following:

$Au(I)\text{-}Au(I)\text{-}Au(I) + e^- \rightarrow Au(0)\text{-}Au(I)\text{-}Au(I)$ $\quad E^0_1$ (eq.1)

$Au(0)\text{-}Au(I)\text{-}Au(I) + e^- \rightarrow Au(0)\text{-}Au(I)\text{-}Au(0)$ $\quad E^0_2$ (eq. 2)

$Au(0)\text{-}Au(I)\text{-}Au(0) + e^- \rightarrow Au(0)\text{-}Au(0)\text{-}Au(0)$ $\quad E^0_3$ (eq. 3)

On the basis of the chemical structure of the **Au_3-($PC_{NHC}P)_2$** complex and the different electronic properties of the ligands coordinated on the gold atoms, it seems plausible that the internal Au atom, coordinated to strong σ-donating NHC moieties, bears a slightly higher electron density when compared to the two external metal atoms. For this reason, the two external metal centers are expected to be easier to reduce when compared to the central atom, since the former are more electron-poor, while the most negative potential is attributable to the latter bearing higher electron density. The difference between E^0_1, E^0_2 and E^0_3 is related to the interaction between the two metal centers: the higher the electronic communication between the metal centers, the greater the separation between their electrochemical potentials. Indeed, a weak interaction is expected to cause splitting of the processes into closely separated peaks as already reported.[20]

Computational Studies.

Structures in gas phase

In order to gain insight into the electronic structures of **Au_3-($PC_{NHC}P)_2$** and **Au_2-($PC_{NHC}P)_2$** and rationalize their photophysical behaviour calculations were performed **XXXX**, The main geometric parameters of the complex optimization at various level of calculation are given in Table 5. For all the functional tested, the Au-Au and Au-P distances are overestimated even with the inclusion of dispersion corrections. On the contrary, the MP2 calculation is in very close to agreement with

For references, see P81

the experimental data, despite a slight underestimation of the Au-C distance. The better agreement of MP2 calculations with the experimental data proves the role played by static correlation effects on the gold interaction. In contrast, the weak influence of dispersion corrections on the geometric parameters suggests that the short distance between the Au centres has not its origin in such interactions.

Table 5. Important interatomic distances (Å) in the **Au_3-($PC_{NHC}P)_2$** in gas phase. The terminal Au atoms are designated by Au(1) and the central by Au(2). The ending +D denotes the inclusion of dispersion corrections in DFT calculations.

Method	P-Au(1)	Au(1)-Au(2)	Au(2)-C
BLYP	2.407	2.880	2.076
BLYP+D	2.382	2.881	2.068
BP86+D	2.350	2.828	2.046
B3LYP	2.378	2.903	2.054
B3LYP+D	2.374	2.880	2.055
MP2	2.315	2.762	2.022
Experimental	2.315	2.758	2.068

A very similar picture has emeged for **Au_2-($PC_{NHC}P)_2$**. Relevant data are given in Table 6. Here too, DFT overestimates the bond distances, even with dispersion corrections, and MP2 gives very accurate results.

Table 6. Important interatomic distances (Å) in **Au_2-($PC_{NHC}P)_2$** in gas phase. The ending +D denotes the inclusion of dispersion corrections in DFT calculations. The non-bonded distance between the Au and the dangling P is quoted as P(NB).

Method	P-Au	Au-Au	Au-C	Au-P(NB)
B3LYP+D	2.334	2.939	2.078	3.390
MP2	2.297	2.821	2.021	3.342
Experimental	2.286	2.830	2.057	3.298

For references, see P81

Absorption spectroscopy

The theoretical absorption spectra of **Au_3-($PC_{NHC}P)_2$** are depicted in Figure 11. Focussing on the two absorption bands between 250 to 500 nm, the lowest localized at 342 nm, corresponds to the peak found experimentally at 350 nm, and that at 285 nm was found experimentally at 275 nm. Both peaks are generated by two pure electronic transitions; an additional peak found at 374 nm has no absorption intensity, however there are no other lower energy transitions (wavelength longer than 285 nm).

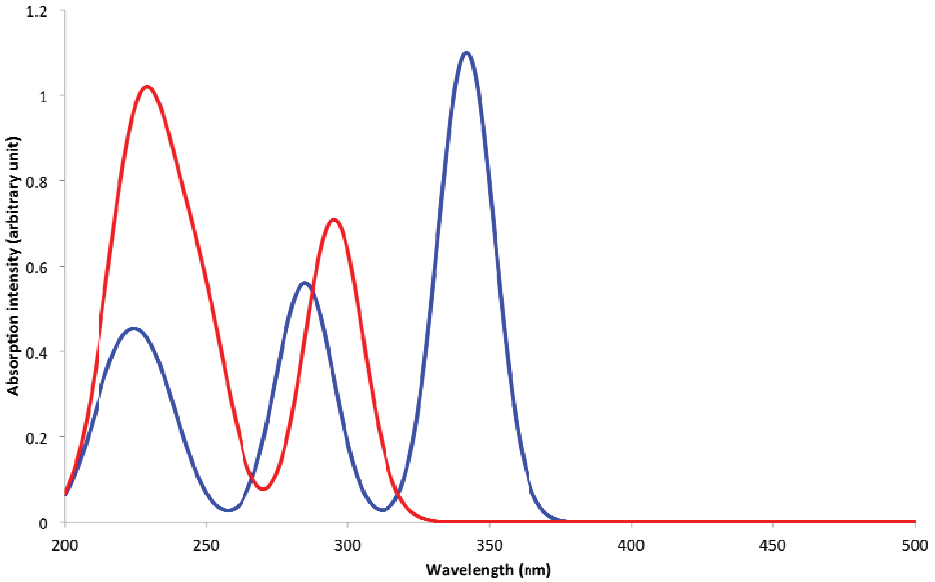

Figure 11. Theoretical absorption spectra of **Au_3-($PC_{NHC}P)_2$** (in blue) and **Au_2-($PC_{NHC}P)_2$** (in red).

The three transitions (S1 = 374 nm, S2 = 342 nm and S3 = 285 nm) possess a Metal-Center (MC) component associated with Metal-to-Ligand Charge Transfer (MLCT) or Ligand-to-Metal Charge Transfer (LMCT); the nature of the three transitions is given in detail in Figure 12. . In S1 and S2, the electron leaves a gold σ* orbital generated by the antibonding combination of the $5d_{x2-y2}$ of the three gold cations. In S1, the orbital populated is a π bonding orbital between the central gold cation and the NHC; in S2, it is mainly a σ gold orbital generated the bonding

For references, see P81

combination of the empty 6pz orbitals of the three cations. S3 is different as it mostly consists in a $\pi-\pi^*$ transition localised on the central gold cation and the NHCs.

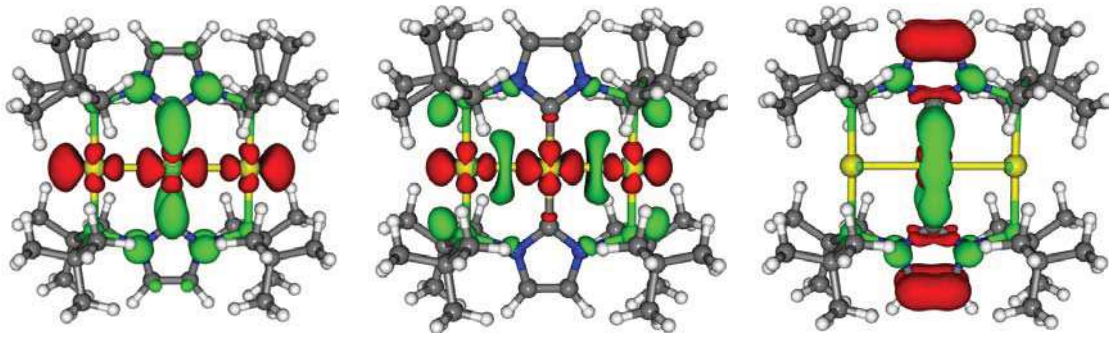

Figure 12: Electronic density differences between the ground state and the excited state for S1 (left), S2 (middle) and S3 (right). The areas in red correspond to electronic depletion and areas in green to electronic enrichment.

The absorption spectrum of the **Au_2-($PC_{NHC}P)_2$** is blue shifted compared to that of **Au_3-($PC_{NHC}P)_2$**. The theoretical absorption spectrum of the former exhibits two peaks at 295 (referred to as DS3) and 225 nm (see Figure 12). However, these peaks do not correspond to the lowest electronic transition. Two singlets are located at 335 (DS1) and 308 (DS2) nm but with no absorption intensities. The peak at 295 nm (DS3) is generated by only one transition the nature of is detailed in Figure 14. The nature of these transitions is similar to those of **Au_3-($PC_{NHC}P)_2$** with one major difference: the involvement of the dangling phosphorus atom in the transition. Indeed, the DS1 transition consists on an excitation of an electron from a σ antibond between the gold atoms and the dangling phosphorus to a bonding p orbital between the gold cation and the carbon of the NHC. This is very similar to the S1 transition of the **Au_3-($PC_{NHC}P)_2$**. We can also associate the DS3 transition to the S2 of the PCP-Au3. The DS2 is the only transition with no MC character and is a mixed MLCT and Ligand Centred (LC) state.

For references, see P81

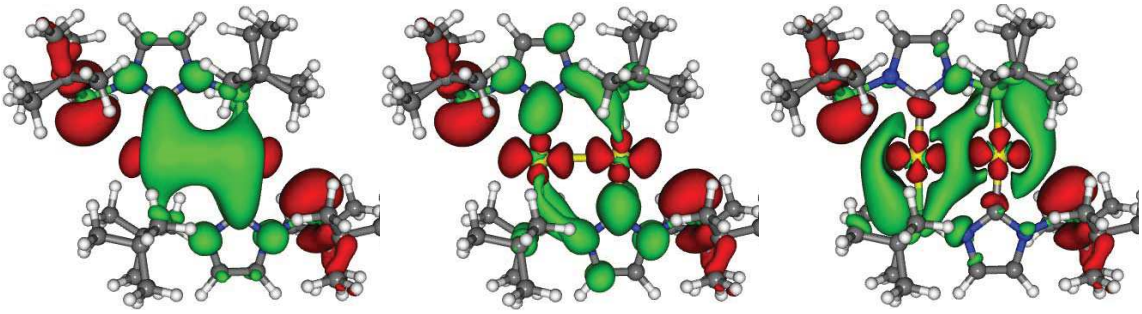

Figure 13. Electronic density differences between the ground and the excited state for DS1 (left), DS2 (middle) and DS3 (right). The areas in red correspond to electronic depletion and areas in green to electronic enrichment.

Emission properties

Based on the computed absorption spectra of **Au_3-($PC_{NHC}P)_2$**, we next focused on the two lowest triplet states, which are of the same nature as the lowest singlets see Figure 14. The main geometric parameters and emission wavelength associated to these triplets state are given in Table 7.

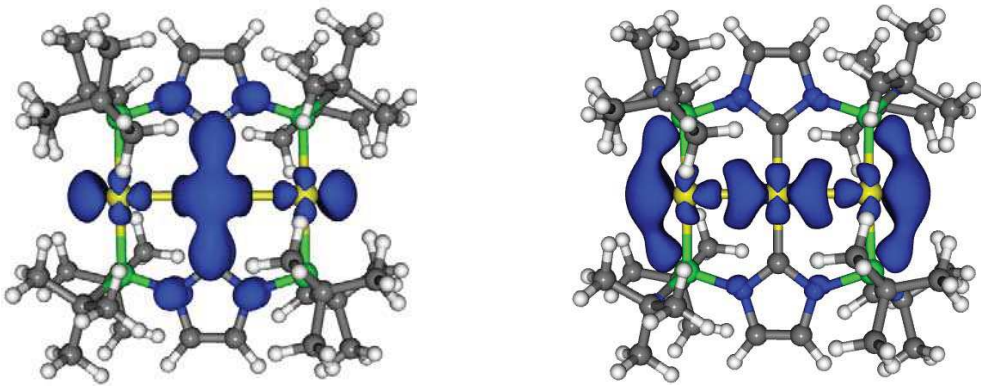

Figure 14. Spin density of the optimized triplet T1 (left) and T2 (right).

For references, see P81

Table 7. Important interatomic distances (Å) of **Au_3-($PC_{NHC}P)_2$** in solution and emission wavelength (in nm) computed by ΔSCF and TD-DFT.

	Fundamental	T_1	T_2
λ_{em} (ΔSCF)		421	409
λ_{em} (TD-DFT)		442	420
Au-P	2.368	2.369	2.345
Au-C	2.048	2.032	2.058
Au-Au	2.865	2.740	2.711

These two triplet states are almost degenerate; T2 (triplet counterpart of S2) is only 0.5 kcal.mol^{-1} more stable than T1 (triplet counterpart of T2), which is not significant at our level of calculation. However, the theoretical emission wavelength of both is very close to the experimental one. Furthermore, the small difference between the emission wavelengths of the two states is also consistent with the experimental narrow emission peak.

Upon geometry optimization, a contraction of the Au-Au distances was observed in both states compared to the geometry of the ground state. This is due to the depopulation of the Au-Au antibond, and for T2 to the population of a σ bonding orbital leading to a greater contraction compared to T1. Simultaneously, we observe for T1 a small contraction of the Au-C distance due to the population of the π Au-C bonding orbitals. In contrast,,this distance increase in T2 compared to the ground state. Eventually, the Au-P distance is not affected in T1 but is slightly reduced in T2.
Theoretical results suggest that both triplets are emissive. This feature can be related to the experimental excitation spectrum. In this spectrum, the experimental peak at 350 splits into two peaks shifted towards red and blue compared to the initial one. On the optimized geometries of T1 and T2, if we perform a TD-DFT on singlet wavefunctions we retrieve a similar feature. On T1 geometry, S2 is blue shifted and absorbs at 340 nm. On T2 geometry, S2 is slightly red shifted and absorbs at 354 nm compared to 352 nm for S2 at the ground state geometry. In consequence, we

For references, see P81

propose that experimentally T1 and T2 states emit and are at the origin of the feature experimentally observed on the excitation spectra.

The presence of a free phosphorus atom has a great influence on the emission properties of **Au_2-($PC_{NHC}P)_2$**. As for **Au_3-($PC_{NHC}P)_2$**, we only optimized the two lowest triplet states referred as DT1 and DT2, (Table 8). reported

Table 8. Important interatomic distances (Å) in **Au_2-($PC_{NHC}P)_2$** in solution and emission wavelength (in nm) computed by ΔSCF and TD-DFT.

	Fundamental	DT1	DT2
λ_{em} (ΔSCF)		532	500
λ_{em} (TD-DFT)		559	520
Au-P	2.334	2.352	2.371
Au-C	2.078	2.035	2.045
Au-Au	2.939	2.774	2.832
Au-P(NB)	3.390	2.880	2.861

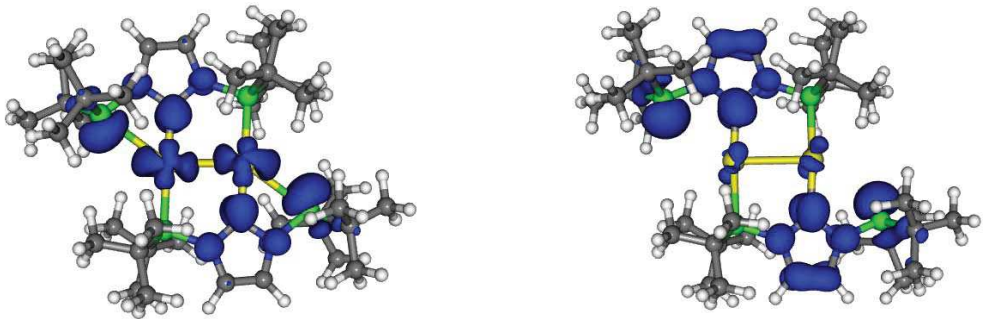

Figure 15. Spin density of the optimized triplet DT1 (left) and DT2 (right).

The nature of the triplet is detailed in Figure 15. The DT1 state is the triplet counterpart of DS1 transition. The situation is less clear for DT2, the contribution of the gold atom in the transition is smaller with less spin density localized on the gold atom. Energetically, there is no ambiguity: the two triplets are well separated, the

For references, see P81

DT1 state is more stable by 7.5 kcal.mol^{-1} compared to DT2. Furthermore, they are subject to greater geometry distortions. Again, we observed a contraction of the Au-Au distance in the excited states and to a lesser extent a Au-C contraction and Au-P elongation. However, the main point is the behaviour of the dangling phosphorus. Upon excited state geometry optimization, the Au-P(NB) distance shortens by as much as 0.5 Å, tending to a square planar ligand field around the gold cation. This change in the gold coordination sphere may explain the greater stabilisation of the excited state compared to the **Au_3-($PC_{NHC}P$)$_2$**. In **Au_2-($PC_{NHC}P$)$_2$**, the absorption is blue shifted whereas the emission is red-shifted. The presence of an available free donor ?? in the surroundings of the partially oxidized cations stabilizes the excited state.

Raman Spectra of Au_3-($PC_{NHC}P$)$_2$

Raman spectra of powder sample of **Au_3-($PC_{NHC}P$)$_2$** complex, collected by using the 473, 532 and 633 nm excitations are displayer in Figure 16. Raman spectra evolved with the excitation wavelengths due to the pre-resonance condition associated to the XXXX transition (absorption maximum around 344 nm). Consequently, several Raman features were observed to enhance when the blue excitation was used. Vibrational spectrum was interpreted according to previous analysis of the vibrations of several molecules containing phosphine, imidazole and Au-Au moieties.[21] In addition quantum chemical calculations were also performed to help to the interpretation of the Raman spectrum, in special the Au-Au stretching vibration. Both symmetric and asymmetric Au-Au-Au stretching modes are expected in vibrational spectra. However, due to the symmetry of the complex (C_{2h}) only the Au-Au-Au symmetric stretching mode is Raman active (asymmetric motion is only IR active) with a fundamental predicted near to 83 cm^{-1}. In our experiments, we observe a Raman band centered to 91 cm^{-1} which was observed strongly to enhance when the blue excitation was used. This vibration can be attributed to the Au-Au-Au symmetric stretching mode of the **Au_3-($PC_{NHC}P$)$_2$** complex on the basis of the comparison with theoretical calculations and the Au-Au stretching vibration of similar compounds investigated

For references, see P81

previously.[21c,21e,21f] The main experimental Raman bands with their proposed assignment are summarized in Table 9.

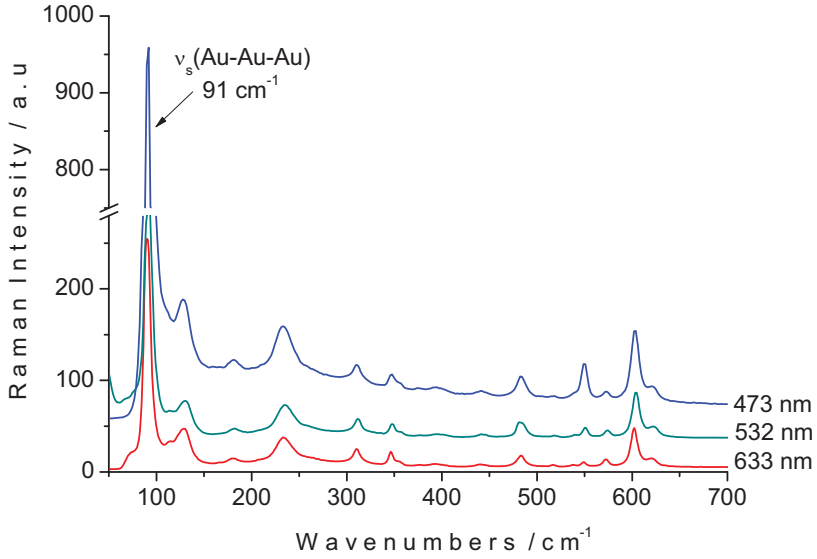

Figure 16. Raman spectra using 473, 532 and 633 nm excitation lines of a solid sample of **Au_3-($PC_{NHC}P)_2$** at room temperature, in the 50–700 cm^{-1} region.

Table 9. Selected experimental Raman and calculated wavenumbers of the **Au_3-($PC_{NHC}P)_2$** complex and proposed assignments

Assignments [a]	**Symmetry**	**Experimental wavenumbers (cm^{-1})**
ν $(CC)_{ring}$	Ag	1562
ν_s (CAuC) + ν_s(NCN)	Ag	1316
$\nu_{ring\ breathing}$	Ag	1206
ν_s $(CN)_{ring}$	Ag	1111
ν_s (CC)	Ag	800
	Bg	
	Ag	
	Bg	
ν_{as}(C-P-C)	Bg	621

For references, see P81

ν_s(C-P-C)	Ag	602
ν (NP)	Ag	550
δ (CPC)	Ag	482
δ (CCP)	Ag	234
ν_{as} (PAuP)	Bg	129
δ (CPN)	Ag	114
ν_s (AuAuAu)	Ag	91

[a] Meaning of symbols: ν_s, symmetric stretching; ν_{as}, asymmetric stretching; δ, deformation

Conclusions

We have provided a new synthetic route for **PCP-Au3** from the transmetallation reaction of **PCP-Ag3** with [AuCl(tht)], which also gave one byproduct **PCP-Au3Cl2THT**. The latter contains a trinuclear metal chain bridged by one **PCP** in a μ_3-κ*P*,κ*C*,κ*P* mode with one chloride on each of the two outer Au and one THT on the central one. The dinuclear gold (I) complex **PCP-Au2** was obtained and the difference between the solid and solution state was also investigated. Adding one equiv. of [M(OTf)] (M = Ag or Au) afforded homotrinuclear complex **PCP-Au3** or heterotrinuclear complex **PCP-Au2Ag**. The work is in progress on photophysics and theory, which are collaborated with Prof. Luisa de Cola (measurements of luminescent properties) and Dr Christophe Gourlaouen (theoretical calculations), respectively, and should give rise to a joint publication.

Experimental section

1. Synthesis and characterisation

1.1 General methods

All manipulations involving organometallics were performed under argon using standard Schlenk techniques. Solvents were dried using standard methods and distilled under nitrogen prior use or passed through columns of activated alumina

For references, see P81

and subsequently purged with nitrogen or argon. ^{1}H, ^{13}C{^{1}H}, and ^{31}P{^{1}H} NMR spectra were recorded at 298 K, unless otherwise specified, on a Bruker Avance 400, 500 or 600 spectrometer and referenced to the residual solvent resonance (^{1}H and ^{13}C) or external 85% H_3PO_4 in D_2O(^{31}P). Elemental analyses were performed by the "Service de microanalyses", Université de Strasbourg. Imidazolium salt **PCHP**,[14c] free carbene **$PC_{NHC}P$**,[14c] **Ag_3-($PC_{NHC}P)_2$**,[14c] [AuCl(tht)][22] and [Au(tht)$_2$](O_3SCF_3)[23] were prepared according to the literature.

1.2 Synthesis of trinuclear Au(I) complexes **Au_3-($PC_{NHC}P)_2$** and **Au_3-$PC_{NHC}P$**.

To a mixture of **Ag_3-($PC_{NHC}P)_2$** (0.080 g, 0.054 mmol) and [AuCl(tht)] (0.064 g, 0.200 mmol) was added 6 ml MeCN at room temperature under protection from light and stirring was maintained for overnight. This reaction was monitored by ^{31}P{^{1}H} NMR until the product peak (at δ 141) becomes dominant. After filtration through Celite, the filtrate was evaporated to dryness, then washed with THF (10 ml) and dried under vacuum to give a solid mixture of **Au_3-($PC_{NHC}P)_2$** and **Au_3-$PC_{NHC}P$**. Pure **Au_3-($PC_{NHC}P)_2$** could be easily obtained by washing the solid with CH_2Cl_2 (1 ml), and drying under vacuum afforded a white powder (0.075 g, 80%). The characterization data agree with our previous report.[14c]

In the above synthesis, when the CH_2Cl_2 solution obtained after filtration was left standing overnight to evaporate in the air and the resulting solid was washed quickly with 1 ml MeCN, **Au_3-$PC_{NHC}P$** was obtained as a white powder (0.010 g, 15%). X-ray quality crystals were obtained by slow diffusion of ether into a MeCN solution. Analysis: Found (Calcd. for $C_{24}H_{46}Au_3Cl_2F_3N_2O_3P_2S_2$) (%): C, 23.25 (22.96), H, 3.72 (3.69), N, 2.19 (2.23). ^{1}H NMR (400 MHz, CD_2Cl_2): δ 8.39 (s, 2H, im-*H*), 3.64 (m, 4H, THT), 2.13 (m, 4H, THT), 1.53 (d, 36H, $^{3}J_{HP}$ = 17.8 Hz, C(C*H*$_3$)$_3$). ^{1}H NMR (400 MHz, CD_3CN): δ 7.78 (s, 2H, im-*H*), 3.33 (m, 4H, THT), 1.87 (m, 4H, THT), 1.53 (d, 36H, $^{3}J_{HP}$ = 17.9 Hz, C(C*H*$_3$)$_3$). ^{13}C{^{1}H} NMR (125 MHz, CD_2Cl_2): δ 193.1 (t, $^{2}J_{CP}$ = 35.1 Hz, N*C*N), 128.6 (im-*C*), 121.3 (q, $^{1}J_{CF}$ = 319.6 Hz, *C*F$_3$), 42.3 (THT), 40.5 (d, $^{2}J_{CP}$ = 16.3 Hz, *C*(CH$_3$)$_3$), 31.0 (THT), 29.2 (d, $^{3}J_{CP}$ = 7.4 Hz, C(*C*H$_3$)$_3$). ^{31}P{^{1}H} NMR (162 MHz, CD_2Cl_2): δ

For references, see P81

132.2 (s). $^{31}P\{^{1}H\}$ NMR (162 MHz, CD_3CN): δ 133.7 (s).

1.3 Synthesis of dinuclear Au(I) complexes **Au_2-($PC_{NHC}P)_2$**.

To a mixture containing the imidazolium **PCHP** (0.104 g, 0.205 mmol), free carbene **$PC_{NHC}P$** (0.010 g, 0.028 mmol) and [(Ph_3P)Au{$N(SiMe_3)_2$}] (0.104 g, 0.168 mmol) was added 5 ml THF at room temperature. After stirring was maintained for 3 days and removal of the supernatant, the residue was dried under vacuum to give a white powder (0.070 g, 59%). X-ray quality crystals were obtained by slow diffusion of ether into a CH_2Cl_2 solution. Analysis: Found (Calcd. for $C_{40}H_{76}Au_2F_6N_4O_6P_4S_2$) (%): C, 34.19 (33.83), H, 5.45 (5.17), N, 3.99 (3.80). ^{1}H NMR (400 MHz, CD_3CN): δ 8.01-8.0 (2H, im-*H*), 7.89-7.87 (2H, im-*H*), 1.51 (d, 36H, $^{3}J_{HP}$ = 17.6 Hz, $C(CH_3)_3$), 1.28 (d, 36H, $^{3}J_{HP}$ = 13.2 Hz, $C(CH_3)_3$). $^{31}P\{^{1}H\}$ NMR (162 MHz, CD_3CN): δ 134.8 (s), 132.7 (s), 119.7 (s) , 110.6 (s). ^{1}H NMR (400 MHz, CD_2Cl_2): δ 8.18-8.17 (2H, im-*H*), 8.11 (d, $^{3}J_{HP}$ = 1.5 Hz) + 8.08 (d, $^{3}J_{HP}$ = 2.2 Hz) (2H, im-*H*), 1.55 (d, 36H, $^{3}J_{HP}$ = 17.7 Hz, $C(CH_3)_3$), 1.29 (d, 36H, $^{3}J_{HP}$ = 13.2 Hz, $C(CH_3)_3$). ^{1}H NMR (400 MHz, CD_2Cl_2, dissolved at -40 ^{o}C): δ 8.15 (s, 2H, im-*H*), 8.07 (s, 2H, im-*H*), 1.53 (d, 36H, $^{3}J_{HP}$ = 17.7 Hz, $C(CH_3)_3$), 1.28 (d, 36H, $^{3}J_{HP}$ = 13.2 Hz, $C(CH_3)_3$). $^{13}C\{^{1}H\}$ NMR (125 MHz, CD_2Cl_2): δ 199.8 (dddd, $^{2}J_{C\text{-trans P}}$ = 116.3 Hz, $^{2}J_{CP}$ = 76.0 Hz, $^{2}J_{CP}$ = 31.9 Hz, $^{5+6}J_{CP}$ = 3.4 Hz, N*C*N), 129.0 (im-*C*), 128.2 + 128.0 (im-*C*), 122.4 (q, $^{1}J_{CF}$ = 320.3 Hz, CF_3), 39.8 (d, $^{2}J_{CP}$ = 15.2 Hz, $C(CH_3)_3$), 36.0 (d, $^{2}J_{CP}$ = 31.1 Hz, $C(CH_3)_3$), 29.1 (d, $^{3}J_{CP}$ = 7.9 Hz, $C(CH_3)_3$), 28.9 (d, $^{3}J_{CP}$ = 15.8 Hz, $C(CH_3)_3$). $^{31}P\{^{1}H\}$ NMR (162 MHz, CD_2Cl_2): δ 134.1 (s), 132.0 (s), 119.9 (s) , 110.7 (s). $^{31}P\{^{1}H\}$ NMR (162 MHz, CD_2Cl_2, dissolved at -40 ^{o}C): δ 131.0 (s), 117.8 (s). $^{19}F\{^{1}H\}$ NMR (564 MHz, CD_2Cl_2): δ -79.9 (s). CP-MAS ^{31}P NMR (202 MHz): δ 130.8 (s), 115.8 (s).

1.4 Synthesis of the heterometallic trinuclear complex **Au_2Ag-($PC_{NHC}P)_2$**.

To a solution of **Au_2-($PC_{NHC}P)_2$** (0.035 g, 0.025 mmol) in MeCN (5 ml) was added AgO_3SCF_3 (0.007 g, 0.027 mmol) at room temperature. After it was stirred for 2 h, the volatiles were removed under reduced pressure and the residue was washed with THF (5 ml) and dried under vacuum to give a white powder (0.037 g, 89%). Analysis: Found (Calcd. for $C_{41}H_{76}Au_2AgF_9N_4O_9P_4S_3$) (%): 29.40 (29.63), H, 4.56 (4.61), N, 3.25

For references, see P81

(3.37). ^{1}H NMR (400 MHz, CD_3CN): δ 8.13 (2H, $^{3}J_{HP}$ = 2.3 Hz, im-*H*), 8.01 (2H, $^{3}J_{HP}$ = 2.1 Hz, im-*H*), 1.55 (t, 36H, $^{3}J_{HP}$ = 9.3 Hz, C(C*H*$_3$)$_3$), 1.49 (d, 36H, $^{3}J_{HP}$ = 8.5 Hz, C(C*H*$_3$)$_3$). ^{13}C{^{1}H} NMR (125 MHz, CD_2Cl_2): δ 195.0 (t, $^{2}J_{CP}$ = 14.2 Hz, N*C*N), 130.0 (im-*C*), 129.7 (im-*C*), 122.4 (q, $^{1}J_{CF}$ = 320.3 Hz, *C*F$_3$), 41.6 (d, $^{2}J_{CP}$ = 6.0 Hz, *C*(CH$_3$)$_3$), 39.4 (*C*(CH$_3$)$_3$), 29.8-29.7 (C(*C*H$_3$)$_3$ and C(*C*H$_3$)$_3$). ^{31}P{^{1}H} NMR (162 MHz, CD_3CN): δ 137.2 (s), two doublets centered at 121.7 ($J_{P\text{-}109Ag}$ = 542.9 Hz, $J_{P\text{-}107Ag}$ = 469.5 Hz).

2. X-ray crystallography

Summary of the crystal data, data collection and refinement for structures of **Au$_3$-PC$_{NHC}$P**•CH_3CN and **Au$_2$-(PC$_{NHC}$P)$_2$** are given in Table S1. X-ray diffraction data collection was carried out on a Bruker APEX II DUO Kappa-CCD diffractometer equipped with an Oxford Cryosystem liquid N_2 device, using Mo-Kα radiation (λ = 0.71073 Å). The crystal-detector distance was 38 mm. The cell parameters were determined (APEX2 software)[24] from reflections taken from three sets of 12 frames, each at 10s exposure. The structure was solved by Direct methods using the program SHELXS-97.[25] The refinement and all further calculations were carried out using SHELXL-97.[26] The H-atoms were included in calculated positions and treated as riding atoms using SHELXL default parameters. The non-H atoms were refined anisotropically, using weighted full-matrix least-squares on F^2. A semi-empirical absorption correction was applied using SADABS in APEX2.[24]

3. Photophysical characterization

Room temperature lifetime measurements. Steady-state emission spectra at both room temperature in organic solvent and 77 K in 2-MeTHF glassy matrix were recorded on a HORIBA Jobin-Yvon IBH FL-322 Fluorolog 3 spectrometer equipped with a 450 W xenon arc lamp as the excitation source, double-grating excitation and emission monochromators (2.1 nm mm^{-1} of dispersion; 1200 grooves mm^{-1}) and a TBX-04 single-photon-counting as the detector. Emission and excitation spectra were corrected for source intensity (lamp and grating) and emission spectral response (detector and grating) by standard correction curves. Time-resolved measurements

For references, see P81

were performed using the time-correlated single-photon-counting (TCSPC) option on the Fluorolog 3. NanoLEDs (402 nm; FWHM<750 ps) with repetition rates between 10 kHz and 1 MHz used to excite the sample. The excitation source were mounted on the sample chamber at 908 to a double grating emission monochromator (2.1 nm mm^{-1} dispersion; 1200 grooves mm^{-1}) and collected by a TBX-4-X single-photon-counting detector. The photons collected at the detector were correlated by a time-to-amplitude converter (TAC) to the excitation pulse. Signals were collected using an IBH DataStation Hub photon counting module and data analysis was performed using the commercially available DAS6 software (HORIBA Jobin Yvon IBH). Alternatively, time resolved measurements were performed by using either the TCSPC electronics PicoHarp300 or the Multi Channel Scaling (MCS) electronics NanoHarp 250 of the PicoQuant FluoTime 300 (PicoQuant GmbH, Germany), equipped with a PDL 820 laser pulse driver. A pulsed laser diode LDH-P-C-375 (λ = 375 nm, pulse FWHM <70 ps, repetition rate 200 kHz – 40 MHz) was used to excite the sample and mounted directly on the sample chamber at 90°. The photons were collected by a PMA-C-192 photomultiplier (PMT) single-photon-counting detector. The data were acquired by using the commercially available software EasyTau (PicoQuant GmbH, Germany), while data analysis was performed using the commercially available software FluoFit (PicoQuant GmbH, Germany).

Low temperature (77 K) lifetime measurements. Steady-state measurements on glassy matrix samples were recorded on a Horiba Jobin–Yvon IBH FL-322 Fluorolog 3 spectrometer as described before. Time-resolved measurements were performed using the time-correlated single-photon-counting option on the Fluorolog 3. NanoLEDs (402 nm; fwhm <200 ns) with repetition rates between 10 kHz and 1 MHz was used to excite the sample. The excitation sources were mounted directly on the sample chamber at 90° to a double-grating emission monochromator (2.1 nm mm^{-1} of dispersion; 1200 grooves mm^{-1}) and collected by a TBX-04 single-photon-counting detector. The photons collected at the detector are correlated by a time-to-amplitude converter to the excitation pulse. Signals were collected using an

For references, see P81

IBH DataStation Hub photon-counting module and data analysis was performed using the commercially available DAS6 software (Horiba Jobin-Yvon IBH).

Methods. The quality of the fit was assessed by minimizing the reduced χ^2 function and by visual inspection of the weighted residuals. For multi-exponential decays, the intensity, namely I*(t)*, has been assumed to decay as the sum of individual single exponential decays (Eqn. 1):

$$I(t) = \sum_{i=1}^{n} \alpha_i exp\left(-\frac{t}{\tau_i}\right) \quad (1)$$

where $_i$ are the decay times and α_i are the amplitude of the component at t = 0. In the tables, the percentages to the pre-exponential factors, α_i, are listed upon normalization. For fluid solution state samples, luminescence quantum yields (PLQY) were measured in optically dilute solution and compared to reference emitters by the method of Demas and Crosby.[27] The $[Ru(bpy)_3]Cl_2$ complex in air-equilibrated water solution at room temperature was used as reference (Φ = 0.04).[28] For solid-state samples as well as for complex **Au_3-($PC_{NHC}P)_2$** in solution, PLQY measurements were performed by using an absolute photoluminescence quantum yield spectrometer Quantaurus C11347 (Hamamatsu, Japan) exciting the sample at λ_{exc} = 350 nm. All solvents were spectrophotometric grade. Deaerated samples were prepared by the freeze-pump-thaw technique.

4. Electrochemical characterization

The electrochemical characterization of complex **Au_3-($PC_{NHC}P)_2$** at concentration of 1 mM has been carried out in both acetonitrile (ACN)/0.1 M tetra-butylammonium hexafluorophosphate ($TBAPF_6$) and ACN/0.1 M sodium trifluoromethanesulfonate (NaOTf). Oxygen was removed by purging the ACN solution with high-purity argon. A typical three-electrode cell was employed, which was composed of a glassy carbon working electrode (3 mm diameter, 66-EE047 Cypress Systems), a platinum wire as counter, and a silver wire as quasi-reference (QRE) electrode. A CHI750C Electrochemical Workstation (CH Instruments, Inc., Austin, TX, USA) was used. The potential of the reference electrode was calibrated after each measurement using

For references, see P81

ferrocene/ferrocenium ($Fc|Fc^+$) redox couple as the internal standard. The GC electrodes were stored in ethanol, and before experiments were polished with a 0.05 µm diamond suspension (Metadi Supreme Diamond Suspension, Buehler) and ultrasonically rinsed with deionized water for 10 minutes and ethanol for 10 minutes. The electrodes were electrochemically activated in the background solution by means of several voltammetric cycles at 0.5 V s^{-1} between the anodic and cathodic solvent/electrolyte discharges. The standard potentials were calculated as the average value between cathodic and anodic peak potentials, when the processes are reversible or quasi-reversible. The CVs were performed at different scan rates, ranging from 0.05 to 1 V s^{-1}. Differential pulse voltammetry (DPV) measurements were performed by applying a differential pulse voltammetric potential scan in the range of the cyclic voltammetry with a step increment of 25 mV (pulse height), an amplitude of 50 mV, a pulse width of 0.2 sec and a pulse period of 0.5 sec.

5. Raman spectra

Raman spectra were recorded in the backscattering geometry with a Labram HR 800 Raman spectrometer (Horiba Jobin-Yvon), equipped with 600 grooves.mm^{-1} grating, CW 473, 532 and 633-nm lasers, a Liquid Nitrogen-cooled CCD camera and a microscope objective (Olympus BX40; 100×). The powder sample of the **Au_3-($PC_{NHC}P)_2$** complex was placed on a glass slide and positioned directly under the Raman microscope. Spectra were normalized using the C-S stretching mode of the counterion centered on 752 cm^{-1}.

For references, see P81

References

(1) (a) Yam, V. W.-W.; Cheng, E. C.-C. *Chem. Soc. Rev.* **2008**, *37*, 1806-1813. (b) Visbal, R.; Gimeno, M. C. *Chem. Soc. Rev.* **2014**, *43*, 3551-3574. (c) Lin, J. C. Y.; Huang, R. T. W.; Lee, C. S.; Bhattacharyya, A.; Hwang, W. S.; Lin, I. J. B. *Chem. Rev.* **2009**, *109*, 3561-3598. (d) Chen, Z.-N.; Zhao, N.; Fan, Y.; Ni, J. *Coord. Chem. Rev.* **2009**, *253*, 1-20. (e) Strasser, C. E.; Catalano, V. J. *J. Am. Chem. Soc.* **2010**, *132*, 10009-10011. (f) Dau, M. T.; Shakirova, J. R.; Karttunen, A. J.; Grachova, E. V.; Tunik, S. P.; Melnikov, A. S.; Pakkanen, T. A.; Koshevoy, I. O. *Inorg. Chem.* **2014**, *53*, 4705-4715. (g) King, C.; Wang, J. C.; Khan, M. N. I.; Fackler, J. P. *Inorg. Chem.* **1989**, *28*, 2145-2149. (h) Ziolo, R. F.; Lipton, S.; Dori, Z. *Journal of the Chemical Society D: Chemical Communications* **1970**, 1124-1125.

(2) (a) Chen, Y.; Cheng, G.; Li, K.; Shelar, D. P.; Lu, W.; Che, C.-M. *Chem Sci* **2014**, *5*, 1348-1353. (b) Tanase, T.; Otaki, R.; Nishida, T.; Takenaka, H.; Takemura, Y.; Kure, B.; Nakajima, T.; Kitagawa, Y.; Tsubomura, T. *Chem.–Eur. J.* **2014**, *20*, 1577-1596. (c) Bestgen, S.; Gamer, M. T.; Lebedkin, S.; Kappes, M. M.; Roesky, P. W. *Chem.–Eur. J.* **2015**, *21*, 601-614. (d) Tong, G. S. M.; Kui, S. C. F.; Chao, H.-Y.; Zhu, N.; Che, C.-M. *Chem.–Eur. J.* **2009**, *15*, 10777-10789.

(3) Wing-Wah Yam, V.; Chung-Chin Cheng, E. In *Photochemistry and Photophysics of Coordination Compounds II*; Balzani, V., Campagna, S., Eds.; Springer Berlin Heidelberg: 2007; Vol. 281, p 269-309.

(4) (a) Pyykkö, P. *Chem. Rev.* **1997**, *97*, 597-636. (b) Pyykkö, P.; Runeberg, N.; Mendizabal, F. *Chem.–Eur. J.* **1997**, *3*, 1451-1457. (c) Muñiz, J.; Wang, C.; Pyykkö, P. *Chem.–Eur. J.* **2011**, *17*, 368-377.

(5) (a) Smith, D. C.; Gray, H. B. *Coord. Chem. Rev.* **1990**, *100*, 169-181. (b) Li, D.; Che, C.-M.; Kwong, H.-L.; Yam, V. W.-W. *J. Chem. Soc., Dalton Trans.* **1992**, 3325-3329. (c) Fu, W.-F.; Chan, K.-C.; Cheung, K.-K.; Che, C.-M. *Chem.–Eur. J.* **2001**, *7*, 4656-4664. (d) Ma, C.; Chan, C. T.-L.; To, W.-P.; Kwok, W.-M.; Che, C.-M. *Chem.–Eur. J.* **2015**, *21*, 13888-13893.

(6) (a) Yeung, M. C.-L.; Yam, V. W.-W. *Chem. Soc. Rev.* **2015**, *44*, 4192-4202. (b) Wing-Wah Yam, V.; Kam-Wing Lo, K. *Chem. Soc. Rev.* **1999**, *28*, 323-334. (c) Chen, Z.;

For references, see P81

Zhang, J.; Song, M.; Yin, J.; Yu, G.-A.; Liu, S. H. *Chem. Commun.* **2015**, *51*, 326-329. (d) Chen, K.; Nenzel, M. M.; Brown, T. M.; Catalano, V. J. *Inorg. Chem.* **2015**, *54*, 6900-6909. (e) Wenger, O. S. *Chem. Rev.* **2013**, *113*, 3686-3733.

(7) Sarcher, C.; Lühl, A.; Falk, F. C.; Lebedkin, S.; Kühn, M.; Wang, C.; Paradies, J.; Kappes, M. M.; Klopper, W.; Roesky, P. W. *Eur. J. Inorg. Chem.* **2012**, *2012*, 5033-5042.

(8) Che, C.-M.; Kwong, H.-L.; Yam, V. W.-W.; Cho, K.-C. *J. Chem. Soc., Chem. Commun.* **1989**, 885-886.

(9) (a) Che, C.-M.; Tse, M.-C.; Chan, M. C. W.; Cheung, K.-K.; Phillips, D. L.; Leung, K.-H. *J. Am. Chem. Soc.* **2000**, *122*, 2464-2468. (b) Leung, K. H.; Phillips, D. L.; Mao, Z.; Che, C.-M.; Miskowski, V. M.; Chan, C.-K. *Inorg. Chem.* **2002**, *41*, 2054-2059. (c) Czerwieniec, R.; Hofbeck, T.; Crespo, O.; Laguna, A.; Concepción Gimeno, M.; Yersin, H. *Inorg. Chem.* **2010**, *49*, 3764-3767.

(10) (a) Visbal, R.; Lopez-de-Luzuriaga, J. M.; Laguna, A.; Gimeno, M. C. *Dalton Trans.* **2014**, *43*, 328-334. (b) Baron, M.; Tubaro, C.; Biffis, A.; Basato, M.; Graiff, C.; Poater, A.; Cavallo, L.; Armaroli, N.; Accorsi, G. *Inorg. Chem.* **2012**, *51*, 1778-1784.

(11) Yersin, H. *Highly Efficient OLEDs with Phosphorescent Materials*; Wiley-VCH Verlag GmbH & Co. KGaA: Weinheim, Germany, 2008.

(12) (a) Zou, T.; Lum, C. T.; Lok, C.-N.; Zhang, J.-J.; Che, C.-M. *Chem. Soc. Rev.* **2015**. (b) Baron, M.; Bellemin-Laponnaz, S.; Tubaro, C.; Basato, M.; Bogialli, S.; Dolmella, A. *J. Inorg. Biochem.* **2014**, *141*, 94-102.

(13) Wang, H. M. J.; Chen, C. Y. L.; Lin, I. J. B. *Organometallics* **1999**, *18*, 1216-1223.

(14) (a) Gaillard, S.; Renaud, J.-L. *Dalton Trans.* **2013**, *42*, 7255-7270. (b) Marchenko, A. P.; Koidan, H. N.; Hurieva, A. N.; Gutov, O. V.; Kostyuk, A. N.; Tubaro, C.; Lollo, S.; Lanza, A.; Nestola, F.; Biffis, A. *Organometallics* **2013**, *32*, 718-721. (c) Ai, P.; Danopoulos, A. A.; Braunstein, P.; Monakhov, K. Y. *Chem. Commun.* **2014**, *50*, 103-105. (d) Marchenko, A.; Koidan, H.; Hurieva, A.; Kurpiieva, O.; Vlasenko, Y.; Kostyuk, A.; Tubaro, C.; Lenarda, A.; Biffis, A.; Graiff, C. *J. Organomet. Chem.* **2014**, *771*, 14-23. (e) Wang, T.; Stephan, D. W. *Chem. Eur. J.* **2014**, *20*, 3036-3039. (f) Brill, M.; Marrwitz, D.; Rominger, F.; Hofmann, P. *J. Organomet. Chem.* **2015**, *775*, 137-151.

(15) Krytchankou, I. S.; Krupenya, D. V.; Karttunen, A. J.; Tunik, S. P.; Pakkanen, T. A.;

For references, see P81

Chou, P.-T.; Koshevoy, I. O. *Dalton Trans.* **2014**, *43*, 3383-3394.

(16) (a) de Frémont, P.; Scott, N. M.; Stevens, E. D.; Nolan, S. P. *Organometallics* **2005**, *24*, 2411-2418. (b) Ai, P.; Danopoulos, A. A.; Braunstein, P. *Inorg. Chem.* **2015**, *54*, 3722-3724.

(17) Kühnel, E.; Shishkov, I. V.; Rominger, F.; Oeser, T.; Hofmann, P. *Organometallics* **2012**, *31*, 8000-8011.

(18) Geiger, W. E.; Barrière, F. *Acc. Chem. Res.* **2010**, *43*, 1030-1039.

(19) Barrière, F.; Geiger, W. E. *J. Am. Chem. Soc.* **2006**, *128*, 3980-3989.

(20) (a) Tkatchouk, E.; Mankad, N. P.; Benitez, D.; Goddard, W. A.; Toste, F. D. *J. Am. Chem. Soc.* **2011**, *133*, 14293-14300. (b) Tubaro, C.; Baron, M.; Costante, M.; Basato, M.; Biffis, A.; Gennaro, A.; Isse, A. A.; Graiff, C.; Accorsi, G. *Dalton Trans.* **2013**, *42*, 10952-10963.

(21) (a) Loo, B. H.; Tse, Y.; Parsons, K.; Adelman, C.; El-Hage, A.; Lee, Y. G. *Journal of Raman Spectroscopy* **2006**, *37*, 299-304. (b) Cao, P.; Gu, R.; Tian, Z. *The Journal of Physical Chemistry B* **2003**, *107*, 769-777. (c) Perreault, D.; Drouin, M.; Michel, A.; Miskowski, V. M.; Schaefer, W. P.; Harvey, P. D. *Inorganic Chemistry* **1992**, *31*, 695-702. (d) Durig, J. R.; Cox Jr, A. W. *Journal of Molecular Structure* **1977**, *38*, 77-88. (e) Leung, K. H.; Phillips, D. L.; Tse, M.-C.; Che, C.-M.; Miskowski, V. M. *Journal of the American Chemical Society* **1999**, *121*, 4799-4803. (f) Phillips, D. L.; Che, C.-M.; Leung, K. H.; Mao, Z.; Tse, M.-C. *Coordination Chemistry Reviews* **2005**, *249*, 1476-1490.

(22) Usón, R.; Laguna, A.; Laguna, M.; Briggs, D. A.; Murray, H. H.; Fackler, J. P. *Inorg. Synth.* **1989**, *26*, 85-91.

(23) Usón, R.; Laguna, A.; Navarro, A.; Parish, R. V.; Moore, L. S. *Inorg. Chim. Acta* **1986**, *112*, 205-208.

(24) 2006.

(25) Sheldrick, G. M. *Acta Crystallogr. Sect. A: Found. Crystallogr.* **1990**, *A46*, 467.

(26) Sheldrick, G. M. 1999.

(27) Crosby, G. A.; Demas, J. N. *J. Am. Chem. Soc.* **1970**, *92*, 7262-7270.

(28) Ishida, H.; Tobita, S.; Hasegawa, Y.; Katoh, R.; Nozaki, K. *Coord. Chem. Rev.* **2010**, *254*, 2449-2458.

For references, see P81

(29) TURBOMOLE V6.2 2010; Vol. a development of university of Karlsruhe and Forschungszentrum Karlsruhe GmbH, 1989-2007, TURBOMOLE GmbH, since 2007; available from http://www.turbomole.com.

(30) ADF2014, SCM, Theoretical Chemistry, Vrije Universiteit, Amsterdam, The Netherlands, http://www.scm.com.

(31) Pai, S. J.; Bae, Y. C. *J. Chem. Phys.* **2010**, *133*, 154104.

(32) Klamt, A.; Schuurmann, G. *Journal of the Chemical Society, Perkin Transactions 2* **1993**, 799-805.

(33) van Lenthe, E.; van Leeuwen, R.; Baerends, E. J.; Snijders, J. G. *Int. J. Quantum Chem* **1996**, *57*, 281-293.

For references, see P81

ESI

Luminescent Properties of Au(I) Complexes Bearing *N*,*N*'-Diphosphanyl NHC Ligands

Pengfei Ai,[a] Matteo Mauro,[b] Christophe Gourlaouen,[c] Andreas A. Danopoulos,*[a,d] Pierre Braunstein,*[a] Luisa De Cola*[b]

[a] Laboratoire de Chimie de Coordination, Institut de Chimie (UMR 7177 CNRS), Université de Strasbourg, 4 rue Blaise Pascal, 67081 Strasbourg Cedex, France. E-mail: danopoulos@unistra.fr, braunstein@unistra.fr

[b] ISIS & icFRC, Université de Strasbourg & CNRS, 8 rue Gaspard Monge, 67000 Strasbourg, France

[c] Laboratoire de Chimie Quantique, Institut de Chimie (UMR 7177 CNRS), Université de Strasbourg, 1 rue Blaise Pascal, 67008 Strasbourg, France

[d] Institute for Advanced Study, USIAS, Université de Strasbourg, France.

For references, see P90

X-ray crystallography:

For **PCP-Au3Cl2THT•CH_3CN**, the atoms C1, Au2, S1; C13, S2, O2, F2; C14, C15 and N2 are in special positions. As the CH_3CN molecule is in special position, the H-atoms on C15 are in half occupancy. There are 6 H atoms in half occupancy, so 3 H in total.

For **PCP-Au2**, there is a high electron density peak near to C1 and Au1.

Table S1. Summary of the crystal data, data collection and refinement for structures of **PCP-Au3Cl2THT**•CH_3CN and **PCP-Au2**.

	PCP-Au3Cl2THT•CH_3CN	**PCP-Au2**
Chemical formula	$C_{24}H_{46}Au_3Cl_2F_3N_2O_3P_2S_2$•$CH_3CN$	$C_{40}H_{76}Au_2F_6N_4O_6P_4S_2$
Formula Mass	1296.54	1404.98
Habit	Colorless prism	colourless block
Crystal size/mm	0.30×0.25×0.15	0.16×0.15×0.10
Crystal system	monoclinic	monoclinic
Space group	*P 21/m*	*P 21/c*
a/Å	10.3495(5)	8.7716(7)
b/Å	16.4819(9)	13.4707(9)
c/Å	11.6668(5)	23.8674(17)
α/°	90	90
β/°	90.964(3)	92.103(2)
γ/°	90	90
Unit cell volume/Å^3	1989.83(17)	2818.3(4)
Formula units / cell, *Z*	2	2
Absorption coefficient, μ/mm^{-1}	11.396	5.450
F (000)	1220	1392
Temperature/K	173(2)	173(2)
θ range for data collection	1.746- 27.481°	2.32-26.87°
No. of reflections measured	11170	41526
No. of independent reflections	4720	6807
R_{int}	0.0585	0.0730
Final R_1 values ($I > 2\sigma(I)$)	0.0431	0.0566
Final $wR(F^2)$ values ($I > 2\sigma(I)$)	0.1076	0.1270
Final R_1 values (all data)	0.0687	0.0805
Final $wR(F^2)$ values (all data)	0.1484	0.1373
Goodness of fit on F^2	1.122	1.093

For references, see P90

Photophysical characterization:

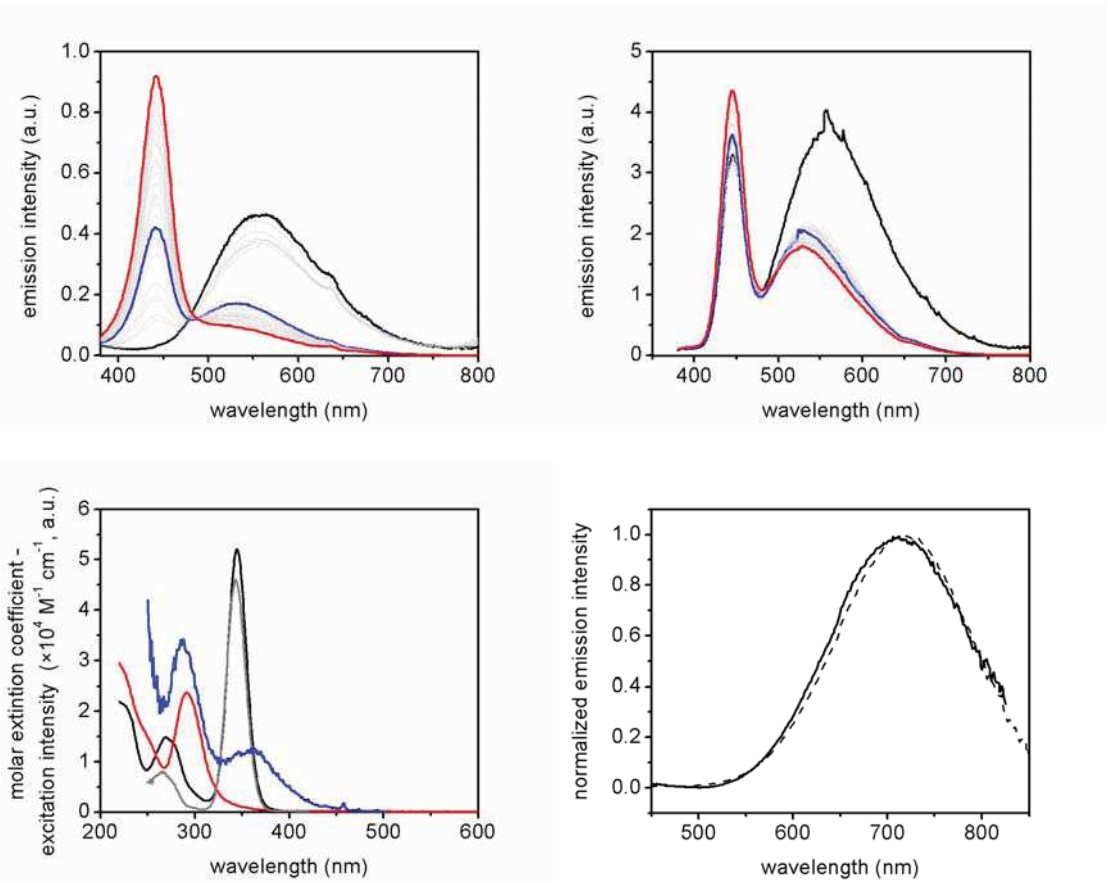

Figure S1. *Top:* Emission spectra of dilute (concentration = 1×10^{-5} M) **Au_2-($PC_{NHC}P$)$_2$** in air-equilibrated (left) and degassed (right) MeCN solution. *Bottom*: (left) comparison of absorption spectrum of **Au_3-($PC_{NHC}P$)$_2$** (black), **Au_2-($PC_{NHC}P$)$_2$** (red) with the excitation spectra of **Au_2-($PC_{NHC}P$)$_2$** recorded at $_{em}$ = 445 (grey) and 530 nm (blue); (right) normalized emission spectra of dilute sample (concentration = 5×10^{-5} M) **Au_3-$PC_{NHC}P$** in air-equilibrated (solid trace) and degassed (dotted trace) CH_2Cl_2 solution. The samples were irradiated at $_{exc}$ = 290 and 300 nm for **Au_2-($PC_{NHC}P$)$_2$** and **Au_3-$PC_{NHC}P$**, respectively.

For references, see P90

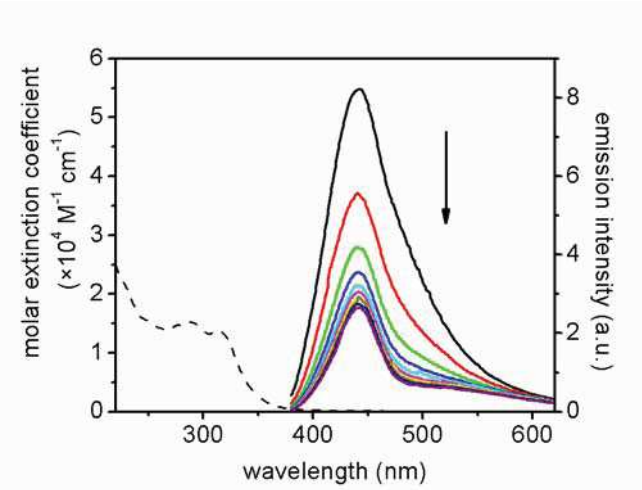

Figure S2. Absorption (dashed line) and emission (solid lines) spectra of complex **Au_2Ag-$(PC_{NHC}P)_2$** in MeCN at room temperature. Emission spectra are recorded upon excitation at $_{exc}$ = 300 nm. Black arrow indicates the change of emission spectra upon different irradiation at $_{exc}$ = 300 nm during the measurements.

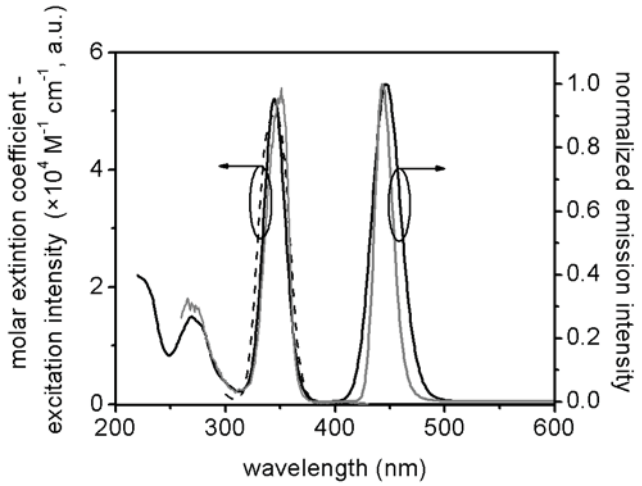

Figure S3. Absorption and emission spectra of complex **Au_3-$(PC_{NHC}P)_2$** in MeCN at room temperature (black traces) and excitation spectrum (dashed trace). Emission and excitation spectra recorded at low temperature (77 K) in MeCN are displayed for comparison as grey traces. All the samples were excited at $_{exc}$ = 340 nm and excitation spectra were recorded at $_{em}$ = 470 nm.

For references, see P90

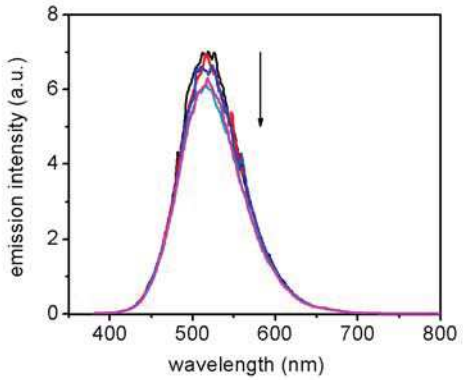

Figure S4. Emission spectra of complex **Au_2-($PC_{NHC}P)_2$** recorded in frozen CH_3CN upon different excitation at $_{exc}$ = 290.

Computational details:

Due to the presence of aurophilic interactions, two sets of calculations were performed using TURBOMOLE[29] and ADF packages[30].

The ground state structures were optimized at MP2 level of calculations with TURBOMOLE and DEF2-SVP basis set for all atoms. Structure optimizations were also performed with ADF at the DFT level of calculations with several functionals (BP86, BLYP and B3LYP) and Grimme's dispersion corrections.[31] TZP basis set was used for ADF calculations. All calculations were performed in gas phase.

The spectroscopic properties were investigated by means of TD-DFT with B3LYP functional and TZP basis set (ADF package). Solvent corrections (acetonitrile) were included through the COSMO model.[32] Scalar relativistic effects were included by ZORA model.[33] For consistency, the ground state structures were reoptimized in these conditions and a TD-DFT performed on the optimized structure to compute the absorption spectra. The nature of the absorbing states was determined by electronic density differences between the excited states and the ground state. The complexes were then optimized in their triplet state to study the luminescence properties. Then, TD-DFT calculations on these geometries were done starting from a singlet wavefunction.

All calculations were done in D_2 point group for the gold trimer except for

For references, see P90

emission properties for which structures were optimized without symmetry. For the gold dimer, all calculations were done in C_i symmetry.

Raman spectra:

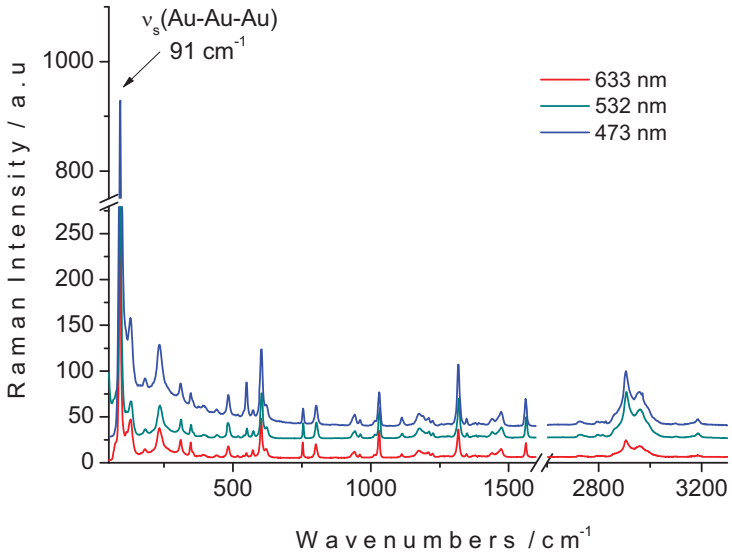

Figure S5. Raman spectra using 473, 532 and 633 nm excitation lines of a solid sample of **Au_3-($PC_{NHC}P)_2$** at room temperature, in the 50–3300 cm^{-1} region.

References:

(1) TURBOMOLE V6.2 2010; Vol. a development of university of Karlsruhe and Forschungszentrum Karlsruhe GmbH, 1989-2007, TURBOMOLE GmbH, since 2007; available from http://www.turbomole.com.

(2) ADF2014, SCM, Theoretical Chemistry, Vrije Universiteit, Amsterdam, The Netherlands, http://www.scm.com.

(3) Pai, S. J.; Bae, Y. C. *J. Chem. Phys.* **2010**, *133*, 154104.

(4) Klamt, A.; Schuurmann, G. *Journal of the Chemical Society, Perkin Transactions 2* **1993**, 799-805.

(5) van Lenthe, E.; van Leeuwen, R.; Baerends, E. J.; Snijders, J. G. *Int. J. Quantum Chem* **1996**, *57*, 281-293.

For references, see P90

Chapter 5

A Mononuclear Bis(diphosphanyl)-N-Heterocyclic Carbene Au Complex as Synthon for Rigid $AuAg_2$ Arrays and Orthogonal or Parallel Homonuclear Au_5 and Cu_6 Luminescent Double Arrays

This chapter is written as a publication to be submitted.

My contribution in this work included the synthesis of the complexes, their characterization and the preparation of the draft of the publication.

A Mononuclear Bis(diphosphanyl)-N-Heterocyclic Carbene Au Complex as Synthon for Rigid $AuAg_2$ Arrays and Orthogonal or Parallel Homonuclear Au_5 and Cu_6 Luminescent Double Arrays

Pengfei Ai,[a] Andreas A. Danopoulos,*[a,b] Pierre Braunstein*[a]

[a] Laboratoire de Chimie de Coordination, Institut de Chimie (UMR 7177 CNRS), Université de Strasbourg, 4 rue Blaise Pascal, 67081 Strasbourg Cedex, France. E-mail: danopoulos@unistra.fr, braunstein@unistra.fr

[b] Institute for Advanced Study, USIAS, Université de Strasbourg, France.

For references, see P107

Résumé du Chapitre 5

Le complexe mononucléaire d'Au(I) **Au1** fut préparé et caractérisé (Schéma 9). Avec quatre fonctions phosphines non-coordinées, il a été utilisé pour la synthèse des complexes trinucléaires **Au3** et **Au-Ag** ou des complexes polynucléaires **Au5** et **Cu6** selon le choix effectué du précurseur métallique.

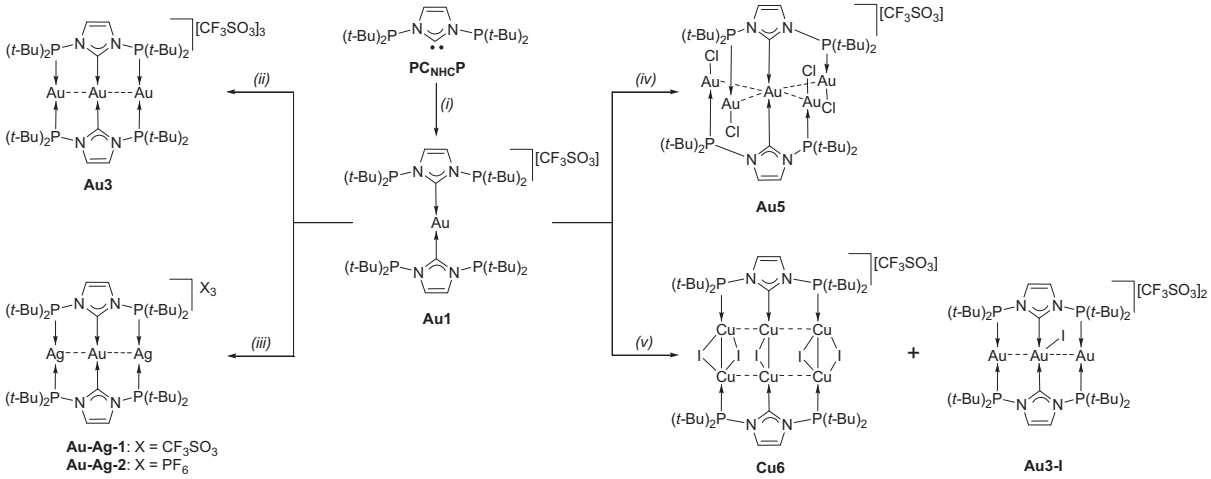

Schéma. Synthèses des complexes d'Au(I) **Au1**, **Au3**, **Au-Ag**, **Au5**, **Au3-I**, **Au3-I3** et **Cu6**. Réactifs et conditions: (*i*) 1 equiv [$(Ph_3P)Au\{N(SiMe_3)_2\}$] et 1 equiv PCHP, dans le THF, 2 jours, temp. amb.; (*ii*) 2 equiv $[Au(tht)_2](CF_3SO_3)$, dans le THF, 3 h, temp. amb.; (*iii*) 2 equiv $[AgO_3SCF_3]$ ou 3 equiv $[AgPF_6]$, dans le CH_3CN, 2 h, temp. amb.; (*iv*) 4 equiv [AuCl(tht)], dans le CH_2Cl_2, 3 h, temp. amb.; (*v*) 2 equiv [CuI], dans le THF, pendant la nuit, temp. amb.

Avec cinq atomes d'Au(I) coplanaires, **Au5** possède une structure en croix très rare qui donne lieu à des d'interactions aurophiles. **Cu6** a quant à lui un cœur métallique hexanucléaire constitué de deux rangées parallèles et coplanaires Cu3 qui sont le siège d'interactions d^{10}-d^{10}. Des résultats préliminaires montrent que **Au1**, **Au-Ag-1**, **Au-Ag-2**, **Au5** et **Cu6** sont luminescents alors que **Au3-I** et **Au3-I3** ne le sont pas.

For references, see P107

A Mononuclear Au(I) Complex Bearing *N*,*N*'-Diphosphanyl NHC Ligands: A Platform for Polynuclear Au(I) or Cu(I) Complexes

Pengfei Ai,[a] Andreas A. Danopoulos,*[a,b] Pierre Braunstein*[a]

[a] Laboratoire de Chimie de Coordination, Institut de Chimie (UMR 7177 CNRS), Université de Strasbourg, 4 rue Blaise Pascal, 67081 Strasbourg Cedex, France. E-mail: danopoulos@unistra.fr, braunstein@unistra.fr

[b] Institute for Advanced Study, USIAS, Université de Strasbourg, France.

ABSTRACT

With four uncoordinated phosphine groups mononuclear Au(I) complex **Au1** was used as a precursor to the trinuclear complexes **Au3** and **Au-Ag** or polynuclear complexes **Au5** and **Cu6** depending on the choice of the metal precursors. **Au5** displays a rare X-type metal arrangement as a result of aurophilic interactions. **Cu6** shows a hexanuclear metal center consisting of two parallel and coplanar Cu3 rows with d^{10}-d^{10} interactions. Preliminary data shows that **Au1**, **Au-Ag-1**, **Au-Ag-2**, **Au5** and **Cu6** are luminescent while **Au3-I** and **Au3-I3** are not luminescent.

For references, see P107

A Mononuclear Bis(diphosphanyl)-N-Heterocyclic Carbene Au Complex as Synthon for Rigid $AuAg_2$ Arrays and Orthogonal or Parallel Homonuclear Au_5 and Cu_6 Luminescent Double Arrays

Pengfei Ai,[a] Andreas A. Danopoulos,*[a,b] Pierre Braunstein*[a]

[a] Laboratoire de Chimie de Coordination, Institut de Chimie (UMR 7177 CNRS), Université de Strasbourg, 4 rue Blaise Pascal, 67081 Strasbourg Cedex, France. E-mail: danopoulos@unistra.fr, braunstein@unistra.fr

[b] Institute for Advanced Study, USIAS, Université de Strasbourg, France.

ABSTRACT

With four uncoordinated phosphine groups mononuclear Au(I) complex **Au1** was used as a precursor to the trinuclear complexes **Au3** and **Au-Ag** or polynuclear complexes **Au5** and **Cu6** depending on the choice of the metal precursors. **Au5** displays a rare X-type metal arrangement as a result of aurophilic interactions. **Cu6** shows a hexanuclear metal center consisting of two parallel and coplanar Cu3 rows with d^{10}-d^{10} interactions. Preliminary data shows that **Au1**, **Au-Ag-1**, **Au-Ag-2**, **Au5** and **Cu6** are luminescent while **Au3-I** and **Au3-I3** are not luminescent.

For references, see P107

Research into the molecular chemistry of gold has intensified in the last decade, largely driven by successful synthetic strategies based on the isolobal analogy between $[Au]^+$ or its complexes of formula $[Au\text{-}L]^+$ (L = 2 electron donor ligand) with the proton H^+ or carbocations R^+, respectively,[1] and by a very fast growing range of applications.[2] The synthetic achievements have triggered structural and theoretical investigations on the intimate nature of the bonding interactions within and between molecules and, in particular, on the propensity for Au(I) to develop attractive d^{10}-d^{10} dispersion interactions, with distances between two gold(I) ions well below the sum of their Van der Waals radii. In polynuclear gold complexes, such aurophilic interactions[3] are crucial in dictating structural motifs in solution and solid, facilitating intramolecular cooperativity and supramolecular reactivity, but also have inconclusively been correlated to emission energies.[3a,4] Other factors that critically influence catalytic reactivity and photophysical properties are the ligand donor and steric properties and rigidity, the arrangement of the metal centres (1D-, 2D-, 3D) and the metal chain length. Short-bite-type ligands, such as $Ph_2PCH_2PPh_2$ (dppm), well suited to stabilize 5-membered rings including two adjacent metal centres, are often used to support these and related d^{10}-d^{10} metallophilic interactions.[5] Ligand imposed rigidity[6] and low coordination numbers[7] are often beneficial to stabilize excited states and improve emission characteristics. Polynuclear (di-, tetra-) Cu complexes with halide bridges, in particular iodides, are also emerging as promising inexpensive photoemitters over a wide range of wavelengths.[8] Furthermore, within the exponential development of N-heterocyclic carbene (NHC) chemistry, gold is again in focus because of increasing applications in e.g. reactivity, catalysis[2e,9] and photophysics.[4c] Beyond gold chemistry and NHC ligands, a third area of high current interest concerns hybrid ligands, that associate within the same molecule different donor functions, often able to bring about unique features to their metal complexes. Functionalized NHC ligands are thus increasingly developed, including phosphine-functionalized NHCs.[10]

For references, see P107

With the objectives to further develop studies at the interfaces between aurophilic interactions, P-functionalized NHC ligands and hybrid, rigid short-bite ligands, we have recently introduced an inherently rigid trifunctional hybrid ligand, of double short-bite architecture, comprising bulky strong σ-donors in a bis(phosphine)-functionalized NHC (**$PC_{NHC}P$**) and described relevant complexes with coinage metals featuring linear M_3 arrays (M = Au, Ag, Cu) characterized by short intermetallic distances.[10h] The rigidity of this **$PC_{NHC}P$** ligand is ensured by the direct N-P link which also facilitates direct electronic communication between the donors. We reasoned that **$PC_{NHC}P$** could lend itself to a platform of ordered arrays of the same or different metals types if selective, sequential complexation methodology to the two different types of donors could be developed, allowing the stepwise construction of unique homo- and heteropolynuclear complexes of the coinage metals. Herein, we describe an important mononuclear homoleptic bis-NHC complex of Au(I) and give examples of transformations that show its potential for the rational design of certain metal arrays. We also give an example where this methodology led to unexpected and unprecedented polynuclear structures. The underlying feature of the reported polynuclear complexes is the rigidity conveyed by the narrow natural bite angle ligand and the occurrence of aurophilic, argentophilic and cuprophilic d^{10}-d^{10} interactions; the latter also gave the incentive to undertake preliminary studies on the luminescence properties of specific complexes.

The mononuclear Au(I) complex **Au1** was prepared from the reaction of the imidazolium salt **PCHP** with 1 equiv. of [Au{$N(SiMe_3)_2$}(**$PC_{NHC}P$**)]. The latter is formed cleanly from [Au{$N(SiMe_3)_2$}(PPh_3)] and **$PC_{NHC}P$** and was characterised by multinuclear NMR spectroscopies (see ESI). Even though it is isolable solid after removal of PPh_3, it was conveniently reacted further *in situ* with the imidazolium salt **PCHP** to yield **Au1**. The $^{31}P\{^1H\}$ NMR singlet at δ 101.4 for **Au1** supports the presence of uncoordinated P(*t*-Bu)$_2$ and the triplet at δ 201.1 ($^2J_{CP}$ = 66.4 Hz) confirms that C_{NHC} is coordinated to Au. Interestingly, this is the first time that [Au{$N(SiMe_3)_2$}(PPh_3)]

For references, see P107

has been used as a versatile synthon for the non-synchronous introduction of NHC ligands with protic-sensitive functionalities (P-N) on Au(I) centres by taking advantage of two different reaction types (substitution, aminolysis). The irreversible formation Au-C_{NHC} under the reaction conditions is crucial for the successful synthesis of [Au{N(SiMe$_3$)$_2$}(**PC$_{NHC}$P**)] and **Au1**. It is noteworthy that addition of two equivalents of **PC$_{NHC}$P** to other Au(I) precursors gave different products.[10h,10i] **Au1** is not air-stable for a long time (*ca.* less than 3-4 h) and should be stored under inert atmosphere.

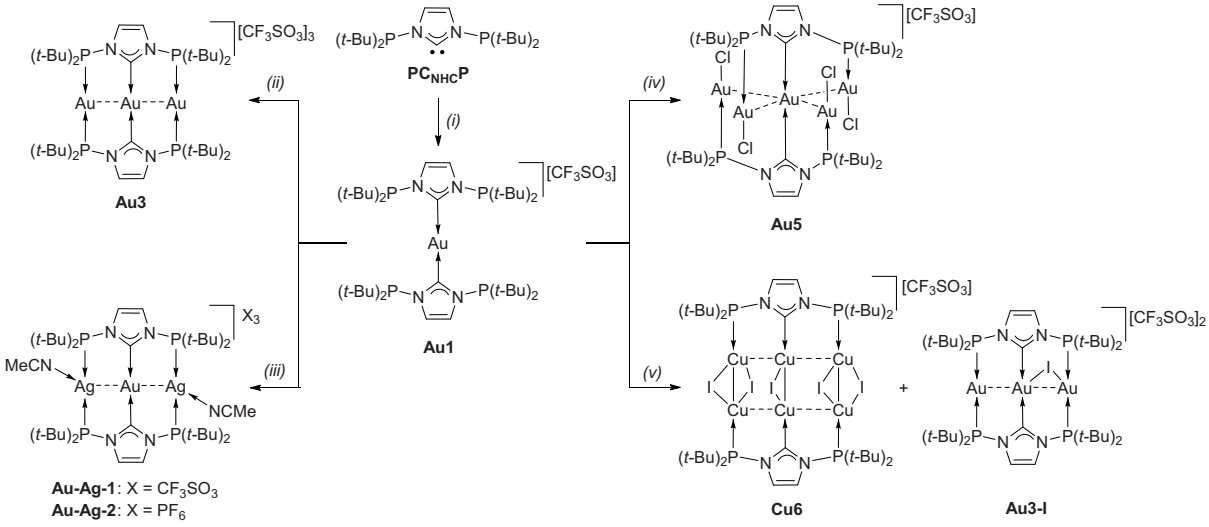

Scheme 1. Synthesis of complexes **Au1**, **Au3**, **Au-Ag**, **Au5**, **Au3-I**, **Au3-I3** and **Cu6**. Reagents and conditions: (*i*) 1 equiv [Au{N(SiMe$_3$)$_2$}(PPh$_3$)] and 1 equiv PCHP, in THF, 2 days, RT; (*ii*) 2 equiv [Au(tht)$_2$](CF$_3$SO$_3$), in THF, 3 h, RT; (*iii*) 2 equiv [AgO$_3$SCF$_3$] or 3 equiv [AgPF$_6$], in MeCN, 2 h, RT; (*iv*) 4 equiv [AuCl(tht)], in CH_2Cl_2, 3 h, RT; (*v*) 2 equiv [CuI], in THF, overnight, RT.

The structure of **Au-1** (Figure 1) features a linear homoleptic Au centre with the two **P-κ^{1}C$_{NHC}$-P** ligands; even though the P(*t*-Bu)$_2$ lone pairs point towards the Au, the Au-P internuclear distances do not imply any bonding interaction in the solid state, as was also confirmed by ^{31}P-NMR spectroscopy in solution; the planes of the NHC heterocycles are staggered. The structural picture revealed points to the possibility of

For references, see P107

using **Au1** as precursor to further homo- or hetero-nuclear complexes *via* P-coordination. This was initially confirmed by accessing the known homo-nuclear **Au3**[10h] through the addition of 2 equiv. of $[Au(tht)_2](CF_3SO_3)$ to a solution of **Au1**.

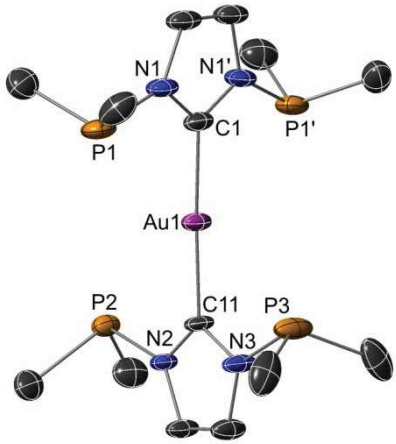

Figure 1. Structure of the cation in **Au1**. H atoms and the *t*-Bu methyl groups are omitted for clarity. Ellipsoids are at the 30% probability. Selected bond lengths (Å) and angles [°]: Au1-C1 2.029(10), Au1-C11 2.041(8); C1-Au1-C11 176.1(4).

The utility of **Au1** as a synthon towards linear hetero-nuclear **$PC_{NHC}P$** complexes was demonstrated by the synthesis of the complex **Au-Ag-1** through the addition of 2 equiv. of $[AgO_3SCF_3]$ to a solution of **Au1** in MeCN (Scheme 1). The $^{31}P\{^1H\}$ NMR of **Au-Ag-1** showed two doublets centered at δ 118.3 ($J_{P\text{-}109Ag}$ = 527.3 Hz, $J_{P\text{-}107Ag}$ = 457.5 Hz) in support of phosphine coordination to Ag. The solid state structure of **Au-Ag-1** confirmed the atom connectivity and the Ag inclusion in the 'P-pockets' of **Au1** (Figure S1) but satisfactory refinement was hampered by persistent disorder of the P(*t*-Bu)$_2$ groups and one of the triflate anions that could not be modeled satisfactorily. A MeCN ligand is bound to each Ag atom. However, by employing $AgPF_6$ as silver source, **Au-Ag-2** was obtained, which is analogous to **Au-Ag-1**, as evidenced by ^{31}P- and ^1H-NMR spectroscopies (δ 118.5 ($J_{P\text{-}109Ag}$ = 525.7 Hz, $J_{P\text{-}107Ag}$ = 455.9 Hz), except for the presence of PF_6^-, which appears as the expected septet at δ -144.4 ($^1J_{PF}$ = 705.9 Hz) in the ^{31}P-NMR spectrum.

For references, see P107

X-ray quality crystals of **Au-Ag-2** were obtained by diffusion of Et_2O into a MeCN solution at 0 °C. Complex **Au-Ag-2** contains a centrosymmetric, linear Ag-Au-Ag array with d^{10}-d^{10} interactions[3b,11] (Ag-Au distance 2.8039(7) Å) (Figure 2). One MeCN molecule is coordinated to each of the outer Ag atoms, resulting in deviation of the P1-Ag1-P2 angle from linearity (152.70(9)°). The Au-C_{NHC} distance (2.089(8) Å), slightly longer than that in **Au1**, are similar to the corresponding one in **Au3** (2.068(5) Å); similarly, the aver. Ag-P distances (2.423 Å) are also similar to those in the trinuclear Ag_3 complex (2.406 Å).[10h]

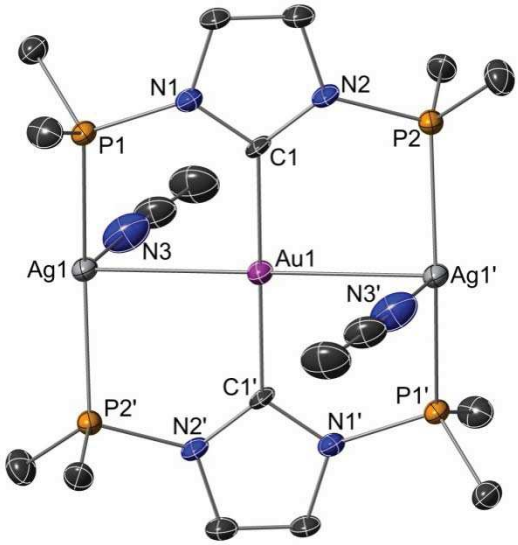

Figure 2. Structure of the trication in **Au-Ag-2**. H atoms and the *t*-Bu methyl groups are omitted. Ellipsoids are at 30% probability level. Selected bond lengths (Å) and angles [°]: Au1-C1 2.089(8), Ag1-N3 2.477(10), Ag1-P1 2.420(2), Ag1-P2' 2.425(2), Ag1-Au1 2.8039(7); P1-Ag1-P2' 152.70(9), P1-Ag1-N3 103.1(3), P2'-Ag1-N3 102.7(3), Au1-Ag1-N3 82.2(3), C1-Au1-C1' 180, Ag1-Au1-Ag1' 180.

Further attempts to use **Au1** for the rational synthesis of novel homonuclear complexes involved its reaction with 4 equiv. of [AuCl(tht)]. This resulted to the isolation of the unique pentanuclear **Au5** (Figure 3) featuring a rare cross-type arrangement of two Au_3 arrays sharing as common intersection point the homoleptic NHC hexacoordinated Au centre. Each metal chain (Au2-Au1-Au3 and Au4-Au1-Au5)

For references, see P107

is spanned by one μ_3-**PC$_{NHC}$P** ligand (μ_3-**PC$_{NHC}$P**, $\kappa P,\kappa C,\kappa P$). All five Au atoms are almost coplanar (max. deviation 0.446 Å for Au2), most likely as a result of aurophilic interactions (aver. Au-Au distance 3.1271 Å).[3,11-12] The planes of the two NHC ligands form a dihedral angle of 88.08°. The Au-C_{NHC} (aver. 2.061 Å), Au-P (aver.2.227 Å) and Au-Cl (aver. 2.287 Å) distances are in the expected range,[10g,10i,13] but the metal-metal separations (aver. 4.416 Å) between the peripheral Au atoms are too long to represent bonding interactions. Although substructures involving five Au atoms have been observed in larger nuclearity Au clusters or pentanuclear complexes, they feature severe pyramidalisations and deviations from planarity unlike the structure observed in **Au5**. [2a,14] Compared to **Au1**, the $^{31}P\{^1H\}$ NMR signal assignable to the coordinated P donors in **Au5** is shifted downfield to δ 128.9 and the $^{13}C\{^1H\}$ NMR signal assignable to C_{NHC} is shifted to δ 196.5 (t, $^2J_{CP}$ = 33.5 Hz). Solid **Au5** is not air-stable for a long time (*ca.* less than 3-4 h) and should be stored under inert atmosphere.

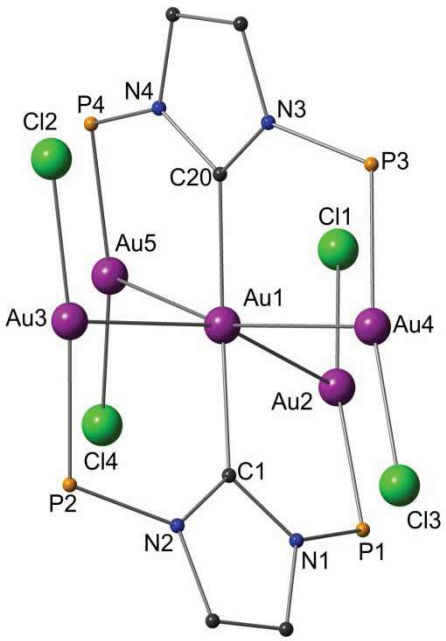

Figure 3. Structure of cationic part of **Au5**. H atoms and the *t*-Bu groups are omitted for clarity. Selected bond lengths (Å) and angles [°]: Au1-C1 2.061(9), Au1-C20 2.061(9), Au2-P1 2.223(3), Au3-P2 2.234(3), Au4-P3 2.223(2), Au5-P4 2.228(3), Au2-Cl1 2.280(3), Au3-Cl2 2.298(3), Au4-Cl3 2.281(2), Au5-Cl4 2.290(3), Au1-Au2

For references, see P107

3.2317(6), Au1-Au3 3.0492(6), Au1-Au4 3.0534(6), Au1-Au5 3.1741(6); Au2-Au1-Au3 160.55(2), Au2-Au1-Au4 105.042(15), Au3-Au1-Au5 104.492(15), Au4-Au1-Au5 162.53(2), C20-Au1-C1 167.5(4), P1-Au2-Cl1 168.1(1), P2-Au3-Cl2 168.8(1), P3-Au4-Cl3 167.4(1), P4-Au5-Cl4 168.7(1).

With a initial objective to prepare heteronuclear Au-Cu complexes, **Au1** was also treated with CuI in 1:6 ratio in THF but an unusual transmetallation reaction from Au(I) to Cu(I) occurred, leading to a mixture of two complexes: (i) the novel hexanuclear Cu(I) complex **Cu6** with two parallel homonuclear Cu_3 arrays bridged by five iodide ligands; (ii) the trinuclear Au(I) iodide complex **Au3-I** with two uncoordinated triflate anions. Complex **Cu6** is sparingly soluble in CH_2Cl_2 and decomposes in acetonitrile, methanol or acetone, leaving pure **Au3-I** in the solution. The $^{31}P\{^1H\}$ NMR spectrum of this reaction mixture showed a broad peak at δ 87.7 and a singlet at δ 135.8 for **Cu6** and **Au3-I**, respectively. Pure **Au3-I** was also obtained as a yellow powder by adding 1 equiv. of NaI to the solution of **Au3** in MeCN; increasing the amount of NaI to 3 equiv. resulted in the complete replacement of the three triflate anions by iodides to give **Au3-I3** as yellow microcrystals (Scheme 2). The $^{31}P\{^1H\}$ NMR spectra in CD_3CN reveal slight differences between **Au3-I** (δ 137.2) and **Au3-I3** (δ 136.6), but no differences in ^1H NMR and $^{13}C\{^1H\}$ NMR were detectable. The structurally similar cations in **Au3-I** and **Au3-I3** are depicted in Figures 4 and S2, respectively. The iodide bridge in **Au3-I** is non-symmetric, I1 being nearer to the central than the outer Au (3.1578(9) Å and 3.538 Å, respectively), while in **Au3-I3** the opposite non-symmetric arrangement is found (*i.e.* 3.085(1) *vs.* 3.388 Å, respectively). The iodide bridge causes a striking non-linear arrangement of P2-Au3-P2' (168.1(1)°) and P1-Au2-P1' (158.6(1)°) in **Au3-I** and **Au3-I3**, respectively. Otherwise, the Au-C_{NHC} and the Au-P distances are similar to those in the parent **Au3**.

For references, see P107

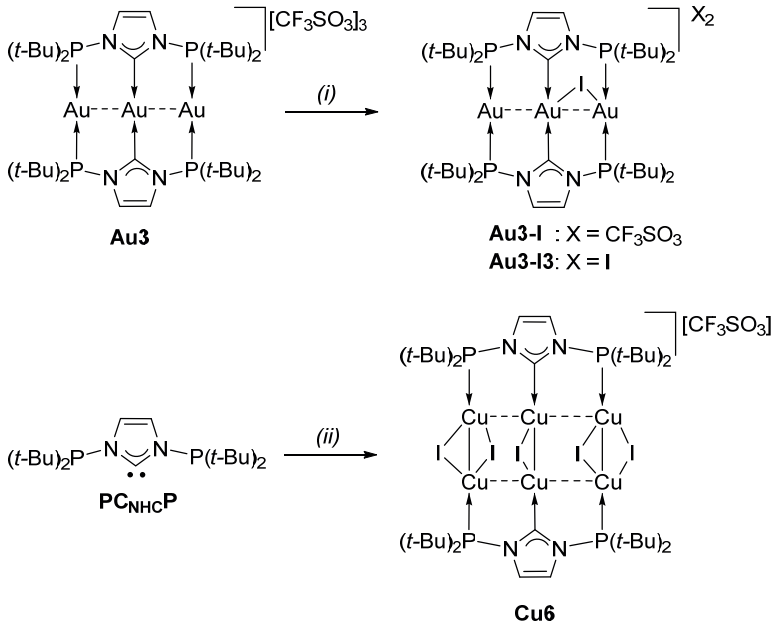

Scheme 2. Synthesis of complexes **Au3-I**, **Au3-I3** and **Cu6**. Reagents and conditions: (*i*) 1 equiv $[CuO_3SCF_3]_2$•toluene and 5 equiv [CuI], in THF, 2 days, RT; (*ii*) 1 or 3 equiv [NaI], in MeCN, 0.5 h, RT.

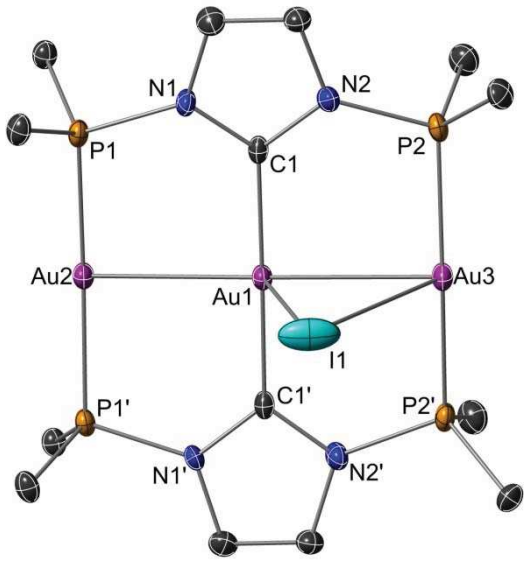

Figure 4. Structure of the dication in **Au3I**. H atoms and the *t*-Bu methyl groups are omitted. Ellipsoids are at 30% probability level. Selected bond lengths (Å) and angles [°]: Au1-C1 2.040(8), Au1-Au2 2.7426(5), Au1-Au3 2.7546(5), Au1-I1 3.1578(9), Au2-P1 2.314(2), Au3-P2 2.329(2); C1-Au1-C1' 179.2(3), Au2-Au1-Au3 177.73(2), P1-Au2-P1' 174.2(1), P2-Au3-P2' 168.1(1).

For references, see P107

The structure of **Cu6** (Figure 5) comprises two parallel and coplanar Cu3 arrays (max. deviation 0.265 Å for Cu5), each spanned by a μ_3-**PC$_{NHC}$P** ligand (μ_3-**PC$_{NHC}$P**,κ*P*,κ*C*,κ*P*). This results in two types of metal-metal separations, one between the opposing metals in different arrays and the other between adjacent metals in the same array, however, there is no substantial difference between them. The seven Cu-Cu distances, in the range 2.669(2) - 2.872(2) Å, are consistent with d^{10}-d^{10} interactions. Five iodides are bonding six Cu atoms in a m_2 fashion with Cu-I bond distances in the range 2.533(2) - 2.680(2) Å, which are comparable to the typical bond lengths in copper clusters with doubly-bridging iodides.[8c] The Cu-C_{NHC} (aver. 1.948 Å) and Cu-P (aver. 2.221 Å) distances are in the expected range.[10h,15] To the best of our knowledge, this Cu_6 arrangement is unprecedented and presumably originates from the unique donor characteristics and rigidity of the **PC$_{NHC}$P**.

Since **Cu6** was always contaminated by **Au3I**, an alternative synthesis was developed comprising the reaction of **PC$_{NHC}$P** with one equiv. of $[Cu(O_3SCF_3)]_2$•toluene and 5 equiv. of CuI in THF for two days (Scheme 2); it was obtained as a white powder which is not air-stable for a long time (*ca.* less than 3-4 h) and should be stored under inert atmosphere.

For references, see P107

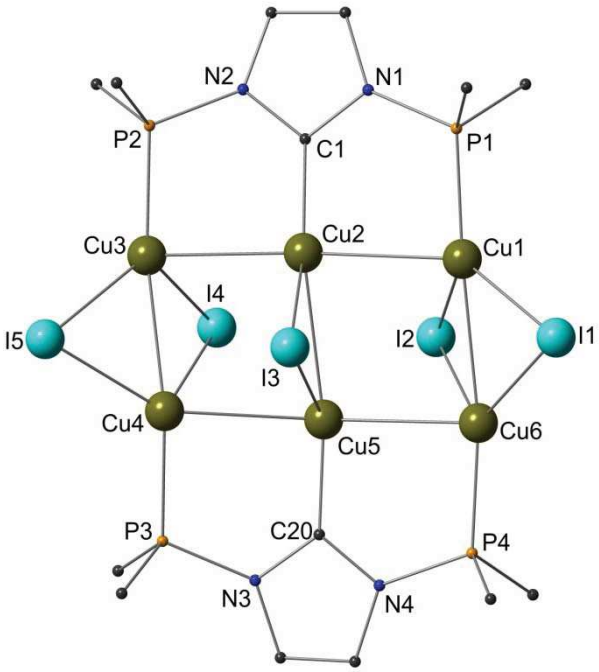

Figure 5. Structure of the cation in **Cu6**. H atoms and the *t*-Bu methyl groups are omitted. Selected bond lengths (Å) and angles [°]: Cu2-C1 1.938(13), Cu5-C20 1.957(13), Cu1-P1 2.223(4), Cu3-P2 2.210(4), Cu4-P3 2.231(4), Cu6-P4 2.220(4), Cu1-I1 2.576(2), Cu1-I2 2.590(2), Cu2-I3 2.531(2), Cu2-I4 2.909(2), Cu3-I4 2.618(2), Cu3-I5 2.533(2), Cu4-I4 2.680(2), Cu4-I5 2.613(2), Cu5-I2 2.809(3), Cu5-I3 2.603(2), Cu5-I4 3.057(2), Cu6-I1 2.564(2), Cu6-I2 2.604(2), Cu1-Cu2 2.802(3), Cu1-Cu6 2.808(2), Cu2-Cu3 2.730(3), Cu2-Cu5 2.872(2), Cu3-Cu4 2.669(2), Cu4-Cu5 2.782(3), Cu5-Cu6 2.754(3); Cu1-Cu2-Cu3 173.71(11), Cu4-Cu5-Cu6 163.16(11), Cu5-Cu2-C1 168.8(5), Cu2-Cu5-C20 169.1(5), Cu6-Cu1-P1 176.0(2), Cu1-Cu6-P4 171.4(2), Cu4-Cu3-P2 171.4(2), Cu3-Cu4-P3 167.5(2).

Though the Au-Au distances (2.7426(5) and 2.7546(5) in **Au3I**, 2.7478(7) and 2.7481(7) Å in **Au3I3**) are even shorter than those in **Au3**, the luminescence was quenched. Similar halide-quenching phenomena were reported separately by Che[16] and Tanase.[13b]

For references, see P107

In conclusion, we have prepared a mononuclear Au(I) complex **Au1** based on the difference of s-donor ability between C_{NHC} and phosphine groups in **$PC_{NHC}P$**. With dangling phosphine donors, it serves as a platform for the synthesis of novel trinuclear or polynuclear complexes depending on the choice of the metal precursors. **Au5** displays a unique X-type pentanuclear gold(I) metal arrangement while the unprecedented **Cu6** shows hexanuclear metal centers consisting of two parallel and coplanar Cu3 rows, both with d^{10}-d^{10} interactions. Preliminary data shows that **Au1**, **Au-Ag-1**, **Au-Ag-2**, **Au5** and **Cu6** are luminescent while **Au3-I** and **Au3-I3** are not luminescent. Further investigation about their photophysical properties is in progress.

For references, see P107

References

(1) (a) Lauher, J. W.; Wald, K. *J. Am. Chem. Soc.* **1981**, *103*, 7648-7650. (b) Braunstein, P.; Rosé, J.; Dusausoy, Y.; Mangeot, J.-P. *C. R. Acad. Sci., Ser. IIc: Chim.* **1982**, *294*, 967. (c) Hoffmann, R. *Angew. Chem. Int. Ed. Engl.* **1982**, *21*, 711-724. (d) Mingos, D. M. *Gold Bull.* **1984**, *17*, 5-12. (e) Braunstein, P.; Rose, J. *Gold Bull.* **1985**, *18*, 17-30.

(2) (a) Mingos, D. M. P. In *Gold Clusters, Colloids and Nanoparticles II*; Mingos, D. M. P., Ed.; Springer International Publishing: 2014; Vol. 162, p 1-65. (b) Louis, C.; Pluchery, O. *Gold Nanoparticles for Physics, Chemistry and Biology*; Imperial College Press: London, 2012. (c) Mohr, F. *Gold Chemistry*; Wiley-VCH Verlag GmbH & Co. KGaA: Weinheim, 2009. (d) Laguna, A. *Modern Supramolecular Gold Chemistry: Gold-Metal Interactions and Applications*; Wiley-VCH Verlag GmbH & Co. KGaA: Weinheim, 2008. (e) Hashmi, A. S. K.; Rudolph, M. *Chem. Soc. Rev.* **2008**, *37*, 1766-1775. (f) Schmidbaur, H. *Gold: Progress in Chemistry, Biochemistry and Technology*; John Wiley & Sons: Chichester, 1999.

(3) (a) Schmidbaur, H.; Schier, A. *Chem. Soc. Rev.* **2008**, *37*, 1931-1951. (b) Schmidbaur, H.; Schier, A. *Chem. Soc. Rev.* **2012**, *41*, 370-412.

(4) (a) Che, C.-M.; Lai, S.-W. In *Gold Chemistry*; Wiley-VCH Verlag GmbH & Co. KGaA: 2009, p 249-281. (b) Wing-Wah Yam, V.; Chung-Chin Cheng, E. In *Photochemistry and Photophysics of Coordination Compounds II*; Balzani, V., Campagna, S., Eds.; Springer Berlin Heidelberg: 2007; Vol. 281, p 269-309. (c) Yam, V. W.-W.; Cheng, E. C.-C. *Chem. Soc. Rev.* **2008**, *37*, 1806-1813. (d) VivianWing-Wah, Y.; Chi-Hang, T. In *Gold*; CRC Press: 2009, p 69-87.

(5) (a) Schmidbaur, H.; Schier, A. *Angew. Chem. Int. Ed.* **2015**, *54*, 746-784. (b) Schmidbaur, H.; Schier, A. *Organometallics* **2015**, *34*, 2048-2066. (c) López-de-Luzuriaga, J. M.; Monge, M.; Olmos, M. E.; Pascual, D. *Organometallics*

For references, see P107

2015, *34*, 3029-3038. (d) Schuh, W.; Braunstein, P.; Bénard, M.; Rohmer, M.-M.; Welter, R. *J. Am. Chem. Soc.* **2005**, *127*, 10250-10258.

(6) (a) Hashimoto, M.; Igawa, S.; Yashima, M.; Kawata, I.; Hoshino, M.; Osawa, M. *J. Am. Chem. Soc.* **2011**, *133*, 10348-10351. (b) Harkins, S. B.; Peters, J. C. *J. Am. Chem. Soc.* **2005**, *127*, 2030-2031.

(7) Krylova, V. A.; Djurovich, P. I.; Aronson, J. W.; Haiges, R.; Whited, M. T.; Thompson, M. E. *Organometallics* **2012**, *31*, 7983-7993.

(8) (a) Mazzeo, P. P.; Maini, L.; Petrolati, A.; Fattori, V.; Shankland, K.; Braga, D. *Dalton Trans.* **2014**, *43*, 9448-9455. (b) Naik, S.; Mague, J. T.; Balakrishna, M. S. *Inorg. Chem.* **2014**. (c) Benito, Q.; Goff, X. F. L.; Nocton, G.; Fargues, A.; Garcia, A.; Berhault, A.; Kahlal, S.; Saillard, J.-Y.; Martineau, C.; Trébosc, J.; Gacoin, T.; Boilot, J.-P.; Perruchas, S. *Inorg. Chem.* **2015**, *54*, 4483-4494. (d) Harvey, P. D.; Knorr, M. *Macromol. Rapid Commun.* **2010**, *31*, 808-826. (e) Ford, P. C. *Coord. Chem. Rev.* **1994**, *132*, 129-140. (f) Wallesch, M.; Volz, D.; Zink, D. M.; Schepers, U.; Nieger, M.; Baumann, T.; Bräse, S. *Chem.–Eur. J.* **2014**, *20*, 6578-6590.

(9) (a) Hashmi, A. S. K.; Hutchings, G. J. *Angew. Chem. Int. Ed.* **2006**, *45*, 7896-7936. (b) Hahn, F. E.; Jahnke, M. C. *Angew. Chem. Int. Ed.* **2008**, *47*, 3122-3172.

(10) (a) Herrmann, W. A.; Köcher, C.; Gooßen, L. J.; Artus, G. R. J. *Chem.–Eur. J.* **1996**, *2*, 1627-1636. (b) Danopoulos, A. A.; Winston, S.; Gelbrich, T.; Hursthouse, M. B.; Tooze, R. P. *Chem. Commun.* **2002**, 482-483. (c) Kühl, O. *Functionalised N-Heterocyclic Carbene Complexes*; Wiley, Weinheim, 2010. (d) Edwards, P. G.; Hahn, F. E. *Dalton Trans.* **2011**, *40*, 10278-10288. (e) Liu, X.; Braunstein, P. *Inorg. Chem.* **2013**, *52*, 7367-7379. (f) Gaillard, S.; Renaud, J.-L. *Dalton Trans.* **2013**, *42*, 7255-7270. (g) Bestgen, S.; Gamer, M. T.; Lebedkin, S.; Kappes, M. M.; Roesky, P. W. *Chem.–Eur. J.* **2015**, *21*, 601-614. (h) Ai, P.; Danopoulos, A. A.; Braunstein, P.; Monakhov, K. Y. *Chem. Commun.* **2014**, *50*, 103-105. (i) Ai, P.; Danopoulos, A. A.; Braunstein, P. *Inorg. Chem.* **2015**, *54*, 3722-3724. (j) Ai, P.; Danopoulos, A. A.; Braunstein, P. *Organometallics* **2015**, *34*, 4109-4116. (k) Salem, H.; Schmitt, M.; Herrlich, U.; Kühnel,

For references, see P107

E.; Brill, M.; Nägele, P.; Bogado, A. L.; Rominger, F.; Hofmann, P. *Organometallics* **2013**, *32*, 29-46. (l) Brown, C. C.; Plessow, P. N.; Rominger, F.; Limbach, M.; Hofmann, P. *Organometallics* **2014**, *33*, 6754-6759. (m) Brill, M.; Marrwitz, D.; Rominger, F.; Hofmann, P. *J. Organomet. Chem.* **2015**, *775*, 137-151. (n) Marchenko, A. P.; Koidan, H. N.; Zarudnitskii, E. V.; Hurieva, A. N.; Kirilchuk, A. A.; Yurchenko, A. A.; Biffis, A.; Kostyuk, A. N. *Organometallics* **2012**, *31*, 8257-8264. (o) Marchenko, A. P.; Koidan, H. N.; Hurieva, A. N.; Gutov, O. V.; Kostyuk, A. N.; Tubaro, C.; Lollo, S.; Lanza, A.; Nestola, F.; Biffis, A. *Organometallics* **2013**, *32*, 718-721. (p) Marchenko, A.; Koidan, H.; Hurieva, A.; Kurpiieva, O.; Vlasenko, Y.; Kostyuk, A.; Tubaro, C.; Lenarda, A.; Biffis, A.; Graiff, C. *J. Organomet. Chem.* **2014**, *771*, 14-23. (q) Danopoulos, A. A.; Tsoureas, N.; Macgregor, S. A.; Smith, C. *Organometallics* **2007**, *26*, 253-263. (r) Tsoureas, N.; Danopoulos, A. A. *J. Organomet. Chem.* **2015**, *775*, 178-187.

(11) Sculfort, S.; Braunstein, P. *Chem. Soc. Rev.* **2011**, *40*, 2741-2760.

(12) Katz, M. J.; Sakai, K.; Leznoff, D. B. *Chem. Soc. Rev.* **2008**, *37*, 1884-1895.

(13)(a) de Frémont, P.; Scott, N. M.; Stevens, E. D.; Nolan, S. P. *Organometallics* **2005**, *24*, 2411-2418. (b) Tanase, T.; Otaki, R.; Nishida, T.; Takenaka, H.; Takemura, Y.; Kure, B.; Nakajima, T.; Kitagawa, Y.; Tsubomura, T. *Chem.–Eur. J.* **2014**, *20*, 1577-1596.

(14) (a) van der Velden, J. W. A.; Bour, J. J.; Vollenbroek, F. A.; Beurskens, P. T.; Smits, J. M. M. *J. Chem. Soc., Chem. Commun.* **1979**, 1162-1163. (b) Bennett, M. A.; Welling, L. L.; Willis, A. C. *Inorg. Chem.* **1997**, *36*, 5670-5672. (c) In *Metal Clusters in Chemistry*; Braunstein, P., Oro, L. A., Raithby, P. R., Eds.; Wiley-VCH Verlag GmbH: 1999; Vol. I, p 459-560. (d) Wilfling, M.; Klinkhammer, K. W. *Angew. Chem. Int. Ed.* **2010**, *49*, 3219-3223.

(15) Kühnel, E.; Shishkov, I. V.; Rominger, F.; Oeser, T.; Hofmann, P. *Organometallics* **2012**, *31*, 8000-8011.

(16)(a) Tong, G. S. M.; Kui, S. C. F.; Chao, H.-Y.; Zhu, N.; Che, C.-M. *Chem.–Eur. J.* **2009**, *15*, 10777-10789. (b) Fu, W.-F.; Chan, K.-C.; Cheung, K.-K.; Che, C.-M. *Chem.–Eur. J.* **2001**, *7*, 4656-4664.

For references, see P107

ESI

A Mononuclear Bis(diphosphanyl)-N-Heterocyclic Carbene Au Complex as Synthon for Rigid $AuAg_2$ Arrays and Orthogonal or Parallel Homonuclear Au_5 and Cu_6 Luminescent Double Arrays

Pengfei Ai,[a] Andreas A. Danopoulos,*[a,b] Pierre Braunstein*[a]

[a] Laboratoire de Chimie de Coordination, Institut de Chimie (UMR 7177 CNRS), Université de Strasbourg, 4 rue Blaise Pascal, 67081 Strasbourg Cedex, France. E-mail: danopoulos@unistra.fr, braunstein@unistra.fr

[b] Institute for Advanced Study, USIAS, Université de Strasbourg, France.

For references, see P119

Experimental section:

1. Synthesis and characterisation

1.1 General methods

All manipulations involving organometallics were performed under argon using standard Schlenk techniques. Solvents were dried using standard methods and distilled under nitrogen prior use or passed through columns of activated alumina and subsequently purged with nitrogen or argon. Imidazolium salt **PCHP**,[1] free carben **$PC_{NHC}P$**,[1] $[Au(tht)_2](O_3SCF_3)$[2] and [AuCl(tht)][3] were prepared according to the literature.

1.2 Synthesis of **Au1**.

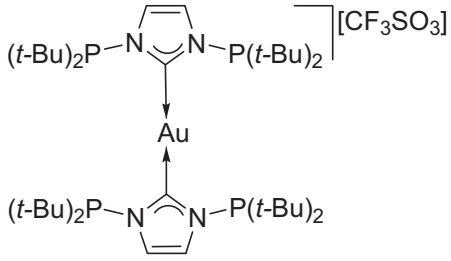

To a schlenk tube containing carbene **$PC_{NHC}P$** (0.072 g, 0.202 mmol) and $[(Ph_3P)Au\{N(SiMe_3)_2\}]$ (0.125 g, 0.202 mmol) was added 5 ml THF at room temperature and the reaction mixture was stirred for 1 h. Then a solution of imidazolium salt **PCHP** (0.102 g, 0.201 mmol) in THF (2 ml) was added and stirring was maintained for 2 days. After concentrating the reaction mixture to ca. 1 ml and removal the supernatant by filtration, the residue was dried under vacuum to give a white powder (80 mg, 38%). X-ray quality crystals were obtained by slow diffusion of ether into its CH_2Cl_2 solution. Analysis: Found (Calcd. for $C_{39}H_{76}AuF_3N_4O_3P_4S$) (%): C, 44.10 (44.23), H, 7.14 (7.23), N, 5.09 (5.29). ^{1}H NMR (400 MHz, CD_2Cl_2): δ 7.51 (s, 4H, im-*H*), 1.25 (d, 72H, $^3J_{HP}$ = 12.3 Hz, C(C*H*$_3$)$_3$). ^{1}H NMR (400 MHz, CD_3CN): δ 7.62 (s, 4H, im-*H*), 1.24 (d, 72H, $^3J_{HP}$ = 12.3 Hz, C(C*H*$_3$)$_3$). ^{13}C{^{1}H} NMR (125 MHz, CD_2Cl_2): δ 201.1 (t, $^2J_{CP}$ = 66.4 Hz, N*C*N), 125.3 (im-*C*), 121.4 (q, $^1J_{CF}$ = 320.8 Hz, *C*F_3), 35.2 (d, $^1J_{CP}$ = 33.5 Hz, *C*(CH$_3$)$_3$), 29.0 (d, $^2J_{CP}$ = 16.8 Hz, C(*C*H$_3$)$_3$). ^{31}P{^{1}H} NMR (162 MHz, CD_2Cl_2): δ 101.5 (s). ^{31}P{^{1}H} NMR (162 MHz, CD_3CN): δ 101.4 (s).

For references, see P119

1.3 Synthesis of **Au3** from **Au1**.

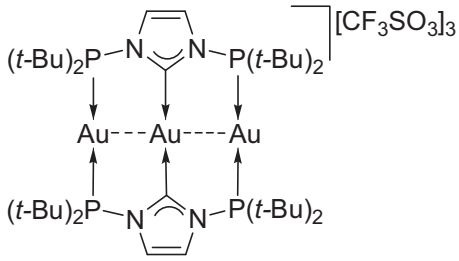

To a mixture of **Au1** (0.025 g, 0.024 mmol) and $[Au(tht)_2](O_3SCF_3)$ (0.025 g, 0.048 mmol) was added 3 ml THF at room temperature and stirring was maintained for 3 h. After removal of the supernatant by filtration, the residue was dried under vacuum to give a white powder (0.039 g, 94%). The characterization data agree with our previous report.[1]

1.4 Synthesis of **Au-Ag-1**.

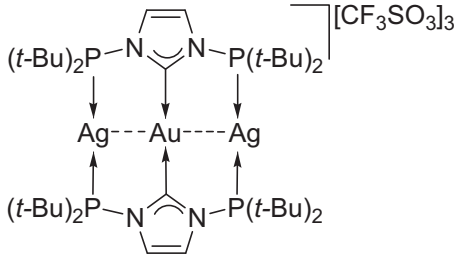

To a mixture of **Au1** (0.030 g, 0.028 mmol) and $[AgO_3SCF_3]$ (0.015 g, 0.058 mmol) was added 5 ml MeCN at room temperature and stirring was maintained for 2 h. After removal of the volatile under vacuum, the residue was washed by THF (2 ml) and dried under vacuum to give a white powder (0.042 g, 95%). Analysis: Found (Calcd. for $C_{41}H_{76}Ag_2AuF_9N_4O_9P_4S_3$) (%): C, 30.95 (31.31), H, 4.90 (4.87), N, 3.65 (3.56). ^{1}H NMR (400 MHz, CD_3CN): δ 7.96 (s, 4H, im-*H*), 1.57 (d, 72H, $^3J_{HP}$ = 17.7 Hz, C(C*H*$_3$)$_3$). ^{13}C{^{1}H} NMR (125 MHz, CD_2Cl_2): δ 195.6 (t, $^2J_{CP}$ = 21.8 Hz, N*C*N), 129.2 (im-*C*), 122.5 (q, $^1J_{CF}$ = 320.4 Hz, *C*F$_3$), 39.0 (*C*(CH$_3$)$_3$), 29.6 (t, $^2J_{CP}$ = 5.2 Hz, C(*C*H$_3$)$_3$). ^{31}P{^{1}H} NMR (162 MHz, CD_3CN): two doublets centered at δ 118.3 ($J_{P\text{-}109Ag}$ = 527.3 Hz, $J_{P\text{-}107Ag}$ = 457.5 Hz).

1.5 Synthesis of **Au-Ag-2**.

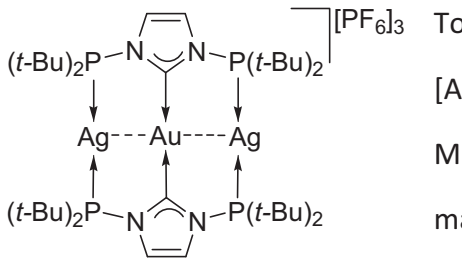

To a mixture of **Au1** (0.030 g, 0.028 mmol) and $[AgPF_6]$ (0.022 g, 0.087 mmol) was added 5 ml MeCN at room temperature and stirring was maintained for 2 h. After removal of the volatile

For references, see P119

under vacuum, the residue was washed by THF (4 ml) and dried under vacuum to give a white powder (0.042 g, 96%). X-ray quality crystals were obtained by slow diffusion of ether into its MeCN solution at 0 °C. Analysis: Found (Calcd. for $C_{38}H_{76}Ag_2AuF_{18}N_4P_7$) (%): C, 29.26 (29.25), H, 4.92 (4.91), N, 3.54 (3.59). ^{1}H NMR (400 MHz, CD_3CN): δ 7.87 (s, 4H, im-*H*), 1.43 (t, 72H, $^3J_{HP}$ = 8.3 Hz, C(C*H*$_3$)$_3$). ^{13}C{^{1}H} NMR (125 MHz, CD_3CN): δ 195.7 (t, $^2J_{CP}$ = 22.4 Hz, N*C*N), 129.1 (im-*C*), 39.0 (*C*(CH$_3$)$_3$), 29.6 (t, $^2J_{CP}$ = 4.9 Hz, C(*C*H$_3$)$_3$). ^{31}P{^{1}H} NMR (162 MHz, CD_3CN): two doublets centered at δ 118.5 ($J_{P\text{-}109Ag}$ = 525.7 Hz, $J_{P\text{-}107Ag}$ = 455.9 Hz, (*t*-Bu)$_2$P), -144.4 (sept, $^1J_{PF}$ = 705.9 Hz, PF_6).

1.6 Synthesis of **Au5**.

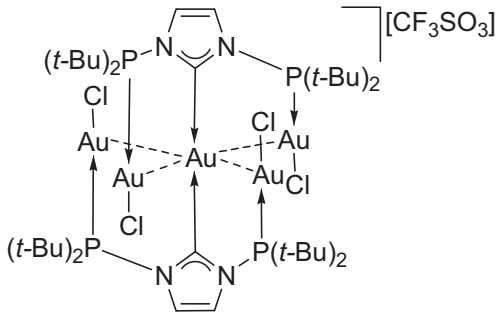

To a mixture of **Au1** (0.030 g, 0.028 mmol) and [AuCl(tht)] (0.037 g, 0.115 mmol) was added 5 ml CH_2Cl_2 at room temperature and stirring was maintained for overnight. After evaporation of the volatile under vacuum, the residue was washed by THF (2 ml) and dried under vacuum to give a white powder (0.040 g, 72%). X-ray quality crystals were obtained by slow diffusion of ether into its CH_2Cl_2 solution. Analysis: Found (Calcd. for $C_{39}H_{76}Au_5Cl_4F_3N_4O_3P_4S$) (%): C, 23.64 (23.55), H, 3.92 (3.85), N, 2,69 (2.82). ^{1}H NMR (400 MHz, CD_3CN): δ 7.96 (s, 4H, im-*H*), 1.57 (d, 72H, $^3J_{HP}$ = 17.7 Hz, C(C*H*$_3$)$_3$). ^{13}C{^{1}H} NMR (125 MHz, CD_3CN): δ 196.5 (t, $^2J_{CP}$ = 33.5 Hz, N*C*N), 129.5 (im-*C*), 122.5 (q, $^1J_{CF}$ = 320.4 Hz, *C*F$_3$), 42.2 (d, $^1J_{CP}$ = 17.2 Hz, *C*(CH$_3$)$_3$), 30.6 (d, $^2J_{CP}$ = 7.5 Hz, C(*C*H$_3$)$_3$). ^{31}P{^{1}H} NMR (162 MHz, CD_3CN): δ 128.9 (s).

1.7 Synthesis of **Cu6** and **Au3-I**.

To a mixture of **Au1** (0.030 g, 0.028 mmol) and CuI (0.033 g, 0.173 mmol) was added 5 ml THF at room temperature and stirring was maintained for overnight. After

For references, see P119

removal of the supernatant by filtration, the residue was extract by CH_2Cl_2 (2 × 10 ml). The extracts was evaporated under vacuum until dryness to give a mixture of **Cu6** and **Au3-I** as yellow powder (0.038 g, the ratio ca. 2:1 was determined from NMR spectra). Adding MeCN in the mixture led to the decomposition of **Cu6** giving the pure **Au3-I** in the solution.

1.8 Synthesis of **Au3-I**.

To a solution of **Au3** (0.035 g, 0.020 mmol) in MeCN (5 ml) was added NaI (0.003 g, 0.020 mmol) at room temperature and stirring was maintained for 30 min. After evaporation of the solvent under reduced pressure, the residue was washed by THF (2 × 5 ml) and dried under vacuum to give a yellow powder (0.030 g, 88%). Analysis: Found (Calcd. for $C_{40}H_{76}Au_3F_6IN_4O_6P_4S_2$) (%): C, 28.27 (27.79), H, 4.51 (4.43), N, 3.97 (3.24). ^{1}H NMR (400 MHz, CD_3CN): δ 8.00 (s, 4H, im-*H*), 1.59 (t, 72H, $^3J_{HP}$ = 9.1 Hz, C(C*H*$_3$)$_3$). ^{1}H NMR (400 MHz, CD_2Cl_2): δ 8.30 (s, 4H, im-*H*), 1.63 (t, 72H, $^3J_{HP}$ = 9.1 Hz, C(C*H*$_3$)$_3$). ^{13}C{^{1}H} NMR (125 MHz, CD_3CN): δ 195.6 (t, $^2J_{CP}$ = 15.6 Hz, N*C*N), 128.5 (im-*C*), 122.1(q, $^1J_{CF}$ = 320.4 Hz, *C*F$_3$), 40.9 (t, $^1J_{CP}$ = 5.2 Hz *C*(CH$_3$)$_3$), 30.0 (C(*C*H$_3$)$_3$). ^{31}P{^{1}H} NMR (162 MHz, CD_3CN): δ 137.2 (s). ^{31}P{^{1}H} NMR (162 MHz, CD_2Cl_2): δ 135.8 (s).

1.9 Synthesis of **Au3-I3**.

By a procedure similar to that for **Au3-I**, treating **Au3** (0.035 g, 0.020 mmol) with 3 equivalent of NaI (0.009 g, 0.060 mmol) in MeCN, yellow microcrystals of **Au3-I3** were obtained. Analysis: Found (Calcd. for $C_{38}H_{76}Au_3I_3N_4P_4$) (%): C, 26.93 (27.09), H, 4.31 (4.55), N, 3.33 (3.33). The NMR spectroscopic data is almost the same as that of **Au3-I**. ^{1}H NMR (400 MHz, CD_3CN): δ 8.05 (s, 4H, im-*H*), 1.59 (t, 72H, $^3J_{HP}$ = 9.1 Hz, C(C*H*$_3$)$_3$). ^{13}C{^{1}H} NMR (125 MHz, CD_3CN): δ 195.6 (t, $^2J_{CP}$ = 15.6 Hz, N*C*N), 128.5 (im-*C*), 122.1(q, $^1J_{CF}$ = 320.4 Hz, *C*F$_3$), 40.9 (t, $^1J_{CP}$ = 5.2 Hz *C*(CH$_3$)$_3$), 30.0 (C(*C*H$_3$)$_3$). ^{31}P{^{1}H} NMR (162 MHz, CD_3CN): δ 136.6 (s).

For references, see P119

1.10 Synthesis of **Cu6**.

To a mixture of free carbene **$PC_{NHC}P$** (0.030 g, 0.084 mmol), $[CuO_3SCF_3]_2$•Toluene (0.022 g, 0.042 mmol) and CuI (0.030 g, 0.420 mmol) was added 5 ml THF at room temperature and stirring was maintained for 2 days. After removal of the supernatant by filtration, the residue was extracted by CH_2Cl_2 (2 × 20 ml). The extracts was evaporated under reduced pressure until dryness to give a white powder (0.040 g, 51%). X-ray quality crystals were obtained by slow diffusion of ether into its CH_2Cl_2 solution. Analysis: Found (Calcd. for $C_{39}H_{76}Cu_6F_3I_5N_4O_3P_4S$) (%): C, 25.20 (24.95), H, 4.21 (4.08), N, 2.97 (2.98). ^{1}H NMR (400 MHz, CD_2Cl_2): δ 7.58 (s, 4H, im-*H*), 1.48 (d, 72H, $^3J_{HP}$ = 15.6 Hz, C(C*H*$_3$)$_3$). ^{13}C{^{1}H} NMR (125 MHz, CD_2Cl_2): δ 197.1 (t, $^2J_{CP}$ = 58.6 Hz, N*C*N), 125.7 (im-*C*), 121.4 (q, $^1J_{CF}$ = 322.4 Hz, *C*F$_3$), 38.4 (*C*(CH$_3$)$_3$), 29.5 (d, $^2J_{CP}$ = 8.3 Hz, C(*C*H$_3$)$_3$). ^{31}P{^{1}H} NMR (162 MHz, CD_2Cl_2): δ 87.7 (br).

2. X-ray crystallography

Summary of the crystal data, data collection and refinement for structures of **Au1, Au-Ag-2**•2MeCN, **Au5**•CH_2Cl_2, **Au3I**•MeCN, **Au3I3**•2MeCN **and Cu6**•CH_2Cl_2 are given in Table S1.

For **Au1**, X-ray diffraction data collection was carried out on a Bruker APEX II DUO Kappa-CCD diffractometer equipped with an Oxford Cryosystem liquid N_2 device, using Mo-Kα radiation (λ = 0.71073 Å). The crystal-detector distance was 38 mm. The cell parameters were determined (APEX2 software)[4] from reflections taken from three sets of 12 frames, each at 10s exposure. The structure was solved by Direct methods using the program SHELXS-97.[5] The refinement and all further calculations were carried out using SHELXL-97.[6] The H-atoms were included in calculated positions and treated as riding atoms using SHELXL default parameters. The non-H atoms were refined anisotropically, using weighted full-matrix least-squares on F^2. A semi-empirical absorption correction was applied using SADABS in APEX2.[4]

For references, see P119

For **Au-Ag-2**, **Au5**•CH_2Cl_2, **Au3I**•MeCN, **Au3I3**•2MeCN and **Cu6**•CH_2Cl_2, X-ray diffraction data collection was carried out on a Nonius Kappa-CCD diffractometer equipped with an Oxford Cryosystem liquid N_2 device, using Mo-Kα radiation (λ = 0.71073 Å). The crystal-detector distance was 36 mm. The cell parameters were determined (Denzo software)[7] from reflections taken from one set of 10 frames (1.0° steps in phi angle), each at 20s exposure. The structures were solved by Direct methods using the program SHELXS-97.[5] The refinement and all further calculations were carried out using SHELXL-97.[6] The H-atoms were included in calculated positions and treated as riding atoms using SHELXL default parameters. The non-H atoms were refined anisotropically, using weighted full-matrix least-squares on F^2. A semi-empirical absorption correction was applied using MULscanABS in PLATON.[8]

For **Au1**, the atoms C1, C11, C12, C13, C22, N2, N3, O1, F2, P2, P3, S1 and Au1 are in a special position (population 50%). The carbons C4, C5, C6, C14, C15, C17, C19, C20 and C21 are disordered on two positions.

For **Au-Ag-2**•2MeCN, the atoms Au1 and P4 are in a special position (population 50%).

For **Au5**•CH_2Cl_2, the carbon C40 of the dichloromethane is disordered on two positions by symmetry (population 50%).

For **Au3I**•MeCN, the atoms C21, C22, N3, Au1, Au2, Au3 and I1 are in a special position (population 50%).

For **Au3I3**•2MeCN, the atoms Au1, Au2, Au3 and I1 are in a special position (population 50%). A squeeze was made. The residual electron density was assigned to two molecules of the acetonitrile.

For references, see P119

2.1 Summary of crystal data

Table S1. Crystal data for compounds **Au1**, **Au-Ag-2**•2MeCN, **Au5**•CH_2Cl_2, **Au3I**•MeCN, **Au3I3**•2MeCN and **Cu6**•CH_2Cl_2.

	Au1	**Au-Ag-2**•2MeCN	**Au5**•CH_2Cl_2	**Au3I**•MeCN	**Au3I3**•2MeCN	**Cu6**•CH_2Cl_2
Chemical formula	$C_{39}H_{76}AuF_3N_4O_3P_4S$	$C_{42}H_{82}Ag_2AuF_{18}N_6P_7$• 2MeCN	2($C_{39}H_{76}Au_5Cl_4F_3N_4O_3P_4S$)• CH_2Cl_2	$C_{40}H_{76}Au_3F_6IN_4O_6P_4S_2$• MeCN	$C_{38}H_{76}Au_3I_3N_4P_4$• 2MeCN	$C_{39}H_{76}Cu_6F_3I_5N_4O_3P_4$ S• CH_2Cl_2
CCDC Number	1429388	1429389	1429392	1429391	1429390	1429393
Formula Mass	1058.94	1724.74	4062.14	1769.90	1766.61	1962.64
Crystal system	Orthorhombic	Triclinic	Monoclinic	Monoclinic	Orthorhombic	Triclinic
a/Å	18.456(2)	11.8254(5)	11.7605(3)	9.02490(10)	16.3895(5)	13.0359(6)
b/Å	17.218(2)	12.6302(4)	18.6546(4)	24.3396(5)	24.3545(5)	16.5959(5)
c/Å	16.464(2)	13.7781(6)	28.9436(4)	13.8812(3)	15.0688(5)	16.8760(8)
α/°	90	101.319(2)	90	90	90	107.396(2)
β/°	90	101.571(2)	111.9230(10)	90.7330(10)	90	101.585(2)
γ/°	90	116.764(2)	90	90	90	104.372(3)
Unit cell volume/Å^3	5231.8(11)	1700.69(12)	5890.7(2)	3048.93(10)	6014.8(3)	3222.1(2)
Temperature/K	173(2)	173(2)	173(2)	173(2)	173(2)	173(2)
Space group	*Pnma*	*P-1*	*$P2_1/c$*	*$P2_1/m$*	*Pnma*	*P-1*
Formula units / cell, *Z*	4	1	2	2	4	2
Absorption coefficient, μ/mm^{-1}	3.020	2.973	12.827	7.942	8.977	4.599
No. of reflections measured	35048	29408	37174	38420	26978	33723
No. of independent reflections	6539	7788	13437	7162	7052	14699
R_{int}	0.0849	0.1170	0.0877	0.0919	0.0919	0.1316
Final R_1 values ($I > 2\sigma(I)$)	0.0663	0.0688	0.0461	0.0519	0.0513	0.0900
Final $wR(F^2)$ values ($I > 2\sigma(I)$)	0.1371	0.1832	0.1084	0.1374	0.1365	0.1736
Final R_1 values (all data)	0.1176	0.1116	0.0793	0.0747	0.0813	0.2111
Final $wR(F^2)$ values (all data)	0.1586	0.2210	0.1503	0.1651	0.1496	0.2519
Goodness of fit on F^2	1.184	1.080	1.035	1.092	1.075	1.010

For references, see P119

2.2 Structure of Au3I3

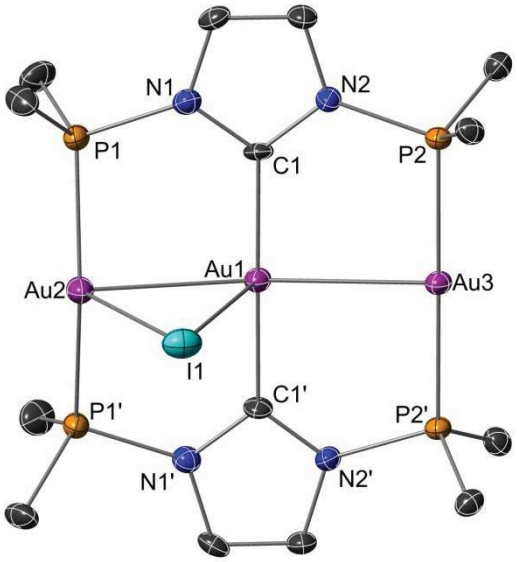

Figure S1. Structure of cationic part of **Au3I3**. H atoms, the *t*-Bu methyl groups and one molecule of MeCN are omitted for clarity. Anisotropic displacement parameters are depicted at the 30% probability level. Selected bond lengths (Å) and angles [°]: Au1-C1 2.043(8), Au2-P1 2.336(2), Au3-P2 2.311(2), Au2-I1 3.085(1), Au1-Au3 2.7478(7), Au1-Au2 2.7481(7); C1-Au1-C1' 179.2(5), Au3-Au1-Au2 166.26(3), P1-Au2-P1' 158.56(13), P2-Au3-P2' 179.17(12).

For references, see P119

References

(1) Ai, P.; Danopoulos, A. A.; Braunstein, P.; Monakhov, K. Y. *Chem. Commun.* **2014**, *50*, 103.

(2) Usón, R.; Laguna, A.; Navarro, A.; Parish, R. V.; Moore, L. S. *Inorg. Chim. Acta* **1986**, *112*, 205.

(3) Usón, R.; Laguna, A.; Laguna, M.; Briggs, D. A.; Murray, H. H.; Fackler, J. P. *Inorg. Synth.* **1989**, *26*, 85.

(4) Bruker AXS Inc Madison USA, 2006.

(5) Sheldrick, G. M. *Acta Crystallogr. Sect. A: Found. Crystallogr.* **1990**, *A46*, 467.

(6) Sheldrick, G. M. Universität Göttingen: Göttingen Germany, 1999.

(7) Nonius, B. V. Delft, The Netherlands, 1997.

(8) Spek, A. L. *J. Appl. Cryst.* **2003**, *36*, 7.

For references, see P119

Chapter 6

Selective Partial or Complete Transmetallation of Trinuclear Cu(I) or Ag(I) Complexes leading to Hetero- or Homo-trinuclear Pd Complexes

This chapter is written as a publication to be submitted.

My contribution in this work included the synthesis of the complexes, their characterization and the preparation of the draft of the publication.

Selective Partial or Complete Transmetallation of Trinuclear Cu(I) or Ag(I) Complexes leading to Hetero- or Homo-trinuclear Pd Complexes

Pengfei Ai,[a] Andreas A. Danopoulos,*[a,b] Pierre Braunstein*[a]

[a] Laboratoire de Chimie de Coordination, Institut de Chimie (UMR 7177 CNRS), Université de Strasbourg, 4 rue Blaise Pascal, 67081 Strasbourg Cedex, France. E-mail: danopoulos@unistra.fr, braunstein@unistra.fr

[b] Institute for Advanced Study, USIAS, Université de Strasbourg, France.

For references, see P135

Résumé du Chapitre 6

Les complexes homotrinucléaires **Cu-1** et **Ag-1** ont servi à réaliser des transmétallations partielles ou totales avec des précurseurs de Pd(0). La réaction of **Cu-1** avec 1 equiv. de $[Pd(PPh_3)_4]$ dans le CH_2Cl_2 a conduit au complexe hétérotrinucléaire **Cu-Pd-1** à interactions d^{10}-d^{10}-d^{10} après qu'un des centres métalliques terminaux ait été remplacé par le Pd(0) (Schéma 1). En augmentant la quantité de $[Pd(PPh_3)_4]$ à 3 équivalents, un produit de réduction a été obtenu, **Cu-Pd-2** qui possède une chaîne Pd-Cu-Pd (d^9-$d^{10}s^1$-d^9). En passant à $[Pd(dba)_2]$ dans MeCN, nous avons obtenu le complexe homotrinucléaire **Pd-1** par transmétallation complète.

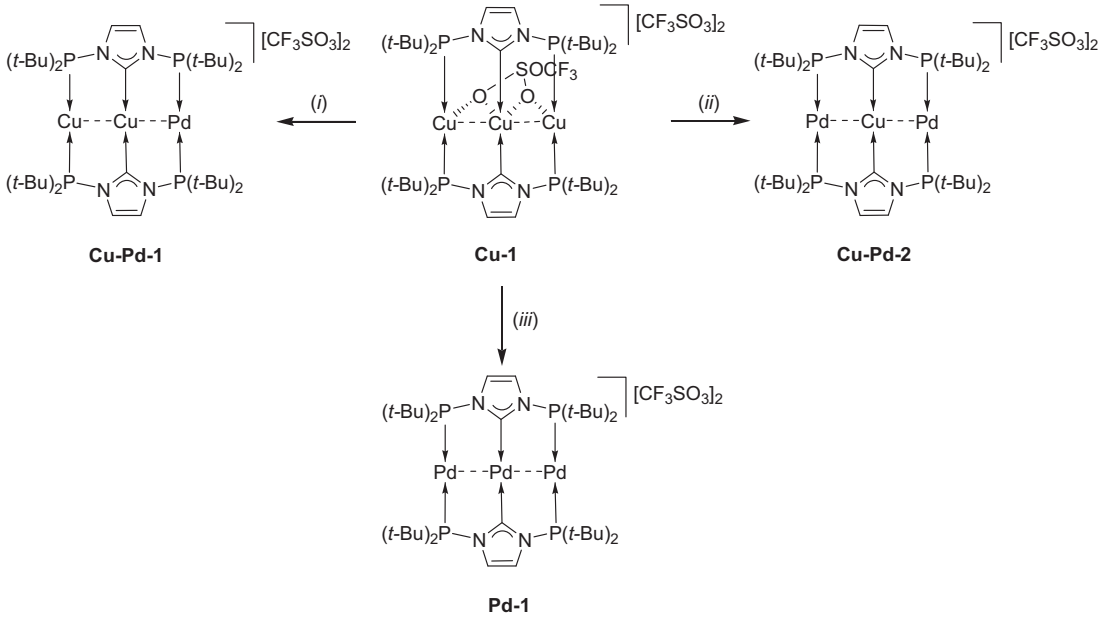

Schéma 1. Réactions de transmétallation du complexe trinucléaire **Cu-1**. Réactifs et conditions: (*i*) 1.2 equiv $[Pd(PPh_3)_4]$, CH_2Cl_2, 12 h, temp. amb.; (*ii*) 3 equiv $[Pd(PPh_3)_4]$, CH_2Cl_2, 12 h, temp. amb.

La réaction de **Ag-1** avec $[Pd(PPh_3)_4]$ a conduit au complexe hétérotrinucléaire **Ag-Pd-1** analogue à **Cu-Pd-1** (Schéma 2). Cependant, la réaction ne va pas plus loin, même en ajoutant davantage de $[Pd(PPh_3)_4]$. L'oxydation de **Ag-Pd-1** par le solvant (CH_2Cl_2) a produit **Ag-Pd-2** qui présente des interactions d^{10}-d^8-d^{10}.

For references, see P135

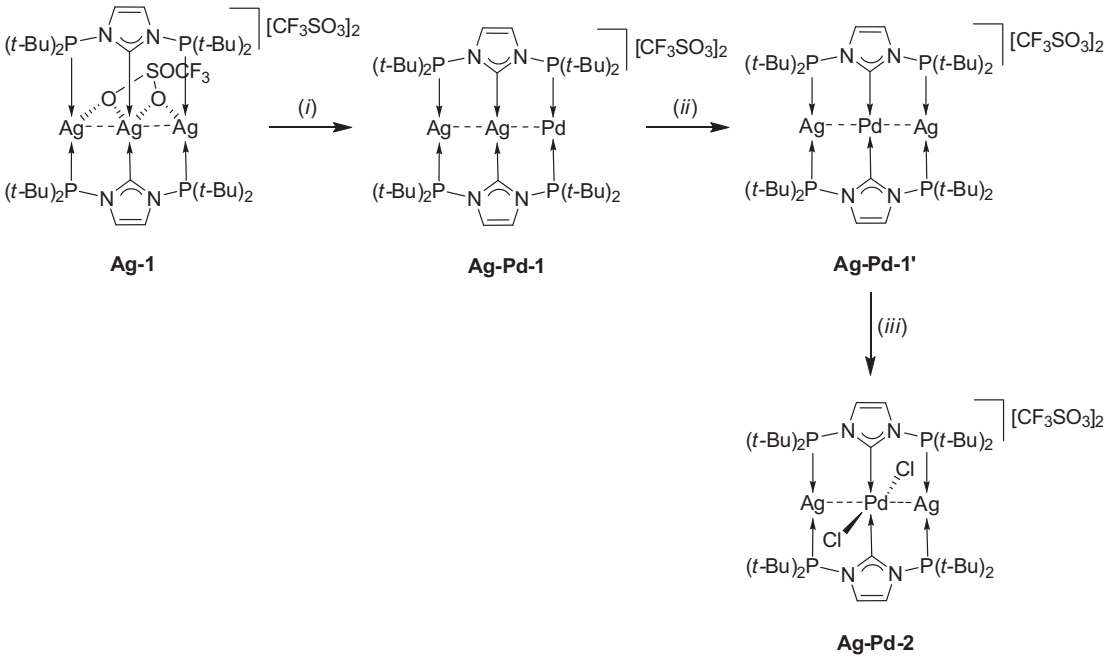

Ag-1 **Ag-Pd-1** **Ag-Pd-1'** **Ag-Pd-2**

Schéma 2. Réactions de transmétallation du complexe trinucléaire **Ag-1**. Réactifs et conditions: (*i*) 1 equiv $[Pd(PPh_3)_4]$, CH_2Cl_2, 1 h, temp. amb.; (*ii*) évaporation lente et complète à l'air; (iii) solide laissé dans $MeCN/CH_2Cl_2$ (10:1) pendant deux semaines à temp. amb.

For references, see P135

Selective Partial or Complete Transmetallation of Trinuclear Cu(I) or Ag(I) Complexes leading to Hetero- or Homo-trinuclear Pd Complexes

Pengfei Ai,[a] Andreas A. Danopoulos,*[a,b] Pierre Braunstein*[a]

[a] Laboratoire de Chimie de Coordination, Institut de Chimie (UMR 7177 CNRS), Université de Strasbourg, 4 rue Blaise Pascal, 67081 Strasbourg Cedex, France. E-mail: danopoulos@unistra.fr, braunstein@unistra.fr

[b] Institute for Advanced Study, USIAS, Université de Strasbourg, France.

ABSTRACT

Homotrinuclear complexes **Cu-1** and **Ag-1** were used for partial or fully transmetallation with Pd(0) precursors. Reaction of **Cu-1** and 1 equiv. of $[Pd(PPh_3)_4]$ in CH_2Cl_2 led to a heterotrinuclear complex **Cu-Pd-1** with d^{10}-d^{10}-d^{10} interactions after one of the outer metal was replaced by Pd(0). Increasing the amount of $[Pd(PPh_3)_4]$ to 3 equivalent resulted in a reducing product **Cu-Pd-2** with a Pd-Cu-Pd (d^9-$d^{10}s^1$-d^9) metal chain. Changing to $[Pd(dba)_2]$ in MeCN afforded one homotrinuclar **Pd-1** after fully tranmetallation. Reacting **Ag-1** with $[Pd(PPh_3)_4]$ led to a heterotrinuclear complex **Ag-Pd-1** analogous to **Cu-Pd-1**. However, no further reaction happened even adding more $[Pd(PPh_3)_4]$. Oxidation of **Ag-Pd-1** by solvent (CH_2Cl_2) gave a novel complex **Ag-Pd-2** with d^{10}-d^8-d^{10} bonding interaction.

For references, see P135

Introduction

The chemistry of heterometallic complexes with metal-metal bonding interactions is continuing to be a very interesting field due to their catalytic applications and photophisical properties.[1] However, synthesis of stoichiometrically defined complexes with M-Pd bond (M = group 11 coinage metals) seems to be very difficult. About 24 structures with the direct Pd-Ag bond (bond distance less than the sum of their Van der Waals radii, 3.35 Å) have been found in CCDC, while the complexes with the direct Pd-Cu bond (bond distance less than the sum of their Van der Waals radii, 3.03 Å) are even less (8 hits). The Cu-Pd bonds include Cu(II)-Pd(II) (d^9-d^8),[2] Cu(I)-Pd(0) (d^{10}-d^{10})[3] and Cu(I)-Pd(II) (d^{10}-d^8)[1c,4]; the Ag-Pd bonds include Ag(I)-Pd(II) (d^{10}-d^8),[1c,4a,5] Ag(I)-Pd(0) (d^{10}-d^{10})[3b,6] and Ag(I)-Pd(I) (d^{10}-d^9)[7], amongst which , most are clusters. Recently, two linear heterotrinuclear complex with Cu(II)-Pd(II) bond interactions are reported with dipyridylamide and 2-naphthyridylphenylamine ligand.[2a,2b]

The nature of ligands plays an important role in assembling the metals in close proximity to form attractive metal-metal bonds. Short-bite ligands can place adjacent metals in constrained geometry, favoring metal-metal interactions.[1b,8] We have recently found that the rigid functional NHC ligand *N,N'*-diphosphanyl-imidazol-2-ylidene ligand, P-C_{NHC}-P, is ideally suited to doubly span a metal-metal bonded chain in trinuclear complexes. The rigidity of our double, short-bite ligand accounts for the short Cu-Cu, Ag-Ag and Au-Au distances observed in the trinuclear complexes **Cu-1**, **Ag-1** and **Au-1**, respectively, as a result of metallophilic d^{10}-d^{10} interactions. In the latter case, they resulted in remarkable photophysical properties. A related P-C_{NHC}-P system has been reported where the donor groups are connected by a flexible linker , which weaken the metallic interactions.[8c] We became interested in extending the use of this rigid, short-bite hybrid ligand P-C_{NHC}-P to heterometallic systems because of the often unique reactivity or photophysical properties associated with heterometallic complexes and clusters, in particular in the presence of d^{10}-d^{10} interactions.[1a,1f]

For references, see P135

N-heterocyclic carbene (NHC) copper(I) complexes have been used as carbene transfer reagents to other transition metals, such as Au(I), Pd(II), Ni(II), Ru(II), Rh(I), Cr(III) or even Ag(I), besides the popularly used Ag(I)-NHCs, because of their effective, practical and cost effective advantages.[9] Considering the different chemical environments of the inner and outer metal atoms in the **Cu-1** and **Ag-1** metal chains, we wondered whether partial and selective transmetallation could be performed, lead to novel heterometallic systems and allow a comparison of the reactivity of the P-Cu(or Ag)-P and C_{NHC}-Cu(or Ag)-C_{NHC} units. Here, we will present the transmetallation of homotrinuclear complex **Cu-1** and **Ag-1** with Pd(0) precusors to form heterotrinuclear complexes with metal-metal interactions.

Results and Discussion

Mixed-metal chains by transmetallation from Cu(I) to Pd(0).

In order to evaluate the possibility to use the homotrinuclear Cu(I) complex **Cu-1** as precursor in transmetallation reactions, we first reacted it with one equivalent of $[Pd(PPh_3)_4]$ in CH_2Cl_2 overnight at room temperature (Scheme 1). This afforded a green compound **Cu-Pd-1**, air stable in the solid-state, which was shown by an X-ray diffraction study to have retained the doubly P-C_{NHC}-P supported chain structure but with one of the two outer Cu(I) atoms replaced by a Pd atom to form a heterotrinuclear complex (Figure 1). The NMR spectroscopic data in solution are consistent with the solid-state structure: the $^{31}P\{^1H\}$ NMR spectrum contains one single peak at δ 122.0 corresponding to the phosphine coordinated to Pd and one broad singlet at δ 101.0 for the phosphine coordinated to the Cu atom. The $^{13}C\{^1H\}$ NMR spectrum shows a triplet at δ 197.6 ($^2J_{CP}$ = 26.8 Hz) for the carbene atom C_{NHC}.

For references, see P135

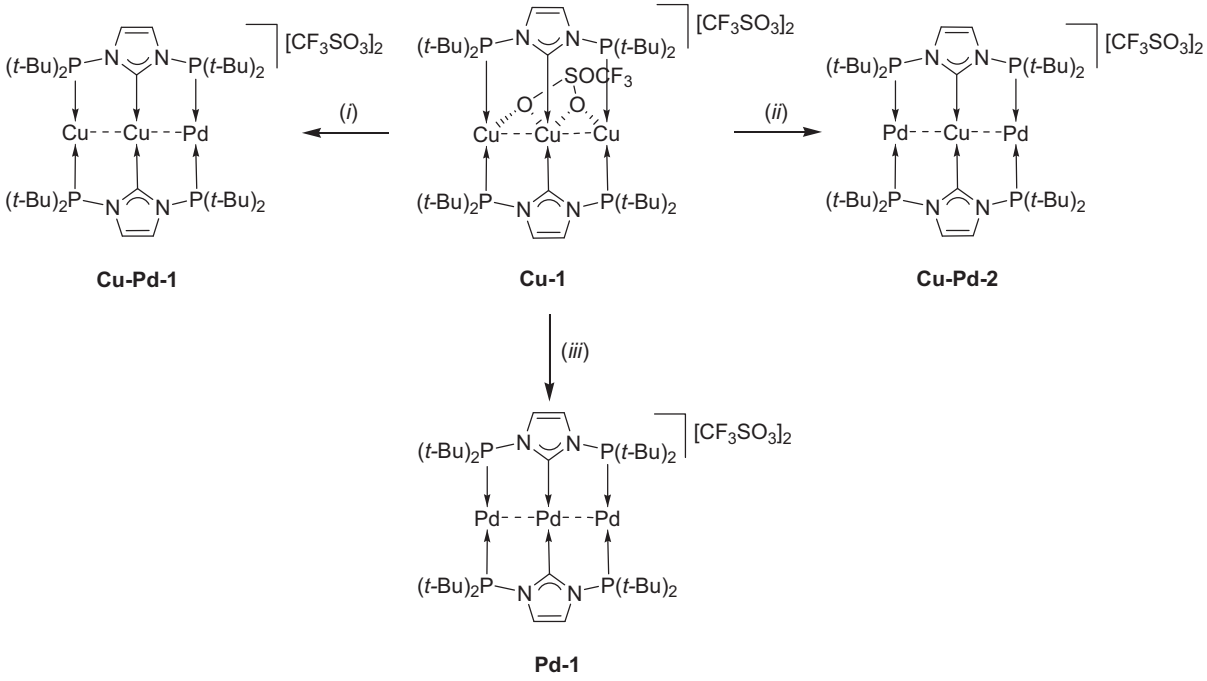

Scheme 1. Transmetallation reactions of trinuclear **Cu-1**. Reagents and conditions: (*i*) 1.2 equiv $[Pd(PPh_3)_4]$, in CH_2Cl_2, overnight, RT; (*ii*) 3 equiv $[Pd(PPh_3)_4]$, in CH_2Cl_2, overnight, RT.

The structure of **Cu-Pd-1**•CH_2Cl_2 contains one complex cation with a linear asymmetric mixed-metal chain Cu-Cu-Pd (178.61(2)°) bridged by two mutually *trans* ligands (Figure 1). The three metal atoms and the six donor atoms are almost coplanar (max. deviation for P1, 0.147 Å). Both triflates act as uncoordinated counterions, at variance with the situation in the precursor complex **Cu-1** where one of the triflates acts as a ($\kappa^1$1O, $\kappa^1$2O')-bridge. The number of anions present indicates that the metal chain contains two Cu(I) and one Pd(0) centers. With a total electron count of 42 (30 metal valence electrons + 12), the heterotrinuclear complex **Cu-Pd-1** is isoelectronic with its homotrinuclear precursor complex **Cu-1**. The P2-Cu2-P4 coordination angle of 166.95(4)° around the outer Cu atom corresponds to a bending towards the central Cu atom while the C1-Cu1-C20 angle of 172.7(2)° around the central Cu(I) corresponds to a slight bending towards the outer Pd atom. The Pd atom is supported by two trans P donors which form a P1-Pd-P3 angle of 175.79(4)°. The slight bending of angles observed and the short metal-metal separations

For references, see P135

(Cu1-Cu2 2.5971(7) Å, Cu1-Pd1 2.6478(5) Å) are consistent with attractive d^{10}-d^{10} interactions between the metals.[1f,1g,10] The Cu-Cu distance is slightly longer than that in **Cu-1** (2.5761(9) Å), which, together with the bending of the central coordination angle, suggests a stronger d^{10}-d^{10} interaction between Cu1 and Pd than that between Cu1 and Cu2. To the best of our knowledge, there are only two reported clusters with d^{10}-d^{10} interactions between Pd and Cu, $[PPh_4]_2\{Cu_4Pd_2[Ru_6C(CO)_{16}]_2Cl_2\}$ (Pd-Cu, 2.677(2) Å)[3a] and $[Pd(\mu\text{-CuI})\{Pd(dmpe)\}_3(\mu_3\text{-GePh}_2)_3]$ (Pd-Cu, 2.462(1) and 2.632(1) Å).[3b] **Cu-Pd-1** represents the first linear heterotrinuclear complex with d^{10}-d^{10} interactions between Pd(0) and Cu(I).

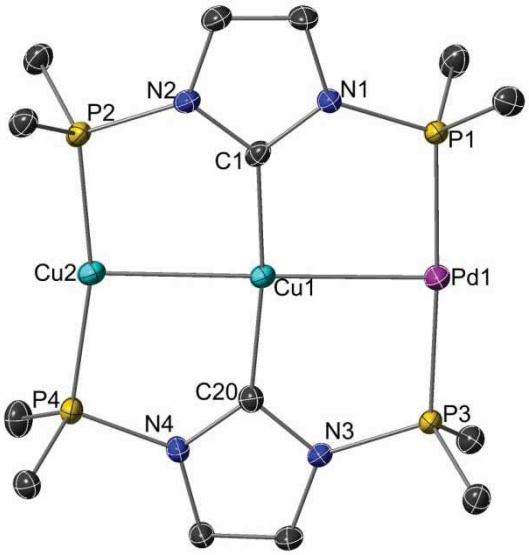

Figure 1. Thermal ellipsoid representation (30% probability level) of the structure of **Cu-Pd-1**. H atoms, one molecule of CH_2Cl_2, two triflate anions and the *t*-Bu Me groups are omitted for clarity. Selected bond lengths (Å) and angles [°]: Cu1-C1 1.954(4), Cu1-C20 1.953(4), Cu2-P2 2.200(1), Cu2-P4 2.203(1), Pd1-P1 2.243(1), Pd1-P3 2.261(1), Cu1-Cu2 2.5971(7), Cu1-Pd1 2.6478(5); C1-Cu1-C20 172.67(16), P2-Cu2-P4 166.95(4), P1-Pd1-P3 175.79(4), Cu1-Cu2-P2 96.65(3), Cu1-Cu2-P4 96.35(3), Cu1-Pd1-P1 88.63(3), Cu1-Pd1-P3 88.58(3), Cu2-Cu1-C1 86.36(11), Cu2-Cu1-C20 86.35(11), Cu2-Cu1-Pd1 178.61(2), Pd1-Cu1-C20 93.93(11), Pd1-Cu1-C1 93.37(11).

To examine whether the intermetallic ratio in the metal chain could be

For references, see P135

controlled by the stoichiometry of the reagents, the amount of $[Pd(PPh_3)_4]$ used in the reaction with **Cu-1** in CH_2Cl_2 was increased to 3 equivalents. This led to the formation of a novel yellow heterotrinuclear complex **Cu-Pd-2** (Scheme 1 and Experimental part). This air-stable complex is paramagnetic (NMR evidence, see below) and it was characterized by elemental analysis and single crystal X-ray diffraction.

In the cation of **Cu-Pd-2** the Cu center occupies a center of symmetry and the strictly linear heterotrinuclear metal arrangement is doubly supported by two trans bridging ligands in a μ_3-P-C_{NHC}-P,κP,κC,κP bonding mode, which is similar to that in **Cu-1**, except than no triflate anion is coordinated to the metals.[11] The two outer Pd atoms are bound to two trans P donors forming an angle of 176.65(7)°, a value which is similar to that in **Cu-Pd-1**, while the Cu is bound to two trans NHC donors in an ideal linear way. The Cu-Pd separation of 2.664(2) Å is slightly longer than that in **Cu-Pd-1**. On the basis of the molecular symmetry and the total charge 2+ of the complex cation, two formal assignments of oxidation states for the metals are possible, Pd(0)-Cu(II)-Pd(0) (d^{10}-d^9-d^{10}) and Pd(I)-Cu(0)-Pd(I) (d^9-$d^{10}s^1$-d^9). Both give 29 metal valence electrons for the 41 electron complex **Cu-Pd-2**, one less than that for **Cu-Pd-1** and **Cu-1**. An EPR study showed no Cu(II) signal in the solid-state or in solution, even at liquid N_2 temperature, which tends to rule out the Pd(0)-Cu(II)-Pd(0) hypothesis. In a Pd(I)-Cu(0)-Pd(I) (d^9- $d^{10}s^1$-d^9) chain, one could envisage spin pairing between the termini d^9 atoms through the central metal but the paramagnetism of the Cu(0) explains the broad $^{31}P\{^1H\}$ and $^{13}C\{^1H\}$ NMR spectra observed for **Cu-Pd-2**.

One can thus view the reactions leading to **Cu-Pd-2** as a partial reduction of the initial Cu_3 chain in **Cu-1** by Pd(0) whereas the Cu centers in **Cu-Pd-1** can still be formally considered as Cu(I). That some of the $[Pd(PPh_3)_4]$ used for the synthesis of **Cu-Pd-2** acted as a reducing agent explains why the reaction of **Cu-1** with only 2 equiv $[Pd(PPh_3)_4]$ afforded a mixture of Cu-Pd-1 and Cu-Pd-2 (NMR evidence and X-ray diffraction). Recently, a dinuclear Cu/Ga complex, $[Cu_2$-$(GaCp^*)(\mu$-$GaCp^*)_3Ga(OTf)_3]$, was reported and suggested as the first structural characterized Cu(0) complex.[12] To the best of our knowledge, **Cu-Pd2** is the first

For references, see P135

heterometallic complex formally involving Pd(I) and Cu(0), and the first Cu(0) complex with NHC ligands.

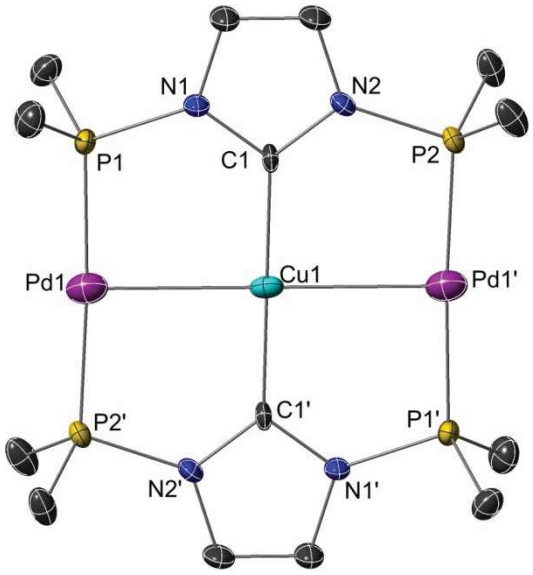

Figure 2. Thermal ellipsoid representation (30% probability level) of the structure of **Cu-Pd-2**. H atoms, two triflate anions and the *t*-Bu Me groups are omitted for clarity. Selected bond lengths (Å) and angles [°]: Cu1-C1 1.974(6), Pd1-P1 2.226(2), Pd1-P2' 2.216(2), Cu1-Pd1 2.664(2); C1-Cu1-C1' 180.0, P2'-Pd1-P1 176.65(7), Pd1-Cu1-C1 91.49(15), Pd1-Cu1-C1' 88.51(15), Pd1-Cu1-Pd1' 180.0, Cu1-Pd1-P2' 92.76(6), Cu1-Pd1-P1 90.58(6).

Since the attempt to replace all the Cu atoms in **Cu-1** to form a homotrinuclear Pd complexes failed by increasing the amount of $[Pd(PPh_3)_4]$ to even 6 equivalent, another Pd(0) precursors, $[Pd(dba)_2]$, was choosen. The reaction of **Cu-1** with 4 equivalent of $[Pd(dba)_2]$ in MeCN (Scheme 1) resulted in a homotrinuclear palladium complex with mixed oxidation states (totally 2+ for three Pd atoms), which was confirmed by X-ray diffraction. **PCP-Pd** is air stable and diamagnetic: one singlet at δ 112.2 ppm in $^{31}P\{^1H\}$ NMR and the C_{NHC} a triplet at δ 181.4 ($^2J_{CP}$ = 18.1 Hz).

The cation of **Pd-1** (Figure 3) features a similar structure to that of trinuclear **Cu-Pd-2**, a almost linear metal arrangement (178.85(2)°) with two trans bridging ligands, but with a distortion coordination plane, the angle of 32.91° between the

For references, see P135

two imidazole ring planes. The terminal and internal Pd atoms retain almost linear two coordination environments (178.13(4) and 179.7(2)°, respectively) with a short distance of 2.5927(3) Å.

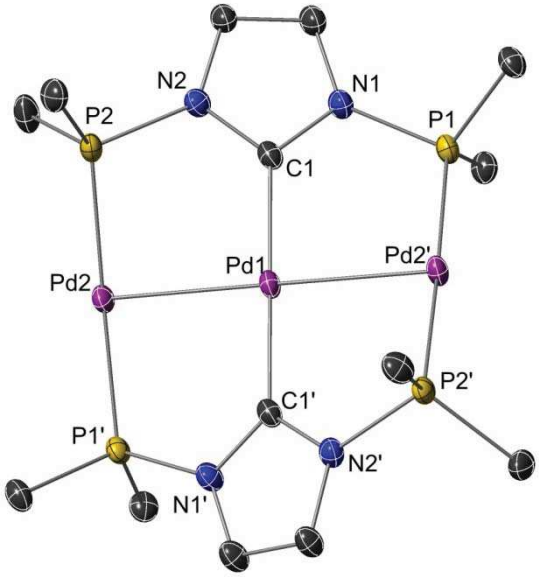

Figure 3. Thermal ellipsoid representation (30% probability level) of the structure of **Pd-1**. H atoms, three triflate anions and the *t*-Bu Me groups are omitted for clarity. Selected bond lengths (Å) and angles [°]: Pd1-C1 2.041(4), Pd2-P1' 2.284(1), Pd2-P2 2.278(1), Pd1-Pd2 2.5927(3); C1-Pd1-C1' 179.7(2), P2-Pd2-P1' 178.13(4), Pd2-Pd1-Pd2' 178.85(2).

Mixed-metal chains by transmetallation from Ag(I) to Pd(0).

In NHC chemistry, transmetallation from Ag(I) is one of the most commonly used methods. Although in the chemistry described above, both NHC and phosphino groups may be involved in the transmetallation reactions, we were anticipating that mixed-metal chain complexes could also be prepared from the homotrinuclear Ag_3 chain complex **Ag-1** analogous to **Cu-1**. Thus, the complex **Ag-1** was reacted with $[Pd(PPh_3)_4]$ in CH_2Cl_2 for 1 h (Scheme 2). The completion of the reaction was indicated by the formation of a metal mirror on the wall of the Schlenk tube and the appearance in the $^{31}P\{^1H\}$ NMR spectrum of one singlet at δ 127 and two doublets at

For references, see P135

δ 120.4 due to P-$^{107/109}$Ag coupling ($^{1}J_{P\text{-}109Ag}$ = 561.4 Hz, $^{1}J_{P\text{-}107Ag}$ = 487.0 Hz). This spectrum implied that one of the phosphine groups was coordinated to Pd and the other to Ag, which would lead to a situation similar to that in the heterotrinuclear complex **Cu-Pd-1**. That the other Ag atom has remained bound to the C_{NHC} donor was confirmed by ^{13}C NMR (δ 204.0 ($^{1}J_{C\text{-}109Ag}$ = 197.8 Hz, $^{1}J_{C\text{-}107Ag}$ = 168.9 Hz). Because of the similar electron density of Ag(I) and Pd(0), a single crystal X-ray diffraction study could not differentiate between the two outer metal atoms and the model suggested the presence of two termini Pd(I) centers with a central Ag(0), giving in total two positive charges. These crystals were redissolved in MeCN and their ^{31}P{^{1}H} NMR spectrum was recorded again. The same results as above were obtained, strongly suggesting that the correct formulation for this complex is as shown for **Ag-Pd-1**, which is similar to that of **Cu-Pd-1**. In view of the disagreement between the single crystal X-ray diffraction data and the NMR data, the crystalline solid was also submitted to energy-dispersive X-ray spectroscopy (EDX), which showed that the 2 : 1 ratio of Ag to Pd. The structure of **Ag-Pd-1** with a Ag-Ag-Pd chain was also supported by its further transformation reaction to **Ag-Pd-2** (see below).

Although **Ag-Pd-1** is air stable in the solid-state for weeks, its CH_2Cl_2 solutions evolve with time (complete transformation in ca. two weeks) by first a mutual exchange between the central Ag(I) and the Pd(0) atom forming an intermediate complex **Ag-Pd-1'** containing a Ag-Pd-Ag metal chain. It was characterized in ^{31}P{^{1}H} NMR by two doublets at δ 114.3 ($^{1}J_{P\text{-}109Ag}$ = 587.5 Hz, $^{1}J_{P\text{-}107Ag}$ = 508.5 Hz). This intermediate evolved further in CH_2Cl_2 to give the new heterotrinuclear complex **Ag-Pd-2**, in quantitative spectroscopic yield, as a result of oxidation by the solvent (CH_2Cl_2) of the central Pd(0) to Pd(II) (see Experimental part). This oxidation was also observed by adding [$PtCl_2(PhCN)_2$] in the solution of **Ag-Pd-1** in MeCN (complete transformation in ca. three days).

The complex **Ag-Pd-2** was characterized by two doublets at δ 112.3 ($J_{P\text{-}109Ag}$ = 590.7 Hz, $J_{P\text{-}107Ag}$ = 512.6 Hz) in ^{31}P{^{1}H} NMR spectroscopy and one triplet in ^{13}C{^{1}H} NMR at δ 184.8 ($^{2}J_{CP}$ = 17.8 Hz) for C_{NHC}. These data suggested a symmetric arrangement of the metal chain and this was confirmed unambiguously by an X-ray

For references, see P135

diffraction analysis of this complex (Figure 4).

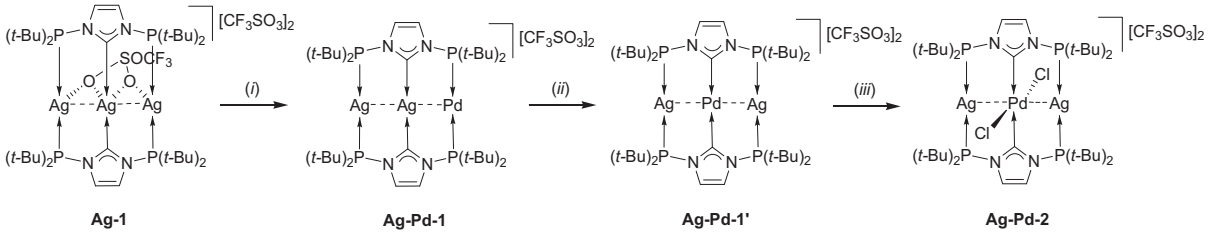

Scheme 2. Transmetallation reactions of trinuclear **Ag-1**. Reagents and conditions: (*i*) 1 equiv $[Pd(PPh_3)_4]$, in CH_2Cl_2, 1h, RT; (*ii*) slow evaporation in air until dryness; (iii) leaving the solid in $MeCN/CH_2Cl_2$ (10:1) for two weeks at RT.

The centrosymmetric cation of **Ag-Pd-2** displays a Ag-Pd-Ag metal chain doubly bridged by the $\mathbf{PC_{NHC}P}$ in a $\mu_3,\kappa P,\kappa C,\kappa P$ bonding mode. The Pd atom occupies a center of symmetry and two chlorido ligands and two C_{NHC} donors form the square planar coordination environment around the Pd center. The presence of two triflate anions leads to consider the metal chain as formally constituted of a 28 metal valence electrons Ag(I)-Pd(II)-Ag(I) chain. Although the chlorido ligands occupy semi-bridging positions between Pd and Ag, the respective bond lengths clearly indicate that they should be assigned to the Pd(II) center. The Pd(II) coordination plane (C1, C1', Cl1, Cl1') forms a dihedral angle of 75.24° with the two imidazole rings as a result of the weak interaction between the outer Ag and Cl atom (2.997 Å).[13] However, this secondary bonding interaction between Ag and Cl does not elongate the Pd-Cl bond distance (2.286(1) Å), which is still in the expected range.[14] The short Ag(I)-Pd(II) bond length of 2.8046(5) (shorter than the sum of van der Waals radii 3.35 Å),[15] is comparable to that reported for the Ag(I)-Pd(II) bonds (2.7637(1) and 2.8014(6) Å) in $Mn_2Pd_2Ag(\mu\text{-Cl})(\mu\text{-}PPh_2)_2(\mu\text{-dppm})(CO)_8$, and indicates the occurrence of d^{10}-d^8-d^{10} interactions in **Ag-Pd-2**.[1c,16]

For references, see P135

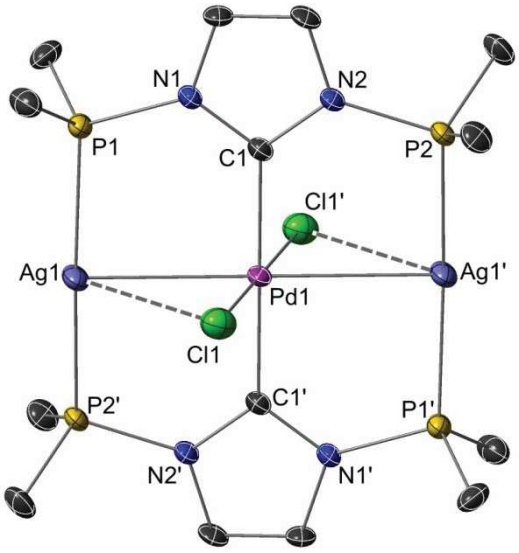

Figure 4. Thermal ellipsoid representation (30% probability level) of the structure of **Ag-Pd-2**. H atoms, two triflate anions and the *t*-Bu Me groups are omitted for clarity. Selected bond lengths (Å) and angles [°]: Pd1-C1 2.065(5), Pd1-Cl1 2.286(1), Ag1-P1 2.395(1), Ag1-P2' 2.392(1), Pd1-Ag1 2.8046(5); C1-Pd1-C1' 180.0, C1-Pd1-Cl1' 90.65(15), C1-Pd1-Cl1 89.35(15), Cl1-Pd1-Cl1' 180.0, P2'-Ag1-P1 168.04(5), Ag1-Pd1-Ag1' 180.0, Ag1-Pd1-C1 90.00(14), Ag1-Pd1-Cl1 71.30(4), Ag1-Pd1-Cl1' 108.71(4), Pd1-Ag1-P2' 88.98(4), Pd1-Ag1-P1 88.46(4).

Conclusion

We have demonstrated in this work that homotrinuclear complexes **Cu-1** and **Ag-1** in which the metal chain is doubly bridged by the recently discovered *N,N'*-diphosphanyl-imidazol-2-ylidene ligand (P-C_{NHC}-P), could be used for partial and selective or fully transmetallation with Pd(0) precursors. When one equivalent of [$Pd(PPh_3)_4$] was used for **Cu-1** and **Ag-1** in CH_2Cl_2, one of the outer metal was replaced by Pd(0) forming **Cu-Pd-1** and **Ag-Pd-1** with d^{10}-d^{10}-d^{10} interactions, respectively. Increasing to more than three equivalent of [$Pd(PPh_3)_4$] to **Cu-1** led to the reducing product **Cu-Pd-2** with a Pd-Cu-Pd (d^9-$d^{10}s^1$-d^9) metal chain. Changing to [$Pd(dba)_2$] in MeCN afforded one homotrinuclar **Pd-1** by fully tranmetallation. However, for **Ag-1** no further reaction happened even adding more [$Pd(PPh_3)_4$] except oxidation of **Ag-Pd-1** by solvent (CH_2Cl_2) giving a novel complex **Ag-Pd-2** with d^{10}-d^8-d^{10} bonding interaction.

For references, see P135

References

(1) (a) Buchwalter, P.; Rosé, J.; Braunstein, P. *Chem. Rev.* **2015**, *115*, 28-126. (b) Dau, M. T.; Shakirova, J. R.; Karttunen, A. J.; Grachova, E. V.; Tunik, S. P.; Melnikov, A. S.; Pakkanen, T. A.; Koshevoy, I. O. *Inorg. Chem.* **2014**, *53*, 4705-4715. (c) Crespo, O.; Gimeno, M. C.; Laguna, A.; Lehtonen, O.; Ospino, I.; Pyykkö, P.; Villacampa, M. D. *Chem.–Eur. J.* **2014**, *20*, 3120-3127. (d) Forniés, J.; Martin, A. In *Metal Clusters in Chemistry*; Wiley-VCH Verlag GmbH: 2008, p 417-443. (e) Bauer, J.; Braunschweig, H.; Dewhurst, R. D. *Chem. Rev.* **2012**, *112*, 4329-4346. (f) Sculfort, S.; Braunstein, P. *Chem. Soc. Rev.* **2011**, *40*, 2741-2760. (g) Katz, M. J.; Sakai, K.; Leznoff, D. B. *Chem. Soc. Rev.* **2008**, *37*, 1884-1895. (h) Yam, V. W.-W.; Cheng, E. C.-C. *Chem. Soc. Rev.* **2008**, *37*, 1806-1813. (i) Díez, Á.; Lalinde, E.; Moreno, M. T. *Coord. Chem. Rev.* **2011**, *255*, 2426-2447.

(2) (a) Liu, I. P.-C.; Lee, G.-H.; Peng, S.-M.; Bénard, M.; Rohmer, M.-M. *Inorg. Chem.* **2007**, *46*, 9602-9608. (b) Liu, I. P.-C.; Chen, C.-H.; Chen, C.-F.; Lee, G.-H.; Peng, S.-M. *Chem. Commun.* **2009**, 577-579. (c) Hosokawa, T.; Takano, M.; Murahashi, S.-I. *J. Am. Chem. Soc.* **1996**, *118*, 3990-3991. (d) Ichieda, N.; Kamimura, T.; Wasada-Tsutsui, Y.; Funahashi, Y.; Ozawa, T.; Jitsukawa, K.; Masuda, H. *Chem. Lett.* **2008**, *37*, 1220-1221. (e) Ichieda, N.; Hakamata, H.; Ozawa, T.; Funahashi, Y.; Jitsukawa, K.; Masuda, H. *The Open Nanoscience Journal* **2009**, *3*, 12-14.

(3) (a) Nakajima, T.; Konomoto, H.; Ogawa, H.; Wakatsuki, Y. *J. Organomet. Chem.* **2007**, *692*, 5071-5080. (b) Tanabe, M.; Ishikawa, N.; Chiba, M.; Ide, T.; Osakada, K.; Tanase, T. *J. Am. Chem. Soc.* **2011**, *133*, 18598-18601.

(4) (a) Ebihara, M.; Tokoro, K.; Maeda, M.; Ogami, M.; Imaeda, K.; Sakurai, K.; Masuda, H.; Kawamura, T. *J. Chem. Soc., Dalton Trans.* **1994**, 3621-3635. (b) Wu, B.; Zhang, W.-J.; Yu, S.-Y.; Sheng, T.-L.; Wu, X.-T. *J. Organomet. Chem.* **1997**, *545–546*, 587-589.

(5) (a) Mechler, M.; Frey, W.; Peters, R. *Organometallics* **2014**, *33*, 5492-5508. (b) Heckenroth, M.; Kluser, E.; Neels, A.; Albrecht, M. *Angew. Chem. Int. Ed.* **2007**, *46*, 6293-6296. (c) Alonso, E.; Forniés, J.; Fortuño, C.; Martín, A.; Orpen, A. G. *Organometallics* **2003**, *22*, 5011-5019. (d) Kessler, F.; Szesni, N.; Maaß, C.; Hohberger,

For references, see P135

C.; Weibert, B.; Fischer, H. *J. Organomet. Chem.* **2007**, *692*, 3005-3018. (e) Alonso, E.; Forniés, J.; Fortuño, C.; Lledós, A.; Martín, A.; Nova, A. *Inorg. Chem.* **2009**, *48*, 7679-7690. (f) Kickham, J. E.; Loeb, S. J. *Organometallics* **1995**, *14*, 3584-3587. (g) Micksch, M.; Herdtweck, E.; Strassner, T. *Z. Anorg. Allg. Chem.* **2013**, *639*, 1237-1241. (h) Khutia, A.; Shen, W.-Z.; Das, N.; Sanz Miguel, P. J.; Lippert, B. *Inorg. Chim. Acta* **2014**, *417*, 274-286. (i) Glaum, M.; Kläaui, W.; Skelton, B. W.; White, A. H. *Aust. J. Chem.* **1997**, *50*, 1047-1052. (j) Ebihara, M.; Tsuchiya, M.; Yamada, M.; Tokoro, K.; Kawamura, T. *Inorg. Chim. Acta* **1995**, *231*, 35-43. (k) Braunstein, P.; Frison, C.; Oberbeckmann-Winter, N.; Morise, X.; Messaoudi, A.; Bénard, M.; Rohmer, M.-M.; Welter, R. *Angewandte Chemie* **2004**, *116*, 6246-6251. (l) Si, T.; Huang, S.; Zhang, j. *CHINESE JOURNAL OF INORGANIC CHEMISTRY* **2003**, *19*, 983-987. (m) Liu, Y.; Lee, K. H.; Vittal, J. J.; Hor, T. S. A. *J. Chem. Soc., Dalton Trans.* **2002**, 2747-2751. (n) Heckenroth, M.; Neels, A.; Garnier, M. G.; Aebi, P.; Ehlers, A. W.; Albrecht, M. *Chem. – Eur. J.* **2009**, *15*, 9375-9386. (o) Arias, A.; Forniés, J.; Fortuño, C.; Martín, A.; Mastrorilli, P.; Gallo, V.; Latronico, M.; Todisco, S. *Eur. J. Inorg. Chem.* **2014**, *2014*, 1679-1693. (p) Tulloch, A. A. D.; Winston, S.; Danopoulos, A. A.; Eastham, G.; Hursthouse, M. B. *Dalton Trans.* **2003**, 699-708.

(6) Mednikov, E. G.; Dahl, L. F. *Angew. Chem. Int. Ed.* **2013**, *52*, 7813-7817.

(7) Usón, R.; Usón, M. A.; Herrero, S. *Inorg. Chem.* **1997**, *36*, 5959-5961.

(8) (a) Tong, G. S. M.; Kui, S. C. F.; Chao, H.-Y.; Zhu, N.; Che, C.-M. *Chem.–Eur. J.* **2009**, *15*, 10777-10789. (b) Tanase, T.; Otaki, R.; Nishida, T.; Takenaka, H.; Takemura, Y.; Kure, B.; Nakajima, T.; Kitagawa, Y.; Tsubomura, T. *Chem.–Eur. J.* **2014**, *20*, 1577-1596. (c) Bestgen, S.; Gamer, M. T.; Lebedkin, S.; Kappes, M. M.; Roesky, P. W. *Chem.–Eur. J.* **2015**, *21*, 601-614.

(9) (a) Furst, M. R. L.; Cazin, C. S. J. *Chem. Commun.* **2010**, *46*, 6924-6925. (b) Liu, X.; Pattacini, R.; Deglmann, P.; Braunstein, P. *Organometallics* **2011**, *30*, 3302-3310. (c) Gierz, V.; Maichle-Mössmer, C.; Kunz, D. *Organometallics* **2012**, *31*, 739-747. (d) Venkatachalam, G.; Heckenroth, M.; Neels, A.; Albrecht, M. *Helv. Chim. Acta* **2009**, *92*, 1034-1045. (e) Badaj, A. C.; Lavoie, G. G. *Organometallics* **2012**, *31*, 1103-1111. (f) Chen, C.; Qiu, H.; Chen, W. *J. Organomet. Chem.* **2012**, *696*, 4166-4172. (g) Al Thagfi,

For references, see P135

J.; Lavoie, G. G. *Organometallics* **2012**, *31*, 2463-2469. (h) Bullough, E. K.; Little, M. A.; Willans, C. E. *Organometallics* **2013**, *32*, 570-577. (i) Slivarichova, M.; Reading, E.; Haddow, M. F.; Othman, H.; Owen, G. R. *Organometallics* **2012**, *31*, 6595-6607. (j) Mormul, J.; Steimann, M.; Nagel, U. *Eur. J. Inorg. Chem.* **2014**, *2014*, 1389-1393.

(10) Pyykkö, P. *Chem. Rev.* **1997**, *97*, 597-636.

(11) Ai, P.; Danopoulos, A. A.; Braunstein, P.; Monakhov, K. Y. *Chem. Commun.* **2014**, *50*, 103-105.

(12)Bollermann, T.; Prabusankar, G.; Gemel, C.; Seidel, R. W.; Winter, M.; Fischer, R. A. *Chem.–Eur. J.* **2010**, *16*, 8846-8853.

(13) (a) Usón, R.; Forniés, J.; Tomás, M.; Ara, I. *Inorg. Chim. Acta* **1991**, *186*, 67-71. (b) Wulfsberg, G.; Kravchenko, E.; Morgunov, V. G.; Miller, S.; Anderson, O.; Barnes, T.; Briggs, R.; MacDougall, P. *Inorg. Chim. Acta* **2008**, *361*, 2471-2482. (c) Chen, J.-H.; Liu, Y.-M.; Zhang, J.-X.; Zhu, Y.-Y.; Tang, M.-S.; Ng, S. W.; Yang, G. *CrystEngComm* **2014**, *16*, 4987-4998.

(14) (a) Lebel, H.; Janes, M. K.; Charette, A. B.; Nolan, S. P. *J. Am. Chem. Soc.* **2004**, *126*, 5046-5047. (b) Altenhoff, G.; Goddard, R.; Lehmann, C. W.; Glorius, F. *J. Am. Chem. Soc.* **2004**, *126*, 15195-15201.

(15) Bondi, A. *J. Phys. Chem.* **1964**, *68*, 441-451.

(16) Doerrer, L. H. *Dalton Trans.* **2010**, *39*, 3543-3553.

For references, see P135

ESI

Selective Partial or Complete Transmetallation of Trinuclear Cu(I) or Ag(I) Complexes leading to Hetero- or Homo-trinuclear Pd Complexes

Pengfei Ai,[a] Andreas A. Danopoulos,*[a,b] Pierre Braunstein*[a]

[a] Laboratoire de Chimie de Coordination, Institut de Chimie (UMR 7177 CNRS), Université de Strasbourg, 4 rue Blaise Pascal, 67081 Strasbourg Cedex, France. E-mail: danopoulos@unistra.fr, braunstein@unistra.fr

[b] Institute for Advanced Study, USIAS, Université de Strasbourg, France.

For references, see P145

Experimental section:

1. Synthesis and characterisation

1.1 General methods

All manipulations involving organometallics were performed under argon using standard Schlenk techniques. Solvents were dried using standard methods and distilled under nitrogen prior use or passed through columns of activated alumina and subsequently purged with nitrogen or argon. $[Pd(PPh_3)_4]$[1] and $[Pd(dba)_2]$[2]were prepared as described. **Ag-1** and **Cu-1** were prepared according to our previous report.[3]

1.2 Synthesis of complex **Cu-Pd-1**.

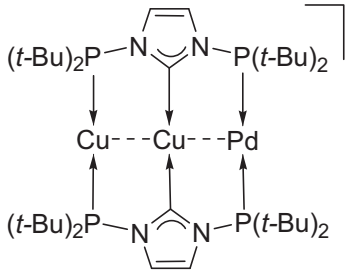

To a solid mixture of **Cu-1** (0.050 g, 0.037 mmol) and $[Pd(PPh_3)_4]$ (0.050 g, 0.043 mmol) was added 4 ml CH_2Cl_2 at room temperature and the solution was stirred overnight. After evaporation of the volatile under vacuum, the residue was washed with Et_2O (20 ml) and THF (4 ml) and dried under vacuum to give a green powder (0.028 g, 61%). X-ray quality crystals (green prisms) were obtained by diffusion of pentane into its CH_2Cl_2 solution. This isolated complex decomposes slowly in CH_2Cl_2 or MeCN. Analysis: Found (Calc. for $C_{40}H_{76}Cu_2F_6N_4O_6P_4PdS_2$) (%): C, 38.44 (38.60), H, 5.99 (6.15), N, 4.20 (4.50). ^{1}H NMR (400 MHz, CD_2Cl_2): δ 7.94 (d, 2H, J_{HH} = 2.0 Hz, im-*H*), 7.87 (d, 2H, J_{HH} = 2.0 Hz, im-*H*), 1.49-1.44 (72H, C(C*H*$_3$)$_3$). ^{13}C{^{1}H} NMR (125 MHz, CD_2Cl_2): δ 197.6 (t, $^2J_{CP}$ = 26.8 Hz, N*C*N), 127.4 (im-*C*), 126.7 (im-*C*), 122.1 (q, $^1J_{CF}$ = 320.6 Hz, *C*F$_3$), 38.5 (*C*(CH$_3$)$_3$), 37.5 (*C*(CH$_3$)$_3$), 29.8 (t, $^2J_{CP}$ = 6.3 Hz, C(*C*H$_3$)$_3$), 29.2 (t, $^2J_{CP}$ = 4.3 Hz, C(*C*H$_3$)$_3$). ^{31}P{^{1}H} NMR (162 MHz, CD_2Cl_2): δ 122.0 (s), 101.0 (br).

1.3 Synthesis of complex **Cu-Pd-2**.

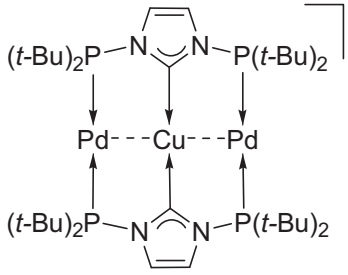

To a solid mixture of **Cu-1** (0.070 g, 0.052 mmol) and $[Pd(PPh_3)_4]$ (0.200 g, 0.173 mmol) was added 5 ml CH_2Cl_2 at room temperature

For references, see P145

and the solution was stirred overnight. After evaporation of the volatile under vacuum, the residue was washed with Et_2O (10 ml). The solid was dissolved again in 2 ml CH_2Cl_2 and then 10 ml pentane was layered on it for crystallization. After two days, the supernatant was removed by pipette and the residue was washed by THF (3×4 ml) and dried under vacuum to give a yellow crystalline material in the form of prisms or plates (0.030 g, 45%). X-ray quality crystals were obtained by diffusion of pentane into its CH_2Cl_2 solution. Analysis: Found (Calc. for $C_{40}H_{76}CuF_6N_4O_6P_4Pd_2S_2$) (%): C, 37.90 (37.32), H, 6.01 (5.95), N, 4.37 (4.35).

1.4 Synthesis of palladium complexes **Pd-1**.

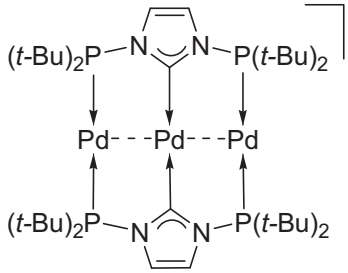

To a mixture of **Cu-1** (0.030 g, 0.022 mmol) and $[Pd(dba)_2]$ (0.050 g, 0.087 mmol) was added 6 ml CH_3CN at room temperature and stirred for 4 days. After filtration with celite, the filtrate was concentrated until 1 ml and Et_2O (10 ml) was layered on it for crystallization. After 3 days the supernatant was removed by pipette and dried under vacuum to give **Pd-1** a dark red-black crystalline material (0.029 g, 55%). X-ray quality crystals were obtained by slow diffusion of ether into its CH_3CN solution. Analysis: Found (Calc. for $C_{40}H_{76}F_6N_4O_6P_4Pd_3S_2$) (%): C, 36.35 (36.11), H, 5.79 (5.76), N, 4.57 (4.21). ^{1}H NMR (400 MHz, CD_3CN): δ 7.56 (s, 4H, im-*H*), 1.48 (t, 72H, $^3J_{HP}$ = 7.9 Hz, C(C*H*$_3$)$_3$). ^{13}C{^{1}H} NMR (125 MHz, CD_3CN): δ 181.4 (t, $^2J_{CP}$ = 18.1 Hz, N*C*N), 126.7 (im-*C*), 121.7 (q, $^1J_{CF}$ = 321.4 Hz, *C*F$_3$), 38.9 (*C*(CH$_3$)$_3$), 29.8 (C(*C*H$_3$)$_3$). ^{31}P{^{1}H} NMR (162 MHz, CD_3CN): δ 112.2 (s).

1.5 Synthesis of complex **Ag-Pd-1**.

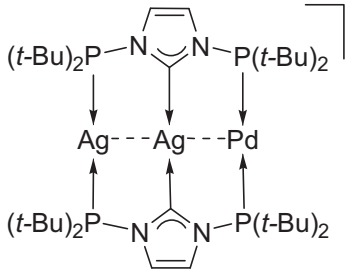

To a solid mixture of **Ag-1** (0.057 g, 0.038 mmol) and $[Pd(PPh_3)_4]$ (0.046 g, 0.040 mmol) was added 5 ml CH_2Cl_2 at room temperature and the solution was stirred for 1 h, leading to the formation of a metal mirror on the walls of the Schlenk tube. After filtering off the metal, the filtrate was evaporated to dryness and washed with THF (10 ml). The solid was dissolved in 1 ml MeCN and

For references, see P145

then 10 ml Et_2O was layered on it for crystallization. After 4 days, the supernatant was removed by pipette and dried under vacuum to give a yellow-green crystalline material (0.030 g, 59%). X-ray quality crystals were obtained by slow diffusion of ether into its MeCN solution. Analysis: Found (Calc. for $C_{40}H_{76}Ag_2F_6N_4O_6P_4PdS_2$) (%): C, 35.93 (36.03), H, 5.90 (5.75), N, 4.11 (4.20). ^{1}H NMR (400 MHz, CD_3CN): δ 7.89 (s, 4H, im-*H*), 1.46-1.41 (72H, C(C*H*$_3$)$_3$). ^{1}H NMR (400 MHz, CD_2Cl_2): δ 8.08 (s, 2H, im-*H*), 7.97 (s, 2H, im-*H*), 1.51-1.45 (72H, C(C*H*$_3$)$_3$). ^{13}C{^{1}H} NMR (125 MHz, CD_3CN): δ 204.0 (m, $^1J_{C\text{-}109Ag}$ = 197.8 Hz, $^1J_{C\text{-}107Ag}$ = 168.9 Hz, N*C*N), 128.2 (d, $^2J_{CP}$ = 5.7 Hz, im-*C*), 127.4 (t, $^2J_{CP}$ = 4.5 Hz, im-*C*), 122.1 (q, $^1J_{CF}$ = 321.5 Hz, *C*F$_3$), 39.0 (*C*(CH$_3$)$_3$), 38.0 (d, $^1J_{CP}$ = 4.8 Hz, *C*(CH$_3$)$_3$), 30.0 (t, $^2J_{CP}$ = 6.9 Hz, C(*C*H$_3$)$_3$), 29.2 (t, $^2J_{CP}$ = 5.8 Hz, C(*C*H$_3$)$_3$). ^{31}P{^{1}H} NMR (162 MHz, CD_3CN): δ 126.8 (s), two doublets at 119.2 ($J_{P\text{-}109Ag}$ = 559.8 Hz, $J_{P\text{-}107Ag}$ = 485.0 Hz). ^{31}P{^{1}H} NMR (162 MHz, CD_2Cl_2): δ 127.0 (s), two doublets at 120.4 ($J_{P\text{-}109Ag}$ = 561.4 Hz, $J_{P\text{-}107Ag}$ = 487.0 Hz).

1.6 Detection of intermediate complex **Ag-Pd-1' and** Synthesis of **Ag-Pd-2**.

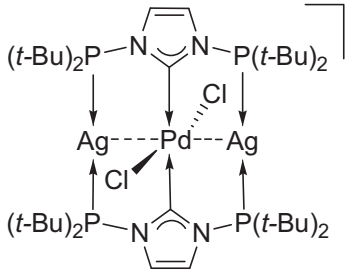

The isolated complex **Ag-Pd-1** is not stable in CH_2Cl_2 for a long period of time and slow evaporation of its solution in CH_2Cl_2 in the air gave the mixture of intermediate **Ag-Pd-1'** and **Ag-Pd-2** as a yellow crystalline material in quantitative yield. The pure intermediate **Ag-Pd-1'** could not be isolated, but leaving the mixture of **Ag-Pd-1'** and **Ag-Pd-2** in MeCN/CH_2Cl_2 (ratio ca. 10:1) for one or two weeks led the complete conversion of **Ag-Pd-1'** to **Ag-Pd-2** and pure **Ag-Pd-2** was isolated. X-ray quality crystals were obtained by slow diffusion of ether into its MeCN solution or by slow evaporation of a solution of **Ag-Pd-1** in CH_2Cl_2 in the air. For **Ag-Pd-2:** Analysis: Found (Calc. for $C_{40}H_{76}Ag_2Cl_2F_6N_4O_6P_4PdS_2$) (%): C, 33.93 (34.22), H, 5.49 (5.46), N, 4.44 (3.99). ^{1}H NMR (400 MHz, CD_3CN): δ 7.85 (s, 4H, im-*H*), 1.50 (t, 72H, $^3J_{HP}$ = 8.5 Hz, C(C*H*$_3$)$_3$). ^{13}C{^{1}H} NMR (125 MHz, CD_3CN): δ 184.8 (t, $^2J_{CP}$ = 17.8 Hz, N*C*N), 128.4 (d, $^2J_{CP}$ = 4.2 Hz, im-*C*), 122.1 (q, $^1J_{CF}$ = 320.7 Hz, *C*F$_3$), 39.0 (d, $^1J_{CP}$ = 4.3 Hz, *C*(CH$_3$)$_3$), 30.0 (t, $^2J_{CP}$ = 5.6 Hz, C(*C*H$_3$)$_3$). ^{31}P{^{1}H} NMR (162 MHz, CD_3CN): two doublets at δ 112.3 ($J_{P\text{-}109Ag}$ = 590.7 Hz, $J_{P\text{-}107Ag}$ = 512.6 Hz).

For references, see P145

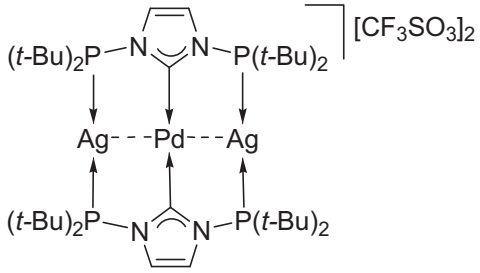

For intermediate **Ag-Pd-1'**: ^{1}H NMR (400 MHz, CD_3CN): δ 7.83 (s, 4H, im-*H*), 1.58 (t, 36H, $^{3}J_{HP}$ = 8.6 Hz, C(C*H*$_3$)$_3$), 1.45 (t, 36H, $^{3}J_{HP}$ = 8.7 Hz, C(C*H*$_3$)$_3$). ^{13}C{^{1}H} NMR (125 MHz, CD_3CN): δ 197.6 (t, $^{2}J_{CP}$ = 19.8 Hz, N*C*N), 134.5 (d, $^{2}J_{CP}$ = 16.3 Hz, im-*C*), 130.3 (d, $^{2}J_{CP}$ = 9.9 Hz, im-*C*), 122.1 (q, $^{1}J_{CF}$ = 320.7 Hz, *C*F$_3$), 39.7 (d, $^{1}J_{CP}$ = 3.3 Hz, *C*(CH$_3$)$_3$), 38.6 (d, $^{1}J_{CP}$ = 5.3 Hz, *C*(CH$_3$)$_3$) 30.1 (t, $^{2}J_{CP}$ = 5.2 Hz, C(*C*H$_3$)$_3$), 29.8 (t, $^{2}J_{CP}$ = 5.8 Hz, C(*C*H$_3$)$_3$). ^{31}P{^{1}H} NMR (162 MHz, CD_3CN): two doublets at δ 114.3 ($J_{P\text{-}109Ag}$ = 587.5 Hz, $J_{P\text{-}107Ag}$ = 508.5 Hz).

2. X-ray crystallography

Summary of the crystal data, data collection and refinement for structures of **Cu-Pd-1•** CH_2Cl_2**, Cu-Pd-2**, **Pd-1** and **Ag-Pd-2** are given in Table S1. X-ray diffraction data collection was carried out on a Bruker APEX II DUO Kappa-CCD diffractometer equipped with an Oxford Cryosystem liquid N_2 device, using Mo-Kα radiation (λ = 0.71073 Å). The crystal-detector distance was 38 mm. The cell parameters were determined (APEX2 software)[4] from reflections taken from three sets of 12 frames, each at 10s exposure. The structure was solved by Direct methods using the program SHELXS-97.[5] The refinement and all further calculations were carried out using SHELXL-97.[6] The H-atoms were included in calculated positions and treated as riding atoms using SHELXL default parameters. The non-H atoms were refined anisotropically, using weighted full-matrix least-squares on F^2. A semi-empirical absorption correction was applied using SADABS in APEX2.[4]

The following special comments apply to the models of the structures:

For **Cu-Pd-1•** CH_2Cl_2, a squeeze was made. The residual electron density was assigned to two molecules of the dichloromethane.

For **Cu-Pd-2**, the copper is in a special position (population 50%).

For references, see P145

For **Pd-1**, the palladium Pd1 is in a special position (population 50%). A squeeze was made. The residual electron density was assigned to one molecule of acetonitrile.

For **Ag-Pd-2**, the palladium is in a special position (population 50%). A squeeze was made to remove residual density peaks. The residual electron density does not correspond to solvent. So there is not explication of the squeeze in the CIF.

For references, see P145

2.1 Summary of crystal data

Table S1. Crystal data for compounds **Cu-Pd-1**• CH_2Cl_2**, Cu-Pd-2**, **Pd-1** and **Ag-Pd-2.**

	Cu-Pd-1• CH_2Cl_2	**Cu-Pd-2**	**Pd-1**	**Ag-Pd-2**
Chemical formula	$C_{40}H_{76}Cu_2F_6N_4O_6P_4PdS_2$•$CH_2Cl_2$	$C_{40}H_{76}CuF_6N_4O_6P_4Pd_2S_2$	$C_{40}H_{76}F_6N_4O_6P_4Pd_3S_2$	$C_{40}H_{76}Ag_2Cl_2F_6N_4O_6P_4PdS_2$
CCDC Number				
Formula Mass	1329.45	1287.38	1330.24	1404.08
Crystal system	Monoclinic	Monoclinic	Monoclinic	Triclinic
a/Å	14.8742(2)	8.837(6)	13.9630(3)	9.2039(10)
b/Å	19.0270(4)	12.438(9)	8.5889(2)	12.4421(13)
c/Å	22.2166(4)	25.885(19)	26.8437(6)	13.5865(15)
α/°	90	90	90	108.966(2)
β/°	95.6480(10)	97.161(17)	117.3280(10)	90.630(2)
γ/°	90	90	90	94.251(2)
Unit cell volume/Å^3	6257.03(19)	2823(4)	2859.98(11)	1466.3(3)
Temperature/K	173(2)	173(2)	173(2)	173(2)
Space group	*P21/c*	*P 21/c*	*P2/c*	*P-1*
Formula units / cell, *Z*	4	2	2	1
Absorption coefficient, μ/mm^{-1}	1.271	1.254	1.180	1.298
No. of reflections measured	54450	23287	20043	20130
No. of independent reflections	14334	6634	6555	7185
R_{int}	0.0850	0.0460	0.0527	0.0513
Final R_1 values ($I > 2\sigma(I)$)	0.0577	0.0757	0.0529	0.0574
Final $wR(F^2)$ values ($I > 2\sigma(I)$)	0.1603	0.2127	0.1465	0.1373
Final R_1 values (all data)	0.0863	0.1051	0.0724	0.0997
Final $wR(F^2)$ values (all data)	0.1742	0.2305	0.1572	0.1511
Goodness of fit on F^2	1.062	1.080	1.111	0.951

For references, see P145

References:

(1) Coulson, D. R. *Inorg. Synth.* **1990**, *28*, 107.

(2) Rettig, M. F.; Maitlis, P. M. *Inorg. Synth.* **1990**, *28*, 110.

(3) Ai, P.; Danopoulos, A. A.; Braunstein, P.; Monakhov, K. Y. *Chem. Commun.* **2014**, *50*, 103.

(4) Bruker AXS Inc Madison USA, 2006.

(5) Sheldrick, G. M. *Acta Crystallogr. Sect. A: Found. Crystallogr.* **1990**, *A46*, 467.

(6) Sheldrick, G. M. Universität Göttingen: Göttingen Germany, 1999.

For references, see P145

Chapter 7

Novel Di- and Tri-nuclear Pd Complexes Supported by *N*,*N*'-Diphosphanyl NHC Ligands and *N*,*N*'-Diphosphanyl Imidazolium Pd, Au and Mixed-Metal Cu-Au Complexes

This chapter is written as a publication to be submitted.

My contribution in this work included the synthesis of the complexes, their characterization and the preparation of the draft of the publication.

Novel Di- and Tri-nuclear Pd Complexes Supported by *N*,*N*'-Diphosphanyl NHC Ligands and *N*,*N*'-Diphosphanyl Imidazolium Pd, Au and Mixed-Metal Cu-Au Complexes

Pengfei Ai,[a] Christophe Gourlaouen,[b] Andreas A. Danopoulos,*[a,c] and Pierre Braunstein*[a]

[a] Laboratoire de Chimie de Coordination, Institut de Chimie (UMR 7177 CNRS), Université de Strasbourg, 4 rue Blaise Pascal, 67081 Strasbourg Cedex, France. E-mail: danopoulos@unistra.fr, braunstein@unistra.fr

[b] Laboratoire de Chimie Quantique, Institut de Chimie (UMR 7177 CNRS), Université de Strasbourg, 1 rue Blaise Pascal, 67008 Strasbourg, France

[c] Institute for Advanced Study, USIAS, Université de Strasbourg, France.

For references, see P177

Résumé du Chapitre 7

La réaction de **Ag-1** avec [Pd(dba)$_2$] a conduit à la formation des complexes trinucléaire **Pd-1** et dinucléaire **Pd-2** (Schéma 1). La réactivité du premier vis-à-vis des isonitriles fut examinée.

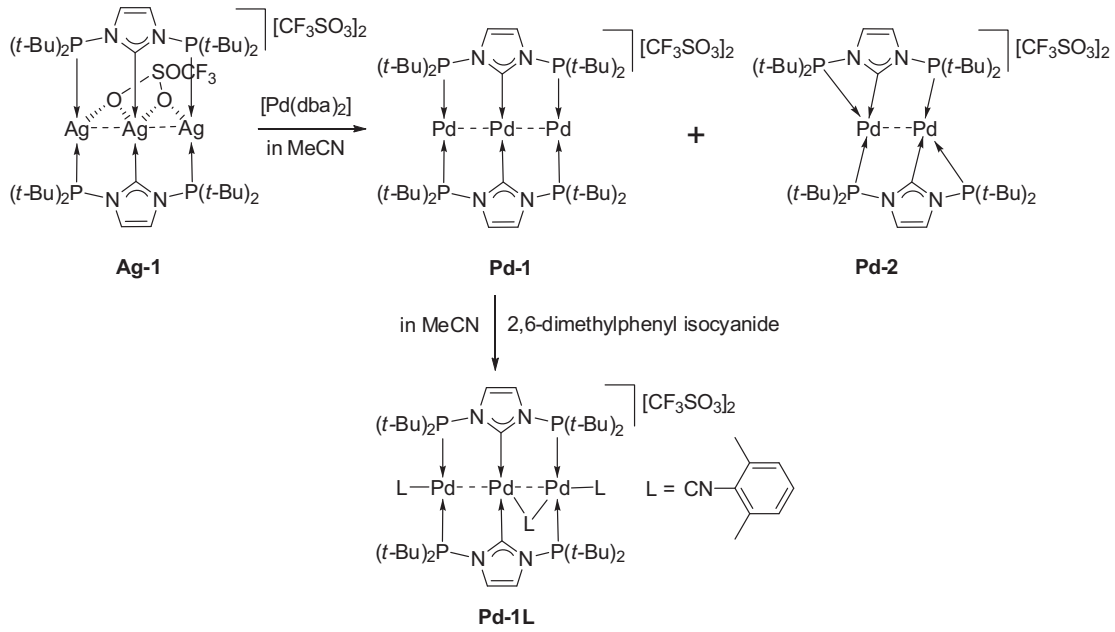

Schéma 1

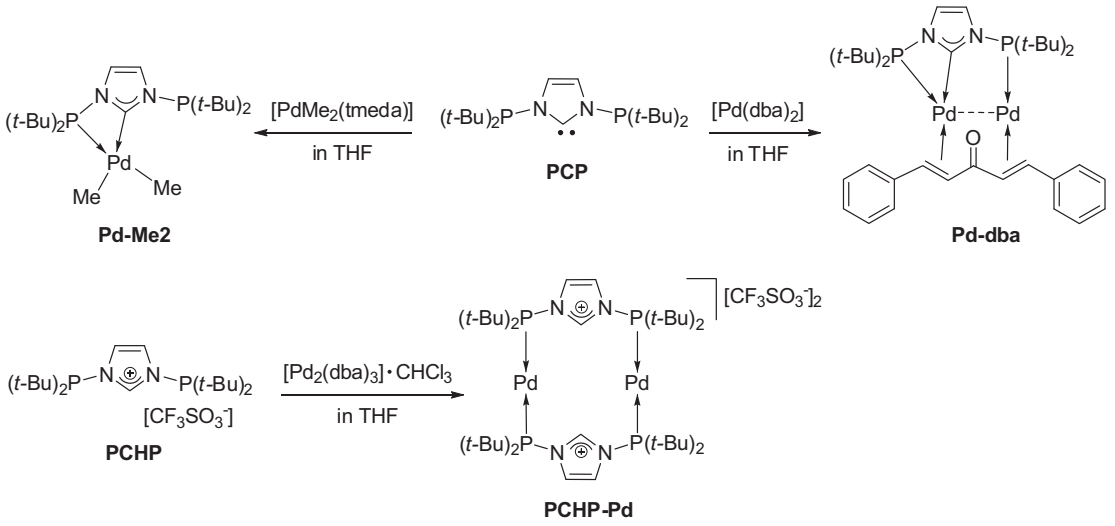

Schéma 2

La coordination directe de **PCP** sur [Pd(dba)$_2$] a conduit au complexe dinucléaire de Pd(0) qui a gardé un ligand dba (Schéma 2). **PCP** joue le rôle d'un chélate dans le complexe diméthyle **Pd-Me2** et montre un angle de pince de

For references, see P177

68.1(2)°. Afin de bloquer les groupes phosphines et de modifier indépendamment l'atome de carbone carbénique, le sel d'imidazolium **PCHP** a été opposé à $[Pd_2(dba)_3]\cdot CHCl_3$ ce qui a conduit au complexe de Pd(0) carré **PCHP-Pd**. Des tentatives de déprotonation ont résulté en la décomposition du complexe.

En utilisant AuCl(tht) à la place du Pd, **PCHP** a donné le complexe **PCHP-Au** ayant une entité Au-Cl liée à chaque donneur P (Schéma 3). Une réaction avec $[(Ph_3P)Au\{N(SiMe_3)_2\}]$ en THF a produit le complexe trinucléaire **Au3** et $[(PPh_3)AuCl]$ (Schéma 3). En passant à [CuMes], un nouveau complexe hétérométallique **PCHP-AuMesCuCl** a été obtenu après perte d'un atome d'or et remplacement d'un chlorure par un groupement mésityle.

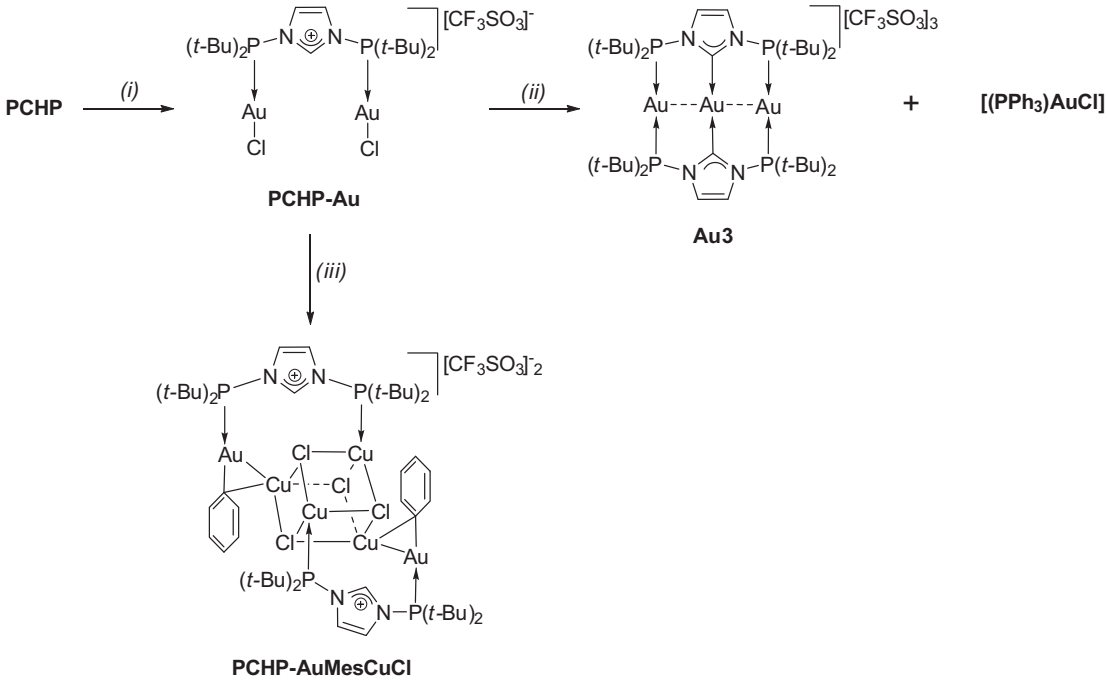

Schéma 3. Synthèse de complexes d'Au(I). Réactifs et conditions: (*i*) 1 equiv. [AuCl(tht)], THF, 3 h, temp. amb.; (*ii*) 1 equiv. $[(Ph_3P)Au\{N(SiMe_3)_2\}]$, THF, 3 h, temp. amb.; (*iii*) 2 equiv. [CuMes], THF, 4 h, temp. amb.

For references, see P177

Novel Di- and Tri-nuclear Pd Complexes Supported by *N*,*N*'-Diphosphanyl NHC Ligands and *N*,*N*'-Diphosphanyl Imidazolium Pd, Au and Mixed-Metal Cu-Au Complexes

Pengfei Ai,[a] Christophe Gourlaouen,[b] Andreas A. Danopoulos,*[a,c] and Pierre Braunstein*[a]

[a] Laboratoire de Chimie de Coordination, Institut de Chimie (UMR 7177 CNRS), Université de Strasbourg, 4 rue Blaise Pascal, 67081 Strasbourg Cedex, France. E-mail: danopoulos@unistra.fr, braunstein@unistra.fr

[b] Laboratoire de Chimie Quantique, Institut de Chimie (UMR 7177 CNRS), Université de Strasbourg, 1 rue Blaise Pascal, 67008 Strasbourg, France

[c] Institute for Advanced Study, USIAS, Université de Strasbourg, France.

ABSTRACT

The reaction of the trinuclear $[Ag_3(\mu_3\text{-}\mathbf{PC_{NHC}P},\kappa P,\kappa C_{NHC},\kappa P)_2](OTf)_3$ (**Ag3**) (**$PC_{NHC}P$** = *N*,*N'*-bis(di-tert-butylphosphanyl)-imidazol-2-ylidene) with $[Pd(dba)_2]$ afforded the trinuclear Pd complex $[Pd_3(\mu_3\text{-}\mathbf{PC_{NHC}P},\kappa P,\kappa C_{NHC},\kappa P)_2](OTf)_2$ (**Pd3**) and the dinuclear Pd(I) complex $[Pd_2(\mu_2\text{-}\mathbf{PC_{NHC}P},\kappa P,\kappa C_{NHC},\kappa P)_2](OTf)_2$ (**Pd2**). The assignment of the oxidation state of the metals in the mixed-valence **Pd3** chain as Pd(0)-Pd(II)-Pd(0) was based on the reactivity of the complex with 2,6-dimethylphenyl isocyanide and DFT calculations. Reaction of **$PC_{NHC}P$** with $[PdMe_2(tmeda)]$ afforded the Pd(II) complex $[PdMe_2(\mathbf{PC_{NHC}P},\kappa P,\kappa C_{NHC})]$ (**Pd-Me2**), with **$PC_{NHC}P$** acting as bidentate ligand**.** Reaction of **$PC_{NHC}P$** with $[Pd(dba)_2]$ led to a dinuclear Pd(0) complex $[Pd_2(\mu_2\text{-}\mathbf{PC_{NHC}P},\kappa P,\kappa C_{NHC},\kappa P)](dba)$ (**Pd2-dba**); attempted replacement of the remaining dba by **$PC_{NHC}P$** failed. The triflate salt of the imidazolium cation **PCHP** was reacted with $[Pd_2(dba)_3]\cdot CHCl_3$ to give the (2+2) metalla-mesocyclic cationic Pd(0) complex $[Pd_2(\mu_2\text{-}\mathbf{PCHP},\kappa P,\kappa P)_2]$ (**PCHP-Pd**), which resisted further deprotonation of the imidazolium cation. In contrast, **PCHP** reacted with [AuCl(tht)] to give $[Au_2Cl_2(\mu_2\text{-}\mathbf{PCHP},\kappa P,\kappa P)]$ (**PCHP-Au**), in which one Au-Cl moiety is bound to each P donor. Further reaction of **PCHP-Au** with $[Au\{N(SiMe_3)_2\}(PPh_3)]$ afforded a mixture of the trinuclear $[Au_3(\mu_3\text{-}\mathbf{PC_{NHC}P},\kappa P,\kappa C_{NHC},\kappa P)_2](OTf)_3$ (**Au3**) and $[AuCl(PPh_3)]$, while reaction with $[CuMes]_5$, Mes = 2,4,6-trimethylphenyl, resulted in a novel,

For references, see P177

centrosymmetric, heterometallic complex [$Au_2Mes_2(Cu_4Cl_4)$(**PCHP**,κP,κP)] (**PCHP-AuCu**) featuring a new **PCHP-AuMes** metalloligand bridging a Cu···Cu diagonal of a Cu_4Cl_4 cubane via the P and Au-Mes functionalities.

For references, see P177

Introduction

NHC coordination chemistry has expanded across the periodic table and now finds applications in *e.g.* catalysis, medicinal chemistry and materials science.[1] Hybrid NHC ligands containing (an) additional 'classical' donor functional group(s), such as a phosphino-, amino-, imino-, *etc.* donor, are now being developed as tools for the precise tailoring of NHC-containing metal coordination spheres.[1e,2]

Initially, NHC ligands have been described as trialkylphosphine (PR_3) mimics, in view of their comparable σ-donor properties towards certain transition metal centers,[3] however, the completed and refined metal-NHC bonding model now includes π-backbonding and even π-donor interactions, depending on the nature of the NHC substituents, the metal, the co-ligands and even the NHC ring conformation relative to the coordination sphere.[4] In addition, NHCs and PR_3 show different steric properties. Therefore, NHCs are subtly different donors than phosphines and both functions may be used in complementary or synergistic approaches for creative ligand design purposes.[2e]

Indeed, the recent years have witnessed the development of phosphine-functionalized NHC ligands of different denticity and architectures, in which the donor groups are linked *via* flexible or semi-rigid alkyl or aryl spacers.[2e,5] *N*-phosphanyl-functionalized NHC ligands of type (**I**) (R' = alkyl or aryl) have also been recently described, that feature a 'fine grading' of the σ-donor ability within the same very rigid ligand.[6] They adopt a bridging coordination mode with certain d^{10} coinage metals, but also a chelating mode $\kappa P,\kappa C_{NHC}$ with small bite angles (*ca*. 68.2°), in particular with platinum group or late transition metals.[6b,6d-f,7]

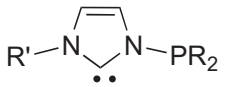

PC_{NHC}

(**type I**)

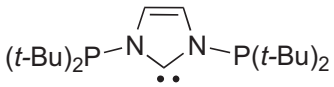

$PC_{NHC}P$

(**type II**)

In this area, we have recently developed a strongly coordinating, tri-functional *N*,*N'*-bis(di-tert-butylphosphanyl)-imidazol-2-ylidene (**$PC_{NHC}P$**) ligand (type (**II**)), which by design should stabilize short arrays of 'σ-loaded' metals,[8] owing to their double

For references, see P177

short-bite, rigid architecture. This has been confirmed with coinage metals, resulting in polynuclear chain complexes.[8] However, **PC$_{NHC}$P** can also act as a **PC$_{NHC}$** chelate ($\kappa P,\kappa C_{NHC}$), or simply a **C**$_{NHC}$ donor, with one or two dangling phosphines, as evidenced in a tribenzyl Cr(III) and a Co(II) silylamide complex, respectively.[9] At first glance, it appears that compared to other short-bite ligands, *e.g.* bis(diphenylphosphino)methane (DPPM),[10] bis(diphenylphosphino)amine (DPPA),[11] diphenyl-2-pyridylphosphine[12] or 1,2-diphosphine imidazole,[13] **PC$_{NHC}$P** is differentiated by the strong σ-donor ability at the central donor, the higher rigidity, the absence of acidic hydrogen atoms at the bridge *etc.* However, detailed insight into the electronic structure of the resulting complexes requires the input from computational methods. Extension of the **PC$_{NHC}$P** coordination chemistry to palladium and gold is the subject of this paper.

Results and discussion

Di- and Tri-nuclear Palladium Complexes with Metal-Metal Bonds.

In view of the broad applicability of NHC transmetallation from silver for the synthesis of NHC complexes, our first approach to access **PC$_{NHC}$P** palladium complexes considered the reaction of the trinuclear complex [Ag$_3$(μ$_3$-**PC$_{NHC}$P**,$\kappa P,\kappa C_{NHC},\kappa P$)$_2$](OTf)$_3$ (**Ag3**) with readily available Pd precursors. Thus, the reaction of **Ag3** with [Pd(dba)$_2$] in MeCN led to the formation of the homotrinuclear [Pd$_3$(μ$_3$-**PC$_{NHC}$P**,$\kappa P,\kappa C_{NHC},\kappa P$)$_2$](OTf)$_2$ (**Pd3**), accompanied by the dinuclear [Pd$_2$(μ$_2$-**PC$_{NHC}$P**,$\kappa P,\kappa C_{NHC},\kappa P$)$_2$](OTf)$_2$ (**Pd2**), in a ratio **Pd1**/**Pd2** of *ca.* 5:2 as determined by ^{31}P{^{1}H} NMR spectroscopy (Scheme 1). Both complexes are air stable and diamagnetic. In solution, **Pd3** shows one ^{31}P{^{1}H} NMR singlet at δ 112.2 and one ^{13}C{^{1}H} NMR triplet at δ 181.4 ($^2J_{CP}$ = 18.1 Hz) for C$_{NHC}$; **Pd2** shows two doublets at δ 139.8 (d, $^2J_{PP}$ = 7.9 Hz) and 94.8 (d, $^2J_{PP}$ = 7.9 Hz) in the ^{31}P{^{1}H}-NMR spectrum, assignable to the P donors of the 4-membered chelate and 5-membered bimetallic rings, respectively, and a singlet at δ 165.6 for C$_{NHC}$ in the ^{13}C{^{1}H}-NMR spectrum. The two complexes were separated by fractional crystallization, and isolated as a dark red-black solid (**Pd3)** and as a brown-yellow solid (**Pd2)** (see Experimental

For references, see P177

part).

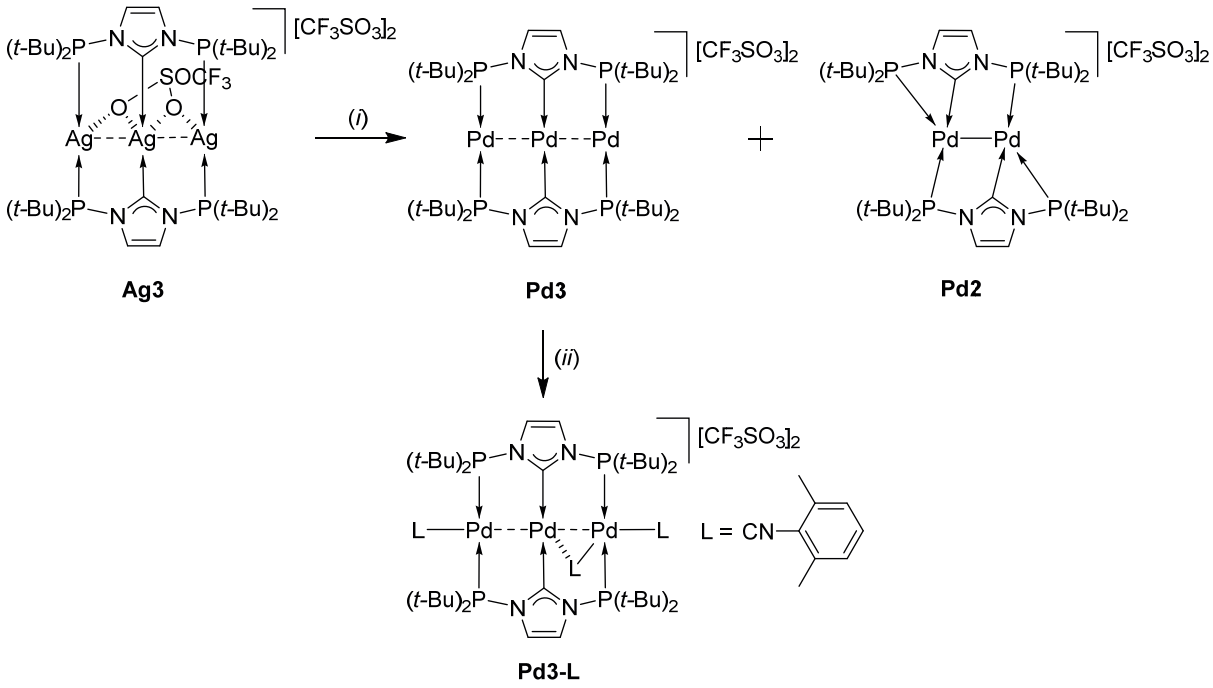

Scheme 1. Synthesis of **Pd3**, **Pd2** and **Pd3-L**. Reagents and conditions: (*i*) 4 equiv. $[Pd(dba)_2]$, in MeCN, 24 h, room temperature; (*ii*) 2,6-dimethylphenyl isocyanide, in MeCN, 1 h, room temperature.

The molecular structures of **Pd2** and **Pd3** were confirmed by X-ray diffraction. The structure of **Pd3** contains a tripalladium complex dication and two triflate counterions (Figure 1). The cation features an almost linear arrangement (178.85(2)°) of metal centers with two triply bridging $\mathbf{PC_{NHC}P}$ ligands on opposite sides of the metal chain, leading to a *trans* arrangement of the respective P and NHC donors at the individual metal centers; this motif is reminescent of that observed in the parent **Ag3,** except for the absence of bridging triflates. At variance with **Ag3**, the two mutually *trans* imidazole rings in **Pd3** are not coplanar (dihedral angle of 32.91°), which results in a staggered arrangement of the P atoms as viewed along the intermetallic axis, possibly due to steric reasons or mismatch of the size of the metal centers. The terminal and internal Pd atoms are almost linearly coordinated by two 2 electron donor ligands, giving P-Pd-P and C_{NHC}-Pd-C_{NHC} environments (178.13(4) and 179.7(2)°, respectively) and they mutually interact, as

For references, see P177

indicated by a short metal-metal separation of 2.5927(3) Å (see below for a bonding analysis).

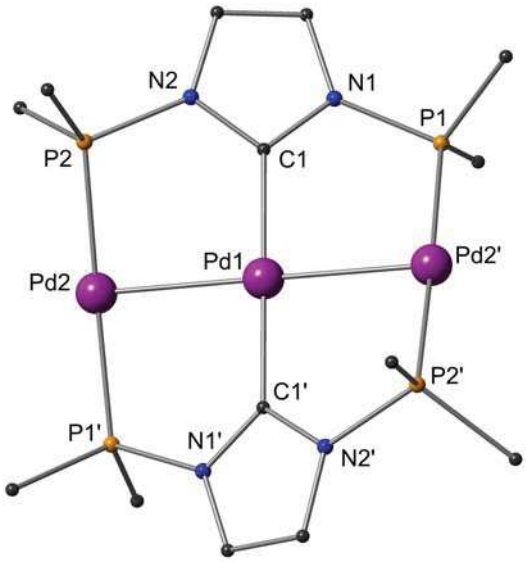

Figure 1. The structure of the dication in **Pd3**. H atoms, two triflate anions and the *t*-Bu methyl groups are omitted for clarity. Selected bond lengths (Å) and angles [°]: Pd1-C1 2.041(4), Pd2-P1' 2.284(1), Pd2-P2 2.278(1), Pd1-Pd2 2.5927(3); C1-Pd1-C1' 179.7(2), P2-Pd2-P1' 178.13(4), Pd2-Pd1-Pd2' 178.85(2).

The trinuclear dication in **Pd3** can be formally described as comprising one (internal) Pd(II) and two equivalent terminal Pd(0) centers. Alternatively, two outer Pd(I) and one central Pd(0) centers are also plausible. To gain evidence in support of any of the two formulations, we attempted to probe the electron density residing on each type of Pd by reacting **Pd3** with a good π-accepting ligand: under thermodynamic control, the π-accepting ligand should preferentially reside on the more electron-rich center. We thus investigated the reaction of **Pd3** with 2,6-dimethylphenyl isocyanide in MeCN. On adding the two reactants, an immediate color change from dark red-black to red was observed, and subsequent crystallization afforded $[Pd_3L_3(\mu_3\text{-}\mathbf{PC_{NHC}P},\kappa P,\kappa C_{NHC},\kappa P)_2](OTf)_2$ (**Pd3-L**, L = 2,6-dimethylphenyl isocyanide) as red crystals. Complex **Pd3-L** was structurally characterized by X-ray diffraction analysis (Figure 2). The structure features a

For references, see P177

trinuclear dication and two triflate anions. The metal chain departs from linearity (165.49(3)°, *cf.* 178.85(2)° in **Pd3**); one 2,6-dimethylphenyl isocyanide is bound at each terminal Pd center and 'trans' to the internal Pd (Pd2-C48 2.050(8) Å, Pd3-C57 2.040(7) Å); a third isocyanide is 'semi-bridging' between one outer and the internal Pd atoms (Pd2-C39 2.029(8) Å, Pd1-C39 2.622(8) Å), and closer to the former. This also leads to significant bending of the P1-Pd2-P3 angle (125.75(7)°, *cf*. 178.13(4) in **Pd3**). The metal-metal distances in this 46 valence electron (VE) complex are slightly longer than in the 40 VE complex **Pd3** (2.6903(7) and 2.7044(7) Å). Assuming that **Pd3-L** is the thermodynamic product of the reaction, the observed regioselectivity implies more electron-rich terminal Pd atoms.

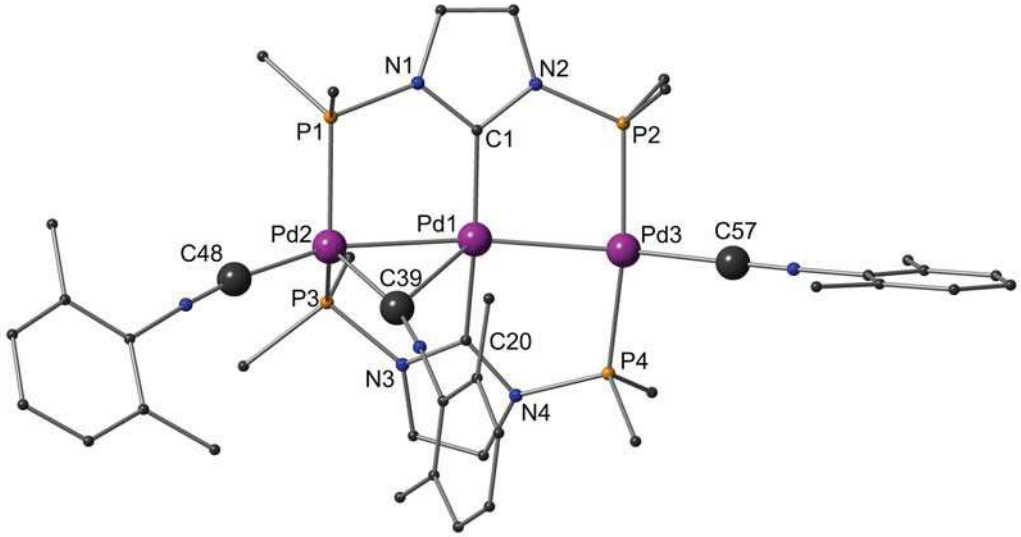

Figure 2. The structure of **Pd3-L**. The H atoms, two triflate anions and the *t*-Bu methyl groups are omitted for clarity. Selected bond lengths (Å) and angles [°]: Pd1-Pd2 2.7044(7), Pd1-Pd3 2.6902(7), Pd1-C1 2.027(6), Pd1-C20 2.007(7), Pd1-C39 2.622(8), Pd2-C39 2.029(8), Pd2-C48 2.050(8), Pd2-P1 2.392(1), Pd2-P3 2.396(2), Pd3-C57 2.040(7), Pd3-P2 2.309(2), Pd3-P4 2.332(2); Pd2-Pd1-Pd3 165.49(3), C20-Pd1-C1 167.4(3), P1-Pd2-P3 125.75(7), P2-Pd3-P4 167.55(7), Pd2-C39-Pd1 69.8(2), C48-Pd2-Pd1 159.8(2), C57-Pd3-Pd1 165.7(2).

The rigid non-symmetric structure observed in the solid state is not retained in solution at room temperature, as inferred by the appearance in the $^{31}P\{^{1}H\}$ NMR

For references, see P177

spectrum of a unique singlet at δ 117.3 and by the equivalence of the three isocyanide ligands on the ^{1}H NMR timescale. When a CD_2Cl_2 solution of **Pd3-L** was cooled to -70 ^{o}C, two P resonances appeared, one broad singlet at δ 115.5 and one singlet at δ 113.5; in the ^{1}H NMR spectrum the methyl groups on the isocyanides gave rise to three different resonances. The IR spectrum shows three absorptions for the ν(CN) stretching vibrations at 2056, 2107 and 2137 cm^{-1}.

The nature of the Pd-Pd interactions and the oxidation state of the metals in **Pd3** were investigated by means of DFT calculations. The optimized geometry is in good agreement with the experimental structure, deviating only by a slight lengthening of the main distances (Pd-Pd at 2.68 Å, Pd-C at 2.07 Å and Pd-P at 2.35 Å). The topological analyses performed on this structure did not provide an unequivocal answer on the nature of the Pd-Pd bonding. The Non-Covalent Analysis showed an electrostatic interaction between the central and the terminal Pd atoms (Figure 3), even though an ELF analysis did not reveal any Pd-Pd valence basin. However, the ELF function along the Pd-Pd axis exhibited a shoulder corresponding to a deformation of the terminal palladium core basin (Figure S1). This suggested the presence of a small Pd-Pd valence basin, which was not separated from the lateral Pd core basin. Therefore, the Pd-Pd bond has some covalent character. The charge analyses performed on the calculated structure of **Pd3** did not allow to clearly differentiate the three Pd atoms. The **Pd1** atom is slightly more positive than the **Pd2** and **Pd3** atoms though it cannot been established that this difference arises from a difference in the nature of the palladium atoms or from a different donor character of the phosphine and the carbene. In searching for alternative ways to assign the oxidation states of the Pd centers in **Pd3** computationally, the NMR chemical shifts of the individual Pd centers were calculated and compared with the values calculated for Pd^{0} and Pd^{2+} model complexes (See Table S1). These calculations unambiguously supported the view that the central Pd1 should be assigned as Pd^{II} and for the terminal Pd2 and Pd2’ as Pd^{0} centers.

For references, see P177

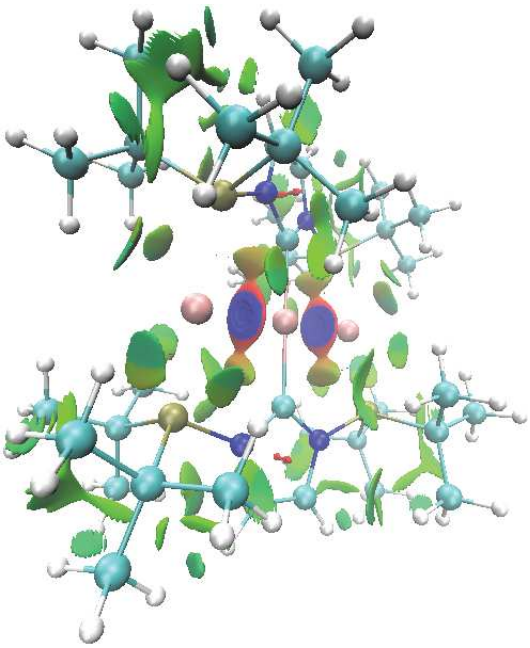

Figure 3. Non Covalent Interaction analysis performed on the DFT optimized structure. The Pd atoms are in pink, the electrostatic attractions in blue, the steric repulsion in red and the van der Waals dispersive interactions in green.

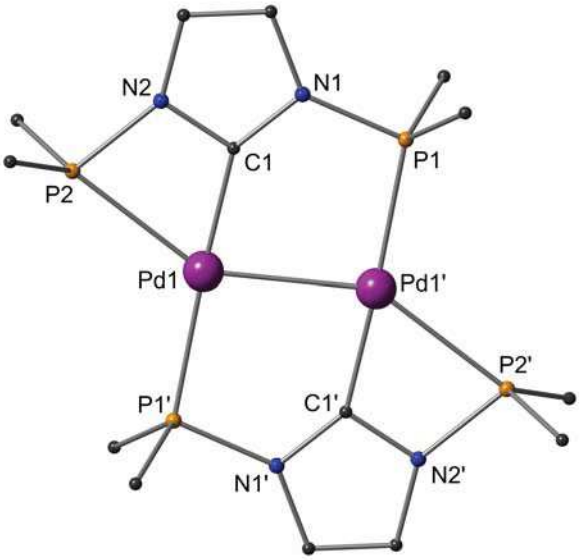

Figure 4. The structure of the dicationic complex in **Pd2** with H atoms, two triflate anions and the *t*-Bu methyl groups omitted for clarity. Selected bond lengths (Å) and angles [°]: Pd1-C1 1.982(3), Pd1-P1' 2.3633(8), Pd1-P2 2.5451(8), Pd1-Pd1' 2.6574(5); C1-Pd1-P1' 177.11(9), C1-Pd1-P2 65.35(9), P1'-Pd1-P2 117.05(3),

For references, see P177

C1-N1-P1 116.2(2), C1-N2-P2 106.5(2).

The crystal structure of **Pd2** revealed the presence of a salt with a dicationic, centrosymmetric dinuclear Pd complex and two triflate counterions (Figure 4). The two Pd centers are coordinated by two chelating-bridging **$PC_{NHC}P$** ligands, each Pd being ligated by one chelating **$PC_{NHC}P$** through the C_{NHC} and P donors and the remaining P donor from the other ligand; the fourth coordination site of the metal being occupied by the neighboring Pd center. Based on this stoichiometry, the metals are formulated as Pd(I) d^9 centers forming a metal-metal bond. The Pd1-P2 (2.5451(8) Å) bond distance is longer than Pd1-P1' (2.3633(8) Å), which indicates a weaker bond between the Pd and the P donor participating in the chelating ring. This is most likely the result of the strain and reduced orbital overlap within the four-membered ring due to the acute bite angle of 65.35(9)°. The Pd-Pd distance (2.6574(5) Å) is in the typical range of Pd(I)-Pd(I) covalent bonds.[14]

It is obvious the the transmetallation reaction is accompanied by oxidation of the Pd^0; however, it is not clear what the speciation of the Ag^+ oxidant is (inner- or outer-sphere electron transfer) or whether the two isolated products are formed in parallel in independent pathways. Further work aiming at exploring the scope of $[M_3(\mu_3\text{-}\mathbf{PC_{NHC}P},\kappa P,\kappa C_{NHC},\kappa P)_2](OTf)_3$ M = Ag, Cu, and understanding the nature of NHC transmetallation reactions with **$PC_{NHC}P$** and related ligand systems is in progress.

The reaction of **$PC_{NHC}P$** with $[PdMe_2(tmeda)]$ in THF afforded the air-sensitive, yellow complex $[PdMe_2(\mathbf{PC_{NHC}P},\kappa P,\kappa C_{NHC})]$ (**Pd-Me2**) (Scheme 2).

For references, see P177

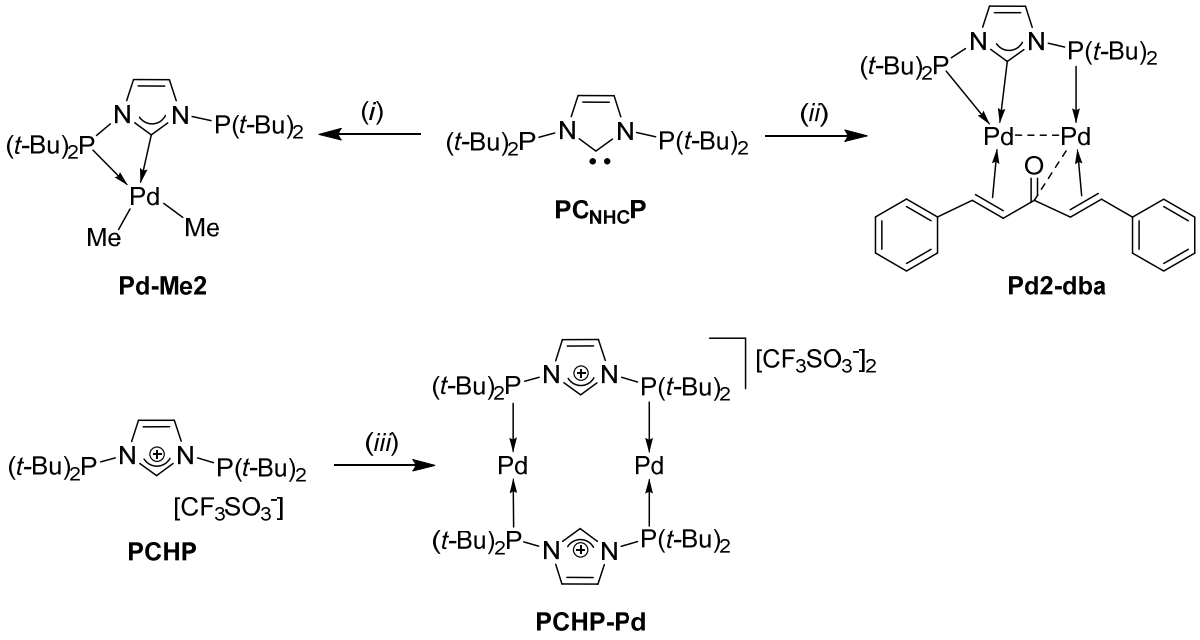

Scheme 2. Synthesis of **Pd-Me2, Pd2-dba** and **PCHP-Pd**. Reagents and conditions: (*i*) 1 equiv. $[PdMe_2(tmeda)]$, in THF, room temperature; (*ii*) 2 equiv. $[Pd(dba)_2]$, in THF, room temperature; (*iii*) 1 equiv. $[Pd_2(dba)_3]\cdot CHCl_3$, in THF, room temperature.

An X-ray diffraction analysis of **Pd-Me2** established that the Pd center adopts a distorted square planar coordination geometry consisting of two methyl ligands and one chelating **$PC_{NHC}P$** ligand through the C_{NHC} and one P donor, with a bite angle of 68.1(2)° (Figure 5). The two Pd-Me distances (2.061(9) and 2.060(8) Å) are almost equal although the two methyl ligands are *trans* to different donor groups (P and C_{NHC}), which implies that the chelate ring strain may have an effect on the *trans* influence of the P donor. The $^{31}P\{^1H\}$ NMR spectrum of **Pd-Me2** contains two singlets at δ 99.1 and 91.2 corresponding to the coordinated and the uncoordinated P, respectively. In the ^1H NMR spectrum, the two methyl groups give rise to two doublets, that were assigned by ^1H-^{13}C-HSQC to the methyl group *cis* to P ($^3J_{P\text{-}H}$ = 8.2 Hz at δ 0.90) and *trans* to P ($^3J_{P\text{-}H}$ = 6.2 Hz at δ 1.60); unexpectedly, the methyl *cis* to P has a larger coupling constant than that *trans* to it. In the ^{13}C NMR spectrum, the coupling constants for the *cis*-P methyl group (2.9 Hz at δ -8.94) is smaller than that for the *trans*-P methyl group (107.7 Hz at δ 2.87), which is typical for such a ligand disposition.[6e,15]

For references, see P177

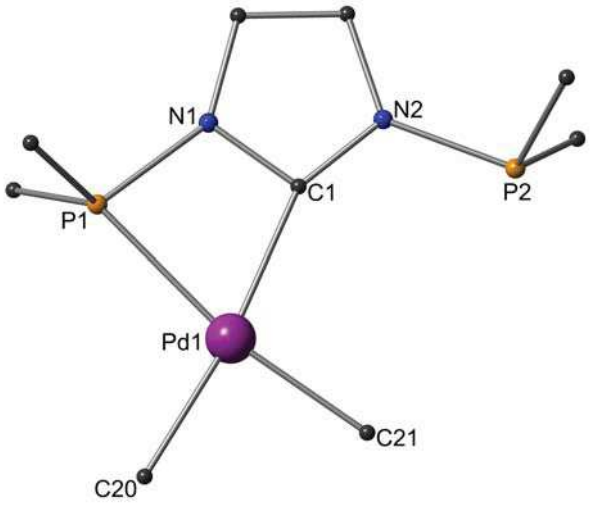

Figure 5. The structure of **Pd-Me2**; H atoms and the *t*-Bu methyl groups are omitted for clarity. Selected bond lengths (Å) and angles [°]: Pd1-C1 2.097(9), Pd1-P1 2.347(2), Pd1-C20 2.061(9), Pd1-C21 2.060(8); C20-Pd1-C21 86.1(4), C1-Pd1-P1 68.1(2), P1-Pd1-C20 104.3(3), P1-Pd1-C21 169.5(3), C20-Pd1-C1 172.4(4).

In contrast to the previous reaction leading to **Pd-Me2**, addition of $[Pd(dba)_2]$ (dba = dibenzylideneacetone) to a solution of $\mathbf{PC_{NHC}P}$ in THF resulted in the formation of the red $[Pd_2(\mu_2\text{-}\mathbf{PC_{NHC}P}, \kappa P, \kappa C_{NHC}, \kappa P)](\mu\text{-dba})$ (**Pd2-dba**) (Scheme 2), the structure of which revealed a neutral dinuclear complex with two Pd(0) centers and one chelating-bridging $\mathbf{PC_{NHC}P}$ and one bridging dba ligand (Figure 6).

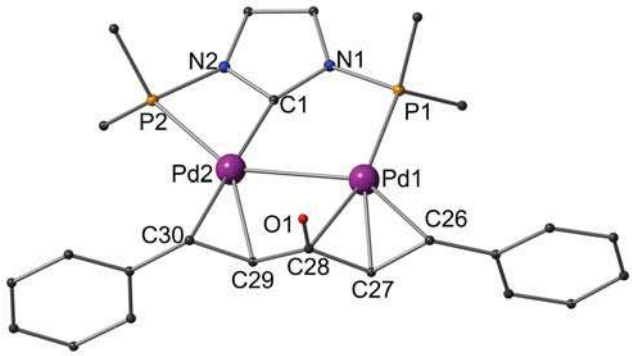

Figure 6. Structure of **Pd2-dba**. H atoms, the *t*-Bu methyl groups and one molecule of CH_2Cl_2 are omitted for clarity. Selected bond lengths (Å) and angles [°]: Pd1-Pd2 2.7799(5), Pd2-C1 2.045(5), Pd2-P2 2.416(1), Pd2-C30 2.169(4), Pd2-C29 2.247(4), Pd1-P1 2.243(1), Pd1-C28 2.336(4), Pd1-C27 2.129(4), Pd1-C26 2.248(4), N1-P1

For references, see P177

1.759(4), N2-P2 1.759(4), C26-C27 1.405(7), C27-C28 1.455(7), C28-C29 1.469(7), C29-C30 1.392(7), C28-O1 1.273(6); C1-N2-P2 104.6(3), C1-N1-P1 114.6(3), C1-Pd2-P2 67.16(13), C1-Pd2-C29 141.91(18), C30-Pd2-C29 36.70(17), C1-Pd2-Pd1 75.03(13), C27-Pd1-C26 37.33(18), C27-Pd1-C28 37.68(17), P1-Pd1-C26 122.81(14), P1-Pd1-C28 162.07(13), C26-Pd1-C28 65.45(17).

One Pd atom (Pd2) is four-coordinate, in an environment consisting of one chelating **$PC_{NHC}P$** ligand (through one P and the C_{NHC} donors, bite angle of 67.16(13)°), one η^2-olefinic group of the dba (mean Pd-C distance 2.208 Å) and the adjacent Pd1 atom. The Pd1 is bound to the remaining P donor of the **$PC_{NHC}P$** and the other olefinic group of the dba ligand. Although the distance between Pd1 and C28 (2.336(4) Å) is slightly longer than the Pd1-C27 (2.129(4) Å) and Pd1-C26 (2.248(4) Å) bonds, it clearly corresponds to a bonding interaction, with a value similar to that in $[Pd_2(\mu\text{-dba})(\mu\text{-}SO_2)(PBz_3)_2]$[16] and in a Pd(II) η^3-boratoxypentadienyl complex.[17] The single bond C27-C28 (1.455(7) Å) is slightly shortened compared to C28-C29 (1.469(7) Å) and is considerably shorter than that in free dba (1.512 Å),[18] while the double bond C26-C27 (1.405(7) Å) is elongated compared to the double bond C29-C30 (1.392(7) Å). These metrical data together with the lengthening of the ketone bond C28-O1 (1.273(6) Å) compared to that in free dba (1.205 Å) imply a partial electronic delocalization. The short Pd-Pd distance of 2.7799(5) Å corresponds to a metal-metal d^{10}-d^{10} interaction.[16,19] The plane formed by C27, C28 and O1 is almost perpendicular to the NHC ring (84.78°). The complex **Pd2-dba** has very poor solubility in Et_2O, THF or MeCN, but is soluble in CH_2Cl_2. It is stable as a solid but decomposes slowly in CD_2Cl_2 (*ca*. 2 h). Its low solubility complicated its purification and characterization in solution. The NMR spectra should be recorded immediately after dissolution. In the ^{31}P NMR spectrum of **Pd2-dba** only one singlet at δ 122.6 is observed, although the two Pd-P bond length are clearly different in the solid state, *i.e.* Pd2-P2 bond (2.416(1) Å) is longer than Pd1-P1 (2.243(1) Å). This feature indicates that the solid structure may be viewed as a snapshot of a dynamic structure in solution. Thus, it can be easily envisaged that the NHC donor, which can

For references, see P177

be considered as semi-bridging (Pd1-C1 2.996(5) Å, Pd2-C1 2.045(5) Å), in a manner reminiscent of phosphine ligands,[20] 'oscillates' between the two metal centers (Scheme 3), rendering the two P donors equivalent on $^{31}P\{^{1}H\}$ NMR time scale.

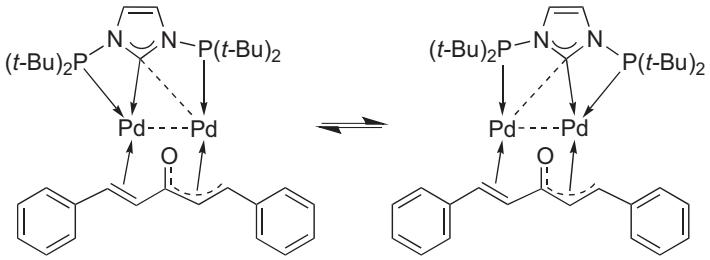

Scheme 3. Suggested 'oscillation' of the NHC carbon between the Pd atoms in solution rendering the P atoms in **Pd2-dba** equivalent on the $^{31}P\{^{1}H\}$ NMR time scale.

Addition of another equiv. of **$PC_{NHC}P$** to **Pd2-dba** in an attempt to displace its dba ligand resulted in decomposition. This may appear surprising since the dba ligand is known for its lability when coordinated to Pd(0). However, there are precedents for this behavior.[21]

Dinuclear Complexes with Remote Metals and a Novel Trinuclear Au and Au_2Cu_4 Cluster.

Since in all complexes described above coordination of the C_{NHC} of **$PC_{NHC}P$** was observed, together with either one or both P donors, we envisaged an alternative rational synthetic strategy consisting of initially promoting P coordination, followed, in a separate step by NHC generation and subsequent coordination, potentially opening the way to homo- or hetero-metallic arrays. A straightforward starting point for this was the reaction of the imidazolium salt **PCHP** with one equiv. $[Pd_2(dba)_3]\cdot CHCl_3$ in THF for 3 h, which led to the formation of the twelve-membered 2+2 metalla-mesocyclic dicationic dipalladium complex $[Pd_2(\mu_2\text{-}\mathbf{PCHP},\kappa P,\kappa P)_2]$ (**PCHP-Pd**) (Scheme 2). Its structure was unambiguously established by X-ray diffraction (Figure 7). It comprises two imidazolium **PCHP**

For references, see P177

cations bridging two 14 valence electron Pd(0) atoms, linearly coordinated by the P atoms (172.70(3)°). The two Pd-P distances (2.2662(4) Å and 2.2664(4) Å) are similar to those in **Pd3** (aver. 2.281 Å).

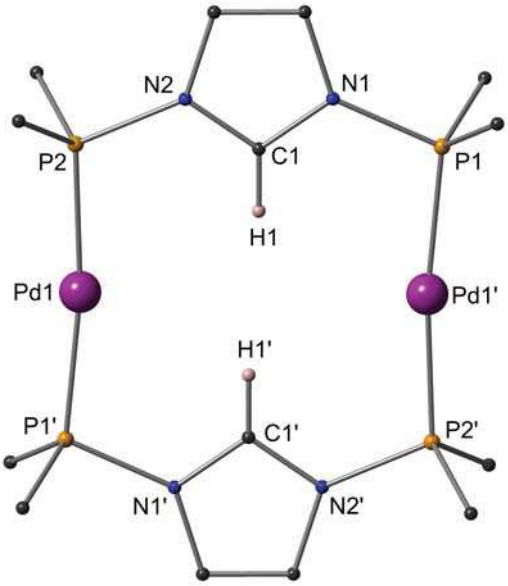

Figure 7. Structure of **PCHP-Pd**. H atoms except H1, two triflate anions and the *t*-Bu methyl groups are omitted for clarity. Selected bond lengths (Å) and angles [°]: Pd1-P1' 2.2662(4), Pd1-P2 2.2664(4); P1'-Pd1-P2 172.70(3).

The complex **PCHP-Pd** was characterized in solution by NMR spectroscopic methods (singlet at δ 139.5 in the $^{31}P\{^{1}H\}$ NMR spectrum, and a quintet ($^{3+5}J_{HP}$ = 1.7 Hz) at δ 10.38 for the imidazolium proton (cf. δ 8.43 (s) in **PCHP**) in the ^{1}H NMR spectrum, this multiplicity resulting from the strong magnetic coupling between the *trans*-P atoms.

The dipalladium complex **PCHP-Pd** can be viewed as a 'metalla-proligand' and was tested as precursor to trinuclear complexes. However, numerous attempted deprotonation/coordination reactions with $[CuN(SiMe_3)_2]$, $[Mg\{N(SiMe_3)_2\}_2]$, $[NaN(SiMe_3)_2]$/AgOTf, Cs_2CO_3/AgOTf, proton sponge, NEt_3, or KO*t*-Bu, resulted in decomposition of the framework.

The suspected complications in **PCHP-Pd** that may arise from the presence of reactive Pd(0) centers led us to explore further the scope and utility of the 'metalla-proligand' in the framework of the above described strategy, by attempting P coordination with other metal fragments. Thus, treating the

For references, see P177

imidazolium salt **PCHP** with 2 equiv. of [AuCl(tht)] in THF resulted in the dinuclear Au(I) complex [Au_2Cl_2(μ_2-**PCHP**,κP,κP)] (**PCHP-Au**). The singlet at δ 135.6 in the $^{31}P\{^1H\}$ NMR spectrum indicated coordination of the phosphine groups and the singlet at δ 10.5 in the ^1H NMR spectrum confirmed the presence of the imidazolium proton at C2.

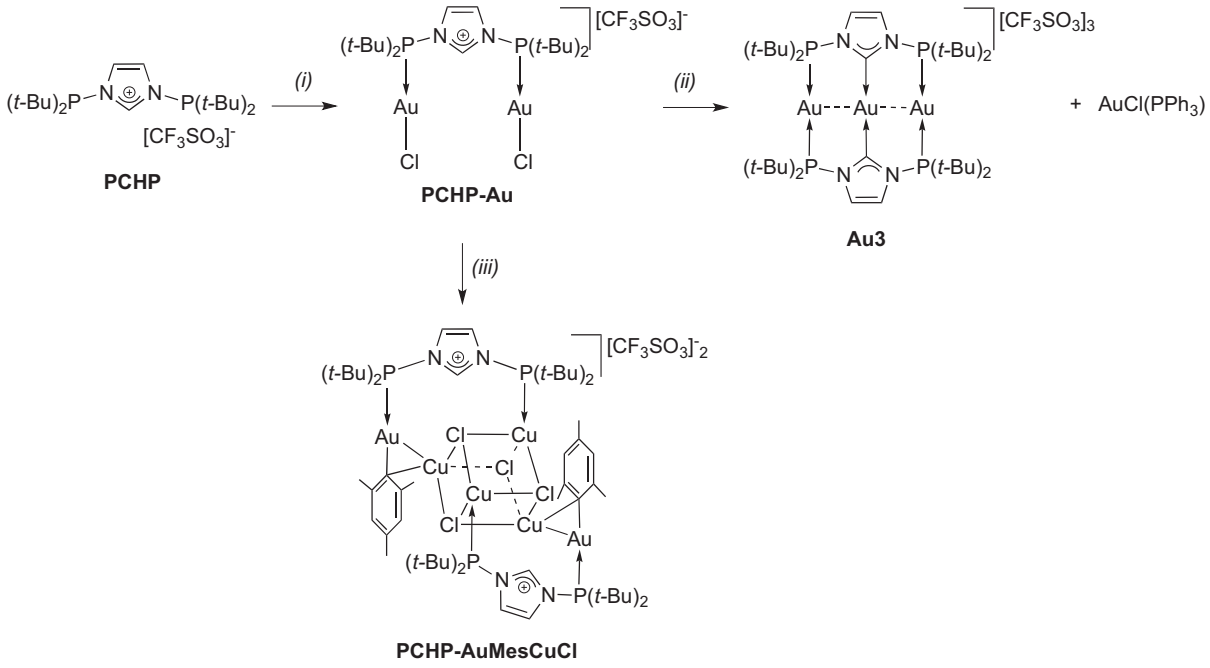

Scheme 4. Synthesis of Au(I) complexes. Reagents and conditions: (*i*) 2 equiv. [AuCl(tht)], in THF, 3h, room temperature; (*ii*) 1 equiv. [Au{$N(SiMe_3)_2$}(PPh_3)], in THF, overnight, room temperature; (*iii*) 0.4 equiv. $[CuMes]_5$, in THF, 4h, room temperature.

In the structure of **PCHP-Au** (Figure 8), a Au-Cl moiety is linearly bound to each P donor (aver. 175.47°). The unit cell contains two molecules of **PCHP-Au** mutually antiparallel ("shaft connector-type") with the corresponding imidazolium planes forming a dihedral angle of 78.44°. This arrangement is likely to be the result of weak hydrogen bonding interactions (aver. distance 2.912 Å) between the Cl atom and the H atom on the imidazolium N*C*N atom (crystallographic C1).

For references, see P177

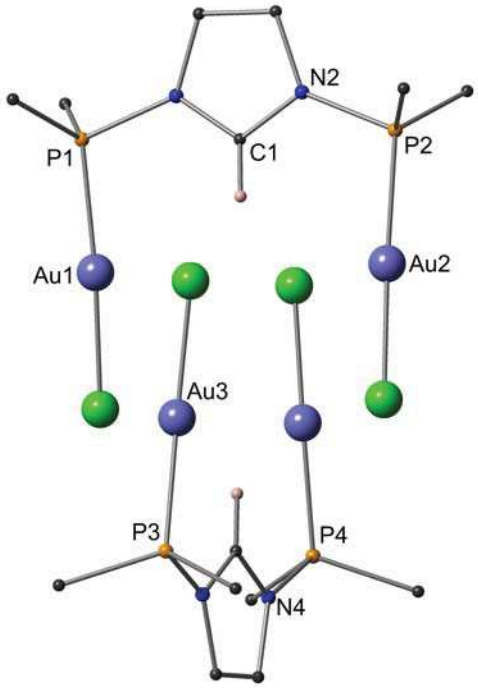

Figure 8. Structure of the cationic parts of two **PCHP-Au** complexes. H atoms except H1 and H20, the *t*-Bu methyl groups are omitted for clarity. Anisotropic displacement parameters are depicted at the 30% probability level. Selected bond lengths (Å) and angles [°]: Au1-P1 2.225(3), Au1-Cl1 2.276(3), Au2-P2 2.223(3), Au2-Cl2 2.265(3), Au3-P3 2.231(3), Au3-Cl3 2.287(3), Au4-P4 2.224(3), Au4-Cl4 2.286(3); P1-Au1-Cl1 174.63(12), P2-Au2-Cl2 176.21(12), P3-Au3-Cl3 174.75(12), P4-Au4-Cl4 176.27(12).

In contrast to the situation encountered with **PCHP-Pd**, deprotonation of **PCHP-Au** occurred without significant decomposition. Thus, reaction of **PCHP-Au** with [Au{$N(SiMe_3)_2$}(PPh_3)], a reagent with a coordinated base, in THF led to the formation of the known trinuclear complex **Au3**[8a] and [AuCl(PPh_3)] (Scheme 4). The thermodynamic stability provided by the two triply bridging **$PC_{NHC}P$** ligands on the Au_3 chain explains the ligand transfer that occurred during the reaction. The reaction of **PCHP-Au** with $[CuMes]_5$ (Mes = 2,4,6-trimethylphenyl) resulted in a yellow complex **PCHP-AuCu** for which the single-crystal X-ray diffraction analysis established an unusual structure, comprising one complex cation and one triflate anion. In the centrosymmetric cation of **PCHP-AuCu** (Figure 9), a central Cu_4Cl_4 cubane is bridged by a 'metalloligand', P-bound to one Cu atom and by a Au-carbon

For references, see P177

σ-bond of a linear Au-mesityl moiety to the Cu atom that is diagonally opposite to the former (C20-Au1-P1 176.48(16)°). The latter Cu atom forms a 3c-2e bond and supports a heterometallophilic d^{10}-d^{10} interaction[22] between the closed shell centers Cu(I) and Au(I), with a Au-Cu distance of 2.7844(9) Å. The short distance (2.111(6) Å) between Cu2 and C20 from the mesityl group also indicates the existence of a bonding interaction.[23] The $^{31}P\{^{1}H\}$ NMR spectrum of **PCHP-AuCu** contained a singlet at δ 149.6 and a quadrupole-broadened peak at δ 107.0, corresponding to the P atoms coordinated to Au and Cu, respectively.

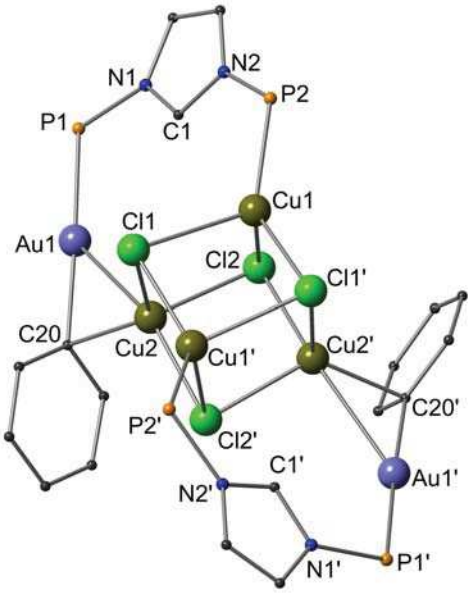

Figure 9. Structure of cationic part of **PCHP-AuCu**. H atoms, the *t*-Bu groups and the mesityl methyl groups are omitted for clarity. Anisotropic displacement parameters are depicted at the 30% probability level. Selected bond lengths (Å) and angles [°]: Au1-P1 2.2901(17), Cu1-P2 2.1908(18), Au1-C20 2.090(6), Cu2-C20 2.111(6), Cu1-Cl1' 2.3326(17), Cu1-Cl1 2.5176(19), Cu1-Cl2 2.4457(19), Cu2-Cl1 2.4820(19), Cu2-Cl2 2.3875(19), Cu2-Cl2' 2.4652(18), Cu2-Au1 2.7844(9); Cl1-Cu1-Cl2 95.86(6), Cl1'-Cu1-Cl2 101.63(6), Cl1-Cu1-Cl1' 95.21(6), Cl2-Cu2-Cl1 98.32(6), Cl2'-Cu2-Cl1 96.98(6), Cl2-Cu2-Cl2' 93.24(6), Cu1'-Cl1-Cu2 81.55(6), Cu1-Cl1-Cu1' 83.36(6), Cu1-Cl1-Cu2 80.82(6), Cu2-Cl2-Cu1 84.22(6), Cu2'-Cl2-Cu1 79.68(6), Cu2-Cl2-Cu2 85.74(6), Au1-C20-Cu2 83.0(2), Au1-Cu2-C20 48.16(18), Cu2-Au1-C20 48.82(16), Cu2-Au1-P1 134.58(5), C20-Au1-P1 176.48(16).

For references, see P177

Rationalization of the formation of **PCHP-AuCu** is not obvious. A plausible proposition may involve a sequence of events during which two **PCHP-Au** entities have each lost one Au-Cl group, the Cl in each of the remaining Au-Cl groups has been replaced by one mesityl originating from $[CuMes]_5$, concomitant formation of the cubane Cu_4Cl_4 and finally assembly to the observed structure.

Conclusion

Two different methodologies to introduce the $\mathbf{PC_{NHC}P}$ ligand on Pd using the $[Pd(dba)_2]$ precursor have been developed, leading to diverse products, in which the ligand adopts different bonding modes: (*i*) the transmetallation from the Ag centers of $[Ag_3(\mu_3\text{-}\mathbf{PC_{NHC}P},\kappa P,\kappa C_{NHC},\kappa P)_2](OTf)_3$ gave two products of bi- or tri-nuclear nature: the $[Pd_3(\mu_3\text{-}\mathbf{PC_{NHC}P},\kappa P,\kappa C_{NHC},\kappa P)_2](OTf)_2$ complex with a linear homonuclear chain cation which is isostoichiometric to the corresponding one in the Ag precursor. Attempts to determine the oxidation state of the individual Pd nuclei in the chain by chemical and computational means support an array with mixed oxidation state Pd(0)-Pd(II)-Pd(0) centers and inter-metallic interactions. Comparison of the structural features of the Pd_3 chain with those of its Ag precursor and the related Cu analogue reveal lack of the bridging triflates. Furthermore, in the Pd_3 array, and in contrast to all three coinage metal arrays (Cu_3, Ag_3, Au_3) that we have previously described, the metal-ligands framework is distorted away from planarity. This may be a manifestation of steric effects and /or the difference in the covalent radii of the Pd(II) and Pd(0) present in the cation and / or the effect of inter-metallic interactions. All these have been accommodated by the rigid complex framework by modulation of the torsion angle between the coordination and ligand planes. We have not been able to analyze satisfactorily by theoretical methods the nature of the inter-metallic interactions in the Pd_3 chain, in contrast to those in the coinage metals arrays which are of the d^{10}-d^{10} type. (*ii*) The direct substitution with the free $\mathbf{PC_{NHC}P}$ led to the binuclear complex $[Pd_2(\mu_2\text{-}\mathbf{PC_{NHC}P}, \kappa P,\kappa C_{NHC},\kappa P)(\mu\text{-dba})]$, which retained one dba ligand. In contrast to the reactivity of the Pd_3 chain complex, for example as revealed by the addition of three aryl isocyanide ligands and their

For references, see P177

fluxionality around the Pd_3 core, the binuclear dba complex is inert towards further substitution. (*iii*) In the Ag transmetallation reaction, a second product was also isolated, the binuclear homometallic $[Pd_2(\mu_2\text{-}\mathbf{PC_{NHC}P},\kappa P,\kappa C_{NHC},\kappa P)_2](OTf)_2$ in which the $\mathbf{PC_{NHC}P}$ ligand adopts a chelating-bridging coordination mode; here the formal oxidation state of each Pd is unequivocally Pd(I). In view of the presence of two species from the transmetallation reaction with oxidation states (0), (I) and (II), its full mechanistic understanding becomes difficult.

A stepwise, rational approach to build homo- or hetero-metallic trinuclear arrays was attempted by the sequential coordination of the phosphine imidazoliums to linear Pd(0) spacers giving (2+2) dimetalla-bis-imidazolium squares; however, in the follow-up step towards a controlled formation of dimetalla-bis-carbene squares or carbene-metal complexes, intractable mixtures were obtained, possibly due to the lack of selectivity in the deprotonation and/or metalation reactions. The coordination of the Au-Cl fragment to the phosphine donors of the imidazolium salt gave a well-defined coordination complex, which assembled in the solid state in a 'shaft-coupling' fashion. From its reaction with $(CuMes)_5$, a remarkable Au/Cu heterometallic cluster was obtained. The overall synthetic strategy for constructing polynuclear arrays requires a careful choice of the base reagent and reaction conditions that do not compete with other reactivity of the precursor molecules (*e.g.* P-N cleavage, substitution at the preformed M-phosphine bond *etc.*).

Experimental section

1. Synthesis and characterization

1.1 General methods

All manipulations involving organometallics were performed under argon using standard Schlenk techniques. Solvents were dried using standard methods and distilled under nitrogen prior use or passed through columns of activated alumina and subsequently purged with nitrogen or argon. ^{1}H, $^{13}C\{^{1}H\}$, and $^{31}P\{^{1}H\}$ NMR spectra were recorded at 298 K, unless otherwise specified, on a Bruker Avance 400, 500 or 600 spectrometer and referenced to the residual solvent resonance (^{1}H and

For references, see P177

^{13}C) or external 85% H_3PO_4 in D_2O(^{31}P). Elemental analyses were performed by the "Service de microanalyses", Université de Strasbourg. The complexes [Pd(dba)$_2$] and [Pd_2(dba)$_3$]·$CHCl_3$ were prepared as described.[24] The ligands **PCHP** and **PC$_{NHC}$P** and complex **Ag3** were prepared as described previously.[8a]

1.2 Synthesis of the palladium complexes **Pd3** and **Pd2**.

To a solid mixture of **Ag3** (0.060 g, 0.040 mmol) and [Pd(dba)$_2$] (0.096 g, 0.167 mmol) was added 6 ml MeCN at room temperature and stirring was maintained for 24 h. After filtration of the reaction mixture through Celite, the filtrate was evaporated to dryness under reduced pressure to give a mixture of **Pd3** and **Pd2** (the ratio of *ca*. 5:2 was determined from ^{31}P{^{1}H} NMR). The mixture was dissolved in 1 ml of MeCN and then Et_2O (8 ml) was layered on it for crystallization. After 3 days, the yellow-brown supernatant was removed by pipette and the residue was evaporated under reduced pressure to give **Pd3** as a dark red-black crystalline material (0.029 g, 55%). Analysis: Found (Calc. for $C_{40}H_{76}F_6N_4O_6P_4Pd_3S_2$) (%): C, 36.35 (36.11), H, 5.79 (5.76), N, 4.57 (4.21). ^{1}H NMR (400 MHz, CD_3CN): δ 7.56 (s, 4H, im-*H*), 1.48 (t, 72H, $^3J_{HP}$ = 7.9 Hz, C(C*H*$_3$)$_3$). ^{13}C{^{1}H} NMR (125 MHz, CD_3CN): δ 181.4 (t, $^2J_{CP}$ = 18.1 Hz, N*C*N), 126.7 (im-*C*), 121.7 (q, $^1J_{CF}$ = 321.4 Hz, *C*F_3), 38.9 (*C*(CH$_3$)$_3$), 29.8 (C(*C*H$_3$)$_3$). ^{31}P{^{1}H} NMR (162 MHz, CD_3CN): δ 112.2 (s).

The brown-yellow supernatant described above, obtained after crystallization, was evaporated to dryness and crystallization from MeCN/Et_2O at -20 ^{o}C gave **Pd2** as a yellow-brown crystalline material (0.008 g, 16% based on **Ag3**).

^{1}H NMR (400 MHz, CD_3CN): δ 7.78 (s, 2H, im-*H*), 7.73 (s, 2H, im-*H*), 1.49-1.42 (72H, C(C*H*$_3$)$_3$). ^{13}C{^{1}H} NMR (125 MHz, CD_3CN): δ 165.6 (N*C*N), 129.5 (im-*C*), 127.8 (im-*C*), 121.8 (q, $^1J_{CF}$ = 320.3 Hz, *C*F_3), 38.9 (t, $^1J_{CP}$ = 6.4 Hz, *C*(CH$_3$)$_3$), 37.3 (t, $^1J_{CP}$ = 2.6 Hz, *C*(CH$_3$)$_3$), 29.3 (t, $^2J_{CP}$ = 3.9 Hz, C(*C*H$_3$)$_3$), 28.6 (t, $^2J_{CP}$ = 4.2 Hz, C(*C*H$_3$)$_3$). ^{31}P{^{1}H} NMR (162 MHz, CD_3CN): δ 139.8 (d, $^2J_{PP}$ = 7.9 Hz), 94.8 (d, $^2J_{PP}$ = 7.9 Hz).

1.3 Synthesis of the palladium complex **Pd3-L**.

To a solution of **Pd3** (0.018 g, 0.014 mmol) in MeCN was added 2,6-dimethylphenyl

For references, see P177

isocyanide (0.008 g, 0.061 mmol) at room temperature and stirring was maintained for 1 h. Layering the reaction mixture with Et_2O for 3 days yielded red crystals (0.021 g, 87%) suitable for X-ray diffraction analysis. Analysis: Found (Calc. for $C_{67}H_{103}F_6N_7O_6P_4Pd_3S_2$) (%): C, 45.80 (46.68), H, 5.97 (6.02), N, 5.57 (5.69). IR(KBr): ν 2056 (CN), 2107(CN), 2137 (CN) cm^{-1}. ^1H NMR (400 MHz, CD_3CN): δ 7.60 (s, 4H, im-*H*), 7.28 (t, 3H, $^3J_{HH}$ = 7.7 Hz, 4-Ar-*H*), 7.18 (d, 6H, $^3J_{HH}$ = 7.7 Hz, 2,6-Ar-*H*), 2.28 (s, 18H, Ar-CH_3), 1.45 (t, 72H, $^3J_{HP}$ = 7.5 Hz, C(CH_3)$_3$). ^1H NMR (400 MHz, CD_2Cl_2): δ 7.68 (s, 4H, im-*H*), 7.26 (t, 3H, $^3J_{HH}$ = 7.6 Hz, 4-Ar-*H*), 7.15 (d, 6H, $^3J_{HH}$ = 7.6 Hz, 2,6-Ar-*H*), 2.32 (s, 18H, Ar-CH_3), 1.49 (t, 72H, $^3J_{HP}$ = 7.3 Hz, C(CH_3)$_3$). ^1H NMR (400 MHz, CD_2Cl_2, -70 °C): δ 7.55 (s, 2H, im-*H*), 7.51 (s, 2H, im-*H*), 7.31 (t, 1H, $^3J_{HH}$ = 7.8 Hz, 4-Ar-*H*), 7.20-7.13 (4H, 4-Ar-*H* and 2,6-Ar-*H*), 7.06-7.02 (4H, 2,6-Ar-*H*), 2.35 (s, 3H, Ar-CH_3), 2.28 (s, 3H, Ar-CH_3), 2.12 (s, 6H, Ar-CH_3), 1.94 (s, 6H, Ar-CH_3), 1.47 (br, 18H, C(CH_3)$_3$), 1.35 (br, 36H, C(CH_3)$_3$), 1.20 (br, 18H, C(CH_3)$_3$). $^{13}C\{^1H\}$ NMR (125 MHz, CD_3CN): δ 135.5 (*C*N), 130.5 (4-Ar-*C*), 129.2 (2,6-Ar-*C*), 128.6 (im-*C*), 122.1 (q, $^1J_{CF}$ = 321.9 Hz, *C*F_3), 39.3 (*C*(CH$_3$)$_3$), 30.1 (C(*C*H$_3$)$_3$), 18.9 (Ar-*C*H$_3$). $^{31}P\{^1H\}$ NMR (162 MHz, CD_3CN): δ 117.3 (s). $^{31}P\{^1H\}$ NMR (162 MHz, CD_2Cl_2): δ 117.8 (s). $^{31}P\{^1H\}$ NMR (162 MHz, CD_2Cl_2, -70 °C): δ 115.5 (br), 113.5 (s).

1.4 Synthesis of the palladium complex **Pd-Me2**.

To a solution of [$PdMe_2$(tmeda)] (0.035 g, 0.139 mmol) in THF (4 ml) was added a solution of ligand **$PC_{NHC}P$** (0.050 g, 0.140 mmol) in THF (4 ml) at room temperature and the reaction mixture was stirred for 6 h. After evaporation of the volatiles under reduced pressure, the residue was washed with pentane (15 ml) and dried to give a light yellow powder (0.048 g, 74%). X-ray quality crystals were obtained by slow evaporation of its Et_2O solution. Analysis: Found (Calc. for $C_{21}H_{44}N_2P_2Pd$) (%): C, 50.69 (51.17), H, 8.84 (9.00), N, 5.48 (5.68). ^1H NMR (400 MHz, C_6D_6): δ 6.70 (s, 1H, imid-*H*), 6.40 (s, 1H, imid-*H*), 1.60 (d, 3H, $^3J_{HP}$ = 6.2 Hz, $CH_{3(trans\text{-}P)}$-Pd), 1.14 (d, 18H, $^3J_{HP}$ = 12.8 Hz, C(CH_3)$_3$), 1.03 (d, 18H, $^3J_{HP}$ = 10.8 Hz, C(CH_3)$_3$), 0.90 (d, 3H, $^3J_{HP}$ = 8.2 Hz, $CH_{3(cis\text{-}P)}$-Pd). $^{13}C\{^1H\}$ NMR (100 MHz, C_6D_6): δ 200.2 (d, $^2J_{CP}$ = 52.8 Hz, N*C*N), 124.2 (d, $^2J_{CP}$ = 7.3 Hz, im-*C*), 121.7 (im-*C*), 36.0 (d, $^1J_{CP}$ = 12.7 Hz, *C*(CH$_3$)$_3$), 34.7 (d,

For references, see P177

$^{1}J_{CP}$ = 32.3 Hz, *C*(CH_3)$_3$), 29.3 (d, $^{2}J_{CP}$ = 17.3 Hz, C(*C*H_3)$_3$), 29.0 (d, $^{2}J_{CP}$ = 8.8 Hz, C(*C*H_3)$_3$), 2.87 (d, $^{2}J_{CP}$ = 107.7 Hz, *C*$H_{3(trans\text{-}P)}$-Pd), -8.94 (d, $^{2}J_{CP}$ = 2.9 Hz, *C*$H_{3(cis\text{-}P)}$-Pd). $^{31}P\{^{1}H\}$ NMR (162 MHz, C_6D_6): δ 99.1 (s), 91.2 (s).

1.5 Synthesis of the palladium complex **Pd2-dba**.

To a solution of [Pd(dba)$_2$] (0.161 g, 0.280 mmol) in THF (8 ml) was added a solution of ligand **PC$_{NHC}$P** (0.050 g, 0.140 mmol) in THF (5 ml) and the reaction mixture was stirred for 4 h. After removal of the supernatant by pipette, the solid was washed with THF (2 × 15 ml) and dried under vacuum to give a brown powder (0.051 g, 45%). X-ray quality crystals were obtained by diffusion of ether into its CH_2Cl_2 solution. Analysis: Found (Calc. for $C_{36}H_{52}N_2OP_2Pd_2$) (%): C, 51.57 (53.81), H, 6.29 (6.52), N, 3.16 (3.49). ^{1}H NMR (400 MHz, CD_2Cl_2): δ 7.44 (s, 2H), 7.42 (s, 2H), 7.17-7.13 (6H, Ar-*H*), 6.97-6.94 (2H, Ar-*H*), 5.35-5.30 (2H and CD_2Cl_2), 4.81 (d, 1H, *J* = 5.4 Hz), 4.78 (d, 1H, *J* = 5.4 Hz), 1.20 (d, 36H, $^{3}J_{HP}$ = 14.2 Hz, C(C*H*$_3$)$_3$), 0.96 (d, 36H, $^{3}J_{HP}$ = 14.0 Hz, C(C*H*$_3$)$_3$). $^{31}P\{^{1}H\}$ NMR (162 MHz, CD_2Cl_2): δ 122.6 (s). The NMR data should be recorded immediately after dissolution since the complex slowly decomposes in CD_2Cl_2.

1.6 Synthesis of the palladium complexes **PCHP-Pd**.

To a suspension of [Pd_2(dba)$_3$]·$CHCl_3$ (0.504 g, 0.487 mmol) in THF (15 ml) was added a solution of the imidazolium salt **PCHP** (0.506 g, 1.000 mmol) in THF (15 ml) and the reddish brown mixture was stirred for 3 h at room temperature. After removal of the supernatant by filtration, the solid was washed with THF (20 ml) and Et_2O (2×20 ml) and dried under reduced pressure to give a grayish green powder (0.442 g, 74%). X-ray quality crystals were obtained by slow diffusion of ether into its CH_2Cl_2 solution. Analysis: Found (Calc. for $C_{40}H_{78}F_6N_4O_6P_4Pd_2S_2$) (%): C, 38.62 (39.19), H, 6.35 (6.41), N, 4.63 (4.57). ^{1}H NMR (400 MHz, CD_2Cl_2): δ 10.38 (quintet, 2H, $^{3}J_{HP}$ = 1.7 Hz, half height width = 7.8 Hz, NC*H*N), 8.31 (d, 4H, $^{3}J_{HP}$ = 1.7 Hz, im-*H*), 1.47 (t, 72H, $^{3}J_{HP}$ = 8.0 Hz, C(C*H*$_3$)$_3$). $^{1}H\{^{31}P\}$ NMR (400 MHz, CD_2Cl_2): δ 10.38 (s, 2H, half height width = 5.4 Hz, NC*H*N), 8.31 (s, 4H, im-*H*), 1.47 (s, 72H, C(C*H*$_3$)$_3$). $^{13}C\{^{1}H\}$

For references, see P177

NMR (100 MHz, CD_2Cl_2): δ 152.3 (t, $^2J_{CP}$ = 16.7 Hz, N*C*HN), 128.8 (im-*C*), 121.4 (q, $^1J_{CF}$ = 320.4 Hz, *C*F_3), 38.8 (*C*$(CH_3)_3$), 29.5 (t, $^2J_{CP}$ = 12.9 Hz, C(*C*$H_3)_3$). $^{31}P\{^1H\}$ NMR (162 MHz, CD_2Cl_2): δ 139.5 (s).

1.7 Synthesis of **PCHP-Au**.

To a solid mixture of the imidazolium salt **PCHP** (0.100 g, 0.197 mmol) and [AuCl(tht)] (0.127 g, 0.396 mmol) was added 10 ml THF at room temperature and stirring was maintained for 3 h. After removal of the supernatant by filtration, the residue was dried under reduced pressure to give a white powder (0.160 g, 84%). X-ray quality crystals were obtained by slow diffusion of ether into its CH_2Cl_2 solution. Analysis: Found (Calcd. for $C_{20}H_{39}Au_2Cl_2F_3N_2O_3P_2S$) (%): C, 25.46 (24.73), H, 4.34 (4.05), N, 2.58 (2.88). ^1H NMR (400 MHz, CD_2Cl_2): δ 10.5 (s, 1H, im-*H*), 8.53 (d, 2H, $^3J_{HH}$ = 1.5 Hz, im-*H*), 1.56 (d, 36H, $^3J_{HP}$ = 18.4 Hz, C(C*H*$_3)_3$). $^{13}C\{^1H\}$ NMR (125 MHz, CD_2Cl_2): δ 152.8 (t, $^2J_{CP}$ = 17.0 Hz, N*C*N), 128.2 (im-*C*), 121.2 (q, $^1J_{CF}$ = 320.1 Hz, *C*F_3), 40.9 (d, $^1J_{CP}$ = 15.6 Hz, *C*$(CH_3)_3$), 29.2 (d, $^2J_{CP}$ = 7.5 Hz, C(*C*$H_3)_3$). $^{31}P\{^1H\}$ NMR (162 MHz, CD_2Cl_2): δ 135.6 (s).

1.8 Synthesis of **PCHP-AuCu**.

To a suspension of the imidazolium salt **PCHP-Au** (0.070 g, 0.072 mmol) in THF (5 ml) was added a solution of $[CuMes]_5$ (0.026 g, 0.028 mmol) in THF (5 ml) at room temperature and the reaction mixture was stirred for 4 h to give a yellow solution. After it was concentrated to 4 ml, Et_2O (20 ml) was added to precipitate the product. The supernatant was removed by filtration and the residue was dried under vacuum to give a yellow powder (0.030 g, 43%). X-ray quality crystals were obtained by slow diffusion of ether into its THF solution. Its instability in solution complicates the purification. Satisfactory elemental analysis data could not be obtained. The NMR data should be recorded immediately after dissolution since the complex rapidly decomposes in CD_2Cl_2. ^1H NMR (400 MHz, CD_2Cl_2): δ 10.69 (t, 2H, $^3J_{HP}$ = 4.0 Hz, im-*H*), 8.37 (s, 2H, im-*H*), 8.28 (s, 2H, im-*H*), 6.93 (s, 2H, Ar-*H*), 6.80 (s, 2H, Ar-*H*), 2.49 (s, 12H, Ar-C*H*$_3$), 2.21 (s, 6H, Ar-C*H*$_3$), 1.52 (d, 36H, $^3J_{HP}$ = 17.0 Hz, C(C*H*$_3)_3$), 1.40 (d, 36H,

For references, see P177

$^{3}J_{HP}$ = 16.1 Hz, C(CH_3)$_3$). $^{31}P\{^{1}H\}$ NMR (162 MHz, CD_2Cl_2): δ 149.6 (s), 106.9 (br).

2. X-ray crystallography

Summary of the crystal data, data collection and refinement for structures of **Pd3**, **Pd3-L**, **Pd2**, **Pd-Me2**, **Pd2-dba**, **PCHP-Pd**, **PCHP-Au** and **PCHP-AuCu** are given in Table S2.

For **Pd2, Pd-Me2, PCHP-Pd**, **PCHP-Au** and **PCHP-AuCu**, X-ray diffraction data collection was carried out on a Bruker APEX II DUO Kappa-CCD diffractometer equipped with an Oxford Cryosystem liquid N_2 device, using Mo-Kα radiation (λ = 0.71073 Å). The crystal-detector distance was 38 mm. The cell parameters were determined (APEX2 software)[25] from reflections taken from three sets of 12 frames, each at 10s exposure. The structure was solved by direct methods using the program SHELXS-97.[26] The refinement and all further calculations were carried out using SHELXL-97.[27] The H-atoms were included in calculated positions and treated as riding atoms using SHELXL default parameters. The non-H atoms were refined anisotropically, using weighted full-matrix least-squares on F^2. A semi-empirical absorption correction was applied using SADABS in APEX2.[25]

For **Pd3**, **Pd3-L**, **Pd2-dba**, X-ray diffraction data collection was carried out on a Nonius Kappa-CCD diffractometer equipped with an Oxford Cryosystem liquid N_2 device, using Mo-Kα radiation (λ = 0.71073 Å). The crystal-detector distance was 36 mm. The cell parameters were determined (Denzo software)[28] from reflections taken from one set of 10 frames (1.0° steps in phi angle), each at 20 s exposure. The structures were solved by direct methods using the program SHELXS-97.[26] The refinement and all further calculations were carried out using SHELXL-97.[27] The H-atoms were included in calculated positions and treated as riding atoms using SHELXL default parameters. The non-H atoms were refined anisotropically, using weighted full-matrix least-squares on F^2. A semi-empirical absorption correction was applied using MULscanABS in PLATON.[29] Specific details about the resolution of the crystal structures are provides in the ESI.

For references, see P177

3. Computational details

Calculations were performed using the ADF 2013 package.[30] Slater type orbitals were used with all-electron triple-ζ quality basis sets at DFT level with BLYP functional.[31] Scalar relativistic effects were included through ZORA Hamiltonian.[32] Full geometry optimization was performed on each structures. NMR results were obtained through single points on these structures. ELF Analyses were done on the ADF wave function with DGRID package[33].

A single point with Gaussian 09 package[34] was done at DFT level with BLYP functional on ADF optimized structure in order to compute wave function suitable for topological analysis. The atoms were all described by a modified version of the def2-SVP[35] basis set with all functions of F-type were deleted. The weak interactions were studied through the NCI analysis[36] of this Gaussian wave function.

ASSOCIATED CONTENT

Supporting Information

Electronic Supplementary Information (ESI) available: ELF analysis, calculated Pd NMR chemical shifts and crystal data for **Pd3, Pd3-L, Pd2, Pd-Me2, Pd2-dba, PCHP-Pd, PCHP-Au** and **PCHP-AuCu.** The Crystallographic information files (CIF) have been deposited with the CCDC, 12 Union Road, Cambridge, CB2 1EZ, U.K., and can be obtained on request free of charge, by quoting the publication citation and deposition numbers 1424765-1424772. This material is also available free of charge via the Internet at http://pubs.acs.org/.

AUTHOR INFORMATION

Corresponding Authors

Pierre Braunstein, braunstein@unistra.fr

Andreas A. Danopoulos, danopoulos@unistra.fr

For references, see P177

Notes

The authors declare no competing financial interest.

ACKNOWLEDGMENT

The USIAS, CNRS, Région Alsace and Communauté Urbaine de Strasbourg are acknowledged for the award of fellowships and a Gutenberg Excellence Chair (2010–11) to AAD. We thank the CNRS and the MESR (Paris) for funding and the Service de Radiocristallographie (UdS) for the determination of the crystal structures. We are grateful to the China Scholarship Council for a PhD grant to P.A. and to Johnson Matthey PLC for a generous loan of Au precursors.

For references, see P177

References

(1) (a) Herrmann, W. A. *Angew. Chem. Int. Ed.* **2002**, *41*, 1290-1309. (b) Crudden, C. M.; Allen, D. P. *Coord. Chem. Rev.* **2004**, *248*, 2247-2273. (c) Peris, E.; Crabtree, R. H. *Coord. Chem. Rev.* **2004**, *248*, 2239-2246. (d) Glorius, F. *N-Heterocyclic Carbenes in Transition Metal Catalysis*; Springer Berlin Heidelberg, 2007. (e) Pugh, D.; Danopoulos, A. A. *Coord. Chem. Rev.* **2007**, *251*, 610-641. (f) Kantchev, E. A. B.; O'Brien, C. J.; Organ, M. G. *Angew. Chem. Int. Ed.* **2007**, *46*, 2768-2813. (g) Díez-González, S.; Marion, N.; Nolan, S. P. *Chem. Rev.* **2009**, *109*, 3612-3676. (h) McGuinness, D. *Dalton Trans.* **2009**, 6915-6923. (i) Riener, K.; Haslinger, S.; Raba, A.; Högerl, M. P.; Cokoja, M.; Herrmann, W. A.; Kühn, F. E. *Chem. Rev.* **2014**. (j) Visbal, R.; Gimeno, M. C. *Chem. Soc. Rev.* **2014**, *43*, 3551-3574. (k) Hopkinson, M. N.; Richter, C.; Schedler, M.; Glorius, F. *Nature* **2014**, *510*, 485-496. (l) Wang, Z.; Jiang, L.; Mohamed, D. K. B.; Zhao, J.; Hor, T. S. A. *Coord. Chem. Rev.* **2015**, *293–294*, 292-326. (m) Zhang, D.; Zi, G. *Chem. Soc. Rev.* **2015**, *44*, 1898-1921.

(2) (a) Kühl, O. *Chem. Soc. Rev.* **2007**, *36*, 592-607 and references cited therein. (b) Kühl, O. *Functionalised N-Heterocyclic Carbene Complexes*; Wiley, Weinheim, 2010. (c) Tornatzky, J.; Kannenberg, A.; Blechert, S. *Dalton Trans.* **2012**, *41*, 8215-8225. (d) Liu, X.; Braunstein, P. *Inorg. Chem.* **2013**, *52*, 7367-7379. (e) Gaillard, S.; Renaud, J.-L. *Dalton Trans.* **2013**, *42*, 7255-7270 and references cited therein. (f) Hameury, S.; de Fremont, P.; R. Breuil, P.-A.; Olivier-Bourbigou, H.; Braunstein, P. *Dalton Trans.* **2014**, *43*, 4700-4710. (g) Jahnke, M. C.; Hahn, F. E. *Coord. Chem. Rev.* **2015**, *293–294*, 95-115. (h) He, F.; Braunstein, P.; Wesolek, M.; Danopoulos, A. A. *Chem. Commun.* **2015**, *51*, 2814-2817. (i) Simler, T.; Danopoulos, A. A.; Braunstein, P. *Chem. Commun.* **2015**, *51*, 10699-10702. (j) Hameury, S.; de Frémont, P.; Breuil, P.-A. R.; Olivier-Bourbigou, H.; Braunstein, P. *Organometallics* **2015**, *34*, 2183-2201.

(3) (a) Herrmann, W. A.; Öfele, K.; Elison, M.; Kühn, F. E.; Roesky, P. W. *J. Organomet. Chem.* **1994**, *480*, c7-c9. (b) Lee, M.-T.; Hu, C.-H. *Organometallics* **2004**, *23*, 976-983. (c) Crabtree, R. H. *J. Organomet. Chem.* **2005**, *690*, 5451-5457.

(4) (a) Kausamo, A.; Tuononen, H. M.; Krahulic, K. E.; Roesler, R. *Inorg. Chem.* **2008**, *47*, 1145-1154. (b) Jacobsen, H.; Correa, A.; Poater, A.; Costabile, C.; Cavallo, L.

For references, see P177

Coord. Chem. Rev. **2009**, *253*, 687-703 and references cited therein. (c) Srebro, M.; Michalak, A. *Inorg. Chem.* **2009**, *48*, 5361-5369. (d) Buhl, H.; Ganter, C. *Chem. Commun.* **2013**, *49*, 5417-5419. (e) Verlinden, K.; Buhl, H.; Frank, W.; Ganter, C. *Eur. J. Inorg. Chem.* **2015**, *2015*, 2416-2425.

(5) Bestgen, S.; Gamer, M. T.; Lebedkin, S.; Kappes, M. M.; Roesky, P. W. *Chem.–Eur. J.* **2015**, *21*, 601-614.

(6) (a) Marchenko, A. P.; Koidan, H. N.; Huryeva, A. N.; Zarudnitskii, E. V.; Yurchenko, A. A.; Kostyuk, A. N. *J. Org. Chem.* **2010**, *75*, 7141-7145. (b) Marchenko, A. P.; Koidan, H. N.; Hurieva, A. N.; Pervak, I. I.; Shishkina, S. V.; Shishkin, O. V.; Kostyuk, A. N. *Eur. J. Org. Chem.* **2012**, *2012*, 4018-4033. (c) Marchenko, A. P.; Koidan, H. N.; Pervak, I. I.; Huryeva, A. N.; Zarudnitskii, E. V.; Tolmachev, A. A.; Kostyuk, A. N. *Tetrahedron Lett.* **2012**, *53*, 494-496. (d) Marchenko, A. P.; Koidan, H. N.; Zarudnitskii, E. V.; Hurieva, A. N.; Kirilchuk, A. A.; Yurchenko, A. A.; Biffis, A.; Kostyuk, A. N. *Organometallics* **2012**, *31*, 8257-8264. (e) Nägele, P.; Herrlich, U.; Rominger, F.; Hofmann, P. *Organometallics* **2013**, *32*, 181-191. (f) Marchenko, A.; Koidan, H.; Hurieva, A.; Kurpiieva, O.; Vlasenko, Y.; Kostyuk, A.; Tubaro, C.; Lenarda, A.; Biffis, A.; Graiff, C. *J. Organomet. Chem.* **2014**, *771*, 14-23. (g) Wang, T.; Stephan, D. W. *Chem. Eur. J.* **2014**, *20*, 3036-3039.

(7) (a) Kühnel, E.; Shishkov, I. V.; Rominger, F.; Oeser, T.; Hofmann, P. *Organometallics* **2012**, *31*, 8000-8011. (b) Marchenko, A. P.; Koidan, H. N.; Hurieva, A. N.; Gutov, O. V.; Kostyuk, A. N.; Tubaro, C.; Lollo, S.; Lanza, A.; Nestola, F.; Biffis, A. *Organometallics* **2013**, *32*, 718-721. (c) Brown, C. C.; Plessow, P. N.; Rominger, F.; Limbach, M.; Hofmann, P. *Organometallics* **2014**, *33*, 6754-6759.

(8) (a) Ai, P.; Danopoulos, A. A.; Braunstein, P.; Monakhov, K. Y. *Chem. Commun.* **2014**, *50*, 103-105. (b) Ai, P.; Danopoulos, A. A.; Braunstein, P. *Inorg. Chem.* **2015**, *54*, 3722-3724.

(9) (a) Ai, P.; Danopoulos, A. A.; Braunstein, P. *Organometallics* **2015**, *34*, 4109-4116. (b) Massard, A.; Braunstein, P.; Danopoulos, A. A.; Choua, S.; Rabu, P. *Organometallics* **2015**, *34*, 2429-2438.

(10) (a) Puddephatt, R. J. *Chem. Soc. Rev.* **1983**, *12*, 99-127. (b) Chaudret, B.;

For references, see P177

Delavaux, B.; Poilblanc, R. *Coord. Chem. Rev.* **1988**, *86*, 191-243.

(11) (a) Bhattacharyya, P.; Woollins, J. D. *Polyhedron* **1995**, *14*, 3367-3388. (b) Appleby, T.; Derek Woollins, J. *Coord. Chem. Rev.* **2002**, *235*, 121-140. (c) Todisco, S.; Gallo, V.; Mastrorilli, P.; Latronico, M.; Re, N.; Creati, F.; Braunstein, P. *Inorg. Chem.* **2012**, *51*, 11549-11561. (d) Ghisolfi, A.; Fliedel, C.; Rosa, V.; Pattacini, R.; Thibon, A.; Yu. Monakhov, K.; Braunstein, P. *Chem. –Asian J.* **2013**, *8*, 1795-1805. (e) Rosa, V.; Fliedel, C.; Ghisolfi, A.; Pattacini, R.; Aviles, T.; Braunstein, P. *Dalton Trans.* **2013**, *42*, 12109-12119. (f) Fliedel, C.; Rosa, V.; Falceto, A.; Rosa, P.; Alvarez, S.; Braunstein, P. *Inorg. Chem.* **2015**, *54*, 6547-6559. (g) Todisco, S.; Mastrorilli, P.; Latronico, M.; Gallo, V.; Englert, U.; Re, N.; Creati, F.; Braunstein, P. *Inorg. Chem.* **2015**, *54*, 4777-4798.

(12) Newkome, G. R. *Chem. Rev.* **1993**, *93*, 2067-2089.

(13) (a) Ai, P.; Danopoulos, A. A.; Braunstein, P. *Dalton Trans.* **2014**, *43*, 1957-1960. (b) Brill, M.; Rominger, F.; Hofmann, P. *Organometallics* **2015**, *34*, 506-521.

(14) (a) Bender, R.; Braunstein, P.; Jud, J. M.; Dusausoy, Y. *Inorg. Chem.* **1983**, *22*, 3394-3407. (b) Braunstein, P.; Ries, M.; de Méric de Bellefon, C.; Dusausoy, Y.; Mangeot, J.-P. *J. Organomet. Chem.* **1988**, *355*, 533-550. (c) Tanase, T.; Kawahara, K.; Ukaji, H.; Kobayashi, K.; Yamazaki, H.; Yamamoto, Y. *Inorg. Chem.* **1993**, *32*, 3682-3688. (d) Tanase, T.; Ukaji, H.; Yamamoto, Y. *J. Chem. Soc., Dalton Trans.* **1996**, 3059-3064. (e) Murahashi, T.; Otani, T.; Mochizuki, E.; Kai, Y.; Kurosawa, H.; Sakaki, S. *J. Am. Chem. Soc.* **1998**, *120*, 4536-4537. (f) Bachert, I.; Braunstein, P.; Guillon, E.; Massera, C.; Rosé, J.; DeCian, A.; Fischer, J. *J. Cluster Sci.* **1999**, *10*, 445-458. (g) Zhang, J.; Pattacini, R.; Braunstein, P. *Inorg. Chem.* **2009**, *48*, 11954-11962. (h) Tanase, T.; Hatada, S.; Mochizuki, A.; Nakamae, K.; Kure, B.; Nakajima, T. *Dalton Trans.* **2013**, *42*, 15941-15952. (i) *CSD version 5.36, Nov 2014*.

(15) Verstuyft, A. W.; Nelson, J. H.; Cary, L. W. *Inorg. Chem.* **1976**, *15*, 732-734.

(16) Burrows, A. D.; Choi, N.; McPartlin, M.; Mingos, D. M. P.; Tarlton, S. V.; Vilar, R. *J. Organomet. Chem.* **1999**, *573*, 313-322.

(17) Emslie, D. J. H.; Blackwell, J. M.; Britten, J. F.; Harrington, L. E. *Organometallics* **2006**, *25*, 2412-2414.

(18) Turowska-Tyrk, I. *Chem. Phys.* **2003**, *288*, 241-247.

For references, see P177

(19) Pyykkö, P. *Chem. Rev.* **1997**, *97*, 597-636.

(20) Braunstein, P.; Boag, N. M. *Angew. Chem. Int. Ed.* **2001**, *40*, 2427-2433.

(21)(a) Andrieu, J.; Braunstein, P.; Burrows, A. D. *J Chem Res-S* **1993**, 380-381. (b) Hii, K. K.; Thornton-Pett, M.; Jutand, A.; Tooze, R. P. *Organometallics* **1999**, *18*, 1887-1896. (c) Reid, S. M.; Mague, J. T.; Fink, M. J. *J. Organomet. Chem.* **2000**, *616*, 10-18. (d) Paul, F.; Moulin, S.; Piechaczyk, O.; Le Floch, P.; Osborn, J. A. *J. Am. Chem. Soc.* **2007**, *129*, 7294-7304.

(22) (a) Bardajía, M.; Laguna, A. *Eur. J. Inorg. Chem.* **2003**, *2003*, 3069-3079. (b) Doerrer, L. H. *Dalton Trans.* **2010**, *39*, 3543-3553. (c) Sculfort, S.; Braunstein, P. *Chem. Soc. Rev.* **2011**, *40*, 2741-2760.

(23) (a) Gambarotta, S.; Floriani, C.; Chiesi-Villa, A.; Guastini, C. *J. Chem. Soc., Chem. Commun.* **1983**, 1156-1158. (b) Stollenz, M.; Meyer, F. *Organometallics* **2012**, *31*, 7708-7727.

(24) (a) Ukai, T.; Kawazura, H.; Ishii, Y.; Bonnet, J. J.; Ibers, J. A. *J. Organomet. Chem.* **1974**, *65*, 253-266. (b) Rettig, M. F.; Maitlis, P. M. *Inorg. Synth.* **1990**, *28*, 110-113.

(25) Bruker AXS Inc Madison USA, 2006.

(26) Sheldrick, G. M. *Acta Crystallogr. Sect. A: Found. Crystallogr.* **1990**, *A46*, 467.

(27) Sheldrick, G. M. Universität Göttingen: Göttingen Germany, 1999.

(28) Nonius, B. V. Delft, The Netherlands, 1997.

(29) Spek, A. L. *J. Appl. Cryst.* **2003**, *36*, 7-13.

(30) ADF2013, SCM, Theoretical Chemistry, Vrije Universiteit, Amsterdam, The Netherlands, http://www.scm.com.

(31) (a) Becke, A. D. *Phys Rev A* **1988**, *38*, 3098-3100. (b) Lee, C. T.; Yang, W. T.; Parr, R. G. *Phys. Rev. B* **1988**, *37*, 785-789.

(32) van Lenthe, E.; Ehlers, A.; Baerends, E.-J. *J. Chem. Phys.* **1999**, *110*, 8943-8953.

(33) Kohout, M. D., version 4.6, Radebeul, 2011.

(34) Gaussian 09, R. D., Frisch, M. J.; Trucks, G. W.; Schlegel, H. B.; Scuseria, G. E.; Robb, M. A.; Cheeseman, J. R.; Scalmani, G.; Barone, V.; Mennucci, B.; Petersson, G. A.; Nakatsuji, H.; Caricato, M.; Li, X.; Hratchian, H. P.; Izmaylov, A. F.; Bloino, J.; Zheng, G.; Sonnenberg, J. L.; Hada, M.; Ehara, M.; Toyota, K.; Fukuda, R.; Hasegawa, J.;

For references, see P177

Ishida, M.; Nakajima, T.; Honda, Y.; Kitao, O.; Nakai, H.; Vreven, T.; Montgomery, J. A., Jr.; Peralta, J. E.; Ogliaro, F.; Bearpark, M.; Heyd, J. J.; Brothers, E.; Kudin, K. N.; Staroverov, V. N.; Kobayashi, R.; Normand, J.; Raghavachari, K.; Rendell, A.; Burant, J. C.; Iyengar, S. S.; Tomasi, J.; Cossi, M.; Rega, N.; Millam, J. M.; Klene, M.; Knox, J. E.; Cross, J. B.; Bakken, V.; Adamo, C.; Jaramillo, J.; Gomperts, R.; Stratmann, R. E.; Yazyev, O.; Austin, A. J.; Cammi, R.; Pomelli, C.; Ochterski, J. W.; Martin, R. L.; Morokuma, K.; Zakrzewski, V. G.; Voth, G. A.; Salvador, P.; Dannenberg, J. J.; Dapprich, S.; Daniels, A. D.; Farkas, Ö.; Foresman, J. B.; Ortiz, J. V.; Cioslowski, J.; Fox, D. J. Gaussian, Inc., Wallingford CT, 2009.

(35) Weigend, F.; Ahlrichs, R. *PCCP* **2005**, *7*, 3297-3305.

(36) Contreras-García, J.; Johnson, E. R.; Keinan, S.; Chaudret, R.; Piquemal, J.-P.; Beratan, D. N.; Yang, W. *J. Chem. Theory Comput.* **2011**, *7*, 625-632.

For references, see P177

ESI

Novel Di- and Tri-nuclear Pd Complexes Supported by *N*,*N*'-Diphosphanyl NHC Ligands and *N*,*N*'-Diphosphanyl Imidazolium Au and Mixed-Metal Cu-Au Complexes

Pengfei Ai,[a] Christophe Gourlaouen,[b] Andreas A. Danopoulos,*[a,c] and Pierre Braunstein*[a]

[a] Laboratoire de Chimie de Coordination, Institut de Chimie (UMR 7177 CNRS), Université de Strasbourg, 4 rue Blaise Pascal, 67081 Strasbourg Cedex, France. E-mail: danopoulos@unistra.fr, braunstein@unistra.fr
[b] Laboratoire de Chimie Quantique, Institut de Chimie (UMR 7177 CNRS), Université de Strasbourg, 1 rue Blaise Pascal, 67008 Strasbourg, France
[c] Institute for Advanced Study, USIAS, Université de Strasbourg, France.

Contents:

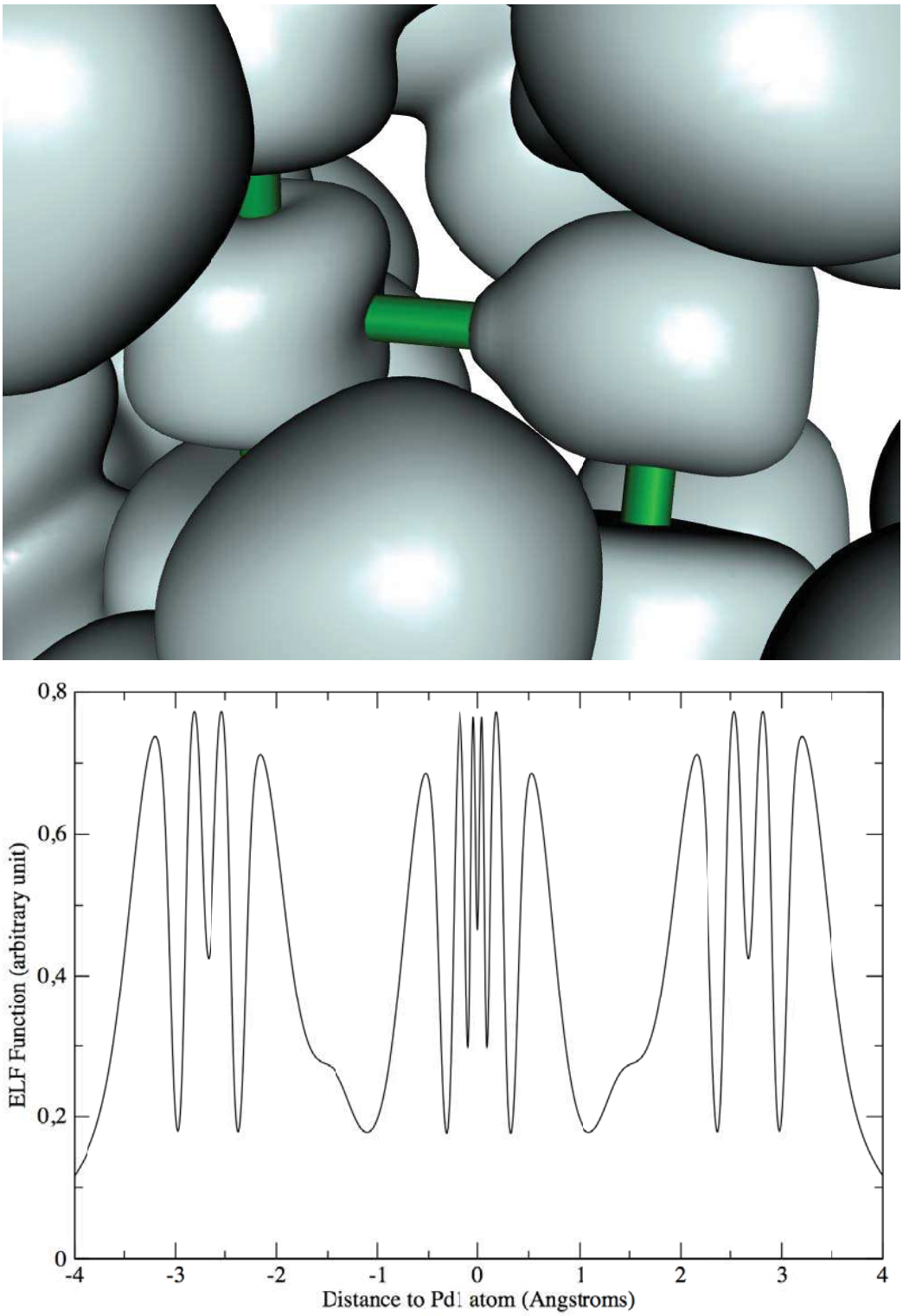

Figure S1. Zoom on the ELF function on the Pd-Pd area (up) and value of the ELF function along the Pd-Pd-Pd axis (down). The core ELF basin of the lateral Pd2 atom presents a small extension directing towards the central Pd1 atom. It appears as a shoulder on the plot of the ELF function along the Pd-Pd-Pd axis.

Table S1. Scheme of the fragments used for the determination of the palladium NMR shielding constants in different oxidation states.

Compound	Oxidation State	NMR Shielding Constant (ppm)
$[Pd(PH_3)_2]$	0	1972.6
$[Pd(PH_3)_2(Cl)]^+$	+II	-831.1
$[Pd(NHC)_2]$	0	1298.8
$[Pd(NHC)_2(Cl)_2]$	+II	-573.1
Complex **Pd3**, Atom Pd1		-423.7
Complex **Pd3**, Atom Pd2		1043.3

Table S2. Crystal data for compounds **Pd3, Pd3-L, Pd2, Pd-Me2, Pd2-dba, PCHP-Pd, PCHP-Au and PCHP-AuCu**.

	Pd3	**Pd2**	**Pd3-L**	**Pd-Me2**
Chemical formula	$C_{40}H_{76}F_6N_4O_6P_4Pd_3S_2$	$C_{40}H_{76}F_6N_4O_6P_4Pd_2S_2$	$C_{67}H_{103}F_6N_7O_6P_4Pd_3S_2$	$C_{21}H_{44}N_2P_2Pd$
CCDC Number	1424772	1424770	1424771	1424768
Formula Mass	1330.24	1223.84	1723.76	492.92
Crystal system	Monoclinic	Monoclinic	Triclinic	Monoclinic
a/Å	13.9630(3)	8.8915(5)	14.9540(5)	8.1647(6)
b/Å	8.5889(2)	12.6197(7)	15.2204(4)	12.4627(10)
c/Å	26.8437(6)	23.7979(14)	18.1728(8)	14.8060(8)
α/°	90	90	82.266(2)	90
β/°	117.3280(10)	93.206(2)	81.606(2)	119.436(3)
γ/°	90	90	86.610(2)	90
Unit cell volume/Å^3	2859.98(11)	2666.1(3)	4051.4(2)	1312.08(16)
Temperature/K	173(2)	173(2)	173(2)	173(2)
Space group	*P2/c*	*P21/c*	*P-1*	*Pc*
Z	2	2	2	2
Absorption coefficient, μ/mm^{-1}	1.180	0.939	0.852	0.837
No. of reflections measured	20043	23495	35264	8922
No. of independent reflections	6555	7739	18416	4780
R_{int}	0.0527	0.0531	0.0634	0.0317

Final R_1 values ($I > 2\sigma(I)$)	0.0529	0.0423	0.0866	0.0458
Final $wR(F^2)$ values ($I > 2\sigma(I)$)	0.1465	0.0927	0.2017	0.0794
Final R_1 values (all data)	0.0724	0.0772	0.1227	0.0709
Final $wR(F^2)$ values (all data)	0.1572	0.1022	0.2199	0.0876
Goodness of fit on F^2	1.111	1.002	1.054	1.022

	PCHP-Pd	**Pd2-dba**•$2CH_2Cl_2$	**PCHP-Au**	**PCHP-AuCu**
Chemical formula	$C_{40}H_{78}F_6N_4O_6P_4Pd_2S_2$	$C_{36}H_{52}N_2OP_2Pd_2$ •$2CH_2Cl_2$	$C_{20}H_{39}Au_2Cl_2F_3N_2O_3P_2S$	$C_{58}H_{100}Au_2Cl_4Cu_4F_6N_4O_6P_4S_2$
CCDC Number	1424767	1424769	1424765	1424766
Formula Mass	1225.86	973.38	971.36	2041.31
Crystal system	Monoclinic	Monoclinic	Monoclinic	Monoclinic
a/Å	8.7420(3)	10.0103(3)	18.9542(11)	33.150(3)
b/Å	12.4928(4)	17.8454(6)	15.9306(10)	11.2586(8)
c/Å	25.8518(8)	24.3889(7)	27.0956(13)	24.5228(18)
α/°	90	90	90	90
β/°	97.0030(10)	100.546(2)	128.601(3)	121.117(2)
γ/°	90	90	90	90
Unit cell volume/Å^3	2802.26(16)	4283.2(2)	6394.0(7)	7835.5(10)
Temperature/K	173(2)	173(2)	173(2)	173(2)

Space group	*P21/c*	*P21/c*	*P21/c*	*C2/c*
Z	2	4	8	4
Absorption coefficient, μ/mm^{-1}	0.893	1.195	9.541	5.128
No. of reflections measured	38382	26697	56353	36965
No. of independent reflections	9717	9798	15377	9491
R_{int}	0.0214	0.0850	0.1003	0.0657
Final R_1 values ($I > 2\sigma(I)$)	0.0298	0.0531	0.0611	0.0495
Final $wR(F^2)$ values ($I > 2\sigma(I)$)	0.0644	0.1098	0.1371	0.1137
Final R_1 values (all data)	0.0378	0.1019	0.1194	0.0818
Final $wR(F^2)$ values (all data)	0.0677	0.1423	0.1524	0.1302
Goodness of fit on F^2	1.137	1.046	1.023	1.116

The following special comments apply to the models of the structures:

For **Pd3**, the palladium Pd1 is in a special position (population 50%). A squeeze was made. The residual electron density was assigned to one molecule of acetonitrile.

For **Pd-Me2**, the carbons C5, C6, C7, C9, C10, C11, C13, C14, C15 are disordered on two positions.

For **PCHP-Au**, a squeeze was made. The residual electron density was assigned to one molecule of the dichloromethane.

Chapter 8

N-Phosphanyl- and *N*,*N*'-Diphosphanyl-N-Heterocyclic Carbene Chromium Complexes: Synthesis, Structures and Catalytic Ethylene Oligomerization

This chapter is written in the form of a publication. This article was published in *Organometallics* **2015**, 34, 4109-4116.

My contribution in this work included the synthesis of the ligands and complexes, their characterization and the preparation of the draft of the publication. The experiments on oligomerization of ethylene were performed by Marc Mermillon-Fournier.

N-Phosphanyl- and *N,N'*-Diphosphanyl-N-Heterocyclic Carbene Chromium Complexes: Synthesis, Structures and Catalytic Ethylene Oligomerization

Pengfei Ai,[a] Andreas A. Danopoulos,*[a,b] Pierre Braunstein*[a]

[a] Laboratoire de Chimie de Coordination, Institut de Chimie (UMR 7177 CNRS), Université de Strasbourg, 4 rue Blaise Pascal, 67081 Strasbourg Cedex, France. E-mail: danopoulos@unistra.fr, braunstein@unistra.fr
[b] Institute for Advanced Study, USIAS, Université de Strasbourg, France.

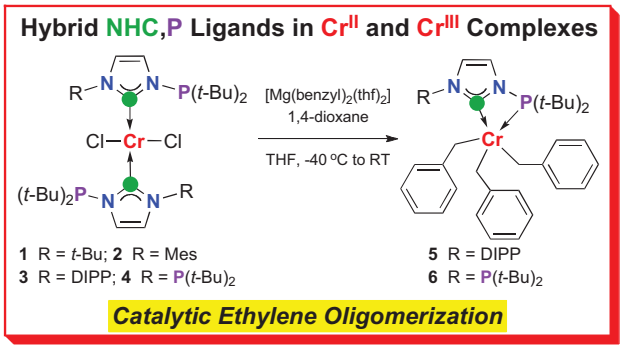

Supporting information for this chapter is available on the internet under

http://pubs.acs.org/doi/suppl/10.1021/acs.organomet.5b00547

For references, see P197

Résumé du Chapitre 8

Les complexes du chrome(II) **1**-**4** contenant des ligands hybrides carbène N-hétérocycliques *N*-phosphanyl- ou *N,N'*-diphosphanyl-substitués (NHC) furent préparés à partir de précurseurs de Cr^{II} ($[CrCl_2(thf)_2]$) ou de Cr^{III} ($[CrCl_3(thf)_3]$ ou de $[Cr(Me)Cl_2(thf)_3]$). Les structures à l'état solide de ces quatre complexes indiquent un environnement plan autour des centres Cr^{II}, avec deux chlorures et deux donneurs C_{NHC} en position mutuellement trans.

L'alkylation de **3** et **4** avec $[Mg(benzyl)_2(thf)_2]$ a conduit respectivement à la formation des complexes σ **5** et **6**. La géométrie de coordination de ces centres Cr^{III} pentacoordinés est pyramide carrée déformée ; elle comporte un chélate lié par C_{NHC} et P et trois groupes benzyles.

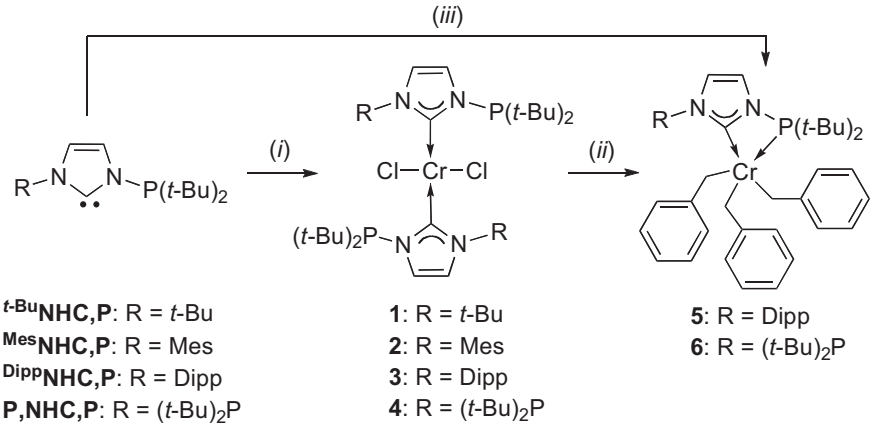

Schéma. Synthèse de complexes de Cr^{II} et Cr^{III}. Réactifs et conditions: (*i*) $[CrCl_2(thf)_2]$, $[CrCl_3(thf)_3]$ ou $[Cr(Me)Cl_2(thf)_3]$, THF, -78 °C à temp. amb.; (*ii*) $[Mg(benzyl)_2(thf)_2]$ et 1,4-dioxane, THF, -40 °C à temp. amb.; (*iii*) $[CrCl_3(thf)_3]$, $[Mg(benzyl)_2(thf)_2]$ et 1,4-dioxane, THF, -78 °C à -40 °C puis temp. amb.

Les systèmes Cr^{III}/MAO ont montré en oligomérisation de l'éthylène des propriétés catalytiques supérieures à celles des complexes du Cr^{II} (valeurs de TOF jusqu'à 16320 mol C_2H_4/((mol Cr)·h) pour **6**) et conduisent principalement à des oligomères. Il est intéressant de noter que les oligomères obtenus à partir du complexe **3** furent presque exclusivement du 1-hexène et du 1-butène lorsque la réaction fut démarrée à 30 °C. Avec $AlEtCl_2$ (EADC) comme cocatalyseur, c'est principalement du polyéthylène qui a été formé.

For references, see P197

ORGANOMETALLICS

Article

pubs.acs.org/Organometallics

N-Phosphanyl- and *N,N′*-Diphosphanyl-Substituted N-Heterocyclic Carbene Chromium Complexes: Synthesis, Structures, and Catalytic Ethylene Oligomerization

Pengfei Ai,[†] Andreas A. Danopoulos,*[,†,‡] and Pierre Braunstein*[,†]

[†]Laboratoire de Chimie de Coordination, Institut de Chimie (UMR 7177 CNRS), and [‡]Institute for Advanced Study, USIAS, Université de Strasbourg, 4 rue Blaise Pascal, 67081 Strasbourg Cedex, France

Supporting Information

ABSTRACT: The chromium(II) complexes $[CrCl_2(^{t\text{-}Bu}\mathbf{NHC,P}\text{-}\kappa C)_2]$ (**1**), $[CrCl_2(^{Mes}\mathbf{NHC,P}\text{-}\kappa C)_2]$ (**2**), $[CrCl_2(^{Dipp}\mathbf{NHC,P}\text{-}\kappa C)_2]$ (**3**), and $[CrCl_2(\mathbf{P,NHC,P}\text{-}\kappa C)_2]$ (**4**) containing the *N*-phosphanyl- or *N,N′*-diphosphanyl-substituted N-heterocyclic carbene (NHC) hybrid ligands $^{t\text{-}Bu}$**NHC,P** (1-(di-*tert*-butylphosphino)-3-*tert*-butylimidazol-2-ylidene), ^{Mes}**NHC,P** (1-(di-*tert*-butylphosphino)-3-mesitylimidazol-2-ylidene), ^{Dipp}**NHC,P** (1-(di-*tert*-butylphosphino)-3-(2,6-diisopropylphenyl)imidazol-2-ylidene), and **P,NHC,P** (1,3-bis(di-*tert*-butylphosphino)imidazol-2-ylidene), respectively, were prepared from Cr^{II} ($[CrCl_2(thf)_2]$) or Cr^{III} ($[CrCl_3(thf)_3]$ or $[Cr(Me)Cl_2(thf)_3]$) precursors. The solid-state structures of these four complexes show square-planar Cr^{II} centers, with two trans chloride and two monodentate C_{NHC} donors. Alkylation of **3** and **4** with $[Mg(benzyl)_2(thf)_2]$ led to the formation of the σ complexes $[Cr(benzyl)_3(^{Dipp}\mathbf{NHC,P}\text{-}\kappa C,\kappa P)]$ (**5**) and $[Cr(benzyl)_3(\mathbf{P,NHC,P}\text{-}\kappa C,\kappa P)]$ (**6**), respectively, with five-coordinate distorted-square-pyramidal Cr^{III} coordination, comprising a chelating ligand through the C_{NHC} and one P donor and three benzyl groups. These complexes were used as precatalysts in ethylene oligomerization, and it was found that the nature of the cocatalyst used and the metal oxidation state have a remarkable influence on the catalytic properties. The Cr^{III}/MAO systems displayed superior catalytic performance (TOF values up to 16320 mol of C_2H_4/((mol of Cr) h) for **6**) and gave mostly oligomers. Interestingly, the oligomers obtained with complex **3** were almost exclusively 1-hexene and 1-butene when the reaction was initiated at 30 °C. The overall activities and selectivities were also affected by the initial reaction temperature and the nature of the solvent. With $AlEtCl_2$ (EADC) as cocatalyst, polyethylene was predominately formed.

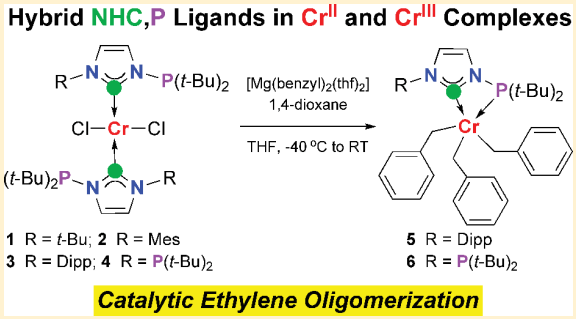

INTRODUCTION

Metal-catalyzed transformations for converting ethylene to linear α-olefins (LAO) or polyethylenes are of continuing interest, due to the industrial importance and value of the end products.[1] For example, LAOs are highly demanded industrial intermediates, in particular as comonomers for the production of linear low-density polyethylene (C4−C8), surfactants (C12−C20), and plasticizers (C6−C10). Chromium is at the core of these transformations, being the active center of the Phillips[2] and Union Carbide[3] SiO_2-supported Cr catalyst, responsible for 40%−50% of the annual world production of polyethylene,[4] or of a number of selective homogeneous oligomerization catalysts affording mainly 1-hexene or 1-octene (Phillips,[5] Mitsubishi,[6] BP Chemicals,[7] Sasol[8]). Since the influence of the Cr oxidation state, the ancillary ligands, and the cocatalyst on the oligomer selectivity has not yet been fully elucidated, considerable efforts have been devoted to the development of well-defined, catalytically active molecular systems, which lend themselves to mechanistic studies and rational tailoring.[1b,f,9]

Although N-heterocyclic carbenes (NHCs) have been established as efficient ancillary ligands in diverse topics of homogeneous catalysis,[10] they have not yet found wide applications in olefin oligomerization and polymerization reactions, in particular with electropositive metals. This may be due to the small metal−NHC bond dissociation energies but also due to the decomposition of the active species with alkyl−NHC−metal bonds via alkylimidazolium reductive elimination.[11] It is conceivable that the side reaction could be suppressed through the donor functionalization and chelation of the NHC functionality, by the introduction of steric bulk and the protection at the NHC, and/or by using early transition metals that are less susceptible to this type of deactivation (e.g. due to unavailable oxidation states etc.). Presently, only a few monodentate, bidentate (N,C; C,S; C,C), and tridentate (N,C,N; C,N,C; C,S,C) functionalized NHC ligands have been employed to prepare Cr complexes as precatalysts for ethylene polymerization or oligomerization.[11,12] Among them, the "pincer" pyridylbis(carbene)chromium(III) complexes of type **A** are the most active precatalysts for the oligomerization of ethylene, with activities up to 7.8×10^5 g/((g of Cr) h).[9a]

Received: June 22, 2015
Published: August 6, 2015

For references, see P197

DOI: 10.1021/acs.organomet.5b00547
Organometallics 2015, 34, 4109−4116

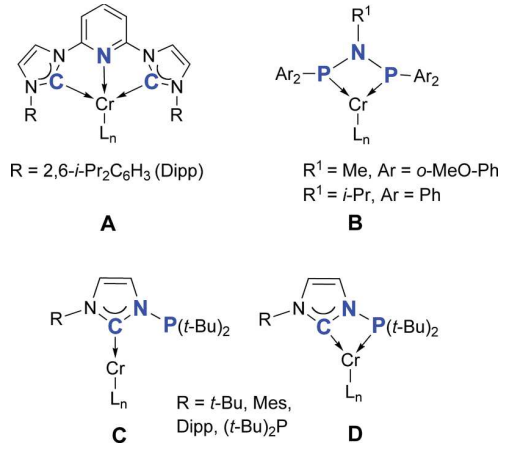

Recently, *N*-phosphanyl-functionalized NHC ligands[13] have received much attention, since they feature vicinal, strong σ donors in rigid, easily tunable sterically and electronically coordination environments. The chemistry that has been explored to date involves coinage, platinum-group, or late transition metals, where the ligands adopt bridging or chelating modes, in the last case giving distorted chelate rings and small bite angles.[14] In contrast, the coordination chemistry with the early and 3d metals is unknown.

Of relevance to the origin of the present work were the versatile ethylene trimerization catalyst PNP-Cr (**B**, Ar = *o*-MeO-Ph), developed by BP Chemicals,[7a] and the analogous ethylene tetramerization catalyst PNP-Cr (**B**, Ar = Ph), developed by Sasol,[8c] both based on a bis(phosphanyl)amine-type (PNP) ligand. The recognition that the nature of the ancillary ligand clearly plays a major role in determining the catalytic activity and selectivity[1e−g] led us to consider the synthesis of complexes with a hybrid ligand containing NHC and phosphine donor groups, in view of the widely accepted similarity of their donor abilities[10b,g,15] and the often unique properties brought about by hybrid ligands.[16] Herein, we report the synthesis of Cr^{II} and Cr^{III} complexes based on a family of P-functionalized NHC ligands of types **C** and **D** and their evaluation in the catalytic oligomerization of ethylene.

RESULTS AND DISCUSSION

Synthesis of the Chromium Complexes. The new complexes $[CrCl_2(^{t\text{-}Bu}\mathbf{NHC,P}\text{-}\kappa C)_2]$ (**1**), $[CrCl_2(^{Mes}\mathbf{NHC,P}\text{-}\kappa C)_2]$ (**2**), $[CrCl_2(^{Dipp}\mathbf{NHC,P}\text{-}\kappa C)_2]$ (**3**), and $[CrCl_2(\mathbf{P,NHC,P}\text{-}\kappa C)_2]$ (**4**) were prepared by the addition of the known *N*-phosphanyl-substituted NHC ligands $^{t\text{-}Bu}$**NHC,P**, ^{Mes}**NHC,P**, ^{Dipp}**NHC,P**, and **P,NHC,P**, respectively,[13c,14a,17] to a suspension of 0.5 equiv of $[CrCl_2(thf)_2]$ in THF at −78 °C (Scheme 1).

They were obtained as purple, paramagnetic, air-sensitive solids in good yields and characterized by X-ray diffraction (see below). Initial attempts to use the same methodology to prepare Cr^{III} complexes, i.e. by reacting excess ligand with $[CrCl_3(thf)_3]$ or $[Cr(Me)Cl_2(thf)_3]$, led unexpectedly to the reduction of Cr^{III} to Cr^{II} and the isolation of **1**−**4**. Similar redox reactions between a Cr^{III} complex and *N*,*N*′-diisopropylimidazol-2-ylidene have been observed previously, but their mechanisms were not fully elucidated.[18]

Further derivatization of **3** and **4** aiming at the introduction of reactive Cr−C σ bonds was attempted by the reaction with $[Mg(benzyl)_2(thf)_2]$. This led to the isolation of $[Cr(benzyl)_3(^{Dipp}\mathbf{NHC,P}\text{-}\kappa C,\kappa P)]$ (**5**) and $[Cr(benzyl)_3(\mathbf{P,NHC,P}\text{-}\kappa C,\kappa P)]$ (**6**), respectively. Whereas substitution of the chlorides by the benzyl moieties was expected, we do not know at which stage the oxidation of Cr^{II} to Cr^{III} took place. One may speculate that disproportionation of an unstable Cr^{II} species has resulted in the formation of **5** and **6**. Subsequently, a more convenient and rational one-pot method was developed to access **5** and **6**, by the reaction of $[CrCl_3(thf)_3]$ with ^{Dipp}**NHC,P** and **P,NHC,P**, respectively, and excess $[Mg(benzyl)_2(thf)_2]$ under a carefully controlled temperature regime (see the Experimental Section). The reaction of $[Cr(benzyl)_3(thf)_3]$ with the ligand ^{Dipp}**NHC,P** also led to **5**, and this procedure could probably be extended to the other NHC,P ligands. However, the difficulties associated with the synthesis of $[Cr(benzyl)_3(thf)_3]$ made this route less attractive. Isolation and purification of the new benzyl complexes were carried out by extraction of the complex into toluene and layering the solution with pentane for crystallization; however, this resulted in lower isolated yields of **5** (8% based on Cr), which has reduced solubility in toluene, and **6** (56%). Attempts to isolate the complexes by extraction into more polar solvents, such as THF, gave impure products. The paramagnetic **5** and **6** are black, extremely air- and moisture-sensitive crystalline materials that were characterized by single-crystal X-ray diffraction.

Scheme 1. Synthesis of Cr^{II} and Cr^{III} Complexes[a]

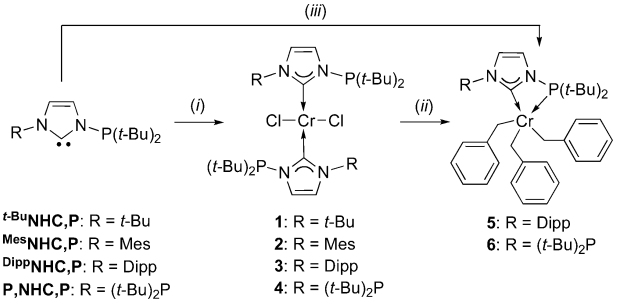

[a]Reagents and conditions: (*i*) $[CrCl_2(thf)_2]$, $[CrCl_3(thf)_3]$ or $[Cr(Me)Cl_2(thf)_3]$, THF, −78 °C to room temperature; (*ii*) $[Mg(benzyl)_2(thf)_2]$ and 1,4-dioxane, THF, −40 °C to room temperature; (*iii*) $[CrCl_3(thf)_3]$, $[Mg(benzyl)_2(thf)_2]$, and 1,4-dioxane, THF, −78 to −40 °C to room temperature.

Solid-State Structures of the Cr^{II} and Cr^{III} Complexes. The structures of **1**−**4** are shown in Figures S1 and S2 in the Supporting Information for **1** and **2** and Figures 1 and 2 for **3** and **4**, respectively. Selected bond lengths and angles are given in Table 1.

In all four complexes, the Cr^{II} center, at a center of molecular and crystallographic symmetry, features a perfect square-planar geometry with mutually trans C_{NHC} and chlorine donors. The coordination plane and the imidazole ring form a dihedral angle of 85.51° in **1**, 87.37° in **2**, 88.30° in **3**, and 85.58° in **4**. The Cr−C_{NHC} and Cr−Cl bond distances are in the ranges 2.152(6)−2.205(2) and 2.3432(6)−2.3525(5) Å, respectively, and are comparable with those in similar complexes.[12a,b,19] No interaction between the phosphine groups and the chromium can be deduced on the basis of the observed set of metrical data and conformations.

The structures of **5** and **6** are shown in Figures 3 and 4, respectively, and selected bond lengths and angles are given in Table 2.

DOI: 10.1021/acs.organomet.5b00547
Organometallics 2015, 34, 4109−4116

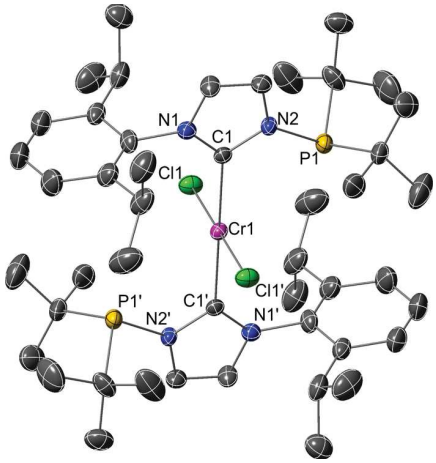

Figure 1. Thermal ellipsoid representation (30% probability level) of the structure of **3**. H atoms are omitted for clarity.

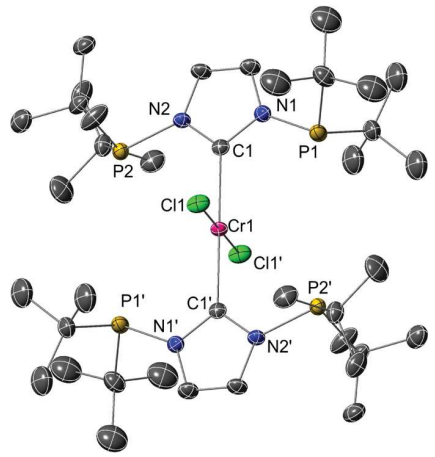

Figure 2. Thermal ellipsoid representation (30% probability level) of the structure of **4**. H atoms are omitted for clarity.

Table 1. Selected Bond Lengths (Å) and Angles (deg) in the Solid-State Structures of 1−4

	1	2	3	4
Cr1−C1	2.205(2)	2.169(2)	2.176(4)	2.152(6)
Cr1−Cl1	2.3525(5)	2.3432(6)	2.346(1)	2.349(2)
C1−N1	1.347(2)	1.347(3)	1.351(5)	1.363(8)
C1−N2	1.382(2)	1.370(3)	1.358(5)	1.370(8)
N2−P1(P2)	1.739(2)	1.755(2)	1.748(3)	1.753(5)
N1−P1				1.755(5)
C1−Cr1−Cl1	89.97(5)	89.98(6)	87.40(9)	87.2(1)
C1−Cr1−Cl1′	90.03(5)	90.02(6)	92.60(9)	92.8 (2)
Cr1- C1−N1	133.3(1)	133.0(2)	131.7(3)	127.4(4)
Cr1- C1−N2	122.6(1)	123.0(2)	123.1(2)	127.5(4)
N1−C1−N2	104.0(2)	103.9(2)	104.6(3)	104.4(5)
C1−N2−P1(P2)	120.9(1)	115.8(2)	117.6(2)	116.9(4)
C1−N1−P1				116.8(4)

Complexes **5** and **6** constitute rare examples of five-coordinate Cr^{III} organometallics.[20] In both, the geometry at Cr^{III} is slightly distorted square pyramidal (τ[21] 0.41 and 0.36 for **5** and **6**, respectively), with the two C_{benzyl} (C31 and C38), the C_{NHC}, and the P donors forming the basal plane. In contrast to

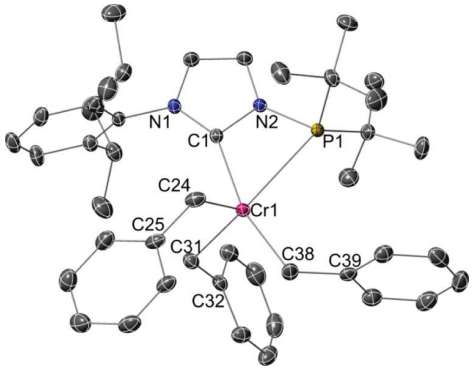

Figure 3. Thermal ellipsoid representation (30% probability level) of the structure of **5**. H atoms are omitted for clarity.

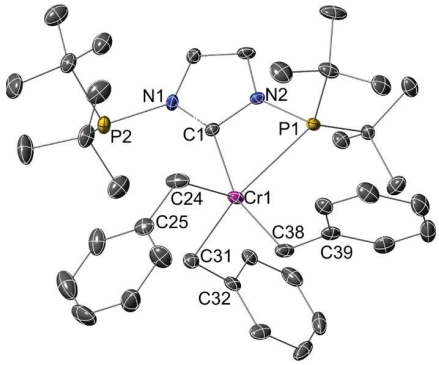

Figure 4. Thermal ellipsoid representation (30% probability level) of the structure of **6**. H atoms are omitted for clarity.

the previously described Cr^{II} species, the phosphanyl NHC ligands in **5** and **6** adopt a chelating bonding mode that results in a strained four-membered ring with an acute bite angle of 60.64(3)° and 61.84(11)°, respectively. The sum of the bond angles within the chelate ring (358.8° for **5**, 360° for **6**) indicates planarity. The short-bite nature of the chelating ligand results in a significant value for the angle θ (Scheme 2), defined as the angle between the axis going through the carbene donor atom C1 and the middle of the imidazole C═C double bond and the C1−Cr bond (18.61 and 21.20°, respectively). This definition is slightly different from that of the yaw distortion angle used by Crabtree (Scheme 2),[22] which is based on a symmetrical imidazole ring (although the two N substituents are not the same), but the θ values obtained according to these two definitions are almost the same.

The Cr−C_{benzyl} bond distances in **5** and **6** (2.095(5)−2.149(1) Å) fall within the expected range[18,23] and are significantly shorter than the Cr−C_{NHC} bonds (2.216(1) Å for **5** and 2.227(4) Å for **6**). In both **5** and **6**, the three angles subtended at $C_{benzylic}$ show considerable differences: the C32−C31−Cr1 angle (107.20(8)° in **5**, 99.8(3)° in **6**) is more acute than the other two (C39−C38−Cr1 121.57(8), 124.7(3)° and C25−C24−Cr1 117.07(9), 118.1(3)° in **5** and **6**, respectively). Even more acute angles of 97.9(2) and 76.6(2)° have been found recently in a Cr^{II} complex of the type [Cr(NHC)-(benzyl)$_2$], the angular distortion at the benzylic carbon having been ascribed to intramolecular polarization-induced metal−arene interactions.[18] In the structure of **6** there is no interaction between the second P(*t*-Bu)$_2$ group and the metal. The lone

DOI: 10.1021/acs.organomet.5b00547
Organometallics 2015, 34, 4109−4116

Table 2. Selected Bond Lengths (Å) and Angles (deg) in the Solid-State Structures of 5 and 6

	5	6
Cr1−C1	2.216(1)	2.227(4)
Cr1−P1	2.8014(3)	2.725(1)
Cr1−C24	2.100(1)	2.095(5)
Cr1−C31	2.080(1)	2.102(4)
Cr1−C38	2.149(1)	2.137(4)
C1−N1	1.358(1)	1.371(5)
C1−N2	1.376(1)	1.369(5)
N2−P1	1.7517(9)	1.740(3)
N1−P2		1.775(4)
C1−Cr1−P1	60.64(3)	61.8(1)
C31−Cr1−C24	96.41(5)	94.6(2)
C31−Cr1−C38	96.22(5)	94.0(2)
C31−Cr1−C1	96.34(5)	100.0(2)
C24−Cr1−C1	94.99(4)	95.4(2)
C38−Cr1−C1	164.02(4)	160.6(2)
C31−Cr1−P1	139.57(4)	139.2(1)
C24−Cr1−P1	116.98(4)	121.8(2)
C38−Cr1−P1	103.40(4)	98.8(2)
Cr1−P1−N2	77.84(3)	79.1(1)
Cr1−C1−N2	109.58(7)	107.5(3)
Cr1−C38−C39	121.57(8)	124.7(3)
Cr1−C31−C32	107.20(8)	99.8(3)
Cr1−C24−C25	117.07(9)	118.1(3)
C1−N2−P1	110.74(7)	111.6(3)
C1−N1−P2		120.0(3)
N1−C1−N2	103.85(9)	103.9(3)

Scheme 2. Distortion Angle θ Resulting from the Short-Bite Character of the NHC,P Chelating Ligands[a]

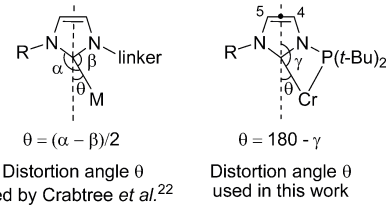

[a]In our case (right), the dashed line goes through the middle of the double bond between C4 and C5 and the C_{NHC} atom.

pair at P2 is oriented toward the benzylic carbons C24 and C31.

Catalytic Ethylene Oligomerization and Polymerization. The complexes **1**−**6** were evaluated as precatalysts for the oligomerization of ethylene at 10 bar of ethylene with 400 equiv of methylaluminoxane (MAO) as cocatalyst. The results are compiled in Table 3. At 30 °C, **1**, **2**, and **4** with MAO as cocatalyst were only poorly active (less than 350 g/((g of Cr) h)) in comparison to the pyridylbis(carbene) Cr^{III} species of type **A** (7.8×10^5 g/((g of Cr) h))[9a] and mostly polyethylene (PE) was formed (entries 1, 2, and 5 in Table 3). The **3**/MAO system showed higher activity (1040 g/((g of Cr) h)) and gave smaller amounts of polymers (32 wt %) and mostly octenes (51%), of which 97% was 1-octene. The C6 fraction (17%) contained almost exclusively 1-hexene; only very small amounts of 3-*cis*-hexene and 2-*trans*-hexene were found in the liquid phase, but no methylcyclopentane and methylenecyclopentane, which are usually produced with other ethylene tetramerization catalysts. When the initial reaction temperature was set at 80 °C, the **3**/MAO system was more than twice as active (2390 g/((g of Cr) h)) and only oligomers were produced (entry 4 in Table 3). Under similar conditions, the Cr^{III} complexes **5** and **6** performed better than the Cr^{II} complexes, with activities of up to 8790 g/((g of Cr) h)) for **6**/MAO (entry 7 in Table 3).[24] The molecular mass distribution of the oligomerization products is of the Schulz−Flory type with a K value of 0.73 ($K = k_{prop}/(k_{prop} + k_{ch\ transfer})$ = (mol of C_{n+2})/(mol of C_n); Figure 5). The nature of the ligand N substituent can significantly affect the nature of the products obtained from catalytic ethylene oligomerization, as found for example in Cr complexes with the pyridine bis(carbene)[9a] and pyridine bis(imine)[21] ligands. The major oligomer produced by the **5**/MAO system was 1-octene, and 4 wt % of polymer was formed, whereas in the case of **6**/MAO, the major oligomers were 1-hexene and 1-octene and 9 wt % waxes were produced. Subsequently, the influence of the reaction conditions on the catalytic performance of **6**/MAO was investigated. The latter system was found to be still active after 35 min and lasted for 90 min, giving an activity of 5360 g/((g of Cr) h)) (entry 8 in Table 3). Methylcyclohexane has been reported to improve the catalytic activity of Cr^{III} complexes with a P,N donor ligand in ethylene oligomerization,[9e] whereas an adverse effect was noted recently with Cr^{III} systems containing dipyrrole-based ligands.[25] In our case, using methylcyclohexane as solvent for the **6**/MAO

Table 3. Oligomerization of Ethylene for Complexes 1−6 with MAO as Cocatalyst[a]

		overall selectivity (wt %)							
entry	cat.	C4 (1-C4)	C6 (1-C6)	C8 (1-C8)	C10 (1-C10)	> C10	PE	productivity[b]	TOF[c]
1	**1**	1 (97)	10 (100)	19 (65)	0	0	70	150	280
2	**2**	0	3 (89)	33 (71)	0	0	64	190	350
3	**3**	0	17 (99)	51 (97)	0	0	32	1040	1930
4[d]	**3**	15 (99)	18 (91)	15 (86)	16 (82)	36	0	2390	4440
5	**4**	0	2 (92)	2 0(96)	1 (12)	2	75	310	580
6	**5**	10 (99)	15 (91)	18 (84)	15 (76)	38	4	6110	11350
7	**6**	14 (95)	16 (95)	15 (91)	13 (85)	33	9[h]	8790	16320
8[e]	**6**	16 (100)	18 (95)	16 (90)	14 (83)	36	0	5360	9950
9[f]	**6**	15 (100)	17 (95)	16 (90)	14 (85)	37	1[h]	6040	11220
10[g]	**6**	12 (99)	15 (84)	16 (87)	14 (80)	33	10	6060	11250

[a]Conditions unless specified otherwise: temperature 30 °C, 10 bar of C_2H_4, reaction time 35 min, 4×10^{-5} mol of catalyst, solvent 9.33 mL of chlorobenzene and 10.66 mL of the cocatalyst solution (1.5×10^{-3} M) for 400 equiv of MAO. [b]In (g of C_2H_4)/((g of Cr) h). [c]In (mol of C_2H_4)/((mol of Cr) h). [d]Temperature 80 °C. [e]Reaction time 90 min. [f]In methylcyclohexane. [g]Temperature 45 °C. [h]Waxes.

DOI: 10.1021/acs.organomet.5b00547
Organometallics 2015, 34, 4109−4116

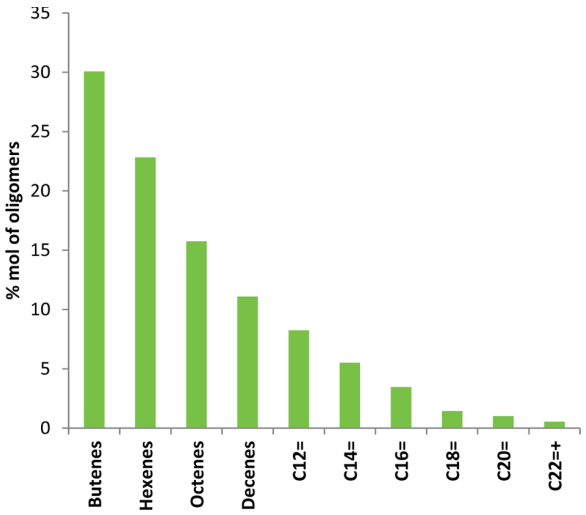

Figure 5. Oligomer distribution with precatalysts **6** (entry 7 in Table 3) using MAO as cocatalyst.

system also had an adverse effect on the activity, which may be ascribed to the poor solubility of **6** in this solvent, but led to a decreased formation of waxes (entry 9 in Table 3). After injection of the catalyst and cocatalyst, **6** consumed ethylene very slowly during the first 7 min. Acceleration of ethylene uptake only started when the reaction temperature reached 45 °C. Subsequently, the **6**/MAO system was tested at an initial temperature of 45 °C, but this resulted in a decreased activity (entry 10 in Table 3). This could be attributed to the rapid formation of polymers instead of waxes, which can encapsulate the catalyst and hamper further reaction.

The use of $AlEtCl_2$ (EADC) as cocatalyst for all of the complexes (**1**−**6**) led predominantly to the formation of polyethylene and less than 5% of oligomers (Table 4). When the R group was changed from *t*-Bu to P(*t*-Bu)$_2$ in the Cr^{II} complexes **1**−**4**, the activity gradually increased from 380 to 1690 g/((g of Cr) h). Increasing the reaction temperature to 80 °C for **3**/EADC (entry 4 in Table 4) and reducing the amount of cocatalyst (3 equiv) for **4**/EADC (entry 6 in Table 4) led to a dramatic decrease in activity. No obvious differences between the Cr^{III} complex **6** and the Cr^{II} complexes **3** and **4** were observed when EADC (entries 3, 5, and 7 in Table 4) was used as a cocatalyst, at variance with the MAO system.

Table 4. Polymerization of Ethylene for Complexes 1−4 and 6 with $AlEtCl_2$ as Cocatalyst[a]

entry	cat.	amt of PE (g)	amt of PE (wt %)	productivity[b]	TOF[c]
1	**1**	0.36	100	380	710
2	**2**	1.37	98	1370	2540
3	**3**	2.09	100	1650	3060
4[d]	**3**	0.26	96	490	910
5	**4**	2.05	97	1690	3140
6[e]	**4**	0.49	95	460	850
7	**6**	1.64	100	1670	3100

[a]Conditions unless specified otherwise: temperature 30 °C, 10 bar of C_2H_4, time 35 min, 4×10^{-5} mol of catalyst, solvent 10 mL of chlorobenzene and 5 mL of the cocatalyst solution (8×10^{-5} M) for 10 equiv of $AlEtCl_2$. [b]In (g of C_2H_4)/((g of Cr) h). [c]In (mol of C_2H_4)/((mol of Cr) h). [d]Temperature 80 °C. [e]1.5 mL of the cocatalyst solution (8×10^{-5} M) for 3 equiv of $AlEtCl_2$ and 13.5 mL of chlorobenzene.

CONCLUSION

Motivated by their donor characteristics and bite angles, we studied the phosphanyl- and diphosphanyl-substituted NHC ligands $^{t\text{-Bu}}$**NHC,P**, $^{\text{Mes}}$**NHC,P**, $^{\text{Dipp}}$**NHC,P**, and **P,NHC,P** as mimics of the *N,N′*-bis(diarylphosphino)amines (PNP) used in Cr complexes for the catalytic oligomerization or polymerization of ethylene. In contrast to the chelating behavior of bis(phosphanyl)amine-type ligands, the functionalized NHC ligands behaved as monodentate C_{NHC} donors with dangling, coordination-inactive PR_2 groups in their Cr^{II} complexes **1**−**4**, obtained from either Cr^{II} or Cr^{III} chlorido precursors. The mechanism of the redox reaction responsible for the formation of the Cr^{II} complexes has not been elucidated but may be relevant to transformations occurring in situ in catalytic systems. In contrast, benzylation of either well-defined Cr^{II} complexes or $[CrCl_3(THF)_3]$/ligand mixtures with $[Mg(benzyl)_2(thf)_2]$ led to $[Cr(NHC)(benzyl)_3]$ species with κ^2-phosphanyl-NHC ligand coordination. Upon activation with MAO, the Cr^{III} complexes were active in ethylene oligomerization, displaying catalytic performances superior to those of the Cr^{II} precursors. However, it is noteworthy that the oligomers obtained with complex **3** were almost exclusively 1-hexene and 1-butene when the reaction was initiated at 30 °C. At 80 °C, a broader mass distribution of oligomers was observed (from C4 to >C10) and polyethylene formation was suppressed. The use of EADC as cocatalyst led predominantly to the formation of polymers. The tri- and tetramerization observed in some cases validates further the idea that NHC-P can mimic the PNP ligands, although each ligand family possesses its own specific features. The significant differences in activities and selectivities observed with catalytic species generated from seemingly similar ligand designs demonstrate further the subtlety of the parameters that determine the catalytic features of metal complexes.

EXPERIMENTAL SECTION

General Methods. All manipulations involving organometallics were performed under nitrogen or argon in a Braun glovebox or using standard Schlenk techniques. Solvents were dried using standard procedures and distilled under nitrogen prior to use or passed through columns of activated alumina and subsequently purged with nitrogen or argon. The ligands $^{t\text{-Bu}}$**NHC,P**, $^{\text{Mes}}$**NHC,P**, $^{\text{Dipp}}$**NHC,P**, and **P,NHC,P** were prepared according to the literature.[13c,14a,17] $[Mg(benzyl)_2(THF)_2]$ was prepared as described,[26] and $[CrCl_2(THF)_2]$ and $[CrCl_3(THF)_3]$ were prepared by continuous Soxhlet extraction of commercial anhydrous $CrCl_2$ with THF under argon for 24−48 h.

Synthesis of the Chromium(II) Complexes 1−4. *Method a.* To a supension of $[CrCl_2(THF)_2]$ (0.133 g, 0.50 mmol) in THF (8 mL) was added a solution of the corresponding ligand (1.05 mmol) in THF (8 mL) at −78 °C. The reaction mixture was warmed slowly to room temperature and stirred overnight. After evaporation of the solvent under reduced pressure, the residue was washed with pentane (5 mL) to give a purple, air-sensitive powder. X-ray-quality crystals were obtained by slow diffusion of pentane into THF solution of the corresponding complex.

Complex **1**: yield 0.274 g, 83%. Anal. Found (calcd for $C_{30}H_{58}Cl_2CrN_4P_2$): C, 54.97 (54.62); H, 8.97 (8.86); N, 8.18 (8.49).

Complex **2**: yield 0.337 g, 86%. Anal. Found (calcd for $C_{40}H_{62}Cl_2CrN_4P_2$): C, 61.22 (61.29); H, 8.15 (7.97); N, 6.64 (7.15).

Complex **3**: yield 0.380 g, 88%. Anal. Found (calcd for $C_{46}H_{74}Cl_2CrN_4P_2$): C, 63.52 (63.65); H, 8.73 (8.59); N, 6.37 (6.46).

DOI: 10.1021/acs.organomet.5b00547
Organometallics 2015, 34, 4109−4116

Complex **4**: yield 0.309 g, 74%. Anal. Found (calcd for $C_{38}H_{76}Cl_2CrN_4P_4$): C, 54.35 (54.60); H, 9.03 (9.16); N, 6.68 (6.70).

Method b. To a suspension of $[CrCl_3(THF)_3]$ (0.093 g, 0.25 mmol) or $[Cr(Me)Cl_2(THF)_3]$ (0.088 g, 0.25 mmol) in THF (8 mL) was added a solution of the corresponding ligand in excess (0.70 mmol) in THF (8 mL) at −78 °C. The reaction mixture was warmed slowly to room temperature and stirred for 4 h. The resulting brown suspension was filtered, and layering the filtrate with pentane afforded crystals of the corresponding Cr(II) complex **1**−**4**.

Synthesis of Chromium(III) Complexes 5 and 6. *Method a.* Solid $[CrCl_3(THF)_3]$ (0.068 g, 0.183 mmol), the corresponding carbene ligand (0.210 mmol), and $[Mg(benzyl)_2(THF)_2]$ (0.150 g, 0.428 mmol) were placed in a Schlenk tube in the glovebox. The tube was connected to the vacuum line and cooled to −78 °C. At this temperature, precooled THF (15 mL) and dioxane (2 mL) were added and the reaction mixture was stirred at −40 °C for 1 h. Then the dark brown reaction mixture was warmed to room temperature and was further stirred for 1 h. After evaporation of the solvent under reduced pressure, the residue was extracted with toluene (30 mL) and the solution was filtered. The filtrate was layered with pentane (60 mL) for 3 days to give a black and air-sensitive crystalline material. X-ray-quality crystals were obtained by slow diffusion of pentane into a dilute toluene solution of the complex.

Complex **5**: yield 0.010 g, 8% based on Cr.

Complex **6**: yield 0.070 g, 56% based on Cr. Due to the extreme sensitivity of **5** and **6**, satisfactory elemental analyses could not be obtained.

Method b. To a solution of **3** (0.174 g, 0.200 mmol) or a suspension of **4** (0.167 g, 0.200 mmol) in THF (10 mL) was added dioxane (2 mL), and the reaction mixture was cooled to −40 °C. At this temperature, a precooled solution of $[Mg(benzyl)_2(THF)_2]$ (0.210 g, 0.60 mmol) in THF (6 mL) was added and the reaction mixture was stirred at −40 °C for 1 h. The dark brown reaction mixture was then warmed to room temperature and was further stirred for 1 h. After evaporation of the solvent under reduced pressure, the residue was extracted with toluene (40 mL) and the solution filtered. The filtrate was layered with pentane (60 mL) for 3 days to give a black, air-sensitive crystalline material.

Complex **5**: yield 0.008 g, 6% based on Cr.

Complex **6**: yield 0.030 g, 22% based on Cr.

General Procedure for the Catalytic Ethylene Oligomerization. All catalytic reactions were performed in a magnetically stirred (1200 rpm) 145 mL stainless steel autoclave. A 125 mL glass container was used to avoid corrosion of the autoclave walls. The preparation of the catalytic solution of the precatalyst was dependent on the nature and the amount of the cocatalyst.

With MAO, 4×10^{-5} mol of Cr complex was dissolved in 9.33 mL of chlorobenzene or methylcyclohexane and the solution was injected into the reactor under an ethylene flux. Then 8 mL of a 1.5×10^{-3} M cocatalyst toluene solution, corresponding to 400 equiv of MAO, was added to the reactor to reach a total volume of 20 mL with the precatalyst solution.

With $AlEtCl_2$ (EADC), 4×10^{-5} mol of Cr complex was dissolved in 13.5 or 10 mL in chlorobenzene and the solution was injected into the reactor under an ethylene flux, followed by 1.5 or 5 mL of a 8×10^{-5} M cocatalyst solution corresponding to 3 or 10 equiv of EADC, respectively. The total volume of the solution inside the reactor was 15 mL.

The catalytic reaction was started at 30, 45, or 80 °C. No cooling of the reactor was applied during the reaction. After injection of the catalyst and cocatalyst solutions under a constant low flow of ethylene, which is considered as the t_0 time, the reactor was immediately pressurized to 10 bar of ethylene. The temperature increased, owing solely to the exothermicity of the reaction. The 10 bar working pressure was maintained through a continuous feed of ethylene from a bottle placed on a balance to allow continuous monitoring of the ethylene uptake. At the end of each test (35 or 90 min to facilitate comparisons with previous studies from this laboratory[1c,9d]), a dry ice bath was used to rapidly cool the reactor. When the inner temperature reached 0 °C, the ice bath was removed, allowing the temperature to slowly rise to 18 °C. The gaseous phase was then transferred into a 10 L polyethylene tank filled with water. An aliquot of this gaseous phase was transferred into a Schlenk flask, previously evacuated, for GC analysis. The amount of ethylene consumed was thus determined by differential weighing of the ethylene bottle (accuracy of the scale 0.1 g). From this amount of ethylene was subtracted the remaining ethylene (calculated using the GC analysis) in the gaseous phase. Although this method is of limited accuracy, it was used throughout and gave satisfactory reproducibility. The reaction mixture in the reactor was quenched in situ by the addition of ethanol (1 mL), transferred into a Schlenk flask, and separated from the metal complexes by trap-to-trap evaporation (20 °C, 0.8 mbar) into a second Schlenk flask previously immersed in liquid nitrogen in order to avoid loss of product for GC analysis. Each catalytic test was performed twice to ensure the reproducibility of the results. For GC analyses, 1-heptene was used as an internal reference.

X-ray Crystallography. A summary of the crystal data, data collection and refinement for structures of **1**−**6** are given in Table S1 in the Supporting Information. For **1** and **3**−**5**, X-ray diffraction data collection was carried out on a Bruker APEX II DUO Kappa-CCD diffractometer equipped with an Oxford Cryosystem liquid N_2 device, using Mo Kα radiation (λ = 0.71073 Å). The crystal−detector distance was 38 mm. The cell parameters were determined (APEX2 software)[27] from reflections taken from 3 sets of 12 frames, each at 10 s exposure. The structure was solved by direct methods using the program SHELXS-97.[28] The refinement and all further calculations were carried out using SHELXL-97.[29] The H atoms were included in calculated positions and treated as riding atoms using SHELXL default parameters. The non-H atoms were refined anisotropically, using weighted full-matrix least squares on F^2. A semiempirical absorption correction was applied using SADABS in APEX2.[27]

For **2** and **6**, X-ray diffraction data collection was carried out on a Nonius Kappa-CCD diffractometer equipped with an Oxford Cryosystem liquid N_2 device, using Mo Kα radiation (λ = 0.71073 Å). The crystal−detector distance was 36 mm. The cell parameters were determined (Denzo software)[30] from reflections taken from one set of 10 frames (1.0° steps in ψ angle), each at 20 s exposure. The structures were solved by direct methods using the program SHELXS-97.[28] The refinement and all further calculations were carried out using SHELXL-97.[29] The H atoms were included in calculated positions and treated as riding atoms using SHELXL default parameters. The non-H atoms were refined anisotropically, using weighted full-matrix least squares on F^2. A semiempirical absorption correction was applied using MULscanABS in PLATON.[31]

■ ASSOCIATED CONTENT

Supporting Information

This material is also available free of charge via the Internet at http://pubs.acs.org/. The Supporting Information is available free of charge on the ACS Publications website at DOI: 10.1021/acs.organomet.5b00547. The Crystallographic information files (CIF) have been deposited with the CCDC, 12 Union Road, Cambridge CB2 1EZ, U.K., and can be obtained on request free of charge, by quoting the publication citation and deposition numbers 1055511−1055516.

Structures of **1** and **2** and crystal data for **1**−**6** (PDF)

Crystal data for **1**−**6** (CIF)

■ AUTHOR INFORMATION

Corresponding Authors

*E-mail for A.A.D.: danopoulos@unistra.fr.

*E-mail for P.B.: braunstein@unistra.fr.

Notes

The authors declare no competing financial interest.

DOI: 10.1021/acs.organomet.5b00547
Organometallics 2015, 34, 4109−4116

■ ACKNOWLEDGMENTS

This paper is dedicated to Professor Ekkehardt Hahn on the occasion of his 60th birthday, with our sincere congratulations and best wishes. The USIAS, CNRS, Région Alsace, and Communauté Urbaine de Strasbourg are acknowledged for the award of fellowships and a Gutenberg Excellence Chair (2010−11) to A.A.D. We are grateful to the China Scholarship Council for a Ph.D. grant to P.A. We thank Marc Mermillon-Fournier for technical assistance, the CNRS and the MESR (Paris) for funding, and the Service de Radiocrystallographie (UdS) for the determination of the crystal structures. We thank Drs. H. Olivier-Bourbigou and P.-A. R. Breuil (IFP Energies nouvelles, Solaize) for discussions and the reviewers for valuable comments.

■ REFERENCES

(1) (a) Vogt, D. Oligomerization of Ethylene to Higher Linear α-Olefins. In *Applied Homogeneous Catalysis with Organometallic Compounds*; Cornils, B., Herrmann, W. A., Eds.; Wiley-VCH: Weinheim, Germany, 2002; Vol. *1*, pp 240−252. (b) Dixon, J. T.; Green, M. J.; Hess, F. M.; Morgan, D. H. *J. Organomet. Chem.* **2004**, *689*, 3641−3668. (c) Speiser, F.; Braunstein, P.; Saussine, L. *Acc. Chem. Res.* **2005**, *38*, 784−793. (d) Forestière, A.; Olivier-Bourbigou, H.; Saussine, L. *Oil Gas Sci. Technol.* **2009**, *64*, 649−667. (e) Peitz, S.; Aluri, B. R.; Peulecke, N.; Müller, B. H.; Wohl, A.; Müller, W.; Al-Hazmi, M. H.; Mosa, F. M.; Rosenthal, U. *Chem. - Eur. J.* **2010**, *16*, 7670−7676. (f) Agapie, T. *Coord. Chem. Rev.* **2011**, *255*, 861−880. (g) McGuinness, D. S. *Chem. Rev.* **2011**, *111*, 2321−2341. (h) van Leeuwen, P. W. N. M.; Clément, N. D.; Tschan, M. J. L. *Coord. Chem. Rev.* **2011**, *255*, 1499−1517. (i) Breuil, P.-A.; Magna, L.; Olivier-Bourbigou, H. *Catal. Lett.* **2015**, *145*, 173−192. (j) Harzschel, S.; Kühn, F. E.; Wohl, A.; Müller, W.; Al-Hazmi, M. H.; Alqahtani, A. M.; Müller, B. H.; Peulecke, N.; Rosenthal, U. *Catal. Sci. Technol.* **2015**, *5*, 1678−1682. (k) Zhou, Y.; Wu, H.; Xu, S.; Zhang, X.; Shi, M.; Zhang, J. *Dalton Trans.* **2015**, *44*, 9545−9550.

(2) (a) Paul, H. J.; Banks, R. L. (Phillips Petroleum Company) U.S. Pat. 2,825,721, 1958. (b) Hogan, J. P. *J. Polym. Sci., Part A-1: Polym. Chem.* **1970**, *8*, 2637−2652.

(3) (a) Karapinka, G. L. (Union Carbide Corporation) U.S. Pat. 3,709,853, 1973. (b) Karol, F. J.; Karapinka, G. L.; Wu, C.; Dow, A. W.; Johnson, R. N.; Carrick, W. L. *J. Polym. Sci., Part A-1: Polym. Chem.* **1972**, *10*, 2621−2637.

(4) (a) McDaniel, M. P. A Review of the Phillips Supported Chromium Catalyst and Its Commercial Use for Ethylene Polymerization. In *Advances in Catalysis*; Bruce, C. G., Helmut, K., Eds.; Academic Press: New York, 2010; Vol. *53*, pp 123−606. (b) Theopold, K. H. *Proc. Natl. Acad. Sci. U. S. A.* **2014**, *111*, 11578−11579.

(5) (a) Reagan, W. K.; Freeman, J. W.; Conroy, B. K.; Pettijohn, T. M.; Benham, E. A. (Phillips Petroleum Company) EP0608447, 1994. (b) Reagen, W. K.; Freeman, J. W.; Pettijohn, T. M. (Phillips Petroleum Company) U.S. Pat. 5,856,257, 1996.

(6) Tanaka, E.; Urata, H.; Oshiki, T.; Aoshima, T.; Kawashima, R.; Iwade, S.; Nakamura, H.; Katsuki, S.; Okano, T. (Mitsubishi Chemical Corporation) EP0611743, 1994.

(7) (a) Carter, A.; Cohen, S. A.; Cooley, N. A.; Murphy, A.; Scutt, J.; Wass, D. F. *Chem. Commun.* **2002**, 858−859. (b) Wass, D. F. (BP Chemicals Ltd) WO2002004119, 2002.

(8) (a) McGuinness, D. S.; Wasserscheid, P.; Keim, W.; Hu, C.; Englert, U.; Dixon, J. T.; Grove, C. *Chem. Commun.* **2003**, 334−335. (b) McGuinness, D. S.; Wasserscheid, P.; Keim, W.; Morgan, D.; Dixon, J. T.; Bollmann, A.; Maumela, H.; Hess, F.; Englert, U. *J. Am. Chem. Soc.* **2003**, *125*, 5272−5273. (c) Bollmann, A.; Blann, K.; Dixon, J. T.; Hess, F. M.; Killian, E.; Maumela, H.; McGuinness, D. S.; Morgan, D. H.; Neveling, A.; Otto, S.; Overett, M.; Slawin, A. M. Z.; Wasserscheid, P.; Kuhlmann, S. *J. Am. Chem. Soc.* **2004**, *126*, 14712−14713. (d) Dixon, J. T.; Wasserscheid, P.; Mcguinness, D. S.; Hess, F. M.; Maumela, H.; Morgan, D. H.; Bollmann, A. (Sasol Technology (Pty) Ltd) WO2003053890, 2003.

(9) (a) McGuinness, D. S.; Gibson, V. C.; Wass, D. F.; Steed, J. W. *J. Am. Chem. Soc.* **2003**, *125*, 12716−12717. (b) Wass, D. F. *Dalton Trans.* **2007**, 816−819. (c) McGuinness, D. S.; Suttil, J. A.; Gardiner, M. G.; Davies, N. W. *Organometallics* **2008**, *27*, 4238−4247. (d) Liu, S.; Pattacini, R.; Braunstein, P. *Organometallics* **2011**, *30*, 3549−3558. (e) Yang, Y.; Gurnham, J.; Liu, B.; Duchateau, R.; Gambarotta, S.; Korobkov, I. *Organometallics* **2014**, *33*, 5749−5757. (f) Yang, Y.; Liu, Z.; Cheng, R.; He, X.; Liu, B. *Organometallics* **2014**, *33*, 2599−2607. (g) Zhang, J.; Qiu, P.; Liu, Z.; Liu, B.; Batrice, R. J.; Botoshansky, M.; Eisen, M. S. *ACS Catal.* **2015**, *5*, 3562−3574. (h) Britovsek, G. J. P.; McGuinness, D. S.; Wierenga, T.; Young, C. *ACS Catal.* **2015**, *5*, 4152−4166.

(10) (a) Herrmann, W. A.; Köcher, C. *Angew. Chem., Int. Ed. Engl.* **1997**, *36*, 2162−2187. (b) Herrmann, W. A. *Angew. Chem., Int. Ed.* **2002**, *41*, 1290−1309. (c) Crudden, C. M.; Allen, D. P. *Coord. Chem. Rev.* **2004**, *248*, 2247−2273. (d) Scott, N. M.; Nolan, S. P. *Eur. J. Inorg. Chem.* **2005**, *2005*, 1815−1828. (e) Nolan, S. P. *N-Heterocyclic Carbenes in Synthesis*; Wiley-VCH: Weinheim, Germany, 2006. (f) Dröge, T.; Glorius, F. *Angew. Chem., Int. Ed.* **2010**, *49*, 6940−6952. (g) Hopkinson, M. N.; Richter, C.; Schedler, M.; Glorius, F. *Nature* **2014**, *510*, 485−496.

(11) McGuinness, D. *Dalton Trans.* **2009**, 6915−6923.

(12) (a) Wang, K.; Zhang, J.; Chen, T.; Zhang, T.; Yang, L. *Chin. J. Struct. Chem.* **2010**, *29*, 933−939. (b) Wang, J.; Tan, G.; An, D.; Zhu, H.; Yang, Y. *Z. Anorg. Allg. Chem.* **2011**, *637*, 1597−1601. (c) Al Thagfi, J.; Lavoie, G. G. *Organometallics* **2012**, *31*, 2463−2469. (d) Conde-Guadano, S.; Hanton, M.; Tooze, R. P.; Danopoulos, A. A.; Braunstein, P. *Dalton Trans.* **2012**, *41*, 12558−12567. (e) Larocque, T. G.; Badaj, A. C.; Dastgir, S.; Lavoie, G. G. *Dalton Trans.* **2011**, *40*, 12705−12712. (f) Thagfi, J. A.; Lavoie, G. G. *Organometallics* **2012**, *31*, 7351−7358.

(13) (a) Gaillard, S.; Renaud, J.-L. *Dalton Trans.* **2013**, *42*, 7255−7270. (b) Marchenko, A. P.; Koidan, H. N.; Hurieva, A. N.; Gutov, O. V.; Kostyuk, A. N.; Tubaro, C.; Lollo, S.; Lanza, A.; Nestola, F.; Biffis, A. *Organometallics* **2013**, *32*, 718−721. (c) Ai, P.; Danopoulos, A. A.; Braunstein, P.; Monakhov, K. Y. *Chem. Commun.* **2014**, *50*, 103−105. (d) Marchenko, A.; Koidan, H.; Hurieva, A.; Kurpiieva, O.; Vlasenko, Y.; Kostyuk, A.; Tubaro, C.; Lenarda, A.; Biffis, A.; Graiff, C. *J. Organomet. Chem.* **2014**, *771*, 14−23. (e) Wang, T.; Stephan, D. W. *Chem. - Eur. J.* **2014**, *20*, 3036−3039. (f) Brill, M.; Marrwitz, D.; Rominger, F.; Hofmann, P. *J. Organomet. Chem.* **2015**, *775*, 137−151. (g) Ai, P.; Danopoulos, A. A.; Braunstein, P. *Inorg. Chem.* **2015**, *54*, 3722−3724.

(14) (a) Nägele, P.; Herrlich, U.; Rominger, F.; Hofmann, P. *Organometallics* **2013**, *32*, 181−191. (b) Brown, C. C.; Plessow, P. N.; Rominger, F.; Limbach, M.; Hofmann, P. *Organometallics* **2014**, *33*, 6754−6759.

(15) Crabtree, R. H. *J. Organomet. Chem.* **2005**, *690*, 5451−5457.

(16) (a) Slone, C. S.; Weinberger, D. A.; Mirkin, C. A. *Prog. Inorg. Chem.* **1999**, *48*, 233−350. (b) Braunstein, P.; Naud, F. *Angew. Chem., Int. Ed.* **2001**, *40*, 680−699. (c) Braunstein, P. *J. Organomet. Chem.* **2004**, *689*, 3953−3967. (d) Zhang, W.-H.; Chien, S. W.; Hor, T. S. A. *Coord. Chem. Rev.* **2011**, *255*, 1991−2024. (e) Chikkali, S. H.; van der Vlugt, J. I.; Reek, J. N. H. *Coord. Chem. Rev.* **2014**, *262*, 1−15.

(17) Marchenko, A. P.; Koidan, H. N.; Pervak, I. I.; Huryeva, A. N.; Zarudnitskii, E. V.; Tolmachev, A. A.; Kostyuk, A. N. *Tetrahedron Lett.* **2012**, *53*, 494−496.

(18) Danopoulos, A. A.; Monakhov, K. Y.; Robert, V.; Braunstein, P.; Pattacini, R.; Conde-Guadaño, S.; Hanton, M.; Tooze, R. P. *Organometallics* **2013**, *32*, 1842−1850.

(19) (a) Danopoulos, A. A.; Hankin, D. M.; Wilkinson, G.; Cafferkey, S. M.; Sweet, T. K. N.; Hursthouse, M. B. *Polyhedron* **1997**, *16*, 3879−3892. (b) Jones, C.; Dange, D.; Stasch, A. *J. Chem. Crystallogr.* **2012**, *42*, 494−497.

(20) (a) Greene, P. T.; Russ, B. J.; Wood, J. S. *J. Chem. Soc. A* **1971**, 3636−3638. (b) Müller, E.; Krause, J.; Schmiedeknecht, K. *J. Organomet. Chem.* **1972**, *44*, 127−140. (c) Cotton, F. A.;

DOI: 10.1021/acs.organomet.5b00547
Organometallics 2015, 34, 4109−4116

Czuchajowska, J.; Falvello, L. R.; Feng, X. *Inorg. Chim. Acta* **1990**, *172*, 135−136. (d) Liang, Y.; Yap, G. P. A.; Rheingold, A. L.; Theopold, K. H. *Organometallics* **1996**, *15*, 5284−5286. (e) Fryzuk, M. D.; Leznoff, D. B.; Rettig, S. J. *Organometallics* **1997**, *16*, 5116−5119. (f) Heintz, R. A.; Leelasubcharoen, S.; Liable-Sands, L. M.; Rheingold, A. L.; Theopold, K. H. *Organometallics* **1998**, *17*, 5477−5485. (g) MacAdams, L. A.; Kim, W.-K.; Liable-Sands, L. M.; Guzei, I. A.; Rheingold, A. L.; Theopold, K. H. *Organometallics* **2002**, *21*, 952−960. (h) Kreisel, K. A.; Yap, G. P. A.; Theopold, K. H. *Organometallics* **2006**, *25*, 4670−4679. (i) Monillas, W. H.; Theopold, K. H.; Yap, G. P. A. Private Communication in CCDC 667984 and 667985. (j) Ronellenfitsch, M.; Wadepohl, H.; Enders, M. *Organometallics* **2014**, *33*, 5758−5766.

(21) Addison, A. W.; Rao, T. N.; Reedijk, J.; van Rijn, J.; Verschoor, G. C. *J. Chem. Soc., Dalton Trans.* **1984**, 1349−1356.

(22) Leung, C. H.; Incarvito, C. D.; Crabtree, R. H. *Organometallics* **2006**, *25*, 6099−6107.

(23) Köhn, R. D.; Kociok-Köhn, G.; Haufe, M. *J. Organomet. Chem.* **1995**, *501*, 303−307.

(24) Jabri, A.; Temple, C.; Crewdson, P.; Gambarotta, S.; Korobkov, I.; Duchateau, R. *J. Am. Chem. Soc.* **2006**, *128*, 9238−9247.

(25) Vadake Kulangara, S.; Haveman, D.; Vidjayacoumar, B.; Korobkov, I.; Gambarotta, S.; Duchateau, R. *Organometallics* **2015**, *34*, 1203−1210.

(26) Wagner, B. O.; Hammond, G. S. *J. Organomet. Chem.* **1975**, *85*, 1−14.

(27) *APEX2*; Bruker AXS Inc., Madison, WI, USA, 2006.

(28) Sheldrick, G. M. *Acta Crystallogr., Sect. A: Found. Crystallogr.* **1990**, *46*, 467−473.

(29) Sheldrick, G. M. *SHELX-97*; Universität Göttingen, Göttingen, Germany, 1999.

(30) *Denzo*; Nonius BV, Delft, The Netherlands, 1997.

(31) Spek, A. L. *J. Appl. Crystallogr.* **2003**, *36*, 7−13.

DOI: 10.1021/acs.organomet.5b00547
Organometallics 2015, 34, 4109−4116

Conclusion Générale

Conclusion Générale

Ce travail de thèse a conduit à la synthèse d'un nouveau ligand tridente, stable et rigide, le *N*,*N'*-diphosphanyl-imidazol-2-ylidene (**PC$_{NHC}$P**). Sa stabilité a été étudiée de manière expérimentale et à l'aide de calculs théoriques.

Sa coordination à des métaux du groupe 11 a conduit à des complexes très originaux au point de vue structural. Les complexes trinucléaires **Cu3**, **Ag3** et **Au3** possédant un arrangement linéaire des métaux furent obtenus par réaction du carbène libre **PC$_{NHC}$P** avec un précurseur cationique des métaux du groupe 11 associés à un anion triflate. Les complexes dinucléaires **Cu2**, **Ag2** ou **Au2** avec ce ligand tridente furent obtenus par réaction du sel d'imidazolium **PCHP** avec MN(SiMe$_3$)$_2$ (M = Cu, Ag ou Au). Les courtes distances métal-métal dans les complexes trinucléaires (2.5761(9) Å pour **Cu3**, 2.7599(3) Å pour **Ag3** et 2.7584(2) Å pour **Au3**) et dans les complexes dinucléaires (2.6827(12) Å pour **Cu2**, 2.8320(6) Å pour **Au2**) impliquent l'existence d'interactions métallophiles d^{10}-d^{10}. Des résultats préliminaires montrent que la forte luminescence de **Au3** au soleil ou sous UV dans l'acétonitrile ou à l'état solide est liée à ces interactions aurophiles.

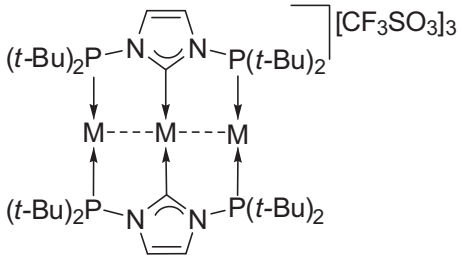

Cu3: M = Cu
Ag3: M = Ag
Au3: M = Au

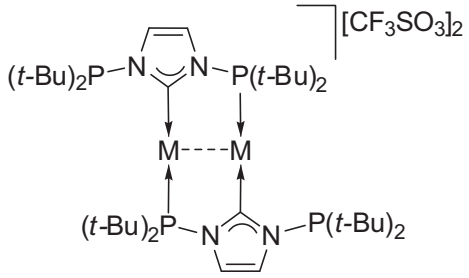

Cu2: M = Cu
Ag2: M = Ag
Au2: M = Au

Le complexe mononucléaire d'Au(I) **Au1** a également été isolé dans la réaction du sel d'imidazolium **PCHP** avec 1 equiv. de [(**PC$_{NHC}$P**)Au{N(SiMe$_3$)$_2$}], ce dernier étant formé *in situ* par addition du carbène libre **PC$_{NHC}$P** à [(Ph$_3$P)Au{N(SiMe$_3$)$_2$}] dans le THF. Avec un ou deux groupes phosphines libres, **Au1** et **Au2** ont servi de précurseurs aux complexes homométalliques **Au3**, **Au5**, un pentanucléaire à

structure très originale en croix, et un hexanucléaire du Cu(I) possédant deux rangées Cu_3 parallèles et coplanaires reliées entre elles par des interactions d^{10}-d^{10} ainsi qu'à des hétérométalliques Ag-Au.

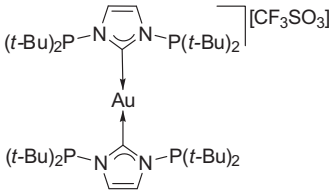

Au1

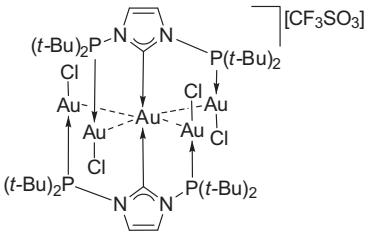

Au5

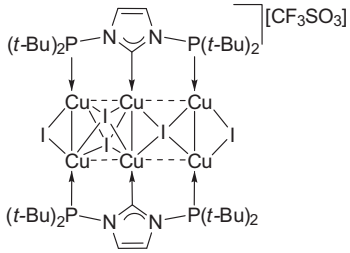

Cu6

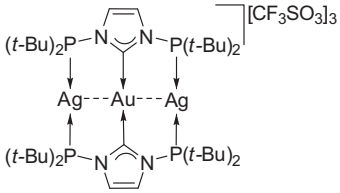

heteronuclear Ag/Au

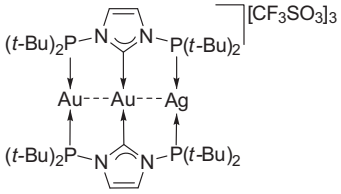

heteronuclear Ag/Au

La nature des produits obtenus dans la reaction de **$PC_{NHC}P$** avec des précurseurs Au(I) depend de l'anion associé à ces derniers. Ainsi, l'utilisation de [Au*Cl*(tht)] a conduit à la rupture d'une liaison N-P pour donner un nouveau complexe triangulaire **Au6**, et non pas le complexe **Au3**, qui est caractérisé par un squelette $Au_6(\mu_3$-**PC**,κ*C*,κ*N*,κ*P*$)_3$. La réaction de l'imidazolidure de lithium **PC-Li** avec [AuCl(tht)] a également conduit à **Au6**, ainsi qu'à un sel original contenant des entités cationiques $[Au_5(\mu_3$-**PC**-κ*P*,κ*C*,κ*N*$)]^+$. A l'état solide, deux de ces cations interagissent via leur centre dicoordiné N-*Au*-N avec un anion $[AuCl_2]^-$.

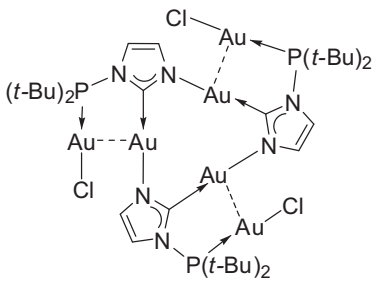

Au6

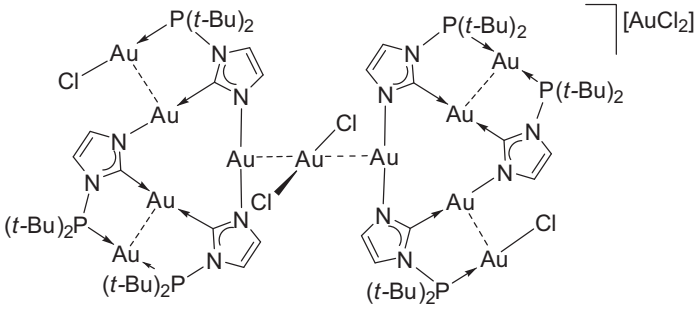

Au12

Inspirés par la migration d'un groupe P(*t*-Bu)$_2$ de N vers C2 lors du chauffage de **$PC_{NHC}P$** à 120 °C pendant 12 h, nous avons preparé deux régioisomères, non

symétriques $P^{C2}P^{N}$-imidazoles, $t\text{-Bu}_2\text{PNCH=CHNC(PPh}_2)$ (**L1**, P^{C2} = PPh_2, P^{N} = P(*t*-Bu)$_2$) et $\text{Ph}_2\text{PNCH=CHNC[P}(t\text{-Bu})_2]$ (**L2**, P^{C2} = P(*t*-Bu)$_2$, P^{N} = PPh_2). Ils présentent des différences de réactivité considérables au niveau de la phosphine liée à N; l'isomère **L2** est extrêmement sensible à la rupture de la liaison P-N par les nucléophiles et lorsque coordiné au fragment PdCl(Me), il conduit d'abord au complexe **2b** qui est ensuite le siège d'un échange mutuel entre un phényle P^{N} et le groupe méthyle du Pd pour donner **2c.**

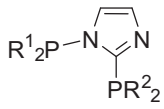

L1: R^1 = *t*-Bu, R^2 = Ph
L2: R^1 = Ph, R^2 = *t*-Bu

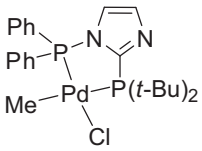

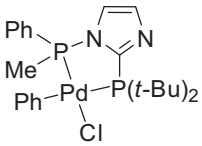

Les complexes homotrinucléaires **Cu3** et **Ag3** furent utilisés pour une transmétallation partielle ou totale avec des précurseurs de Pd(0) pour donner des complexes hétérotrinucléaires. La réaction de **Cu3** ou **Ag3** avec un équivalent de $[Pd(PPh_3)_4]$ dans le CH_2Cl_2 conduit au remplacement de l'un des métaux en position terminale par le Pd(0) pour former respectivement **Cu-Pd-1** et **Ag-Pd-1** à interactions d^{10}-d^{10}-d^{10}. L'utilisation de plus de 3 équivalents de $[Pd(PPh_3)_4$ a donné le complexe hétérotrinucléaire **Cu-Pd-2** avec une chaine métallique Pd-Cu-Pd (d^9-$d^{10}s^1$-d^9). Dans la cas de l'argent par contre, l'addition d'un excès de $[Pd(PPh_3)_4]$ n'a conduit qu'à l'oxydation de **Ag-Pd-1** par le solvant (CH_2Cl_2) pour donner le complexe **Ag-Pd-2** à interactions d^{10}-d^{8}-d^{10}. Dans les deux cas conduisant à **Cu3** et **Ag3**, $[Pd(dba)_2]$ dans le MeCN permet une transmétallation complète donnant le complexe homotrinucléaire **Pd3**.

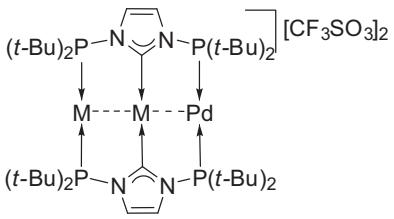

Cu-Pd-1: M = Cu
Ag-Pd-1: M = Ag

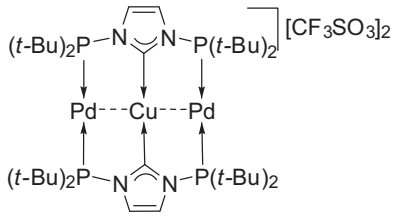

Cu-Pd-1

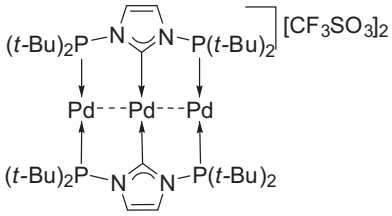

Pd3

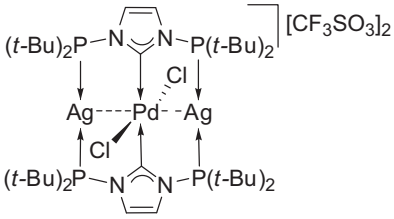

Ag-Pd-2

En plus de son comportement pontant, **$PC_{NHC}P$** peut aussi chélater un métal, comme observé lors de sa coordination à des précurseurs ([$PdMe_2$] ou [$Pd(dba)_2$]).

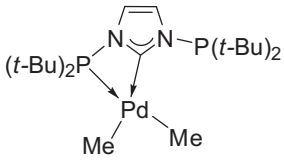

Pd-Me2

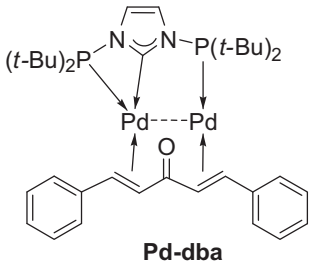

Pd-dba

Une série de complexes du Cr(II) contenant des ligands NHC *N*-phosphanyl- ou *N,N'*-diphosphanyl-substitués furent préparés dans lesquels le centre Cr^{II} a un environnement plan carré avec deux ligands chlorures en trans et deux ligands carbènes monodentates C_{NHC}. L'alkylation avec [$Mg(benzyl)_2(thf)_2$] fournit le dérivé pentacoordiné tribenzyle du Cr(III) avec une géométrie pyramide à base carrée déformée, comprenant un chélate C_{NHC}, P et les trois ligands benzyles. Le système Cr^{III}/MAO a montré des performances catalytiques supérieures au Cr^{II} en oligomérisation de l'éthylene (valeur du TOF jusqu'à 16320 mol C_2H_4/((mol Cr)·h)) et fournit principalement des oligomères.

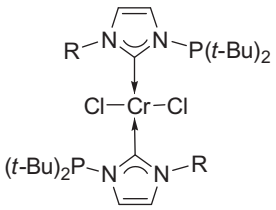

1: R = *t*-Bu
2: R = Mes
3: R = DIPP
4: R = $(t\text{-Bu})_2$P

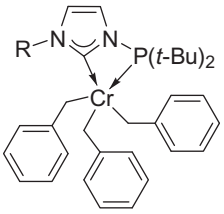

5: R = DIPP
6: R = $(t\text{-Bu})_2$P

Certains complexes de l'or et du cuivre présentent d'excellentes propriétés de luminescence et leur étude est en cours. Le manque de temps n'a pas permis de faire varier les substituants de **$PC_{NHC}P$** et seuls des travaux préliminaires ont été realises dont on peut espérer qu'ils seront poursuivis dans le futur.

Pengfei AI

Synthèse et réactivité de complexes métalliques contenant des ligands carbéniques N-hétérocycliques et des ligands fonctionnels pour des applications catalytiques

Résumé

L'objectif de ce travail fut la synthèse de ligands fonctionnels de type *N*,*N'*-diphosphanyl-NHC (NHC = carbènes N-hétérocycliques) et l'étude de leur chimie de coordination. La synthèse du nouveau ligand tridentate, stable et rigide, *N*,*N'*-diphosphanyl-imidazol-2-ylidene a permis des études expérimentales et théoriques et l'accès à des complexes mono-, di-, tri-, penta-, et hexanucléaires des métaux du groupe 11 (Cu, Ag et Au) originaux et aux propriétés structurales uniques. Les complexes mono- et dinucléaires avec un ou deux atomes de phosphore libres ont permis d'accéder à des complexes hétérotrinucléaires à interactions d^{10}-d^{10} qui sont luminescents. La transmétallation partielle ou totale des complexes homotrinucléaires de Cu ou d'Ag avec des réactifs contenant du Pd(0) ont conduit à des complexes hétérotrinucléaires à interactions d^{10}-d^{10}. En plus de son comportement pontant, ce ligand peut se agir en chélate dans des complexes du palladium et du chrome. Dans le cas du Cr(III), ils montrent une activité catalytique en oligomérisation de l'éthylène supérieure à celle des complexes du Cr(II) et conduisent principalement à des oligomères.

Mots-clés: carbènes N-hétérocycliques, fonctions phosphanyles, complexes polynucléaires, liaisons métal-métal, interactions d^{10}-d^{10} (interactions aurophiles), luminescence, oligomérisation catalytique de l'éthylène.

Résumé en anglais

The purpose of this work was the synthesis of *N*,*N'*-diphosphanyl-functionalized NHC ligands and their coordination chemistry. The novel stable and rigid tridentate *N*,*N'*-diphosphanyl-imidazol-2-ylidene was synthesized and experimental and computational information on its stability were gained. It served as a unique platform for the synthesis of novel mono-, di-, tri-, penta-, hexa-nuclear complexes with the coinage metals (Cu, Ag and Au), exhibiting rare structural features. The mono- and dinuclear complexes with one or two dangling P-donors provided rational access to heterotrinuclear complexes. All these coinage metal complexes have short metal-metal separations, indicating the presence of d^{10}-d^{10} interactions, and display excellent luminescent properties. Partial or complete transmetallation of the homotrinuclear Cu or Ag complexes with Pd(0) precursors led to hetero-trinuclear complexes with d^{10}-d^{10} interactions. In addition to its bridging behavior, this ligand also showed its chelating behavior in Pd or Cr(III) complexes. The latter displayed superior performance in ethylene oligomerization than the Cr(II) complexes and gave mostly oligomers.

Keywords: N-heterocyclic carbenes, phophanyl-functionalization, polynuclear complexes, metal-metal bonds, d^{10}-d^{10} interactions (aurophillic interactions), luminescence, catalytic ethylene oligomerization